PNNL-15465

Pacific Northwest
National Laboratory
Operated by Battelle for the
U.S. Department of Energy

STOMP: Subsurface Transport Over Multiple Phases

Version 1.0

Addendum: Sparse Vegetation Evapotranspiration Model for the Water-Air-Energy Operational Mode

A. L. Ward
M.D. White
E.J. Freeman
Z.F. Zhang

September 2005

Prepared for the U.S. Department of Energy
under Contract DE-AC05-76RL01830

DISCLAIMER

PACIFIC NORTHWEST NATIONAL LABORATORY
operated by
BATTELLE
for the
UNITED STATES DEPARTMENT OF ENERGY
under Contract DE-AC05-76RL01830

PNNL-15465

STOMP: Subsurface Transport Over Multiple Phases

Version 1.0

Addendum:
Sparse Vegetation Evapotranspiration Model for the Water-Air-Energy Operational Mode

A. L. Ward
M. D. White
E. J. Freeman
Z. F. Zhang

September 2005

Prepared for the U.S. Department of Energy
under Contract DE-AC05-76RL01830

Pacific Northwest National Laboratory
Richland, Washington 99352

Preface

This addendum describes the theory, input file formatting, and application of a sparse vegetation evapotranspiration model for the Water-Air-Energy Operational Mode of the Subsurface Transport Over Multiple Phases (STOMP) numerical simulator. The STOMP simulator is a scientific tool for analyzing single and multi-fluid subsurface flow and transport. Its general use, input file formatting, compilation, and execution are described in a companion user's guide. A description of the simulator's governing equations, constitutive functions and, numerical solution algorithms are provided in a companion theory guide.

The Water-Air-Energy Operational Mode (STOMP-WAE) solves the coupled conservation equations for water mass, air mass, and thermal energy transported over three phases: aqueous, gas, and soil matrix. This model operates in multiple dimensions. The evapotranspiration model is implemented as a boundary condition on the upper surface of the computational domain and has capabilities for modeling evaporation from bare surfaces as well as evapotranspiration from sparsely vegetated surfaces populated with multiple plant species. This mode is the *barrier* extension of the WAE mode and is designated as STOMP-WAE-B. Input for STOMP-WAE-B is specified via three input cards and includes the following: atmospheric conditions through the *Atmospheric Conditions Card*, time-invariant plant species data through the *Plant Properties Card*, and time varying plant species data through the *Boundary Conditions* Card. Two optional cards, the *Observed Data* and *UCODE Control* Cards, allow use of STOMP-W-I and STOMP-WAE-I, inverse operational modes of STOMP-W and STOMP-WAE, to estimate model parameters.

In writing this addendum, it is assumed that the reader is a *qualified user* of the STOMP simulator who is familiar with the code and comprehends concepts and theories associated with multiple-phase hydrology, heat transfer, thermodynamics, relative permeability-saturation-capillary pressure constitutive relations, and, more importantly, the soil-vegetation-atmosphere continuum. The authors further assume that readers are familiar with the computing environment in which they plan to compile and execute the STOMP simulator. The STOMP simulator is written in the FORTRAN 77 and 90 languages, following the American National Standards Institute standards. The simulator uses a variable source code configuration, which allows the execution memory and speed to be tailored to the specific problem to be solved, and essentially requires that the source code be assembled and compiled through a software maintenance utility. The memory requirements for executing the simulator are dependent on the complexity of the physical system to be modeled and the size and dimensionality of the computational domain. Likewise, the execution speed depends on the problem complexity, the size and dimensionality of the computational domain, and the computer performance.

Summary

It is anticipated that some 200 surface barriers, covering nearly 1000 acres, will be built at Hanford to reduce the local flux of meteoric water into subsurface waste zones. Because of the complexity of atmospheric-surface and surface-subsurface interactions, barrier design is considered one of four Science and Technology Challenges at Hanford contributing to the uncertainty in long-term performance. Given the combination of climatic conditions and barrier designs being considered for use at the Hanford Site, there is a clear need for a scientific tool capable of simulating non-isothermal unsaturated flow to support barrier design and performance assessment. Such a tool should be capable of simulating the effects of subsurface capillary breaks, lateral drainage, side-slope performance, and evapotranspiration as well as the impacts of spatial and temporal changes in physical and hydraulic properties that might influence long-term performance. The ideal model would be the capability to predict the migration of contaminant transport to help evaluate the efficacy of barriers in containing subsurface contaminant migration and protect groundwater quality. In addition to these requirements, the tool should have inverse capabilities for calibrating key parameters.

A soil-vegetation-atmosphere-transfer scheme (SVAT) based on a sparse vegetation evapotranspiration model was used to extend the Water-Air-Energy Operational Mode of the Subsurface Transport Over Multiple Phases (STOMP) simulator. STOMP was developed by the Pacific Northwest National Laboratory[(a)] for modeling the performance of protective barriers in arid and semi-arid environments. This extension, STOMP-WAE-B (Water-Air-Energy-Barriers) provides the needed scientific tool to design and evaluate candidate barriers for the Hanford Site. This addendum provides background to the concept of engineered barriers for waste management and the basis of the conceptual model; it also describes the mathematical theory and numerical solution techniques of the SVAT scheme. In addition, it provides technical guidance for the use of the simulator and includes example input files and the simulation results for several test problems, including a benchmark problem comparing model simulations with published performance.

The sparse vegetation evapotranspiration model was designed as a boundary condition to extend the Water-Air-Energy Operational Mode of the STOMP simulator. With this extension, the model calculates water mass, air mass, and thermal energy across a boundary surface and root-water transport between the subsurface and atmosphere. The model solves sets of nonlinear conservation equations for water mass, air mass and thermal energy at the ground surface, plant leaves, and canopy. The conservation equations mathematically describe the transport of water, air, and thermal energy across the ground surface, either directly or through plants. Nonlinearities in the solved governing equations are resolved via Newton-Raphson iteration. The subsurface equations are coupled to the surface evapotranspiration equations as a boundary condition, whose effects impact deeper subsurface nodes through plant roots. The STOMP simulator uses numerical derivatives, which requires that the nonlinear boundary condition system be resolved four times (i.e., one plus the number of field domain unknowns) for each boundary surface and Newton-Raphson iteration of the subsurface domain.

(a) Pacific Northwest National Laboratory is operated by Battelle for the U.S. Department of Energy under Contract DE-AC05-76RL01830.

The sets of solved governing conservation equations differ, depending on whether the ground surface is bare or vegetated and whether the temperatures of different plant species are distinguished. The bare-surface system of equations comprises steady-flow conservation equations for water mass, air mass, and thermal energy at the ground surface. The air-mass equation is implicit, yielding a system of two equations and two unknowns to be resolved at each boundary surface. The single-plant-temperature system of equations comprises steady-flow conservation equations for water mass at the ground surface and mean canopy height (canopy) and thermal energy at the ground surface, plant leaves, and canopy. An air-mass conservation equation at the ground surface and water-mass conservation equation at the plant leaves are implicit, yielding a system of five equations and five unknowns to be resolved at each boundary surface. If rainfall interception and condensation accumulation are considered, the water mass conservation equation at the plant leaves changes from steady-flow to transient, including plant-leaf storage of water. The multiple-plant-temperature system is similar to the single-plant-temperature system, except that three additional equations are needed for each plant species: a water-mass conservation equation at the canopy for the plant species and a thermal-energy conservation equation at the plant leaves and canopy for the plant species.

The intended users of the sparse vegetation evapotranspiration model and Water-Air-Energy Operational Mode of the STOMP simulator include scientists and engineers who are investigating hydrologic and multi-fluid flow phenomena associated with the soil-vegetation-atmosphere-transfer schemes, particularly the design and performance of surface barriers and landfill covers. Principal design goals for these numerical simulation tools include broad applicability, verified algorithms, quality assurance controls, and simulations validated against laboratory and field-scale experiments. The calibration of key input parameters, including hydrologic, thermal, and plant properties, is afforded via inverse simulation through STOMP's linkage to UCODE. Quantitative predictions from the STOMP simulator are generated from the numerical solution of partial differential equations that describe surface and subsurface environment transport phenomena. The STOMP simulator and sparse vegetation evapotranspiration model were written in FORTRAN 77, following American National Standards Institute (ANSI) standards. The STOMP simulator is provided as source coding, configured either for a direct-banded linear system solver or an iterative conjugate gradient solver. Compilation of the code with a FORTRAN 77 compiler is required before executing, and the conjugate gradient solver version of the code requires installation of the conjugate gradient solver package.

A series of eleven verification problems related to infiltration, redistribution, evaporation and transpiration in homogeneous and layered soils were simulated. In addition water balance calculations were performed for a grass-covered site in Hanford's 300 Area and a bare-surface monofill barrier in Idaho. A comparison of simulation results with published analytical and numerical solutions and experimental results demonstrates that STOMP is able to describe the dynamics of mass and energy transport over a range of meteorological and soil conditions with or without plants present. Use of field-scale hydraulic properties determined for the grass site by automatic calibration resulted in very good agreement between observed and predicted water balance. In an inter-code comparison with seven public domain codes used to simulate barrier performance, not only was the STOMP simulator capable of matching the field observations, but in all cases, it produced superior results. Using this tool to guide barrier design will result in optimized designs with reduced construction costs, reduced environmental impacts at borrow sites, and minimized post-closure care and monitoring needs while meeting regulatory requirements.

KEYWORDS: STOMP, soil-vegetation-atmosphere-transfer scheme, evapotranspiration, sparse vegetation, surface barrier, landfill cover, numerical simulation, Hanford

Acknowledgments

This work was partly supported by Fluor Hanford, Inc, through its technology management in the Groundwater Protection Program. In addition to programmatic support, the continued development of the Subsurface Transport Over Multiple Phases simulator in its sequential and parallel implementations has been funded by the Laboratory Directed Research and Development (LDRD) program at the Pacific Northwest National Laboratory. In particular, the development of a scalable implementation has been funded through the Computational Science and Engineering Initiative, and the development of new operational modes for modeling carbon dioxide sequestration has been supported through the Carbon Management Initiative. LDRD at Pacific Northwest National Laboratory is a productive and efficient program that develops technical capabilities for solving complex technical problems that are important to the Department of Energy and to the nation. U.S. Department of Energy (DOE) Order 413.2A sets forth the Department's LDRD policy and guidelines for DOE multi-program laboratories and authorizes the national laboratories to allocate up to six percent of their operating budgets to fund the program.

Glossary of Symbols

Roman Symbols

c_a	fractional cloud cover
c_{p_g}	gas specific heat, J/kg K
C^i	extinction coefficient for plant species *i*
C^i_{coef}	crop coefficient for plant species *i*
d_c	canopy zero plane displacement, m
dz_{ns}	z-direction distance between subsurface node and ground surface, m
d_p	stored water depth of plant species, m
d_p^d	maximum dew depth of plant species, m
D_g^w	gas water-vapor diffusion coefficient, m^2/s
E_{ca}	diffusive water-vapor flux from canopy to atmosphere, kg/s m^2
E_{ns}	diffusive water-vapor flux from subsurface node to ground surface, kg/s m^2
E_{pc}	diffusive water-vapor flux, via evaporation, from plant to canopy, kg/s m^2
E_{sa}	diffusive water-vapor flux, via evaporation, from ground surface to atmosphere, kg/s m^2
E_t	equation of time, min
g	acceleration of gravity, m/s^2
G_{ns}	advective gas flux from subsurface node to ground surface, m^3/s m^2
G_{sa}	advective gas flux from ground surface to atmosphere, m^3/s m^2
h	soil water matric head at a particular spatial location, m
h_{50}	soil water matric head at which root water uptake is reduced by 50 percent, m
h_c	crop height, m
h_{cf}	mean canopy flow height, m
h_g	gas enthalpy, J/kg
h_g^w	gas water-vapor enthalpy, J/kg
h_l	aqueous enthalpy, J/kg

H_{ns}	conductive heat flux from subsurface node to ground surface, W/m^2
H_{sa}	conductive-convective heat flux from ground surface to atmosphere, W/m^2
H_{sc}	conductive-convective heat flux from ground surface to canopy, W/m^2
I_a	irrigation intensity, m^3/s m^2
I_o	extraterrestrial irradiance (1367 W/m^2)
j	Julian day divided by 100
J	Julian day
k_e	effective thermal conductivity, W/m K
k_g	gas thermal conductivity, W/m K
k_{rg}	gas relative permeability
k_{rl}	aqueous relative permeability
$\mathbf{k}_z$	z-direction intrinsic permeability, m^2
K	eddy diffusion coefficient, m^2/s
K_c	canopy eddy diffusion coefficient, m^2/s
K_{ca}	canopy-atmosphere eddy diffusion coefficient, m^2/s
K_{sc}	ground-canopy eddy diffusion coefficient, m^2/s
L_a	rainfall intensity, m^3/s m^2
L_{ai}^i	leaf area index of plant species *i*, m^2 leaf area/m^2 plant footprint
L_l	local longitude, deg
L_m	local meridian, deg
L_{ns}	advective aqueous flux from subsurface node to ground surface, m^3/s m^2
L_{sa}	advective aqueous flux from ground surface to atmosphere, m^3/s m^2
L_{sp}	shed rainfall or condensate flux from ground surface to plants, m^3/s m^2
m_p^w	mass of stored water on plant species, kg/m^2
n_D	diffusive porosity
n_{ps}	number of plant species
Nu	Nusselt number
P_{ai}^i	plant area index of plant species *i*, m^2 plant footprint/m^2 ground
P_{atm}	atmospheric pressure (101325.0 Pa)

P_g	gas pressure, Pa
P_g^w	water-vapor partial pressure, Pa
P_l	aqueous pressure, Pa
ΔP_{l_s}	correction to the ground surface aqueous pressure, Pa
Pr	Prandtl number
P_{sat}^w	saturated water-vapor pressure, Pa
r_{ca}^a	aerodynamic resistance between the canopy and atmosphere, s/m
r_{sa}^a	aerodynamic resistance for bare surface (ground-atmosphere), s/m
r_{pc}^a	aerodynamic resistance between plant and canopy, s/m
r_{pc}^s	stomatal resistance between plant and canopy, s/m
r_{sc}^a	aerodynamic resistance between ground and canopy, s/m
R_a^{ld}	downward long-wave radiation from the atmosphere, W/m^2
R_a^{sd}	downward short-wave radiation from the atmosphere, W/m^2
R_i^{sd}	incident clear-sky solar radiation, W/m^2
R_l	aqueous gas constant, J/kmol K
R_p^n	net radiation into the plant, W/m^2
R_p^{ln}	net long-wave radiation into the plant, W/m^2
R_p^{sn}	net short-wave radiation into the plant, W/m^2
R_s^{ld}	downward long-wave radiation at the ground surface, W/m^2
R_s^{ln}	net long-wave radiation into the ground surface, W/m^2
R_s^{lu}	upward long-wave radiation at the ground surface, W/m^2
R_s^n	net radiation into the ground surface, W/m^2
R_s^{sd}	downward short-wave radiation at the ground surface, W/m^2
R_s^{sn}	net short-wave radiation into the ground surface, W/m^2
R_s^{su}	upward short-wave radiation at the ground surface, W/m^2

$\mathbf{R}_s^e$	residual of the energy balance at the ground surface, W/m^2
$\mathbf{R}_s^w$	residual of the water mass balance at the ground surface, kg/s m^2
R_{stress}^i	root stress factor for plant species *i*
R_{wu}^n	root water uptake for node *n*, kg/s m^2
Re	Reynolds number
s	phase saturation
$S\left(z_r\right)$	normalized root water uptake function
Δt	time step, s
t_h	standard time, hr
t_o	solar noon time, hr
T	temperature, K
T_a	atmospheric temperature, K
T_{abs}	absolute temperature (273.15 K)
T_{dp}	dew point temperature, K
T_n	subsurface temperature, K
T_{pc}	diffusive water-vapor flux, via transpiration, from plant to canopy, kg/s m^2
T_s	ground surface temperature, K
ΔT_s	correction to the ground surface temperature, K
u	wind speed, m/s
u_c	wind speed at the mean canopy flow height, m/s
u_{ref}	wind speed at the measurement height, m/s
u^*	friction velocity, m/s
W_p^l	leaf width, m
z	height above ground surface, m
z_0	aerodynamic roughness length, m
z_b^n	bottom depth of node *n*, m
z_h	thermal roughness length, m
z_m	momentum roughness length, m
z_{mr}	maximum root depth, m

z_r	root depth, m
z_{ref}	measurement height above the ground surface, m
z_t^n	top depth of node *n*, m

Greek Symbols

α^i	albedo of plant species *i*
α_s	ground surface albedo
α_z	solar zenith angle adjustment for α_s
α_g	ground surface albedo expressed as a function of soil moisture
α_r	albedo at solar zenith angle, $\omega=60^o$
$\beta(z_r)$	root distribution function
$\gamma(h)$	soil water stress function
δ	solar declination, deg
ε^i	emissivity of plant species *i*
ε_a^0	clear-sky emissivity
ε_s	emissivity of the ground surface
θ	solar altitude, deg
κ	von Karman's constant (0.4)
μ_g	gas viscosity, Pa s
μ_l	aqueous viscosity, Pa s
ρ_g	gas density, kg/m^3
ρ_g^w	water-vapor density, kg/m^3
ρ_l	aqueous density, kg/m^3
σ	Stefan-Boltzmann constant (5.67×10^{-8} W/m^2 K)
τ_g	gas tortuosity factor
ϕ	relative humidity
ϕ_l	local latitude, deg
ω	solar hour angle, deg

ω_g^a	gas air mass fraction
ω_g^w	gas water mass fraction
ω_l^w	aqueous water mass fraction

Mathematical Symbols

$[\ ]_{ns}$	interfacial average between subsurface node and ground surface
$[\ ]_{sa}$	interfacial average between ground surface and atmosphere
$(\ )_a$	atmosphere state condition
$(\ )_n$	subsurface node state condition
$(\ )_s$	ground surface state condition

Subscripts

a	atmosphere
c	canopy
g	gas phase
l	aqueous phase

Acronyms

ANSI	American National Standards Institute
ASME	American Society for Mechanical Engineers
CASTNET	Clean Air Status and Trends Network
DOY	day of year
HMS	Hanford Meteorological Station
LDRD	Laboratory Directed Research and Development
PNNL	Pacific Northwest National Laboratory
STOMP	Subsurface Transport Over Multiple Phases
SVAT	soil-vegetation-atmosphere-transfer scheme
WAE	Water-Air-Energy
WAE-B	Water-Air-Energy-Barriers

Contents

Figures

Tables

1.0 Introduction

In-place containment of subsurface contaminants is viewed as one of the final remedial options for many U.S. Department of Energy (DOE) waste sites expected have residual contaminants after remediation. In-place containment has also been proposed as a viable option for sites with low to intermediate levels of buried contaminants and those that pose few risks to human health and the environment. This technology relies heavily on engineered barriers and at Hanford alone, it is estimated that some 200 barriers will be used to cover almost 1000 acres of waste sites. Yet, barrier development remains one of four top science and technology challenges within the DOE complex, primarily because of uncertainty in long-term performance.

Design standards for engineered barriers require that these structures minimize infiltration through the system in the long-term; function with minimal maintenance; minimize erosion; and accommodate settling and subsidence (Suter et al. 1993). The primary functions of engineered barriers are therefore to isolate near surface and subsurface waste from human and biotic intrusion, thereby limiting interaction with environmental processes that could cause contaminant migration from the site. Several years of barrier research at Hanford and other sites across the United States have demonstrated designs that may provide these functions along with other economic and technical advantages (Ward and Gee 1997; Gee et al. 1997; DOE-RL 1999).

Designing field-scale final covers, however, is a challenging undertaking because of the large number of variables that can influence performance. Barrier design for long-term waste isolation requires consideration of the nature of the waste site, hydrogeological characteristics of the waste site, geochemical characteristics of the waste, the availability of suitable construction materials, required design life, and the acceptable risk to human health and the environment. Consequently, barrier designs may have to be site specific rather than prescriptive. A basic need therefore is a simulation model that can be used to evaluate candidate designs while taking into account economic, technical, and regulatory concerns. At present, there are a number of approaches and models that have been applied to predict barrier performance. These range from simple storage routing models to the more mechanistic Richards' (1931) equation-based models that simulate water flow and heat transport in response to meteorological forcing and plant water uptake. Nevertheless, the ideal model should be capable of supporting barrier design and performance assessment within the complex interaction of physical, hydrologic, and biotic processes that control field-scale at the site of interest.

Predicting the performance of field-scale barriers requires consideration for unsaturated flow processes, including precipitation, snow accumulation and melting, surface runoff, water storage, evaporation, transpiration, lateral diversion along sloped layers, and, ultimately, deep percolation (Ward and Gee 1997; Ward et al. 2005a). All of these processes occur in response to forcing meteorology that leads to temporal variability in air temperature, relative humidity, wind speed, and barometric pressure and therefore require the solution of coupled equations for mass and energy transport. Although significant progress has been made in modeling the performance of engineered covers, there are still some challenges in accurately predicting the complicated flow diversion and leakage patterns typical of field-scale flow in heterogeneous subsurface sediments. There is also a need to understand the processes that may lead to barrier failure in the long term and the importance of these processes to development of post-closure stewardship protocols.

The needs described above were the primary drivers for the work summarized in this report. The primary objective was to develop a simulation model to support the design of engineered barriers at Hanford. The scope of the project was to integrate plant-soil-atmosphere dynamics into Pacific Northwest National Laboratory's (PNNL's) STOMP Numerical Simulator to provide a design and evaluation tool for field-scale barriers and verify performance relative to existing codes to the extent possible. This effort involved adding a soil-vegetation-atmosphere-transfer (SVAT) module to account for meteorological forcings on variably saturated water flow, heat transport, and plant water uptake. The result is an extension to the widely used water-air-energy (WAE) operational mode of STOMP for barrier simulation, STOMP-WAE-B (White and Ward 2005). STOMP-WAE-B is a comprehensive, numerically efficient, mechanistic tool capable of addressing the dominant aspects of barrier functionality as well as potential failure mechanisms. This extension to the simulator provides the capability to evaluate candidate barriers, beforehand, to allow identification of any technical or regulatory problems inherent in their design, and to assess their projected long-term performance. To simplify the calibration process and facilitate parameter sensitivity analysis, an inverse mode of STOMP-WAE (STOMP-WAE-I), which couples STOMP-WAE with UCODE (Poeter and Hill 1998) is available. In addition, the code can be easily incorporated into a decision support system to perform a complete risk assessment of different remediation options.

This report documents the modifications made to STOMP-WAE to incorporate the SVAT schemes for sparse canopy ecosystems. To put the scope of these changes involved in the development of STOMP-WAE-B into proper perspective, the factors affecting the near-surface water and energy dynamics of field-scale barriers are reviewed in Section 2. Section 3 describes the theory governing the soil-vegetation-atmosphere-transfer scheme. Section 4 describes the steps for compilation and execution of the code while Section 5 discusses the input file structure. Seven verification problems ranging from the verification of infiltration to evapotranspiration from a mixed grass canopy and finally an inter-code comparison to be used as a benchmark problem are described and analyzed in Section 6. Section 7 lists the references cited in the development of the code. Details on the input format notation are presented in Appendix A; input control format in Appendix B; example input files for verification problems and associated output files for the verification problems in Appendix C. Because of the size of the input and output files, Appendix C is included in electronic format on an accompanying compact disc.

2.0 Barrier Conceptual Model

Functional performance of engineered barriers can be expected to be influenced by several interactive and dynamic processes that control water balance (Ward and Gee 1997). Thus, the conceptual model of these structures must account for the both biotic and abiotic processes that influence the dynamics of water and energy in the system. Figure 2.1 illustrates the primary environmental interactions that govern performance of a typical vegetated barrier. The physical system is essentially a soil-vegetation-atmosphere continuum in which the flow of mass and energy may be multidimensional. Water impacting the surface can evaporate, be diverted as runoff from the surface, or enter the soil surface as infiltration. Infiltrating water can be stored in the fine soil layers until it is removed by evaporation or plant uptake, or it can redistribute deeper in the system. Redistribution may result in water moving downward into the native sediments or being diverted laterally. Thus, successful performance requires that most of the precipitation (P) be stored in the upper soil layers until it can be recycled to the atmosphere by evaporation (E) from bare surfaces and by evapotranspiration (ET) from vegetated surfaces. Alternatively, water may be diverted via lateral drainage, D_L.

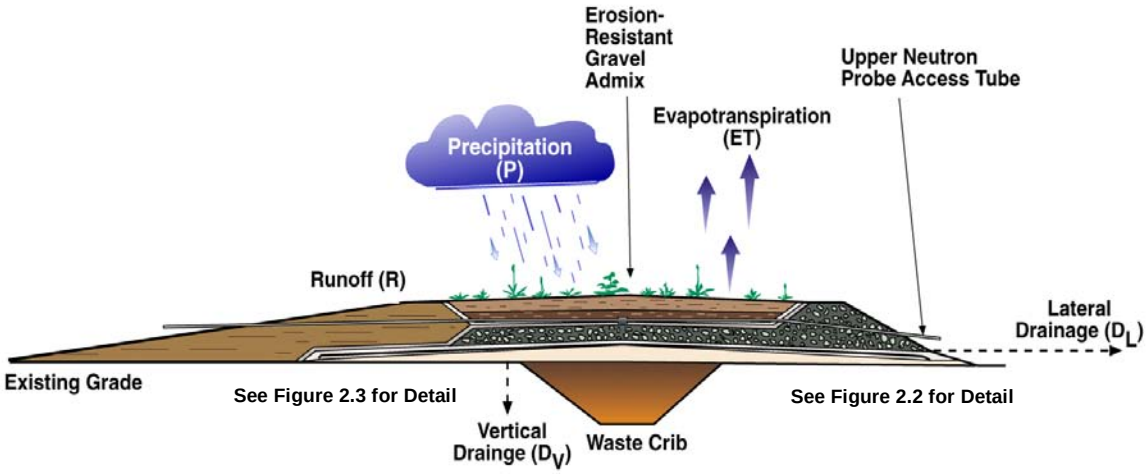

Figure 2.1. Primary Environmental Interactions Governing Functional Performance of a Typical 1000-Year Multilayer, Vegetated, Capillary Barrier (after Ward et al. 1997)

If the storage capacity of the fine soil layer is adequate, and there is sufficient ET or D_L to remove the stored water, percolation or vertical drainage (D_V) into the underlying waste can be virtually eliminated. Most of the reported failures of surface covers not tied directly to consolidation or collapse have been attributed to problems caused by the impact of D_L on slope stability and underflow. Where ever an above-grade cover is planned or exists, there is a potential risk of failure from mechanisms such as differential settlement, subsidence, water, and wind erosion, but more importantly, from elevated water infiltration along the edges with the potential for slope failure and underflow.

A potential complication with above-grade barriers is therefore the need to understand the effects of protective side slopes on performance, which can only be accomplished by a multidimensional model.

Protective side slopes form an integral part of above-grade covers and may occupy as much as 70 percent of the footprint (Figure 2.2 and Figure 2.3).

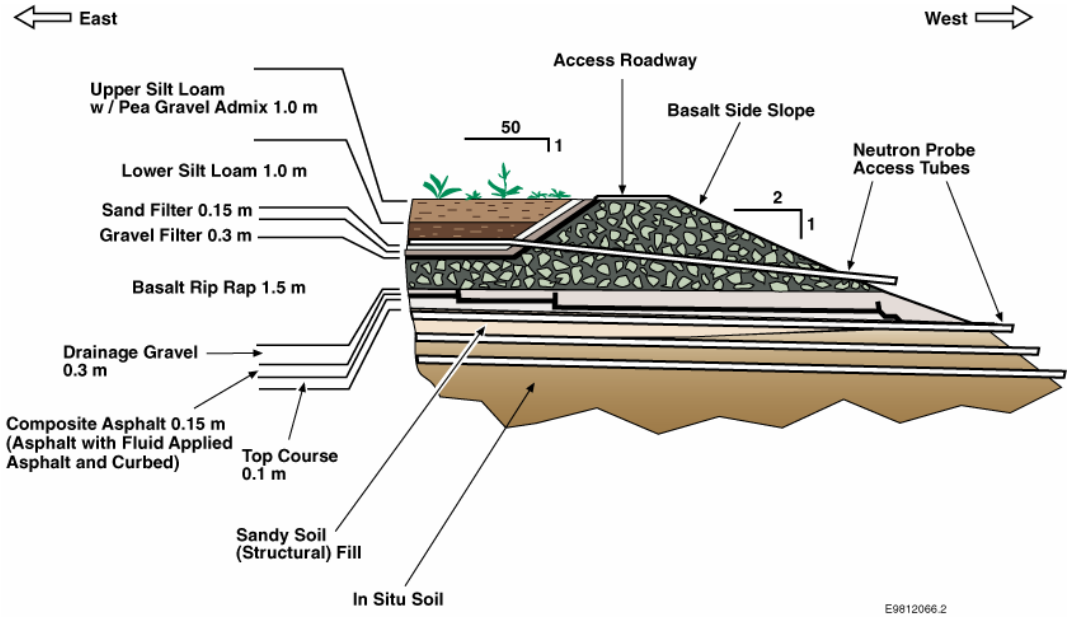

Figure 2.2. Hanford Prototype Surface Barrier Cross Section, Basalt Riprap Side Slope

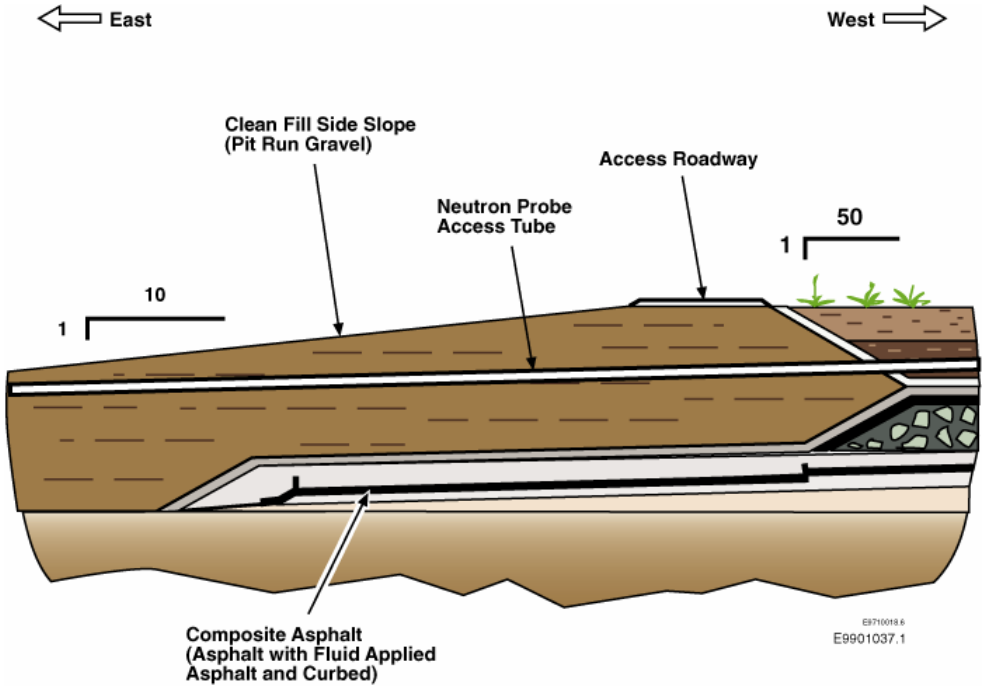

Figure 2.3. Hanford Prototype Surface Barrier Cross Section, Gravel Side Slope

However, there is essentially no design standard or practice for side-slope construction and little or no data on long-term side-slope stability and hydrologic performance needed to support barrier design and

model development (Ward et al. 2005a). Protective side slopes, which are typically constructed of coarse materials, can be quite steep and may drain most of the natural precipitation. This water can move under the barrier as underflow and potentially come in contact with and remobilize buried waste protected by the barrier itself. Underflow is a key factor to be considered when barrier design as the extent of barrier overhang affects how closely barriers can be placed next to each other. A need therefore exists for the ability to 1) assess the possible failure modes, 2) assess current technologies, and 3) evaluate innovative methods that could protect side slopes from failure. Possible options for reducing the risk of side-slope failure include terracing, water harvesting with plants, and air convective embankments. While difficult to study at the field scale, these concepts could be easily evaluated with the appropriate model.

2.1 Water Balance

Developing a conceptual model for an engineered cover, influenced by coupled and dynamic processes controlling the flow of energy and mass, is best formulated on the concept of the water balance. A water balance is an expression of how precipitation is partitioned after it reaches the land surface or bare covers or the top of the vegetative canopy on vegetated covers. The relative contribution of each component of the water balance is strongly influenced by the energy balance, and together, these two relationships dictate the dynamics of water movement as well as the vegetative patterns that persist on an engineered cover. A simplified water budget for an engineered cover may be written as follows:

$$P + I = R + \Delta W + D + G_D + E + T \tag{2.1}$$

where
- P = natural precipitation
- I = irrigation
- R = overland flow
- D = drainage out of the soil cover (diverted by reduced-permeability layer)
- G_D = ground water recharge (deep percolation past a reduced-permeability layer)
- ΔW = change in soil water storage
- E = Evaporation
- T = transpiration.

Precipitation is the total amount of water incident on the site and includes water in both the liquid and solid phases. Irrigation, which is sometimes used in the establishment of the plant cover or in performance testing to evaluate performance of a cover in response to precipitation stresses, is treated as a separate component (Ward et al. 1997). Overland flow includes both surface runoff, through which water is lost from the surface, thereby constituting a negative term in the water balance, and run-on, which may deliver water onto the surface and thereby constitutes a positive term. Water that does not run off the surface can be recycled to the atmosphere by evaporation from the soil or plant surfaces, or it infiltrates into the soil profile. The amount of water that must be stored in the fine-soil layers of a candidate barrier depends on the interactions of precipitation, temperature, vegetation, and albedo changes, and can therefore be expected to be quite variable from season to season. The design storage capacity is therefore controlled by a combination of the accepted flux of contaminants out of the waste zone and the maximum precipitation amounts expected during the life of the barrier. The components of the water balance and their contribution to barrier performance are described in the following sections.

2.1.1 Precipitation

Precipitation occurring at the site of an engineered barrier includes all natural sources of moisture that may reach the surface in the form of rain, snow, sleet, hail, etc. The deposition of dew is a common meteorological phenomenon that has been recognized as an important ecosystem element, especially in arid areas. Thus, in arid ecosystems, precipitation can also be in the form of dew and fog. Precipitation at Hanford ranges from less than 7.6 cm to 31.3 cm with an average about 18 cm since 1946 (Hoitink et al. 1999). Most of the precipitation occurs in the winter months with an average of 60 percent of the annual total occurring between October and February. Snow typically accounts for 22 percent of the annual precipitation and 37 percent of the winter total. There is a pronounced mid-summer dry season in most years (Stone at al. 1983). An important consideration in the assessment of barrier performance is therefore the effect of natural seasonal climatic variation in precipitation at the site of interest.

In addition to the low annual rates, precipitation in eastern and south-central Washington can be quite variable. Over 59 years of climatic data for south-central Washington shows that annual precipitation ranged from 91.3 mm to 348.5 mm, a difference of nearly 400 percent, which could lead to significant variation in the soil water storage (Kremer et al. 1996). Compared to estimates resulting from global climate change models, these differences are quite large. Mean global precipitation change estimates range from +15 percent, due to increased atmospheric moisture (Mitchell 1989), to -21 percent, due to increased surface albedo that may decrease convective activity (Rowntree 1988). Thus, the predicted variation in soil water storage and availability resulting from climatic changes will be equally variable. Yet, the potential impact of climate change may be quite small when compared to the natural, inter-annual variation in precipitation. Candidate barriers should be capable of handling these extremes in water-storage requirements without failing. More importantly, a barrier design tool should be capable of handling short-term episodic precipitation events as well as longer-term inter-annual variations.

Not all precipitation reaching the barrier is available for infiltration. Some precipitation may be intercepted by the plant canopy, from which it is evaporated or transpired without ever contacting the soil. In areas where snow is a significant component of the total precipitation, sublimation, the direct conversion of water from the solid phase to the vapor phase, can remove substantial amounts of water from the water budget.

In addition, the presence of a snow cover may delay infiltration, reduce evaporation rates, and in the event of rapid snowmelt, lead to surface runoff. In the current version of STOMP-WAE-B, winter precipitation falling as snow is treated as an equivalent rainfall amount. This water may then infiltrate or pond on the surface until there exists conditions conducive to infiltration. Dew, fog, and water condensing on plant surfaces is referred to as condensate and is allowed to fall to the soil surface after a maximum accumulation depth is exceeded on plant leaves.

For model simulations, precipitation data are available from the Hanford Meteorological Station (HMS) and include hourly measurements dating back to the 1950s. The National Climatic Data Center for Prosser, Washington, which is approximately 30 km north-west of Hanford, has daily climate records dating back to 1931. A utility has been developed for converting hourly weather data to the correct format for input into STOMP-WAE-B. This utility can generate input files with hourly data, with daily, weekly, or monthly averages. Precipitation data are treated as hourly rainfall intensities (L_a) for input into the model.

2.1.2 Irrigation

In the water balance equation, irrigation is used to account for artificial sources of water that may impact the barrier's surface. Irrigation water is sometimes used during construction as a dust control agent and post construction to support the establishment of vegetation. On the 200-BP-1 prototype barrier, for example, the northern half of the barrier was irrigated a rate of three times the long-time average precipitation during the 3-year treatability test with a simulated 1000-year return storm occurring in late March of each year (Ward et al. 1997; DOE-RL 1999). In STOMP-WAE-B, irrigation water is also subject to evaporation from soil and plant surfaces with the remainder becoming available for runoff or infiltration. Water may also condense on plant surfaces and ultimately fall to the ground once the maximum storage depth in the canopy is exceeded. The net precipitation reaching the surface is calculated as the sum of the natural precipitation and irrigation. Irrigation data are treated as hourly irrigation intensities (I_a) and are combined with hourly rainfall intensities (L_a) for input into the model.

2.1.3 Surface Runoff

In a real system, precipitation at a rate in excess of the hydraulic conductivity for the local soil conditions will result the accumulation of water caused by microtopography of the soil surface. If the ponding height is exceeded, surface runoff may occur because of variable surface topography or large scale surface slope. Surface runoff can only be simulated with a multidimensional model, and it is partly because of this requirement that many of the existing models are unable to accurately describe this process. Nevertheless, a well constructed, vegetated cover can be expected to have excellent infiltration capacity and may offer little opportunity for surface buildup and runoff. In such systems, surface runoff would be uncommon except in cases of saturated and/or frozen surface soils or a matted organic matter layer. Extensive testing at the 200-BP-1 prototype barrier, including three simulated 1000-year return storm events, showed only two runoff events. One runoff event occurred shortly after construction of the barrier and before it was vegetated. This event was likely caused by high rainfall intensity that caused slaking and the formation of a surface seal with reduced permeability (Ward et al. 1997; DOE-RL 1999). The second event occurred after warm winds induced a rapid snowmelt on frozen soil of reduced permeability (Ward et al. 1997; DOE-RL 1999). In the current version of STOMP-WAE-B, water can accumulate on the surface when the precipitation rate exceeds the infiltration rate. Under these conditions, the surface boundary will automatically change to a specified or falling head. However, no runoff is allowed in the current version. Run-on, the flow of water over the surface onto the barrier, is not considered in the current conceptual model as most covers are expected to be above grade.

2.1.4 Infiltration

Infiltration is not explicitly defined in the water balance equation but is an important process that affects water balance. Infiltration is the process of water entry into soil and generally follows precipitation events if the appropriate conditions exist. Unlike many of the existing models that simplify infiltration as a multistage process described by algebraic equations, STOMP-WAE-B calculates infiltration based on the capability of the soil profile to transmit water away from the surface. Under unsaturated conditions, this rate is a function of the matric potential gradient, the saturation, and the relative permeability. In multilayered barriers, particularly those with contrasting textures, infiltrating water can accumulate at the contacts of fine over coarse sequences in response to differences in the effective permeability between the layers (Fayer 2000). The difference in effective permeability between a fine-textured layer and an underlying coarse-textured layer at a given pressure head is the fundamental basis of the capillary barrier concept. As water accumulates at the interface, saturation increases in the fine layer, and water may

move laterally in multidimensional systems, provided there is a slope to the interface. The functionality of capillary barriers is therefore dependent on two coupled processes: (1) the exclusion of infiltration from the coarse layer and (2) the down dip diversion of infiltration above the fine/coarse contact (Oldenburg and Pruess 1993). Water that has infiltrated the soil can be stored or lost to drainage and deep percolation or recharge.

2.1.5 Water Storage

Soil water storage, W, is the amount of water in the soil profile at a given time, *t*. This water is available for evaporation, transpiration by plants, or drainage out of the root zone. Soil water storage is calculated from measurements of volumetric soil water content, θ, over some depth, L, by integrating a θ depth profile. The change in storage, ΔW, is calculated as the difference in W measured at different times. At any given time, W between the surface and depth L is calculated as follows:

$$W = \int_0^L \theta(z)dz \approx L_1\theta_1 + \sum_{i=1}^{n-1} L_{i+1}\frac{(\theta_i - \theta_{i+1})}{2} \tag{2.2}$$

where L = total depth of characterization (thickness of fine soil layer)
θ_1 = volumetric soil water content at the first measurement point
L_1 = distance from surface to first measurement point
n = number of measurement points
θ_I = volumetric soil water content at the i^{th} depth in the profile
L_i = distance between successive measurement points.

In general, W can be expected to increase in the winter months when most of the precipitation occurs as evapotranspiration losses are minimal because of dormant plants. Over time, changes in water storage will occur in response to lateral drainage, D_L, deep percolation or drainage, or evapotranspiration (Figure 2.1). The change in water storage is simply the average volumetric water content of the soil multiplied by the depth of the soil. Any water that is not recycled to the atmosphere by evapotranspiration may leave the root after which it can be diverted to the edge of the barrier, along a low-permeability layer in some barrier designs, or continue deeper into the soil profile, eventually becoming groundwater recharge.

2.2 Drainage

A primary role of protective barriers is to minimize percolation to buried waste by limiting drainage out of the root zone. Water infiltrating beyond the depth of evaporation of vegetation-free covers and beyond the root zone of vegetated covers is typically diverted down dip, towards the edge of the barrier (Figure 2.1). Water that drains below the root zone has little chance of being recycled to the atmosphere by plants. Thus, in monofill barriers and barriers without diversion or low-permeability layers, water exiting the root zone will continue to redistribute down towards the water table, i.e., deep percolation (G), and could come in contact with buried contaminants. Any water leaving the root zone is therefore considered to be drainage in the water balance of Equation (2.1). In covers that include a diversion layer or a low-permeability layer, this water is diverted laterally towards the edge of the barrier (Figure 2.1). Water reaching the edge of the barrier may move under the edge as underflow. Thus, an important component of barrier evaluation is the analysis of underflow and the determination of the amount of overhang that is required to keep wastes isolated. In strongly anisotropic soils, the minimization of underflow becomes

very important and requires optimization of the amount of overhang, i.e., the distance between the edge of the protective region of the barrier and the underlying waste.

Water moves because of potential gradients from regions of high potential to regions of low potential. In porous media, the total potential is defined as the sum of the contributions from the gravity potential, matric potential, the pneumatic potential, the osmotic potential, and the overburden potential (Philip and Smiles 1969). Temperature gradients are also indirect driving forces for water movement because at constant water content, the matric potential is affected by temperature (Philip and de Vries 1957). Temperature also influences the pneumatic, osmotic, and overburden potentials as well as the hydraulic conductivity. In the simplest conceptual model of a contaminant-free isothermal system, the energy state of water is described by the sum of the gravitational and matric potentials. Water continually redistributes from areas of high hydraulic potential to areas of low hydraulic potential, regardless of direction. However, in more complex conceptual models in which the system is non-isothermal, the flux of water vapor is included in the redistribution and drainage calculations. Water vapor moves in response to vapor-pressure gradients, which can arise from matric and osmotic potential gradients in the liquid phase and from temperature gradients within the soil. STOMP-WAE-B is a fully coupled, enthalpy-based code (White and Ward 2005). A major difference between the conceptual model on which STOMP-WAE-B is based is that STOMP addresses convective and radiative heat flow processes between the soil and atmosphere, convective transport of latent heat associated with condensation and evaporation, and radiative heat transfer within the soil profile. Most of the models that are routinely used for barrier design and performance model are based on loosely coupled processes.

2.2.1 Groundwater Recharge

Water not recycled by evapotranspiration may continue to move through the barrier. In multilayered systems with a sloping drainage layer, some of this water may move laterally (interflow) to be discharged at or near the edges of the barrier. Any remaining water may continue to percolate deeper into the soil, eventually exiting at the base, especially if there is no low permeability layer. This body of water may eventually reach the saturated zone and replenish or recharge the groundwater. The recharge area can potentially include the entire footprint of the barrier as deep percolation may occur from water moving vertically through the barrier or from interflow that is discharged at the edge of the barrier or from side slopes. The recharge rate from a candidate barrier is an important characteristic as water moving towards the water table can potentially mobilize contaminants. Understanding the recharge process and the conditions under which it occurs is therefore of critical importance to evaluating barrier performance.

In general, only a few millimeters of water will move beyond the root zone of vegetated semi-arid and arid ecosystems each year. Potential evapotranspiration (PET) typically exceeds precipitation and actual evapotranspiration is generally equal to precipitation (West 1983; Gee and Hillel 1988). Therefore, most of the water stored in the soil will eventually be evaporated or transpired. High PET and fine-textured silt loam soils with relatively high water holding capacity combine to limit recharge. Nevertheless, recharge in these ecosystems can be quite variable. On the Hanford Site, the mean recharge rate has been reported to range from 50 to 100 mm yr^{-1}, on bare surfaces, to less than 0.1 mm yr^{-1} on surfaces vegetated with native shrubs (Figure 2.4). We should therefore be capable of simulating flow in multiple-sloped layers of contrasting properties, including those with low permeability. Processes, such as convective and radiative heat flow, thermal convection of air driven by buoyancy forces arising from soil-air density gradients, and barometric pumping, all of which can contribute to reduce the amount of water draining through side slopes, are also important processes to be considered.

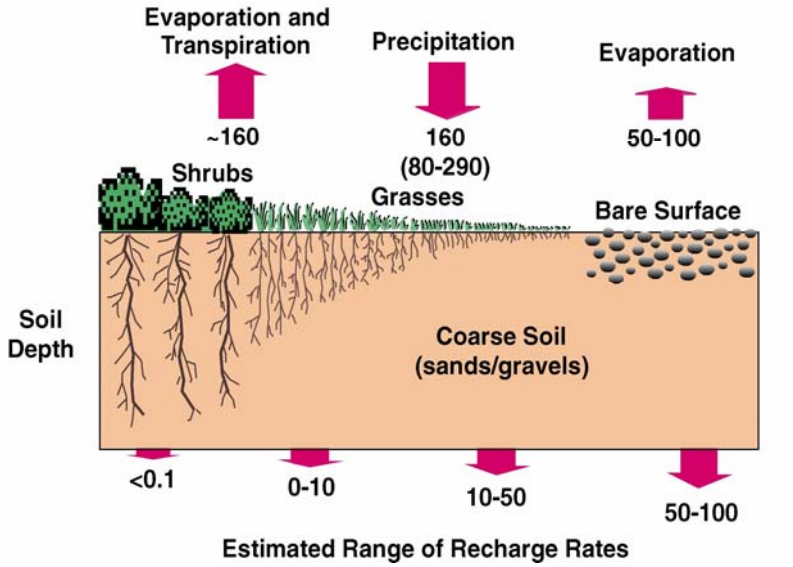

Figure 2.4. Schematic Representation of Hanford Site Water Balance Showing Variable Recharge Rates

2.2.2 Evapotranspiration

ET includes all the processes that convert water from the aqueous phase into water in the gaseous phase, i.e., water vapor. In the current conceptual model, ET is composed of bare soil evaporation, canopy evaporation, and transpiration. These components are typically difficult to measure and as a result, the total evapotranspiration is sometimes measured (Wilcox et al. 2003). Total ET may be determined directly from the energy budget (Evett 1999). Perhaps the most common approach for determining ET for engineered barriers is indirectly from the water balance equation. When the inputs, storage, and drainage losses are known, ET can be determined from Equation (2.1) as the difference between the inputs, losses, and storage (Ward and Gee 1997; Ward et al. 2005a, 2005b). However, this approach is susceptible to error because of uncertainty in the measured components. In the current conceptual model, water loss via ET is partitioned into evaporation from soil and plant surfaces and plant transpiration, i.e.,

$$ET = C + E + T \tag{2.3}$$

where C is canopy interception, E is the evaporation from bare soil and crop canopy, and T is transpiration. These components can all vary with soil properties and structure of the plant canopy. The components of evapotranspiration considered in the current conceptual model are discussed below.

2.2.3 Canopy Interception

Canopy interception is the process by which precipitation falling on vegetative surfaces, i.e., the plant canopy, collects on these surfaces. Intercepted water may be absorbed by plant surfaces, evaporated from these surfaces, or eventually dripped to the ground surface after the interception capacity is exceeded. Water that avoids interception completely or is intercepted and then drips off the canopy is known as throughflow. Intercepted water can also flow along stems and branches, becoming known as stemflow.

Canopy interception can constitute a significant portion of the incident precipitation in certain types of canopies (Calder 1977), especially in arid ecosystems. There is a strong relationship between interception of rainfall and rainfall intensity.

In general, interception is highest under low rainfall intensities and under misty, drizzle-like conditions. Conversely, interception is generally small under intense precipitation conditions (Bultot et al. 1972; Wells and Blake 1972). Very few studies have addressed the interception of precipitation in rangelands and shrub steppe ecosystems of semi-arid and arid areas (West and Gifford 1976). Interception rates in shrub steppe ecosystems are often assumed to be minor because the vegetation canopies are typically small, and total ground cover is often less than 50 percent. However, on a percentage basis, these regions lose considerably more water via interception than more humid environments (Dunkerly 2000). For example, interception losses from rangelands may range from 1 to 80 percent of the annual water budget, although they are generally between 20 and 40 percent (Wilcox et al. 2003). Average losses from sagebrush (*Artemisia* sp.) in these ecosystems have been reported at around 30 percent. In grass-dominated systems, interception loss may exceed that of shrubs, especially if the plant area index is high. In general, plant canopy characteristics control the magnitude of interception loss with the maximum being determined by the interception capacity. Because evaporation of intercepted water can have a significant impact on the energy and water balance of engineered covers, it is an important component of the water and energy balance and is included in the conceptual model on which STOMP-WAE-B is based.

2.2.4 Evaporation

Evaporation is defined as the process by which liquid water is transformed into a gaseous state and the subsequent transfer of this vapor to the atmosphere. Significant soil evaporation can take place only when the top few millimeters of soil are wet while canopy evaporation requires wet plant surfaces. Once the soil surface is dry, evaporation decreases sharply. Thus, significant evaporation occurs after rain or irrigation. Furthermore, as the growing season progresses, and canopy cover increases, evaporation from the wet soil surface gradually decreases. When the crop reaches full cover, as much as 95 percent of water loss may be caused by transpiration and evaporation from the crop canopy where most of the solar radiation is intercepted. Two types of evaporation are important to understanding the soil-vegetation-atmosphere transfer of water and energy (1) potential evaporation and (2) actual evaporation.

Potential evaporation is the amount of water that could be evaporated were it freely available. It is sometimes referred to as “wet-surface evaporation” and is the evaporation governed by available energy and atmospheric conditions. It is a function of surface and air temperatures, insulation, and wind speed, all of which affect water-vapor concentrations immediately above the evaporating surface. In general, potential evaporation in arid ecosystems is quite high and often exceeding precipitation. Actual evaporation is the quantity of water evaporated from an evaporating surface. Actual evaporation is equal to potential evaporation only when the evaporating surface is saturated. Evaporation can only occur when water is available, and it requires the humidity of the atmosphere be less than that of the evaporating surface. Evaporation involves three processes: (1) a flow of energy to the evaporating surface, (2) a flow of liquid to these surfaces, and (3) a flow of vapor away from these surfaces. Significant evaporation takes place only when the evaporating surface (soil or plant) is wet. Thus, evaporation rates are highest after precipitation events, especially those that resulted in canopy interception. Evaporation requires large amounts of energy. For example, the evaporation of one gram of water requires 600 calories of heat energy; the process is powered by the withdrawal of sensible heat from the air.

Evaporation of free water from soil pores involves two main physical processes: (1) molecular diffusion from the water surface to the land surface to the land surface level, defined as the humidity roughness height and (2) laminar and turbulent exchanges from the land surface to the atmosphere. Exchanges between the surface and the atmosphere are controlled by the aerodynamic or atmospheric boundary-layer resistance, which is controlled by the drag coefficient and the wind speed. Significant evaporation from soil surfaces can occur only when the soil is wet, and there is a vapor pressure gradient. Once the soil surface is dry, evaporation decreases sharply. Thus, significant evaporation occurs after rain or irrigation. Furthermore, as the growing season progresses and canopy cover increases, evaporation from the wet soil surface gradually decreases. When the crop reaches full cover, approximately 95 percent of ET is caused by transpiration and evaporation from the crop canopy where most of the solar radiation is intercepted. Prevailing weather conditions, available water in the soil, plant species, and growth stage influence crop water use and therefore evaporation.

Evaporation from wet vegetated surfaces depends on the amount of water that has accumulated on the leaves and stems following precipitation events. The evaporation rate is determined by the amount of energy available, i.e., the solar radiation that is intercepted, the relative humidity of the air, and the vapor pressure of the air above the evaporating surface. For evaporation to occur, the vapor pressure of the free water in or on plants must be greater than the vapor pressure of water in the air. Evaporation ceases when the saturation vapor pressure is reached (relative humidity=100%), unless there is a gradient in vapor pressure from the plant surface to the air; air of lower vapor pressure is moving over the plant in a breeze or wind to produce turbulent transport. In other words, no evaporation will take place when the air is saturated. There must be either a gradient in vapor pressure from the soil or plant surface into the air, or air of lesser vapor pressure must be moving over the soil or plant in a breeze or wind to produce turbulent transport. Air flow over the plant surface removes water molecules from above the evaporating surface, thereby maintaining a vapor pressure gradient.

This complex interaction of processes and the difficulty in estimating the evaporative depth required by models in which water flow and heat transport are only loosely coupled makes simulation of evaporation from soil a challenging task. In most of the existing models, the evaporative depth is an arbitrary input parameter that can be changed at will to dictate barrier performance. In the development of the current conceptual model, mass and energy transfer are tightly coupled, and the evaporative depth, which is essentially the lower boundary of the dry soil layer formed during the drying process, is determined implicitly. In this unique approach, the evaporative depth is determined by balancing the water and energy fluxes as the SVAT process proceeds. The current conceptual model includes evaporation from soil and plant surfaces. Evaporation from these surfaces reduces the amount of water available for infiltration and subsequent transpiration. An interception capacity is defined as a function of rainfall intensity; therefore, evaporation from plant surfaces can be predicted as a function of rainfall intensity.

2.2.5 Transpiration

Transpiration is the loss of water from plants through their stomata to the atmosphere. Water loss is caused by diffusion of water vapor from the open stomata to the atmosphere. Stomata are small openings found on the underside of leaves that are connected to vascular plant tissues. The opening of stomata is a necessary function to allow the exchange CO_2 and O_2 with the atmosphere. One of the most important factors affecting water demand is solar radiation. As energy input increases, the demand for water increases. Whether or not there is water available in the soil, the plant will demand water. In most plants,

transpiration is a passive process controlled by the humidity of the atmospheric and the moisture content of the soil. To avoid desiccation, the plant compensates for transpiration losses by taking up water from the soil. In dry ecosystems, many plants have developed the capability to open and close their stomata to control water loss and the capability to take up water held at very high matric potentials. These adaptations limit the loss of water from plant tissues, and without them, plants would have a difficult time surviving the conditions typical of arid and semi-arid ecosystems.

Of the water taken up by plants, over 95 percent is returned to the atmosphere through their stomata. Transpiration also transports nutrients from the soil into the roots and carries them to the various cells of the plant and is used to keep tissues from becoming overheated. Of the transpired water passing through a plant, only about 1 percent is used in the actual growth process. As with evaporation, there are two types of transpiration important to understanding the soil-vegetation-atmosphere transfer of water and energy: (1) potential transpiration and (2) actual transpiration.

Potential transpiration is the water loss by a plant (or vegetated surface) when soil water is not limiting. It is usually determined empirically for a plant or vegetation type and referenced to evaporation from a class-A evaporation pan. It is not uncommon for the potential transpiration to exceed pan evaporation, especially in arid environments. The potential transpiration rate depends on the leaf area and the evaporative demand of the atmosphere. The evaporative demand is controlled by incoming solar radiation and its partitioning into sensible and latent heat fluxes, vapor pressure deficit, and wind speed. Over the years, a number of approaches have been developed to calculate potential transpiration (Penman 1948; Monteith 1965). Most of these methods were developed for crop plants growing under non-limiting water supply and well developed canopies. However, neither of these conditions is typical of the shrub steppe ecosystems typical of the arid western United States. These ecosystems are characterized by sparse canopies (plant spacing ≥ plant height) with mostly limited water supplies, thereby requiring different approaches for calculating potential transpiration. Actual transpiration is the water limited transpiration rate, and the ratio between actual and potential transpiration is indicative of the extent to which the plant suffers from water stress. In general, actual transpiration increases as temperature increases as long as there is water for plants to transpire. The amount of transpiration therefore depends on the available soil water, which is controlled by soil hydraulic properties, and atmospheric demand, which is controlled by climatic conditions.

In the current conceptual model, both full vegetation canopies and sparse vegetation canopies are considered. Actual transpiration is determined by the atmospheric demand and is controlled by climatic conditions. If incoming solar radiation is less than a specified amount and air temperature is less than a specified minimum, both the actual transpiration and the transfer of vapor from the canopy ceases. However, evaporating water may still be intercepted by the canopy. Potential evaporation and potential transpiration are partitioned according to the fraction of soil cover or a plant area index. The actual transpiration is related to potential transpiration through root water uptake reductions caused by water stress.

2.3 Thermal-Energy Balance

In the current conceptual model, the plant canopy regulates the exchanges of mass, energy, and momentum in the soil-vegetation-atmosphere continuum. The canopy dominates the energy balance through its effect on soil and plant albedo, momentum and thermal roughness, and ultimately the water balance. The interplay between the plant canopy and the energy and water balance is predominantly

through the control exerted by the areal distribution of vegetation on the partitioning of incoming solar energy into sensible and latent heat fluxes. Because the plant canopy controls the partitioning of energy and the microclimate of the cover, the conceptual model for an engineered cover must also consider the energy balance.

In the generalized energy balance, the net solar radiation, R_s^n, is the available thermal energy from which the net change in energy storage within the canopy, *S*, is subtracted (Samson and Lemeur 2001). Canopy storage *S* can be further subdivided into five terms (McCaughey and Saxton 1988) including soil heat storage, S_g; sensible heat storage in the canopy air, S_a; latent heat storage in the canopy air, S_w; biomass heat storage, S_v; and photosynthetic energy storage, S_p. Soil heat storage, S_g, can be further subdivided in the measured soil heat flux at depth *z*, *G*; and the soil heat storage to that depth, $S_g(z)$. In most studies, S is simplified to G, while the other terms are considered to be negligible (Shuttleworth 1994). In the sparse canopied shrub steppe ecosystems of the arid western United States, the latter simplification is not unreasonable. Sometimes *S* may be defined simply as a fraction of R_s^n; sometimes, one or more components of *S* are also assumed to be negligible. The most commonly ignored storage component, perhaps because of the difficulty of determination, is the photosynthetic energy storage S_p (Samson and Lemeur 2001). The surface energy balance is determined by the different fluxes of thermal energy at the ground surface. The relative contribution of each component of the energy balance is strongly influenced by the water balance, and together, these two relationships dictate the overall performance of the cover. A simple energy balance for a vegetated surface may be written as follows:

$$R_s^n + G = \lambda E + H \tag{2.4}$$

where R_s^n = net solar radiation
λE = latent heat flux equivalent to evapotranspiration
H = sensible heat flux
G = soil heat flux.

The exchange processes are governed by different temperatures and vapor pressure conditions in the soil and atmosphere. All fluxes are assumed to positive when directed away from the ground surface and negative when directed toward the surface.

2.3.1 Net Solar Radiation

A surface receiving solar radiation can disperse energy in different ways. Part of the incoming solar radiation is absorbed by the Earth's surface, water vapor, gases, and aerosols in the atmosphere as well as by the canopy. Another part is reflected by the Earth's surface, by clouds, by the atmosphere, and by the canopy. Energy that is absorbed by the Earth-atmosphere system is re-emitted as long-wave radiation with fluxes in the downward (from clouds and gases) and upward directions. Absorbed energy raises the Earth's temperature while emitted radiation lowers the temperature. After summing the absorbed solar radiant energy (a positive value by convention), the outgoing surface thermal irradiance (a negative value by convention) and the downward thermal irradiance (a positive value by convention), the result is the net solar radiation, R_s^n. This is the available thermal energy from which the net change in energy storage within the canopy is subtracted. This energy is a key driver for heating the atmosphere, plant canopy, and

soil. Because the soil warms up as the result of solar heating, a temperature gradient develops between the surface and subsurface sediments and the atmosphere above. The resulting temperature gradient determines the direction of flow of energy. The net radiation is partitioned into turbulent fluxes of heat and water vapor.

2.3.2 Sensible-Heat Flux

Sensible heat flux, H, is that which is used to change the soil temperature, and it flows down the temperature gradient resulting from differences in temperature between the soil, vegetative surfaces, and the atmosphere, induced by solar heating. The sensible heat flux therefore includes the heat flux as energy flows upwards from the ground surface into the air, by conduction, and by convection. In STOMP-WAE, the sensible heat flux also includes heat flux carried by water in the vapor phase, a quantity that is typically ignored in other models. Because H is a turbulent flux driven by the temperature-gradient, it depends on the direction of the temperature gradient between the ground surface and the air as well as the wind speed and the degree of turbulence. The stronger turbulence, the greater the flow of heat. In STOMP-WAE, the sensible-heat flux is considered positive when heat is transferred upward from the subsurface across the surface boundary and negative when heat is transferred downward into the soil. When warm air flows over a cold surface, H is therefore negative as sensible heat flows from the air into the ground. Conversely, cold air flowing over a warm surface would result in a positive H as sensible heat flows from the ground to the air. During the day, the soil surface heats up, and the temperature gradient causes heat to flow from the ground to the air. At night, as the soil surface cools, the temperature gradient is reversed, and sensible heat flows downward toward the soil surface, producing a negative H because of cooling of the ground surface.

2.3.3 Latent-Heat Flux

Some of the radiant energy serves to evaporate liquid water from the soil and plant surfaces, and the water vapor flux is typically expressed as the latent heat flux. The latent-heat flux, which is given by λE, is composed of the rate of evaporation of water (or ice), E, and the latent heat of condensation, λ. The latent-heat flux is therefore the flow of latent thermal energy that occurs when water evaporates from the ground surface or condenses onto the surface. Recall that the ground surface cools in response to evaporation and warms up in response to condensation. In general, λE is quite large over open water; it can also be large over wet soil and is significantly affected by evapotranspiration. The flux of water vapor is driven by vertical changes in the water vapor concentration as opposed to the sensible heat fluxes that are driven by temperature gradients. Moisture gradients in the atmosphere are expressed in units of specific humidity or vapor pressure. In principle, water vapor can flow down the vapor gradient and therefore, on occasion, towards the soil surface. However, the water content of the soil surface does not increase directly because of the downward flux of water vapor, nor does dew form directly as the result of downward latent-heat flux. Dew forms when air cools below the saturation temperature as the result of long-wave emission to space. Nevertheless, both the downward movement of vapor and the formation of dew are considered in the conceptual model. Vapor or dew can condense on plant surfaces and ultimately drip to the ground. The ratio of sensible heat flux to latent heat flux is also an important parameter in micrometeorology known as the *Bowen ratio*. In STOMP-WAE, the latent-heat flux is considered positive when vapor is transferred upward to the atmosphere and negative when the transfer is downward.

2.3.4 Soil-Heat Flux

The soil-heat flux, *G*, represents energy moving upward to the surface from the deeper soil layers or downward through the soil surface. Rapid increases in surface temperature, for example in the morning, cause a downward flux of energy as heat flows towards the cooler, deeper layers. Conversely, with the decrease in surface temperature at night, the deeper soil layers will be relatively warm, and energy will flow upwards to the surface. The extent of the subsurface temperature change depends on the heat capacity of the subsurface porous media. In practice, *G* may be determined from measurements of the soil temperature profile, provided the soil thermal properties are known. The soil heat flux can also be estimated from remote sensing measurements. One simplified approach defines the ratio of the soil flux to net solar radiation in terms of vegetative cover, which, in turn, may be determined from visible and near infrared measurements (Clothier et al. 1986; Kustas and Daughtry 1990). In simulations of barrier performance, soil heat flux is predicted as a function of moisture from the soil temperature gradients, soil thermal properties, and the flux of vapor. In STOMP-WAE, the flux of energy down through the soil gives rise to negative soil-heat flux while an upward flux energy gives rise to a positive soil-heat flux. During the daytime, a negative soil-heat flux results from surface heating whereas at night, the soil-heat flux is positive as energy moves upward toward the cooler soil surface.

2.4 Wind and Turbulent Transport

The surface energy balance of an engineered cover is determined by the different fluxes of heat energy at the surface. Estimates of sensible and latent heat fluxes from the soil surface to the atmosphere are therefore critical for water and energy balance in soil-vegetation-atmosphere-transfer schemes and hydrologic models (Reifsnyder 1988; Driese and Reiners 1997). These fluxes are driven mostly by wind turbulence, which in turn is controlled by the nature of roughness elements. The surface of the barrier will be “rough” at multiple scales because of the roughness associated with soil particles to grass and shrubs protruding into the air. As the wind flows over the surface and other obstacles, it produces turbulence on a horizontal scale similar to that of the obstacle. Air close to these obstacles, or close to a bare surface, is slowed down because of the turbulence. Air in contact with the surface or protruding obstacles has virtually zero velocity (Rosenburg 1974). Knowledge of the shape of the wind speed profile above the surface is therefore a requirement for quantifying the effects of turbulent transport, which influences the water and energy balance, and for predicting wind speed at unmeasured elevations.

2.4.1 The Wind Speed Profile

The shape of a typical wind profile within and above a canopy of height, H, is shown in Figure 2.5. Above the canopy (Region II, or external boundary layer), wind speed, *u*, increases exponentially with elevation. With increasing depth into the canopy (Region I, internal boundary layer), wind speed decreases exponentially with elevation, eventually becoming zero at the surface (Rosenburg 1974). In a system with densely packed roughness elements, the tops of the roughness elements act like a displaced surface. To retain the logarithmic form of the wind profile in neutral conditions, the concept of the zero plane displacement height, *d*, is introduced. Thus, projection of the Region II curve to a displaced surface where $u = 0$ yields an intercept given by $z_0 + d$. The parameter z_0 is known as the roughness parameter, or aerodynamic roughness length, and *d* is the zero plane displacement.

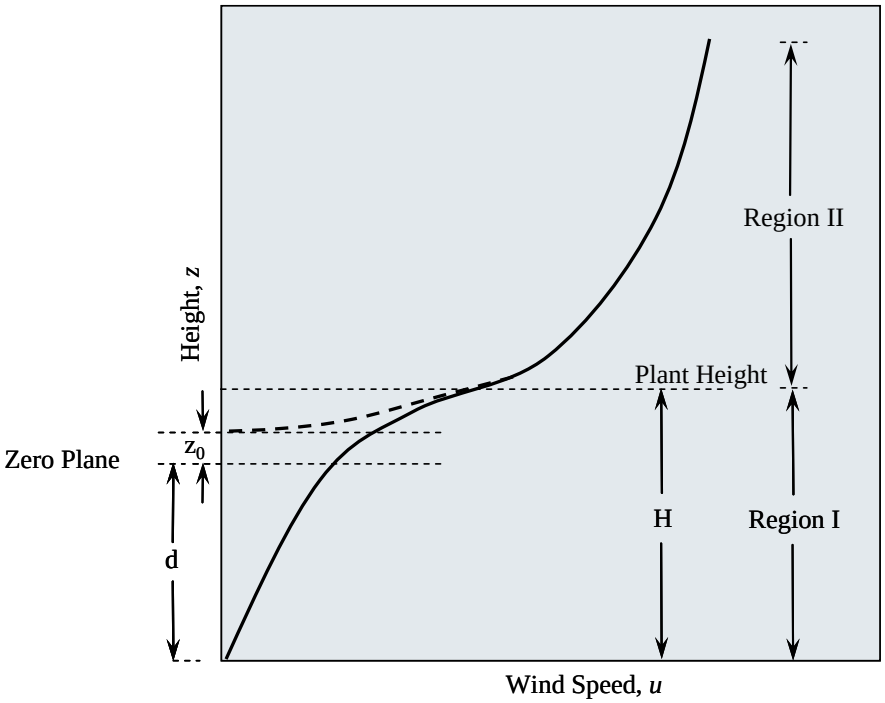

Figure 2.5. Schematic Representation of Wind Speed Distribution Within and Above a Plant Canopy (after Rosenburg 1974)

The aerodynamic roughness length, z_0, is essentially a surface length scale defined by the logarithmic wind speed profile under neutral conditions where the wind speed equals zero at the height $z = z_0$. This theoretical height must be determined from the wind-speed profile, but once determined for a particular surface, it remains invariant with wind speed, stability, stress, and time of day (Sun 1999). However, as the density of roughness elements increases (because of canopy closure on vegetated surfaces), drag increases, and so does the value of the roughness length. At some intermediate density where z_0 is relatively large, flow will cease to enter the inter-element spaces and become a skimming flow. Further increases in the density of roughness elements could possibly decrease drag and the roughness length. In general, the aerodynamic roughness length is near zero over very smooth surfaces and increases with the height of roughness elements. Values of 0.001 to 0.01 m been reported for bare soil; on surfaces with short crops or grass (e.g., height of a typical lawn), values of 0.001 to 0.003 m have been reported but increase to 0.04 to 0.1 m in tall grass (Monteith and Unsworth 1990). The aerodynamic roughness length appears to be related to shrub structure, as expressed by the dominant species, and shrub density. A range of 0.012 to 0.028 m with an average z_0/H ratio of 0.04 was reported for sagebrush sites in Wyoming (Driese and Reiners 1997). Ward and Keller (2005) provide a summary of z_0 values useful for simulations of barrier performance.

The zero plane displacement, *d*, is nothing more than a conceptual tool used to force the wind profile over rough surfaces to conform to the exponential relation between *u* and height *z* so that certain mathematical parameters may be determined. It represents the height above which active turbulent exchange first commences (Rosenburg 1974). At elevations less than *d*, turbulent exchange is essentially non existent, and transport is primarily by molecular diffusion. A number of relationships have been developed to allow estimation of z_0 and *d* as functions of plant height on vegetated surfaces (Szeicz et al. 1969; Stanhill

1969). However, most of these relationships were developed for tall canopies. The shrub steppe canopies typical of engineered barriers in the arid west, on the other hand, are considered sparse as the plant spacing is typically larger than the plant height. More importantly, values of z_0 and d estimated from measurements on crop plants will not be applicable to surface barriers vegetated with native plant species. In one of the few published studies of aerodynamic roughness parameters for shrub steppe ecosystems, Driese and Reiners (1997) reported that identical or similar solutions for z0 were obtained when d was fixed at 0.0 m as when it was allowed to vary between 0 and plant height. This suggests that the actual d may be in fact close to zero. This is consistent with the findings of Garratt et al. (1993) who suggested that in extremely sparsely placed roughness elements, the ground surface is the true reference plane, and d should be close to zero. Given the sparse canopies common in shrub steppe ecosystems and engineered covers, values of d close to ground level are not unreasonable. The aerodynamic roughness parameters offer the greatest flexibility for minimizing differences between observed and predicted evaporation and ultimately in the water balance. Thus, in the current conceptual model, the two aerodynamic roughness parameters, z_0 and d, can be adjusted to optimize predictions of evapotranspiration and ultimately the water balance. However, there are insufficient data to allow adequate estimation of aerodynamic roughness parameters for Hanford conditions (Ward et al. 1997). Ward et al. (2005b) provide a summary, based on literature values, that can be used in the simulation of barrier performance onsite.

2.5 Coupling the Soil-Vegetation-Atmosphere-Transfer Scheme to STOMP

In the context of the water balance and energy balance and the component processes, the need for a coupled soil-vegetation-atmosphere-transfer scheme is readily apparent. Such a scheme is required to simultaneously represent the atmospheric and hydrological processes that control plant water uptake and ultimately barrier performance. In the coupled model, the plant canopy regulates the exchanges of mass, energy, and momentum in the soil-vegetation-atmosphere continuum. It dominates hydrological processes through modification of interception, infiltration, and surface runoff. Its influence on the energy balance is through its effect on surface albedo, roughness, and ultimately evapotranspiration. The areal distribution of vegetation controls the partitioning of incoming solar energy into sensible and latent heat fluxes and consequently temporal changes in vegetative cover, which result in changes to the microclimate and barrier response.

In the SVAT scheme, the model solves coupled sets of nonlinear conservation equations for water mass, air mass, and thermal energy at the ground surface, plant leaves, and canopy. The conservation equations mathematically describe the transport of water, air, and thermal energy across the ground surface, either directly or through plants. The governing conservation equations that are solved depend on whether the ground surface is bare or vegetated and whether the temperatures of different plant species are distinguished. In the current conceptual model, vegetative growth is not implicit but is handled explicitly through temporal changes in plant parameters, such as leaf area index, plant height, maximum root depth, albedo, and crop coefficient as functions of the plant phenophase. This information is then used to partition energy between plant canopy and soil as well as in the parameterization of turbulent transport and evapotranspiration. The surface boundary condition is based on the approach of Shuttleworth and Wallace (1985) that was developed for sparse canopies. This approach considers soil and vegetation as two different sources of latent and sensible heat fluxes with the incoming solar energy being partitioned between bare soil and vegetation through a screen factor.

Solution of the nonlinear conservation equations for water mass, air mass, and thermal energy requires specification of soil thermal and hydraulic properties and plant parameters. The equations are parameterized according to rock/soil type and implicitly describe the transfer of heat as well as water in the aqueous and vapor phases within the soil and through the canopy. At the upper boundary, the equations for the coupled SVAT scheme are numerically solved for surface temperature, soil volumetric moisture, aqueous pressure, and vapor pressure. The atmospheric component of the SVAT scheme is driven by meteorological forcing parameters including precipitation, solar radiation, air temperature, relative humidity, and wind speed. Nonlinearities in the solved governing equations are resolved via Newton-Raphson iteration. The subsurface equations are coupled to the surface evapotranspiration equations as a boundary condition, whose effects impact deeper subsurface nodes through plant roots. The temporal and spatial behavior of these processes is represented in the STOMP simulator.

The STOMP simulator is a scientific tool for analyzing single and multi-fluid subsurface flow and transport. A description of the simulator's governing equations, constitutive functions, and numerical solution algorithms are provided in the STOMP theory guide (White and Oostrom 2000). The general use of the simulator, input file formatting, compilation, and execution are described in a companion user's guide (White and Oostrom 2003). The STOMP simulator uses numerical derivatives, which requires that the nonlinear boundary condition system be resolved four times (i.e., one plus the number of field domain unknowns) for each boundary surface and Newton-Raphson iteration of the subsurface domain. The next section describes the theory behind the soil-vegetation-atmosphere-transfer scheme of the Water-Air-Energy-Barrier mode of STOMP known as STOMP-WAE-B.

3.0 Model Theory

The sparse vegetation evapotranspiration model of STOMP-WAE-B comprises three options: 1) *bare surface*, 2) *single plant temperature*, and 3) *multiple plant temperature*. The option is user defined with selection occurring during development of the conceptual model. The bare surface option is ideally suited to bare surfaces (e.g., lysimeters) and newly constructed covers before revegetation. It is also applicable to previously vegetated covers following a catastrophic event like a wild fire. The *single plant temperature* option is ideal for simulation of sparse canopies, single-storied ecosystems, or mono-cropped systems. The *multiple-plant-temperature* option, however, would be ideal for simulation of forested or multi-plant ecosystems with a well developed multi-storied canopy.

The *bare-surface* option considers water, air, and energy exchange between the atmosphere and subsurface without plants. Conservation equations for water mass, air mass, and thermal energy are solved at the ground surface. The air-mass conservation equation is implicit, yielding a two-equation system for water mass and thermal energy. The *single-plant-temperature* option considers water, air, and thermal energy exchange between the atmosphere and subsurface, assuming a single temperature at the plant leaves and mean canopy height (canopy), and a single water-vapor density at the canopy. This option requires the solution of five coupled nonlinear equations: water mass and thermal energy at the ground surface, thermal energy at the plant leaves, and water mass and thermal energy at the canopy. All equations are expressed in steady-flow form unless rainfall and condensate interception are considered; in this case, the implicit water mass balance equation on the plant leaves is converted to a transient form (i.e., to include water storage on the plant leaves).

The *multiple-plant-temperature* option also considers water, air, and energy exchange between the atmosphere and subsurface. However, it assumes a unique temperature as well as water-vapor density at the plant leaves and canopy for each plant species. This option requires the solution of two plus three times the number of plant species coupled nonlinear equations: water mass and thermal energy at the ground surface; thermal energy at the plant leaves for each plant species; and water mass and thermal energy at the canopy for each plant species. The rainfall and condensate interception option is additionally possible with the multiple-plant-temperature option. The difference in canopy temperatures is typically small for sparse canopies. Owing to the computational burden added to the overall solution scheme by the multiple-plant-temperature option, the single-plant-temperature option is generally recommended for typical arid site conditions.

3.1 Bare Surface Option

The *bare-surface* option is invoked whenever plants are absent, and the surface boundary is specified as bare. To resolve the bare surface boundary system, two coupled conservation equations are resolved: 1) water mass and 2) thermal energy. The primary unknowns for these two equations are the surface temperature and aqueous pressure. The choice of the aqueous pressure is somewhat arbitrary, as the water-vapor partial pressure or water-vapor density could also have been chosen. The gas pressure at the surface is assumed to equal the atmospheric pressure.

3.1.1 Ground-Surface Water-Mass Balance

The water mass balance equation at the ground surface is a steady-flow expression, balancing the water flux from the subsurface to the ground surface with the water flux from the ground surface to the atmosphere. This balance of fluxes is described by:

$$E_{ns} + G_{ns}\left[\omega_g^w \rho_g\right]_{ns} + L_{ns}\left[\omega_l^w \rho_l\right]_{ns} = E_{sa} + G_{sa}\left[\omega_g^w \rho_g\right]_{sa} + L_{sa}\left[\omega_l^w \rho_l\right]_{sa} \tag{3.1}$$

where $-L_{sa}$ represents the rainfall intensity (m s^{-1}) on the ground surface, and interfacial values of the component densities are upwind averaged. The diffusive water-vapor flux between the subsurface node and ground surface is computed via the expression for binary diffusion in porous media

$$E_{ns} = \left[\tau_g n_D \rho_g s_g D_g^w\right]_{ns} \frac{\left(\omega_g^w\right)_n - \left(\omega_g^w\right)_s}{dz_{ns}} \tag{3.2}$$

where the interfacial values are determined by harmonic averaging. The advective gas and aqueous fluxes between the subsurface node and ground surface are computed via the expression for unsaturated Darcy flux

$$G_{ns} = \left[\frac{k_{rg}\mathbf{k}_z}{\mu_g}\right]_{ns} \left\{\frac{\left(P_g\right)_n - \left(P_g\right)_s - dz_{ns}\, g\left[\rho_g\right]_{ns}}{dz_{ns}}\right\} \tag{3.3}$$

$$L_{ns} = \left[\frac{k_{rl}\,\mathbf{k}_z}{\mu_l}\right]_{ns} \left\{\frac{\left(P_l\right)_n - \left(P_l\right)_s - dz_{ns}\; g\left[\rho_l\right]_{ns}}{dz_{ns}}\right\} \tag{3.4}$$

where the interfacial values of relative permeability are upwind averaged, and those for intrinsic permeability and viscosity are harmonically averaged.

The diffusive water-vapor flux between the ground surface and atmosphere is computed using an aerodynamic resistance (Figure 3.1). The diffusive water-vapor or latent flux between the ground surface and atmosphere is defined as

$$E_{sa} = \frac{\left(\rho_g^w\right)_s - \left(\rho_g^w\right)_a}{r_{sa}^a} \tag{3.5}$$

where the aerodynamic resistance, r_{sa}^a, between the ground surface and atmosphere is an averaged quantity for the boundary. Evaporation from the soil is assumed to take place at the soil surface or within soil pores directly adjacent to the soil surface and can occur from wet or dry surfaces.

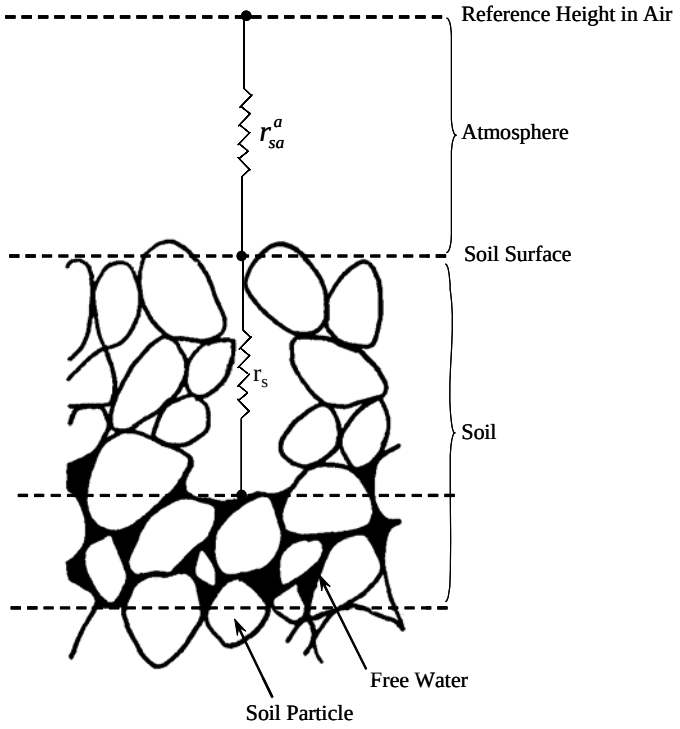

Figure 3.1. Schematic Illustration of Resistance Associated with Evaporation from a Bare Surface

3.1.1.1 Aerodynamic Resistance for Momentum Transfer

The aerodynamic resistance, r_{sa}^{a}, between the soil and canopy is entirely controlled by atmospheric properties, predominantly turbulent exchange (Hicks et al. 1987). Atmospheric turbulence itself depends on the sensible heat flux as well as the roughness length and the wind speed. Computing the aerodynamic resistance above a bare surface therefore requires knowledge of the wind speed profile or its parameters. As discussed in Section 2.3.1, under conditions of neutral or nearly neutral atmospheric stability, the relationship between wind speed and elevation can be described by a logarithmic function. The stability corrections in non-neutral flow can be neglected because in this analysis, the focus is on the lowest 1 m or so of the atmosphere. The wind speed profile from the measurement height to the ground surface is then calculated as

$$u = \frac{u^*}{\kappa} \ln\left(\frac{z + z_m}{z_m}\right) \tag{3.6}$$

where u^* is the friction velocity, and z_m is the roughness length. The friction velocity is a measure of the strength of the turbulent variations in wind speed and is computed from the wind speed at the measurement height, z_{ref}, as

$$u^* = \frac{u_{ref}\ \kappa}{\ln\left(\frac{z_{ref}+z_m}{z_m}\right)} \tag{3.7}$$

The parameter z_m is the roughness length associated with momentum transfer. For simplicity, stability effects are ignored, and the eddy diffusion coefficient describing heat and mass transport are assumed equal to those for momentum. Thus, the two diabatic correction factors for heat and momentum, both of which depend on atmospheric stability, can be neglected. Following Campbell (1985), the eddy diffusion coefficient is equal to some value, characterized by the roughness length, and increases linearly with the friction velocity and height such that

$$K = \kappa u^* \left(z + z_m\right) = \kappa\left[\frac{u_{ref}\ \kappa}{\ln\left(\frac{z_{ref}+z_m}{z_m}\right)}\right]\left(z + z_m\right) \tag{3.8}$$

The bare-surface aerodynamic resistance for heat and mass transport are determined by integrating the inverse of eddy diffusion coefficient over the height range from z_m to z_{ref}:

$$r_{sa}^a = \ln\left(\frac{z_{ref}+z_m}{2\cdot z_m}\right)\left(\frac{\ln\left(\frac{z_{ref}+z_m}{z_m}\right)}{\kappa^2 u_{ref}}\right) \tag{3.9}$$

A widely used estimate for the momentum surface roughness length, z_m, is 0.01 m (van Bavel and Hillel 1976), and this may be used in scoping calculations. However, z_m is known to vary with surface conditions, particularly soil texture, and in STOMP-WAE-B, z_m is an input parameter. To illustrate the effects of aerodynamic roughness on the bare-surface aerodynamic resistances, r_{sa}^a was calculated according to Equation (3.9) for different soil textures. For a reference height, z_{ref}, of 2.0 m, a reference wind speed, u_{ref}, of 2 m s^{-1}, and typical roughness lengths for bare soils (Monteith and Unsworth 1990), estimated r_{sa}^a, for sand (z_m=3·10^{-4} m), silt (z_m=1·10^{-5} m), and clay (z_m=1.4·10^{-7} m) were 223.2 s m^{-1}, 439.1 s m^{-1}, and 846.8 s m^{-1}, respectively. A bare surface under similar conditions but with a roughness length of 0.01 m gives a bare-surface aerodynamic resistance of only 76.4 s m^{-1}. The bare-surface aerodynamic resistance clearly increases as the aerodynamic roughness length (particle diameter) decreases. Thus, the effect of reduced roughness length is to restrict fluxes. Values of z_m for different surfaces relevant to the simulation of bare surfaces are summarized by Ward and Keller (2005).

3.1.2 Ground-Surface Thermal-Energy Balance

The thermal energy balance equation at the ground surface is a steady-flow expression, balancing the energy flux from the subsurface to the ground surface, plus the net short- and long-wave radiation into the ground surface with the energy from the ground surface to the atmosphere such that

$$R_s^n + R_s^{\ln} + E_{ns}\left[h_g^w\right]_{ns} + G_{ns}\left[\omega_g^w \rho_g h_g\right]_{ns} + L_{ns}\left[\omega_l^w \rho_l h_l\right]_{ns} + H_{ns} = E_{sa}\left[h_g^w\right]_{sa} + G_{sa}\left[\omega_g^w \rho_g h_g\right]_{sa} + L_{sa}\left[\omega_l^w \rho_l h_l\right]_{sa} + H_{sa} \tag{3.10}$$

In Equation 3.10, the energy fluxes comprise water-vapor diffusion, gas advection, aqueous advection, thermal conduction, gas convection, and thermal radiation components. All interfacial values of enthalpy are upwind averaged. With this approach, the thermal energy balance is defined entirely with an enthalpy approach, thus implicitly including the heats of evaporation and condensation. The contribution of aqueous dissolved-air is ignored.

To solve the two-equation bare surface system, the governing equations are expressed in residual form

$$\mathbf{R}_s^w = E_{ns} + G_{ns}\left[\omega_g^w \rho_g\right]_{ns} + L_{ns}\left[\omega_l^w \rho_l\right]_{ns} - E_{sa} - G_{sa}\left[\omega_g^w \rho_g\right]_{sa} - L_{sa}\left[\omega_l^w \rho_l\right]_{sa} \tag{3.11}$$

$$\mathbf{R}_s^e = R_s^n + E_{ns}\left[h_g^w\right]_{ns} + G_{ns}\left[\omega_g^w \rho_g h_g\right]_{ns} + L_{ns}\left[\omega_l^w \rho_l h_l\right]_{ns} + H_{ns} - E_{sa}\left[h_g^w\right]_{sa} - G_{sa}\left[\omega_g^w \rho_g h_g\right]_{sa} - L_{sa}\left[\omega_l^w \rho_l h_l\right]_{sa} - H_{sa} \tag{3.12}$$

and linearized using a two-variable Newton-Raphson iteration scheme

$$\begin{vmatrix} \dfrac{\partial \mathbf{R}_s^w}{\partial P_{l_s}} & \dfrac{\partial \mathbf{R}_s^w}{\partial T_s} \\ \dfrac{\partial \mathbf{R}_s^e}{\partial P_{l_s}} & \dfrac{\partial \mathbf{R}_s^e}{\partial T_s} \end{vmatrix} \begin{vmatrix} \Delta P_{l_s} \\ \Delta T_s \end{vmatrix} = \begin{vmatrix} -\mathbf{R}_s^w \\ -\mathbf{R}_s^e \end{vmatrix} \tag{3.13}$$

Convergence is achieved when

$$\frac{\Delta P_{l_S}}{P_{atm}} \le 10^{-7} \quad and \quad \frac{\Delta T_S}{T_{abs}} \le 10^{-7} \tag{3.14}$$

To stabilize the nonlinear solution, temperature corrections are limited to 1K, and aqueous pressure corrections are relaxed during saturated-unsaturated phase transitions at the ground surface, using a 0.6 relaxation factor. The components of the ground surface thermal energy balance are derived below.

The diffusive water-vapor, or latent heat, flux between the ground surface and atmosphere is computed using an aerodynamic resistance, r_a^{sa}. The latent heat flux between the ground surface and atmosphere is defined as

$$E_{sa} = \frac{\left(\rho_g^w\right)_s - \left(\rho_g^w\right)_a}{r_{sa}^a} \tag{3.15}$$

The water-vapor density at the surface is computed from the water-vapor partial pressure at the surface and temperature at the surface using the steam table formulations (ASME 1967). The water-vapor partial pressure at the surface is computed from the saturated water-vapor pressure and the capillary pressure at the surface as

$$\left(P_g^w\right)_s = \left(P_{sat}^w\right)_s \exp\left(\frac{\left(P_l\right)_s - \left(P_g\right)_s}{\left(\rho_l R_l T\right)_s}\right) \tag{3.16}$$

where the aqueous pressure and temperature are the primary unknowns for the bare-surface system of equations.

A major advantage of this approach for calculating the water vapor partial pressure at the ground surface is that it eliminates the need to calculate a surface resistance of the soil for water-vapor transport as required by Shuttleworth and Wallace (1985). The water-vapor density in the atmosphere is calculated from the atmospheric water-vapor partial pressure and temperature, using the steam table formulations (ASME 1967); where the atmospheric water-vapor partial pressure is computed from the atmospheric relative humidity and saturated water-vapor pressure

$$\left(P_g^w\right)_a = \left(P_{sat}^w \phi\right)_a \tag{3.17}$$

The advective gas flux from the surface, or ground heat flux, to the atmosphere is computed via an implicit air mass balance at the ground surface as

$$G_{sa} = \frac{G_{ns}\left[\omega_g^a \rho_g\right]_{ns}}{\left[\omega_g^a \rho_g\right]_{sa}} \tag{3.18}$$

The conductive heat flux from the subsurface to the ground surface is computed via Fick's law for conductive heat transfer

$$H_{ns} = \left[k_e\right]_{ns} \frac{T_n - T_s}{dz_{ns}} \tag{3.19}$$

where the interfacial value of effective thermal conductivity is a harmonic average. The conductive-convective heat flux (sensible heat flux) from the ground surface to the atmosphere is computed using the

turbulent transport formulations of Campbell (1985), while ignoring the differences among momentum, mass, and heat transport eddy diffusion coefficients, as

$$H_{sa} = \left(\frac{T_s - T_a}{r_{sa}^a} \right) \left[\rho_g c_{p_g} \right]_{sa} \tag{3.20}$$

where the interfacial value of the sensible thermal capacitance is harmonic averaged. Calculating the sensible heat flux requires the roughness length for heat, z_h. It is commonly assumed that the momentum roughness length, z_m, equals the z_h. This would suggest that there is no distinction between the temperature at the ground surface and the temperature at the height of the roughness length (Beljaars and Holtslag 1991). However, the analogy between the transport of momentum and other species (heat and water vapor) is not valid. This is because momentum transport not only involves viscous shear but also local pressure gradients, which are related to form drag on roughness elements, whereas the transport of other heat and vapor, especially close to the surface, can only take place by molecular diffusion (Duynkerke 1992). Like the wind speed profile, the temperature profile has been shown to vary logarithmically with height. Thus, an approach similar to that for calculating the aerodynamic resistance to momentum transfer is used.

3.1.2.1 Aerodynamic Resistance for Heat Transfer

In Equation (3.20), the aerodynamic resistance, r_{sa}^a, between the soil and canopy is entirely controlled by molecular diffusion. Computing the aerodynamic resistance above a bare surface therefore requires knowledge of the temperature profile or its parameters. As in Section 2.3.1, under conditions of neutral or nearly neutral atmospheric stability, the relationship between temperature and elevation can be described by a logarithmic function. The temperature profile from the measurement height to the ground surface is then calculated as

$$T_a - T_s = \left(\frac{-H_{sa}}{u^*} \right) \frac{1}{\kappa} \ln \left(\frac{z + z_h}{z_h} \right) \tag{3.21}$$

where u^* is the friction velocity, and z_h is the roughness length for heat transfer. Both experimental and theoretical studies have shown that there is a difference between the roughness length for heat and momentum (Garratt and Hicks 1973; Brutsaert 1979; Beljaars and Holtslag 1991). The difference is related to the additional resistance for heat exchange caused by molecular diffusion. Momentum is transferred to the surface by means of pressure forces on roughness elements from drag. However, heat and moisture are transferred towards the atmosphere by molecular diffusion. Data from homogeneous vegetated surfaces (grass, agricultural crops, and woodlands) suggest that $z_h \approx z_m/10$ (Garratt and Hicks 1973; Beljaars and Holtslag 1991). For sparse to very sparse vegetation cover, there are conceptual arguments for anticipating small values of z_h/z_m. To demonstrate this, Garrat et al. (1993) considered a hypothetical heated evaporating surface of variable roughness density but with the same z_m. For the same insulation and evaporation per unit roughness element, the temperature can be expected to be greater and z_m to be much smaller from the low density surface than on the high density surface. Beljaars and Holstag (1991) reported a ratio of $z_h \approx z_m/6.4 \cdot 10^3$ for sparse canopies.

To illustrate the effects of aerodynamic roughness on the bare-surface aerodynamic resistance, r_{sa}^{a} was calculated according to Equation (3.9) for different soil textures by replacing z_m with z_h. For a reference height, z_{ref}, of 2.0 m, a reference wind speed, u_{ref}, of 2 m s^{-1}, and a typical roughness length for bare soils (Monteith and Unsworth 1990), the estimated r_{sa}^{a} for sensible heat over sand (z_m=3·10^{-4} m), silt (z_m=1·10^{-5} m), and clay (z_m=1.4·10^{-7} m) were 926.5 s m^{-1}, 1.33·10^{3} s m^{-1}, and 1.99·10^{3} s m^{-1}, respectively. A bare surface under similar conditions but with a roughness length of 0.01 m gives a bare-surface aerodynamic resistance of 587.5 s m^{-1} compared to only 76.4 s m^{-1} for momentum transfer.

3.1.2.2 Net Radiation

The energy flux at the surface boundary is computed from weather observations of air temperature, wind speed, relative humidity, and solar radiation. The potential solar radiation is the radiation of an unobstructed or cloudless sky. The magnitude of the potential solar radiation depends on the position of the sun, i.e., the solar altitude or solar angle, during the day, the inclination of the solar rays within the earth's surface, the amount of radiation at the outer layer of the earth's atmosphere; the transmissivity of the sky, and the altitude of the earth's surface. During the day when the sun is above the horizon, all surface nodes are assumed to receive the same amount of radiation.

The net short-wave radiation into the ground surface includes short-wave (solar) and long-wave (thermal) components. Flerchinger (2000) further divided short-wave (solar) radiation into direct-beam and diffuse components, and considered exchanges between plant canopy layers and the ground surface. As the principal target application for this model is sparsely vegetated arid environments, the short-wave (solar) radiation is treated as a single component, including both direct-beam and indirect radiation. The net radiation into the ground surface can then be expressed in terms of upward and downward radiation fluxes

$$R_s^n = R_s^{sn} + R_s^{ln} = R_s^{sd} - R_s^{su} + R_s^{ld} - R_s^{lu} \tag{3.22}$$

The downward short-wave radiation at the ground surface is obtained as input from the atmospheric data. The upward short-wave radiation at the ground surface is the reflected downward radiation. Therefore, the net short-wave radiation into the ground surface is computed from the downward radiation and ground-surface albedo as

$$R_s^{sn} = \left(1-\alpha_s\right)R_s^{sd} \tag{3.23}$$

Computing net short-wave radiation therefore requires an estimate of albedo. In the *bare-surface* option, albedo, α_s, is essentially a measure of reflectivity or absorptivity of the bare surface. The higher the albedo of a surface, the less energy it absorbs, and the cooler a temperature it maintains. Ground-surface albedo is known to be a function of the solar altitude and aqueous water saturation, s_l, described as (Pleim and Xiu 1995)

$$\alpha_s = \alpha_z(\omega) + \alpha_g(s_l) \tag{3.24}$$

Pleim and Xiu (1995) defined $\alpha_z(\omega)$

$$\alpha_z(\omega) = 0.01[\exp(0.003286\,\omega^{1.5}) - 1] \tag{3.25}$$

Two approaches for calculating α_z were recently proposed by Wang et al. (2005), based on an analysis of remote sensing data. They showed that bare soil albedo, normalized to its value at a solar altitude $\omega=60^o$, could be adequately represented by the following function:

$$\alpha_z(\omega) = \alpha_r \cdot \{1 + B_1 \cdot [g_1(\omega) - g_1(60^o)] + B_2 \cdot [g_2(\omega) - g_2(60^o)]\} \tag{3.26}$$

where α_r is the albedo at $\omega=60^o$ and depends on season and location. The functions g_1 and g_2 are given by:

$$g_1(\omega) = -0.007574 - 0.070987\,\omega^2 + 0.307588\,\omega^3 \tag{3.27}$$

$$g_2(\omega) = -1.284909 - 0.166314\,\omega^2 + 0.04184\,\omega^3 \tag{3.28}$$

In Equations 3.27 and 3.28, $B_1 = 0.346$, and $B_2 = 0.063$. Wang et al. (2005) also reported a simpler formulation based on work by Briegleb et al. (1986), which may be written as follows:

$$\alpha_z(\omega) = \alpha_r \cdot \frac{1 + C}{1 + 2C \cdot \cos\omega} \tag{3.29}$$

where *C* is an empirical parameter with values of 0.4 for arable grass, grassland, and desert; and 0.1 for all other surfaces. Equations 3.10 and 3.13 were shown to describe α_z equally well, and both are offered as options in STOMP-WAE-B. A third option is that of constant albedo in which α_s is independent of texture, ω, or θ for the duration of the simulation. This value, which cannot be changed via the input file, is fixed at 0.25.

Soil albedo has also been shown to be a function of soil type, moisture content, and surface roughness (Dirmhirn and Belt 1971; Idso et al. 1975). In the current conceptual model, the effects of roughness are ignored. The relationship between α_s and aqueous saturation is best described by a decreasing exponential function given by

$$\alpha_s(s_l) = \alpha_{wet} + (\alpha_{dry} - \alpha_{wet}) \cdot \exp(-\kappa \cdot s_l) \tag{3.30}$$

where α_{wet} = soil albedo when the surface is near saturation (minimum albedo)
α_{dry} = dry soil albedo (maximum albedo)
κ = albedo attenuation factor that controls the rate of decrease albedo with moisture
θ = moisture content at the surface.

Literature values for wet and dry values of α as a function of texture have been reported by a number of authors (Idso et al. 1975; Post et al. 2000; Lobell and Asner 2002). Post et al. (2000) also showed that α_{wet}, α_{dry} can be predicted quite accurately from the Munsell color value component (R^2=0.93). Values of

κ have been reported by Muller and Décamp (2001). Appropriate parameter values for predicting α_s have been summarized by Ward and Keller (2005).

3.1.2.3 Long-wave Radiation

The downward long-wave radiation incident on the surface is given by Campbell (1985)

$$R_s^{ld} = \varepsilon_a^0 \left(1 - 0.84 c_a\right) \sigma T_a + 0.84 c_a \sigma T_a^4 \tag{3.31}$$

where the clear sky emissivity is an empirical factor that takes into account the difference between the atmospheric and clear-sky temperature. Calculating the downward long-wave radiation by Equation (3.15) requires the clear-sky emissivity and fractional cloud cover. Various equations have been developed for estimating clear-sky emissivity from air temperature and humidity. The method of Berdahl and Fromberg (1982) was chosen for its relatively low error and is expressed as

$$\varepsilon_a^0 = 0.741 + 0.0062 \left(T_{dp}\right)_a \tag{3.32}$$

The atmospheric dew-point temperature, T_{dp}, is determined via an iterative calculation using the air temperature, relative humidity, and saturated water-vapor pressure function. A fractional cloud in cover can be determined from insolation data for solar altitudes greater than 10°. For solar altitudes less than 10°, the last computed fractional cloud cover is used. Fractional cloud cover is measured at some meteorological stations like the HMS, but not at all. Thus, fractional cloud cover is computed from the equation proposed by Kasten and Czeplak (1980), as

$$c_a = 1.088 \left(1 - \frac{R_s^{sd}}{R_i^{sd}} \right)^{0.294} \tag{3.33}$$

where the incident clear sky solar radiation is obtained by multiplying the extraterrestrial solar radiation by the global transmissivity, using the formulation of Caroll (1985)

$$R_i^{sd} = \left(0.79 - \frac{3.75}{\theta} \right) I_o \tag{3.34}$$

where the solar altitude is computed as

$$\sin\left(\theta\right) = \sin\left(\delta\right)\sin\left(\phi_l\right) + \cos\left(\delta\right)\cos\left(\phi_l\right)\cos\left(\omega\right) \tag{3.35}$$

The solar declination, δ, is the annual fluctuation of the sun between the two tropics and varies between -23 and +23 degrees of latitude. Solar declination is computed according to an equation reported by Llasat and Snyder (1998), as

$$\begin{aligned} \sin\left(\delta\right) = &- 0.37726 - 0.10564\, j + 1.2458\, J^2 \\ &- 0.75478\, J^3 + 0.13627\, J^4 - 0.00572\, J^5 \end{aligned} \tag{3.36}$$

where J is the Julian day. In the solar altitude expression, Equation (3.19), the solar hour angle is the position or height of the sun above the horizon and therefore describes the movement of the sun around the earth in 24 hours. The solar-hour angle is computed as

$$\omega = 15\left(t - t_o\right) \tag{3.37}$$

Solar noon equals 0 with each additional hour equal to 15° of longitude per hour (360°/24 hr),with positive values in the mornings and negative values in the afternoons. In Equation (3.30), solar noon time is computed using longitude and equation-of-time corrections, as

$$t_o = 12 + \frac{15\left(L_l - L_m\right)}{60} - \frac{E_t}{60} \tag{3.38}$$

In Equation (3.31), the local meridians are separated by 15° (75° Eastern Time Zone; 90° Central Time Zone; 105° Mountain Time Zone; 120° Pacific Time Zone). This equation for time corrects for the eccentricity of the Earth's orbit around the sun and is expressed as (Llasat and Snyder 1998),

$$\begin{aligned} &\textit{for } J < 181 \\ E_t &= -0.04056 - 0.74503\,J + 0.08823\,J^2 + 2.0516\,J^3 \\ &\quad - 1.8111\,J^4 + 0.42832\,J^5 \\ &\textit{for } J > 180 \\ E_t &= -0.05039 - 0.33954\,J + 0.04084\,J^2 + 1.8928\,J^3 \\ &\quad - 1.7619\,J^4 + 0.4224\,J^5 \end{aligned} \tag{3.39}$$

The upward long-wave radiation is a combination of the reflected-downward and emitted radiation and is calculated as

$$R_s^{lu} = \left(1 - \varepsilon_s\right) R_s^{ld} + \varepsilon_s\,\sigma\,T_s^{\,4} \tag{3.40}$$

The emissivity of the ground surface, ε_s, is modeled as a function of aqueous saturation using the relationship of van Bavel and Hillel (1976)

$$\varepsilon_s = \min\left[0.9 + 0.18\left(n_D\,s_l\right)_s, 1.0\right] \tag{3.41}$$

3.2 Single-Plant-Temperature Configuration

Whenever plants are specified on the boundary surface, the *single-plant-temperature* option is invoked, unless the *multiple-plant-temperature* option is specified via the *Plant Card*. To resolve the single-plant-temperature boundary system, five coupled conservation equations are resolved: 1) water mass at the

ground surface, 2) thermal energy at the ground surface, 3) thermal energy at the plant leaves, 4) water mass at the canopy, and 5) thermal energy at the canopy. The primary unknowns for these five equations are the aqueous pressure and temperature at the ground surface, the plant leaf temperature, and the water-vapor partial pressure and temperature at the canopy. As with the bare-surface option, the gas pressure at the ground surface is assumed to equal the atmospheric pressure.

The presence of plants increases the aerodynamic roughness of the surface, thereby reducing energy available for momentum transfer at the soil surface and the convective exchanges of heat, water vapor, and trace gases between the soil and canopy. Plants therefore alter convective exchanges and near-surface (<0.05 m) wind speeds by absorbing kinetic energy and modifying aerodynamic roughness. These effects are typically quantified as a log-linear decrease in wind velocity relative to distance above the land surface. However, extending wind speed profile theory to sparse canopies requires estimates of the aerodynamic roughness parameters z_m and d_c for these conditions.

We hypothesize that momentum and thermal roughness parameters are proportional to the plant area index. Thus, a fundamental assumption of the sparse vegetation evapotranspiration model is therefore that plant canopies do not overlap and that the plant distributions can be described through a plant-species areal distribution or plant area index, P_a^i, for each species. The P_a^i is a widely used method to describe the amount of foliage when referring to all light blocking elements (stems, twigs, leaves) for that species. Simply put, it is the surface area footprint of a particular plant species per unit ground surface area. This is different from the more familiar leaf area index, L_a^i, which accounts for leaves only. Although P_a^i and L_a^i are dimensionless, they can be thought of as m^2 (one-sided) foliage per m^2 ground area. The plant area index describes the fraction of ground surface covered by a particular plant species as shown in Figure 3.2. For the typical environment of interest, the sparse canopy assumption is quite reasonable as water-limited shrub steppe ecosystems typically show sparse canopies, i.e., canopies in which plant spacing ≥ plant height. The summation of the plant area index over all plant species can not exceed 1.0, and the difference between 1.0 and this summation equals the exposed ground or the ground area index.

3.2.1 Ground-Surface Water-Mass Balance

The governing conservation equations are written with the simplifying assumption that the ground surface beneath the canopy of a particular plant species exchanges water mass and thermal energy with the atmosphere via the canopy nodal point, and that exposed ground surface exchanges water mass and thermal energy directly with atmosphere. Figure 3.3 shows a nodal network for the single-plant-temperature option.

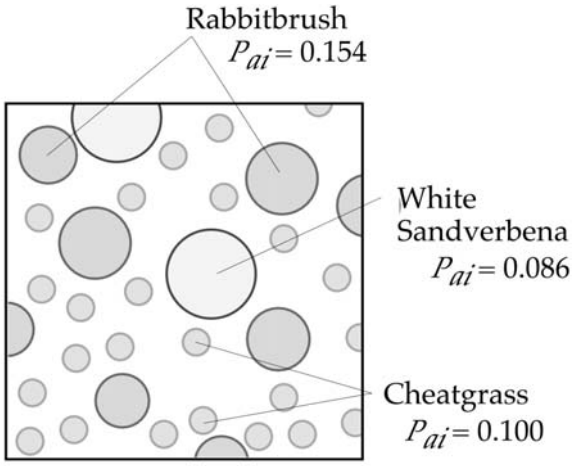

Figure 3.2. Plant Area Indices for Three Plant Species

The water mass balance equation at the ground surface is a steady-flow expression that balances the water flux from the subsurface to the ground surface with the water flux from the ground surface to the canopy or atmosphere. Thus,

$$E_{ns} + G_{ns}\left[\omega_g^w \rho_g\right]_{ns} + L_{ns}\left[\omega_l^w \rho_l\right]_{ns} = E_{sa} + G_{sa}\left[\omega_g^w \rho_g\right]_{sa} + L_{sa}\left[\omega_l^w \rho_l\right]_{sa} + E_{sc} + L_{sp}\left[\omega_l^w \rho_l\right]_{sp} \tag{3.42}$$

where $-L_{sa}$ represents the rainfall intensity on the ground surface, and $-L_{sp}$ represents the shed rainfall or condensate intensity from the plants on the ground surface. Shed rainfall or condensate is only possible when the *rainfall-interception* option is invoked, and the water stored on the plant leaves exceeds the storage capacitance, or maximum condensate depth. In Equation (3.33), the diffusive water-vapor flux, advective gas flux, and advective aqueous flux components of the water mass balance equation are identical to those given for the bare-surface system in Equations (3.2) through (3.4), respectively.

The diffusive water-vapor flux between the subsurface node and ground surface is computed via the expression for binary diffusion in porous media where the interfacial values are determined by harmonic averaging. The advective gas and aqueous fluxes between the subsurface node and ground surface are computed via the expression for unsaturated Darcy flux

$$E_{ns} = \left[\tau_g n_D \rho_g s_g D_g^w\right]_{ns} \frac{\left(\omega_g^w\right)_n - \left(\omega_g^w\right)_s}{dz_{ns}} \tag{3.43}$$

$$G_{ns} = \left[\frac{k_{rg}\mathbf{k}_z}{\mu_g}\right]_{ns} \left\{\frac{\left(P_g\right)_n - \left(P_g\right)_s - dz_{ns}\, g\left[\rho_g\right]_{ns}}{dz_{ns}}\right\} \tag{3.44}$$

$$L_{ns} = \left[\frac{k_{rl}\mathbf{k}_z}{\mu_l} \right]_{ns} \left\{ \frac{(P_l)_n - (P_l)_s - dz_{ns}\, g[\rho_l]_{ns}}{dz_{ns}} \right\} \tag{3.45}$$

where the interfacial values of relative permeability are upwind averaged and those for intrinsic permeability and viscosity are harmonically averaged.

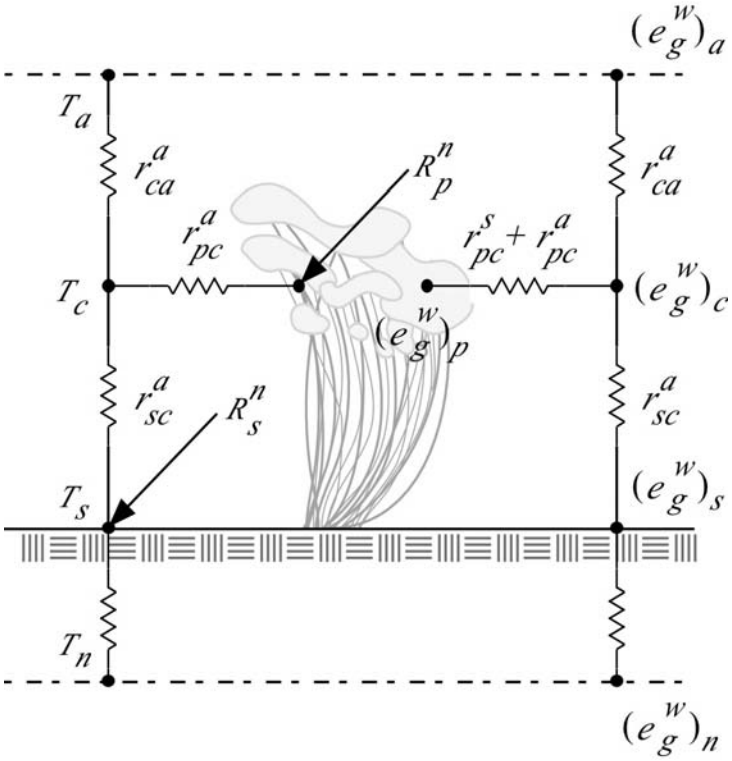

Figure 3.3. Nodal Network for the Single-Plant-Temperature System

The diffusive water-vapor flux between the ground surface and atmosphere, E_{sa}, is fundamentally the same as that for the bare-surface system except that it has been modified to take into account the exposed ground surface

$$E_{sa} = \frac{\left(\rho_g^w\right)_s - \left(\rho_g^w\right)_a}{r_{sa}^a} \left(1 - \sum_{i=1}^{n_{ps}} P_{ai}^i \right) \tag{3.46}$$

where the aerodynamic resistance is divided into two components, one for below and one for above the canopy, as shown in Figure 3.3.

The diffusive water-vapor flux between the ground surface and the canopy, E_{sc}, is computed for the ground surface beneath the plant canopy as

$$E_{sc} = \frac{\left(\rho_g^w\right)_s - \left(\rho_g^w\right)_c}{r_{sc}^a}\left(\sum_{i=1}^{n_{ps}} P_{ai}^i\right) \tag{3.47}$$

where the aerodynamic resistance between the ground surface and canopy is an averaged quantity for the boundary surface. Above the canopy, the eddy diffusion is assumed to vary linearly with elevation and friction velocity. Below the canopy, the eddy diffusion is assumed to decrease exponentially with height (Shuttleworth and Wallace 1985). Thus,

$$K_{ca} = \kappa u^* \left(z + z_0 - d_c\right) \tag{3.48}$$

$$K_{sc} = K_c \exp\left\{-2.5\left(1 - \frac{z}{h_c}\right)\right\} \tag{3.49}$$

$$K_c = \kappa u^* \left(h_c + z_0 - d_c\right) = \kappa\left[\frac{u_{ref}\,\kappa}{\ln\left(\frac{z_{ref} + z_0 - d_c}{z_0}\right)}\right]\left(h_c + z_0 - d_c\right) \tag{3.50}$$

where the eddy diffusion at the canopy is computed from the above-canopy eddy diffusion expression, Equation (3.44), at the canopy height.

A number of relationships have been developed to allow estimation of z_0 and d_c based on micrometeorological measurements. For example, Szeicz et al. (1969) summarized a number of studies and derived a log linear relationship between z_0 and canopy height, h_c

$$\log z_0 = 0.997 \log h_c - 0.883 \tag{3.51}$$

A companion estimate for d_c is that of Stanhill (1969) relating d_c to h_c, which for vegetated surfaces is written as

$$\log d_c = 0.979 \log h_c - 0.154 \tag{3.52}$$

More common approximations of z_0 and d_c are those of (Monteith 1973), written as

$$z_0 = 0.13\, h_c \tag{3.53}$$

$$d_c = 0.63\, h_c \tag{3.54}$$

While these relations can be used to bound values of z_0 and d_c in the absence of site specific data, it is worth noting that none of the measurements on which these relations are based were made over the

vegetation typical of engineered covers in arid and semi arid environments. In fact, these were mostly derives for tall, relatively well developed canopies. The problem of estimating z_0 and d_c is compounded by the fact that plants typically adjust to the mechanical force of the wind (Rosenburg 1974). Shrub steppe canopies, on the other hand, are considered sparse as the plant spacing is typically larger than the plant height. Thus, values estimated under one set of conditions for a specific canopy may not be applicable to another set of conditions or species. More importantly, values of z_0 and d_c estimated from measurements on crop plants will not be applicable to surface barriers vegetated with native plant species.

3.2.1.1 Aerodynamic Resistance for Momentum Transfer

The canopy-atmosphere aerodynamic resistances are simply defined as the ratio of the differential in the quantities being fluxed to the flux itself; e.g., for the latent heat flux, E_{sa}, which is driven by a vapor density gradient between two points, the resistance is defined simply as $\Delta\rho_g^w \cdot E_{sa}^{-1}$. The ground surface to atmosphere aerodynamic resistance is determined by integrating the inverse of the eddy diffusion coefficient over the height range from z_m to z_{ref}, giving rise to Equation (3.50). Above the canopy, the eddy diffusion coefficient is assumed to vary linearly with elevation and friction velocity; and below the canopy, the eddy diffusion is assumed to decrease exponentially with height following Shuttleworth and Wallace (1985). Using the assumptions of Equations (3.36) through (3.38), (3.41), and (3.42), the ground-canopy and canopy-atmosphere resistances can be determined by integrating the inverse of the eddy diffusion coefficient over the height ranges from 0 to $d_c + z_{0m}$ and $d_c + z_{0m}$ to z_{ref}, respectively:

$$r_{sc}^a = \left(\frac{0.4h_c}{K_c}\right)\left\{\frac{1}{\exp(-2.5)} - \frac{1}{\exp\left(-2.5\left(\frac{h_c - d_c - z_{0m}}{h_c}\right)\right)}\right\} \tag{3.55}$$

$$r_{ca}^a = \left\{\ln\left(\frac{z_{ref} + z_{0m} - d_c}{z_{0m}}\right)\right\}\left\{\frac{\ln\left(\frac{z_{ref} + z_{0m} - d_c}{2z_0}\right)}{\kappa^2 u_{ref}}\right\} \tag{3.56}$$

where the 2.5 parameter in Equation (3.55) was determined by Monteith (1973) for agricultural crops. For a reference height, z_{ref}, of 2.0 m, a reference wind speed, u_{ref}, of 2 m s^{-1}, and a plant height, h_c, of 0.3 m, Equations (3.55) and (3.56) give a ground-canopy aerodynamic resistance, r_{sc}^a, of 99.7 s m^{-1} and a canopy-atmosphere aerodynamic resistance, r_{ca}^a, of 38.2 s m^{-1}. In contrast, for a bare-surface with a roughness length of 0.01 m, Equation (3.9) gives a bare-surface aerodynamic resistance, r_{sa}^a, of 76.4 s m^{-1}. The effect of roughness as a consequence of plant height is less straightforward than in the bare surface option. Increasing h_c causes a decrease in r_{ca}^a, which would result in an increase in the ground-canopy flux. Increasing h_c initially causes an increase in r_{sc}^a, which would lead to a decrease in the canopy-atmosphere flux.

The plant-canopy aerodynamic resistance, r_{pc}^{a}, is computed following the approach of Stannard (1993)

$$r_{pc}^{a} = \frac{0.7\, W_p^{l}\, \rho_g\, c_{p_g}}{k_g\, Nu} \tag{3.57}$$

In Equation (3.57), *Nu* is the Nusselt number, the ratio of total heat transfer to convective heat transfer. The Nusselt number is a measure of the enhancement of heat transfer from a surface that occurs in a "real" situation, compared to the heat transfer by conduction only. Typically, it is used to measure the enhancement of heat transfer when convection takes place. The Nusselt number is defined as:

$$Nu = (2/3) Re^{1/2}\, Pr^{1/3} \tag{3.58}$$

where *Re* and *Pr* are the Reynolds and Prandtl numbers, respectively. The Reynolds number, the ratio of inertial forces to viscous forces, is used to determine whether flow is laminar or turbulent and is defined as:

$$Re = \frac{W_p^{l}\, u_c\, \rho_g}{\mu_g} \tag{3.59}$$

The Prandtl number is the ratio of momentum diffusivity to thermal diffusivity with the later being the ratio of thermal conductivity to heat capacity. The Prandtl number is defined as

$$Pr = \frac{\mu_g\, c_{p_g}}{k_g} \tag{3.60}$$

Calculating *Re* requires knowledge of the wind speed at the mean canopy flow height, u_c. This is determined from the wind velocity profile, assuming a mean canopy flow height, h_{cf}, as

$$u_c = \left(\frac{u^*}{\kappa}\right) \ln\left(\frac{h_{cf} + z_0 - d_c}{z_0}\right) = \left(\frac{u_{ref}}{\ln\left(\frac{z_{ref} + z_0 - d_c}{z_0}\right)}\right) \ln\left(\frac{h_{cf} + z_0 - d_c}{z_0}\right) \tag{3.61}$$

The mean canopy flow height, h_{cf}, is estimated as $0.5h_c$.

The final resistance required to calculate the diffusive water-vapor flux between the ground surface and atmosphere is the stomatal resistance, r_{pc}^{s}. The stomatal resistance is influenced by atmospheric turbulence intensities, climate, water availability, radiation intensity, temperature, and vapor pressure

deficit (Jarvis 1976). The resistance increases when the plant is water stressed, and the soil water availability limits evapotranspiration. There are two options for calculating the stomatal resistance. The first option assumes that r_{pc}^{s} is affected only by the net solar radiation, in which case r_{pc}^{s} is calculated simply as

$$r_{pc}^{s} = r_{pc,\min}^{s} \cdot f_T \tag{3.62}$$

where f_T is a correction factor and is calculated as follows:

$$f_T = \frac{400 + R_n^s}{1.4 \cdot R_n^s} \tag{3.63}$$

In Equation (3.62), $r_{pc,\min}^{s}$ is the minimum stomatal resistance (s m^{-1}) and is fixed for all plant species at 50 s m^{-1}. The second option assumes that r_{pc}^{s} varies with time of day because of the effects described by Jarvis (1976). Values of r_{pc}^{s} are then calculated using a simplification of the model of Hicks et al. (1987) written as

$$r_{pc}^{s} = r_{pc,\min}^{s} \cdot \left(1 + \beta \cdot I^{-1}\right) f_T{}^{-1} \tag{3.64}$$

where f_T is a factor that corrects for humidity, water stress, temperature, and diffusivity. The correction factor is calculated as follows:

$$f_T = \frac{(T - T_c)}{(T_0 - T_c)} \left[\frac{T_H - T}{T_H - T_0} \right]^{\left(\frac{T_H - T_0}{T_0 - T_c} \right)} \tag{3.65}$$

In Equations (3.64) and (3.65),

$r^s_{pc,\min}$ = minimum stomatal resistance (s m^{-1})
β = light response coefficient (Wm^{-2})
I = sunlight intensity (Wm^{-2})
f_T = correction factor accounting for closing of stomata outside a given temperature range
T ambient temperature (K)
T_C minimum temperature for stomatal opening (K)
T_H maximum temperature (K)
T_0 optimum temperature (K).

The parameters T_H and T_C are the species-dependent upper and lower temperature extremes at which stomata no longer open (typically 40°C and 5°C, respectively).

Hicks et al. (1987) also suggested a method for extending the elemental surface resistance, r^s_{pc}, to the entire canopy, while taking into account the impact of shading on the lower canopy. The stomatal resistance in the canopy of the i^{th} species is calculated by scaling r^s_{pc} according to the leaf area index regardless of the stomatal resistance model as:

$$R^i_{pc} = \frac{r^s_{pc}}{L^i_a} \tag{3.66}$$

The EPA has estimated stomatal resistance parameters for a variety of vegetation types as part of the deposition calculations for the Clean Air Status and Trends Network (CASTNET). Battye and Barrows (2004) recently summarized these parameters for "natural vegetation." Ward et al. summarized stomatal resistance parameters for plant species typical of the shrub steppe ecosystem that may be used on barriers. Using sagebrush in the month of March on the Hanford Site as an example, the input parameters are $r^s_{pc,\min}$ =100 s m^{-1}; β = 20 W m^{-2}; T_c=278.15 K; T_0 = 298.15 K; T_h = 318.15 K. In March, the average temperature is 280.59K while the solar radiation is 140.367 W m^{-2}. The calculated value of r^s_{pc} for sagebrush is then 19.86 s m^{-1}. A similar calculation for a "grass" with $r^s_{pc,\min}$ =50 s m^{-1}; β = 20 W m^{-2}; T_c=278.15 K; T_0 = 298.15 K; T_h = 318.15 K gives a significantly lower r^s_{pc} of 9.28 s m^{-1}. The effect of increased stomatal resistance is to reduce transpiration from the plants, which could lead to an overall decrease in diffusive water-vapor flux from the canopy.

3.2.1.2 Canopy Interception and Condensation

Precipitation striking the plants may either be intercepted or pass through to the ground surface. The actual rainfall intensity striking the ground surface depends on whether the *Rainfall Interception* option is invoked. Without the *Rainfall Interception* option, there is no attenuation by the plant canopy, and rainfall specified via the *Boundary Conditions Card* is applied directly to the ground surface.

The interception capacity is the maximum volume of water that can be stored on the projected storage area of the vegetation, that is, on the area of leaves, twigs, and branches that can retain water against gravity under still air conditions (Ramirez and Senarath 2000). It is a measure of the efficiency of the vegetation in collecting and retaining precipitation as well as rainfall intensity (Massman 1980). A dependence of interception capacity on rainfall intensity has been reported by several authors (Massman 1980; Aston 1979; Ramirez and Senarath 2000). One model that has proven to be convenient with respect to parameterization assumes an exponential decay of interception capacity with rainfall intensity,

$$h_0(L_a) = d_p^d \, e^{-c L_a}, \qquad L_a \geq 0 \tag{3.67}$$

where h_0 is interception capacity (m). The maximum dew depth, d_p^d, depends only on the vegetative characteristics of the canopy and constitutes an upper limit to the interception capacity; the constant c depends on both vegetative and climatic conditions and characterizes the rate of decay of interception capacity with rainfall intensity (Ramirez and Senarath 2000). Although it has been hypothesized that desert plants could channel precipitation to the soil near the base of their stems (Wallace and Romney 1972), the only published studies of interception rates of semi-arid shrub steppe ecosystems are those of Hull (1972) and Hull and Klomp (1974). West and Gifford (1976) suggested that an average of about 0.59 cm of rain is intercepted yearly by the sagebrush and shadscale plant communities in Idaho in storms over 0.15 cm. This is equivalent to 4 percent of the total annual precipitation that falls as rain (West and Gifford 1976).

The actual amount of precipitation intercepted by the canopy, h_a, is equal to the total precipitation depth, h, when interception capacity exceeds the total precipitation depth. At rates equal to or greater than the infiltration capacity, the actual interception becomes equal to the infiltration capacity. The actual interception, h_a, is given by Ramirez and Senarath (2000).

$$h_a = \begin{cases} h & h < h_0 \\ h_0 & h \geq h_0 \end{cases} \tag{3.68}$$

where h is total precipitation depth.

The maximum amount of water that can accumulate from interception or condensation within the canopy is the maximum dew- or condensate-depth, d_p^d. The maximum condensate depth for species i is defined as (Ramirez and Senarath 2000):

$$d_p^d = \gamma^i \, (L_{ai}^i + S_{ai}^i) \tag{3.69}$$

where γ^i is the maximum depth of water per unit L_{ai}^i and stem area index, S_{ai}^i. Data for minimum and maximum L_{ai}^i and S_{ai}^i values exist mostly for forest and crop species (Dickinson et al. 1988), but there are very few for shrubs and grasses. Typical values for shrubs and grasses are 0.1 and 0.2 mm, respectively (Sellers et al. 1989). Hull and Klomp (1974) observed leaf drip from big sagebrush in Idaho during heavy storms but never observed stemflow. Thus, in the current version of STOMP-WAE-B, the default value is S_{ai}^i. A comparison between interception in heavy brush and in brush-free areas showed

that the heavy brush intercepted 31 percent of the rain that fell between April 1 and October 30. During the winter months, snow interception averaged 37 percent. The potential interception per rainfall event, derived from a sample size of 10 plants, was 0.11 cm. Based on the work of West and Gifford (1976), the best estimate of γ^* for big sagebrush appears to be about 0.22 cm.

The fraction of leaves covered by intercepted water depends on both the actual interception and the maximum dew depth. The fraction of leaves covered is defined by Deardoff (1978) as

$$p^* = \left[\frac{L_{pa}}{d_p^d} \right]^{2/3} \tag{3.70}$$

The interception fraction, based on the L_{ai}^i, is then subtracted from the gross precipitation and allowed to be adsorbed by the plant, evaporate from the plant surfaces, or run off to the ground.

If the *Rainfall Interception* option is invoked, then the rainfall specified via input is reduced according to the summed plant area indices. Precipitation is divided according to the plant-area index into that which is incident on the ground surface or plant leaves, i.e.,

$$- L_a = L_{sa} + L_{pa} \tag{3.71}$$

in which L_{sa} is calculated as:

$$L_{sa} = - L_a \left(1 - \sum_{i=1}^{n_{ps}} P_{ai}^i \right) \tag{3.72}$$

Precipitation or condensate that forms on the plant leaves is shed from the plants when the stored water exceeds the specified maximum dew or condensate depth, d_p^d, at leaf area index, L_{ai}. The stored water mass is computed as

$$\left(m_p^w \right)^i = \left(d_p^d \omega_l^w \rho_l^w L_{ai} P_{ai} \right)^i \tag{3.73}$$

The total stored water mass is computed by summing contributions from individual plant species

$$m_p^w = \left(\omega_l^w \rho_l^w \right) \sum_{i=1}^{n_{ps}} \left(d_p^d L_{ai} P_{ai} \right)^i \tag{3.74}$$

Condensate forms on the plant whenever the plant temperature is below the atmospheric dew point temperature. The rate of condensation is controlled by the convective-diffusive mass transfer from the atmosphere to the plant canopy according to

$$\left(E_{pc}\right)^i = \frac{\left(e_g^w\right)_p - \left(e_g^w\right)_c}{\left(r_{pc}^a\right)^i} P_{ai}^i \;;\; \left(e_g^w\right)_p = \left(\omega_g^w\, \rho_g\right)_p \;;\; \left(e_g^w\right)_c = \left(\omega_g^w\, \rho_g\right)_c \tag{3.75}$$

where for the single-plant-temperature option, the plant and canopy water-vapor densities are single valued, and the plant area index and plant-canopy aerodynamic resistance are species dependent. The plant water-vapor density is computed as a function of temperature and saturated water-vapor partial pressure using the steam table formulations (ASME 1967). The total rate of condensation is computed by summing contributions from individual plant species, i.e.,

$$E_{pc} = \left\{\left(\rho_g^w\right)_p - \left(\rho_g^w\right)_c\right\} \sum_{i=1}^{n_{ps}} \frac{P_{ai}^i}{\left(r_{pc}^a\right)^i} \tag{3.76}$$

For a given time step, the flux of shed water is dependent on the incident precipitation flux, condensate flux, stored water mass, and maximum stored water mass. The flux of shed water is defined as

$$L_{sp} = -\max\left[-L_{sa}\sum_{i=1}^{n_{ps}} P_{ai}^i - \frac{E_{pc}}{\omega_l^w \rho_l^w} - \frac{m_p^w}{\omega_l^w \rho_l^w \Delta t} + \sum_{i=1}^{n_{ps}} \frac{\left(d_p L_{ai} P_{ai}\right)^i}{\Delta t}, 0\right] \tag{3.77}$$

3.2.2 Canopy Water-Mass Balance

Water-mass conservation at the canopy is a steady-flow equation that balances water flux from the ground surface and plant leaves with that released to the atmosphere:

$$E_{sc} + G_{sc}\, e_{g_{sc}}^w + E_{pc} + F_{pc} = E_{ca} \tag{3.78}$$

The total mass flux from the canopy to the atmosphere, E_{ca}, is computed using an aerodynamic resistance derived from the wind speed above the canopy,

$$E_{ca} = \left(e_g^w\right)_c - \left(e_g^w\right)_a \sum_{i=1}^{n_{ps}} \frac{P_{ai}^i}{\left(r_{ca}^a\right)^i} \tag{3.79}$$

where the aerodynamic resistance above the canopy, r_{ca}^a, is given by Equation (3.55). Evaporation from the plant leaves to the canopy, E_{pc}, refers only to water stored on the plant leaves and is calculated according to Equation (3.72). The diffusive water-vapor flux between the ground surface and the canopy, E_{sc}, is computed for the ground surface beneath the plant canopy according to Equation (3.46). Transpiration from the plants is computed using an equation similar to that for evaporation of stored water but with an additional stomatal resistance calculated according to Equation (3.61). The diffusive water-vapor flux, via transpiration, from the plant leaves of all species to the canopy is calculated using the root water uptake reduction caused by stress and the crop coefficient according to

$$F_{pc} = \left[\left(e_g^w\right)_p - \left(e_g^w\right)_c\right] \sum_{i=1}^{n_{ps}} \left(P_{ai}^i C_c^i S_r^i\right)\left(\left(r_{pc}^a\right)^i + \left(r_{pc}^s\right)^i\right) \tag{3.80}$$

where the crop coefficient, C_c^i, accounts for the phenophases of plant species, *i*, and the root stress factor, S_r^i, accounts for the effects of soil saturation around the plant roots. In Equation (3.80), S_r^i is computed from the soil-water stress or plant limiting function and the root spatial distribution (van Genuchten 1987)

$$S_r^i = \int_0^{\zeta^*} \gamma[h_c(\zeta)]\, S_d^i(\zeta)\, d\zeta \tag{3.81}$$

The amount of water removed from a subsurface cell by transpiration therefore depends on the overall root stress factor, a normalized vertical root spatial distribution, and a plant limiting function integrated over the height of the cell.

3.2.2.1 Crop Coefficient

The crop coefficient for species *i*, C_c^i, is a parameter used to scale actual transpiration to potential transpiration for the plant species of interest. It is essentially the ratio between actual transpiration of a particular species to the potential transpiration and is usually computed as a function of total accumulated growing days (Figure 3.4). Different species have different phenophases and as a result will reach full canopy cover and maximum transpiration rates at different times after planting. To standardize transpiration calculations, a potential transpiration or reference crop transpiration is used to estimate actual transpiration for other plants. Under a non limiting water supply, a plant can easily achieve its maximum transpiration rate (the reference transpiration rate or potential transpiration rate) for the associated leaf area index and C_c^i=1.0. If C_c^i <1, then the plant uses less water than the potential transpiration. Conversely, when C_c^i >1, the plant uses more water. The temporal distribution of C_c^i therefore dictates when transpiration begins, when it ends, and, depending on time of year, to what degree of maximum transpiration the plant responds. At the beginning and end of the season, C_c^i = 0 signifies a cessation of plant transpiration. In the mid-season stage when the plant is mature, C_c^i = 1.0, which indicates a maximum potential for transpiration.

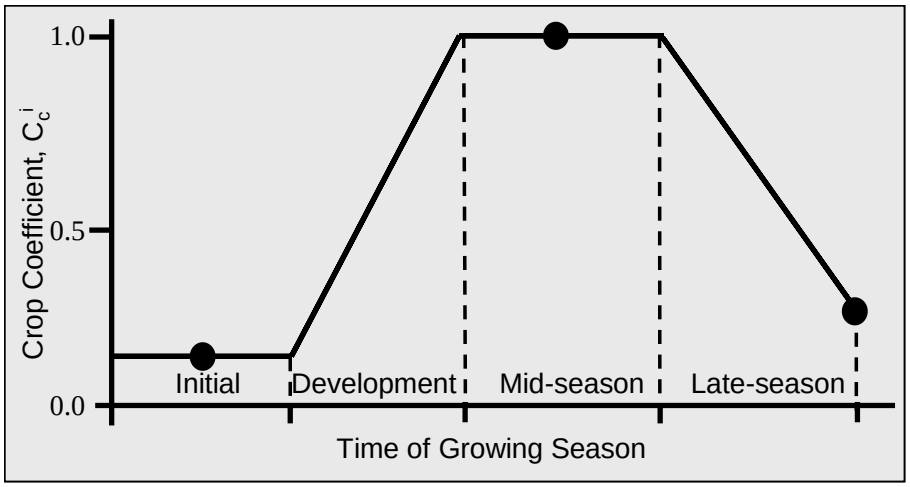

Figure 3.4. The Relation Between C_c^i and the Total Accumulated Growing Days. The crop coefficient is essentially the ratio between actual and potential transpiration, or the transpiration of a reference crop. It is used to scale the actual transpiration to the potential.

One of the strategies of native perennials that allows them survive extended water stress is the ability to extract water from an increasingly dry soil. These plants retain green leaves through the summer and must therefore be able to extract water from an increasingly dry soil. Sagebrush has green leaves all summer long because it is able to concentrate its cell fluids with compounds that will attract water from very dry soil. In modeling native perennials, therefore, C_c^i may decline from 1.0 in the late season, but never returns to zero. Annual plants complete their life cycle in 1 year or less; thus, the late season C_c^i returns to zero, signaling an end of transpiration, and will therefore have a significantly different growth cycle and distribution of C_c^i. In ecosystems with wet winters and dry summers, such as Hanford, some annuals have adapted to maximize growth when water is available. Cheatgrass, for example, is a winter annual grass and begins growth in the fall when the rains begin and dies in late spring when it becomes dry. This means the plant usually germinates in the fall and grows during winter when most native bunchgrasses are still dormant. The key to its success is that it spends the summer as a seed that does not need water, thereby avoiding drought conditions. As a prolific seed producer, cheatgrass is a dominant plant in many places. The function for C_c^i will be significantly different from that of a perennial like sagebrush, and unlike sagebrush, $C_c^i \rightarrow 0$ at a time when C_c^i is still increasing for perennials.

The crop coefficient is a user-specified function used to model the plant phenophases. To parameterize C_c^i, five time points and three average values of C_c^i are used, allowing for the classical crop growing season stages: 1) initial, 2) crop development, 3) mid-season, and 4) late season. Linear interpolation is used between the intermediate time points and between the end of the late-season stage and the end of the calendar year (Day 365) for a given simulation to model perennial plants such as sagebrush.

3.2.2.2 Root Spatial Distribution

Root water uptake is distributed through the root system based on the fraction of the root density present in discrete intervals extending from the top to the bottom of the root zone. One-dimensional root water uptake models are used primarily because in a sparse canopy, the boundary surfaces will contain multiple plants, and the sum of the plant area index for a given species will be less than the boundary surface area. The root distribution at a particular interval is described using the method of Vrugt et al. (2002), chosen because of the flexibility it offers for multidimensional distributions, if needed, as well as its capability to describe complex distributions. With this model, the root distribution in a particular depth interval is calculated according to Vrugt et al. (2001) as

$$\beta^i(z) = \left[1 - \frac{z}{z_m}\right] e^{-\left(p_z / z_m\right)\left|z^* - z\right|} \tag{3.82}$$

where z is the depth (m), z_m is the maximum root depth (m), and p_z and z^* are empirical parameters that provide for zero root uptake at $z = z_m$ and allow for maximum root uptake at some depth z_0. The one-dimensional, normalized root distribution is then calculated as

$$S_d^i(\zeta) = \frac{\beta^i(\zeta)}{\int_0^{\zeta^*} \beta^i(\zeta)\, d\zeta} \tag{3.83}$$

3.2.2.3 Plant Limiting Function

As water is removed from the soil, the remaining water available to the roots diminishes. To account for changes in the availability of water and root water uptake, a root stress or plant limiting function is used. Figure 3.5 shows a schematic of a normalized plant-limiting function, γ^I, as it varies with soil water suction. The plant-limiting function regulates the amount of water that can be extracted from the root zone and is essentially equal to the ratio of actual transpiration to potential transpiration. The stress factor accounts for conditions that are either too dry or too wet for the plant to function. When soil moisture becomes limiting, evapotranspiration decreases and will eventually cease.

The plant-limiting function is a user-specified function that models the root water uptake distribution according to the soil moisture distribution. Parameterizing γ^i requires four suction stress points, h_{wp}, h_{cr}, h_{fc} and h_s, which can be calculated from the soil water contents or saturations using an appropriate water retention function. The four stress points, h_{wp}, h_{cr}, h_{fc} and h_s are specified in the input file, and values of h^i between the four stress points are obtained by linear interpolation. Between the critical suction, h_{cr} and h_{fc}, the normalized stress function, $h^i = 1$, and transpiration occurs at a rate equivalent to the potential or unlimited rate. At $h < h_{cr}$ and $h > h_s$, $h^i < 1$ and transpiration occur at a reduced rate. At $h = h_{wp}$ (permanent wilting point) and at saturation, $h = h_{sat}$ (oxygen deficiency), transpiration and hence crop growth cease. The parameters h_{wp} and h_{fc} are controlled by soil hydraulic properties, and the approach to these conditions is determined by the coupled processes in the soil-vegetation-atmosphere-transfer scheme. The parameter, h_{cr}, on the other hand, depends on both plant type and meteorological conditions. For example, a combination of high evaporative demand, typical of arid sites, coupled with a drought resistant shrub would lead to high values of h_{cr}. Thus, actual transpiration, T_a, is related to the potential

transpiration, T_p, by the factor γ^i, which in turn is affected by the soil hydraulic functions (Feddes et al. 1978).

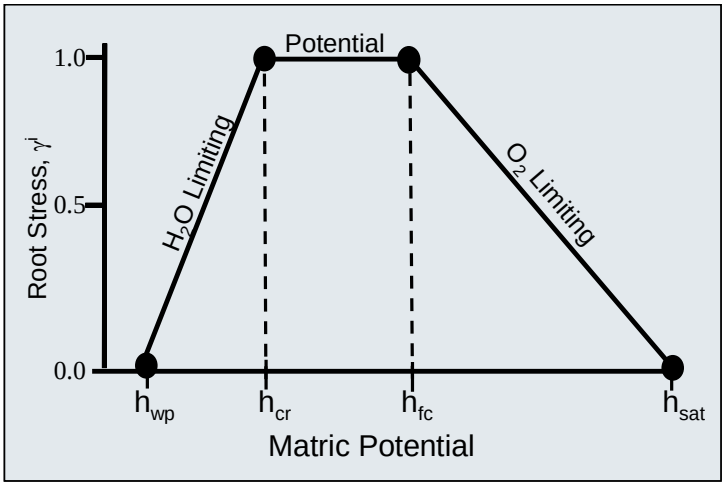

Figure 3.5. The Relation Between γ^i and Soil Water Suction, ψ, for a Plant/Soil Combination. Parameters ψ_{wp} , ψ_{cr} , ψ_{fc}, and ψ_s represent the soil water suction at the at the wilting point, the critical point for potential transpiration, field capacity, and saturation, respectively.

In the Vrugt (2002) model, the stress function depends on the normalized vertical root distribution, Equation (3.81), and the soil-water stress or plant limiting function. The plant limiting function is computed as (van Genuchten and Gupta 1993)

$$\gamma^i[h_c(\zeta)] = \frac{1}{\left[1+\left(\frac{h_c(\zeta)}{h_c^{50}}\right)^{\lambda}\right]} \tag{3.84}$$

At present, the exponent γ has a default value of 3.

In the plant-limiting function described by Vrugt (2002), there is another option based on the normalized root distribution of Jarvis (1989). The main difference between the two formulations is that the Jarvis function incorporates a water stress-compensating factor defined as,

$$\overline{\gamma} = \sum_{i=1}^{k} S_d^i \gamma_i \tag{3.85}$$

where γ_i is the stress index. The stress index is a function of saturation, Θ_i, which is determined relative to the saturated water content (θ_s) and wilting point (θ_{wp}) as,

$$\Theta_i = \frac{\theta_i - \theta_{wp}}{\theta_s - \theta_{wp}} \tag{3.86}$$

The stress index, $\gamma_{i,}$, is calculated as follows

$$\begin{aligned} \gamma_i &= \frac{1-\Theta_i}{1-\Theta_{c2}} && \Theta_{c2} < \Theta_i \le 1 \\ \gamma_i &= 1 && \Theta_{c1} \le \Theta_i \le \Theta_{c2} \\ \gamma_i &= \frac{\Theta_i}{\Theta_{c1}} && 0 \le \Theta_i < \Theta_{c1} \end{aligned} \tag{3.87}$$

where Θ_{c1} and Θ_{c2} are the normalized water contents that describe the stress function. This definition results in a stress function of essentially the same general shape at that shown in Figure 3.5, except that the stress points are now described in terms of a saturation rather than suction. This form of the plant-limiting function is also user specified, and parameterization of γ^i requires four critical saturation points that essentially correspond to θ_{wp}, θ_{cr}, θ_{fc} and θ_s.

For values of θ between the critical soil moisture content, θ_{cr}, and the field capacity, θ_{fc}, $\gamma_i = 1$, and water uptake occurs at an unlimited rate. At $\theta < \theta_{cr}$ and $\theta > \theta_{fc}$, $\gamma_i < 1$, and uptake occurs at a reduced rate. At the $\theta = \theta_{wp}$ (permanent wilting point) and $\theta = \theta_s$ (at saturation), transpiration and hence crop growth ceases. While θ_{wp}, θ_{fc}, and θ_{st} are controlled by soil hydraulic properties, θ_{cr} is controlled by plant type and the prevailing meteorological conditions. For example, a combination of high evaporative demand typical of arid sites coupled with a drought-resistant shrub would lead to low values of θ_{cr}.

3.2.3 Ground-Surface Thermal-Energy Balance

Similar to the water-mass balance at the ground surface, the thermal-energy balance has both canopy and atmospheric components that are defined by the plant areal distributions via the plant area index. Outside of the areal plant distribution, the ground surface is directly coupled to the atmosphere; whereas, within the areal plant distribution, the ground surface is coupled to the atmosphere indirectly through the canopy. At the ground surface, energy from the subsurface plus the net short- and long-wave radiation into the ground surface is balanced with the thermal energy to the canopy and atmosphere

$$\begin{aligned} &R_s^n + R_s^{\ln} + E_{ns}\left[h_g^w\right]_{ns} + G_{ns}\left[\omega_g^w \rho_g h_g\right]_{ns} + L_{ns}\left[\omega_l^w \rho_l h_l\right]_{ns} + H_{ns} = \\ &E_{sa}\left[h_g^w\right]_{sa} + G_{sa}\left[\omega_g^w \rho_g h_g\right]_{sa} + L_{sa}\left[\omega_l^w \rho_l h_l\right]_{sa} + H_{sa} \\ &+E_{sc}\left[h_g^w\right]_{sc} + G_{sc}(\rho_g h_g)_{sc} H_{sc} + L_{sp}\left[\omega_l^w \rho_l h_l\right]_{sp} + H_{sc} \end{aligned} \tag{3.88}$$

where the interfacial values of enthalpy and component mass are upwind weighted. As with the bare-surface option, the thermal energy balance has been written using an enthalpy approach, thus implicitly including the heats of evaporation and condensation.

3.2.3.1 Net Radiation

As in the bare-surface option, the energy flux at the surface boundary is computed from weather observations of air temperature, wind speed, relative humidity, and solar radiation. The potential solar radiation is the radiation of an unobstructed or cloudless sky. The magnitude of the potential solar

radiation depends on the position of the sun, i.e., the solar altitude or solar angle, during the day; the inclination of the solar rays within the earth's surface; the amount of radiation at the outer layer of the earth's atmosphere; the transmissivity of the sky; and the altitude of the earth's surface. During the day when the sun is above the horizon, all surface nodes are assumed to receive the same amount of radiation.

The net short-wave radiation into the ground surface includes short- and long-wave components and considers the attenuation by plants. Direct-beam and diffuse short-wave radiation is treated as a single component. The net radiation into the ground surface is expressed in terms of downward and upward radiation fluxes according to Equation (3.15). The downward short-wave radiation from the atmosphere is derived from the atmospheric data. A portion of this radiation strikes the ground surface directly, without being intercepted by plants, while another portion is attenuated by intervening plants. The net short-wave radiation striking the ground surface is defined as

$$R_s^{sn} = \left(1 - \alpha_s\right) R_a^{sd} \left[\left(1 - \sum_{i=1}^{n_{ps}} P_{ai}^i \right) + \left(\sum_{i=1}^{n_{ps}} P_{ai}^i \exp\left\{ - C^i L_{ai}^i \right\} \right) \right] \tag{3.89}$$

where the attenuated component of short-wave radiation is based on the equation for plant canopy transmissivity of Goudriann (1988).

Computing net short-wave radiation therefore requires an estimate of albedo. On a vegetated surface, albedo is a measure of reflectivity or absorptivity of the entire surface and includes contributions from the ground-surface or soil albedo, α_s, as well as the plant canopy. Plant albedo is known to vary with solar angle, spatial distribution of vegetation (height, density, etc.), and, to some extent, with the spectral properties of the individual surface components. Changes in solar angle and physical structure will therefore affect the total reflected radiation, and both seasonal and diurnal trends in albedo have been reported as a result of these phenomena (Baldocchi et al. 2004). Baldocchi et al. reported a decrease in albedo of grassland as the grass canopy greened and grew, gradually obscuring bare soil and litter. In comparison, the albedo of the dormant and bare woodland was slightly greater than the open grassland during the same period as the bare trees were more reflective. A sharp change in albedo occurred in response to changes in the phenophase, such as the formation of reproductive heads on the grasses, and was reinforced by their sequential senescence (Baldocchi et al 2004). The albedo for grass increased as the summer progressed, and the grass dried to a golden brown color and became more reflective. Woodland and shrubs showed a similar temporal trend with sharp changes coinciding with leaf expansion. In general, the woodland and shrubs had a lower albedo than grassland during the summer, perhaps because the multi-storied structure trapped sunlight even though the grass understory was dry and more reflective.

Similar temporal trends could be expected for shrub steppe ecosystems, although the specific timing of changes in albedo and the absolute values would be expected to differ as the phenophases are different. In fact, Hanson (2001) reported seasonal trends in albedo for stands of Wyoming big sagebrush (*Artemisia tridentata wymomingensis*) and bluebunch wheatgrass (*gropyron spicatum*) that appear correlated with phenophase. To describe the dependence of a_s on phenophase, an approach was used similar to that used for the crop coefficient (Figure 3.4). In this case, the α_s curve is defined simply at the

start and end of four stages of the developmental cycle (initial, development, mid-season, and late season) with four stage lengths (initial, development, mid, and late) as shown in Figure 3.6.

The plant albedo is a user-specified function used to model the change with phenophases. To parameterize α_p^i, five time points and three average values of α_p^i are required. This approach is consistent with the description of crop developmental stages: 1) initial, 2) crop development, 3) mid-season, and 4) late season. Linear interpolation is used between the intermediate time points and between the end of the late-season stage and the end of the calendar year (Day 365). The input requirements include plant albedo at the start of the simulation, α_1; the minimum albedo that typically occurs between the initial and developmental stages, α_2; albedo at the end of the developmental stage (start of the mid-season), α_3; albedo at the start of the late-season stage, α_4.

As discussed in Section 3.1.2.1, the ground-surface albedo is a function of the solar altitude and aqueous water saturation, s_l. Thus, the albedo for a sparse canopy includes the plant albedo for the i^{th} species, α_p^i, and the bare soil albedo which is applied to the fraction of soil not covered by plants.

$$\alpha_s = \left[\alpha_z(\omega) + \alpha_g(s_l)\right] + \alpha_c^i \tag{3.90}$$

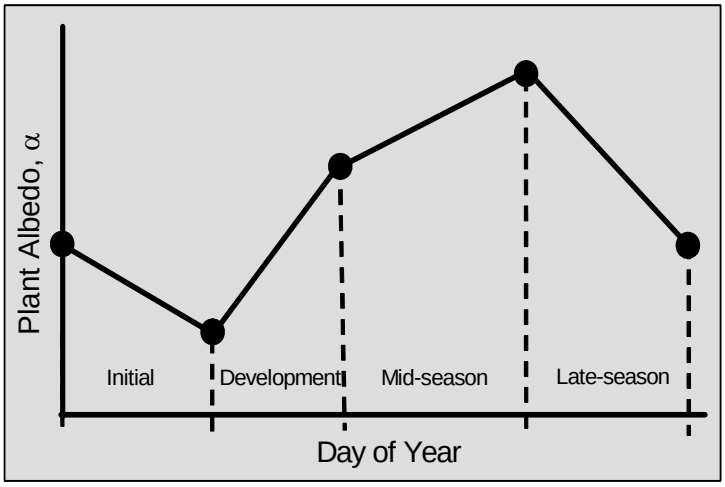

Figure 3.6. The Relation Between Plant Albedo and the Total Accumulated Growing Days

The downward long-wave radiation is given by Equation (3.15), modified for intervening plant attenuation. The upward long-wave radiation is a combination of the reflected-downward radiation and the emitted radiation. Long-wave radiation from the sky to the ground surface is computed as a function of the clear-sky emissivity, fractional cloud cover, and atmospheric temperature (Campbell 1985):

$$R_s^{ld} = \varepsilon_a^0 (1 - 0.84 c_a) \sigma T_a^4 + 0.84 c_a \sigma T_a^4 \tag{3.91}$$

In Equation (3.91),

$$\varepsilon_a^0 = 0.741 + 0.0062\,(T_{dp})_a \tag{3.92}$$

where the clear-sky emissivity is an empirical factor that accounts for the difference between atmospheric and clear-sky temperature (Berdahl and Fromberg 1982), and fractional cloud cover is estimated from atmospheric insolation for solar altitudes greater than 10° (Kasten and Czeplak 1980) and (Caroll 1985); otherwise from the previous computed value:

$$c_a = 1.088\left(1 - \frac{R_s^{sd}}{R_i^{sd}}\right)^{0.294} \tag{3.93}$$

$$R_i^{sd} = \left(0.79 - \frac{0.375}{\theta}\right) I^0 \tag{3.94}$$

Solar altitude is computed from the solar hour angle, local latitude, and solar declination following the approach of Duffie and Beckman (1974) and that of Llasat and Snyder (1998).

The downward long-wave radiation is given by Equation (3.87), modified for plant attenuation per Equation (3.85). The upward long-wave radiation, which is a combination of reflected and emitted radiation, does not consider multiple reflections and is written as:

$$R_s^{\ln} = \varepsilon_s\, R_s^{ld}\left[\left(1 - \sum_{i=1}^{n_{ps}} P_{ai}^i\right) + \left(\sum_{i=1}^{n_{ps}} P_{ai}^i \exp\left\{-C^i\, L_{ai}^i\right\}\right)\right] - \varepsilon_s\, \sigma\, T_s^4 \tag{3.95}$$

The convective-diffusive heat flux between the ground surface and canopy occurs within the areal distribution of plants, whereas, the convective-diffusive heat flux between the ground surface and atmosphere occurs outside of the areal distribution of plants. The convective-diffusive heat flux between the ground surface and canopy is calculated as

$$H_{sc} = (T_s - T_c)\left[\rho_g c_{p_g}\right]_{sc} \sum_{i=1}^{n_{ps}} \frac{P_{ai}^i}{\left(r_{sc}^a\right)^i} \tag{3.96}$$

while the convective-diffusive heat flux between the ground surface and the atmosphere is calculated as:

$$H_{sa} = \frac{(T_s - T_a)}{r_{sa}^a}\left[\rho_g c_{p_g}\right]_{sa}\left(1 - \sum_{i=1}^{n_{ps}} P_{ai}^i\right) \tag{3.97}$$

3.2.4 Canopy Thermal-Energy Balance

The energy balance at the canopy is a steady-flow equation that balances energy fluxes from the ground surface and plant leaves with those from the canopy to the atmosphere:

$$E_{sc}\left[h_g^w\right]_{sc} + H_{sc} + E_{pc}\left[h_g^w\right]_{pc} + F_{pc}\left[h_g^w\right]_{pc} + H_{pc} = E_{ca}\left[h_g^w\right]_{ca} + H_{ca} \tag{3.98}$$

where the interfacial average values of enthalpy are upwind averaged. As with the evaporative and transpirative components, the convective-diffusive heat fluxes between the ground surface and canopy, plant and canopy, and canopy and atmosphere are only considered for the areal region covered by plants. Thus, the sensible heat flux from the ground surface to the canopy is written as:

$$H_{sc} = \left(T_s - T_c\right)\left[\rho_g c_{p_g}\right]_{sc} \sum_{i=1}^{n_{ps}} \frac{P_{ai}^i}{\left(r_{sc}^a\right)^i} \tag{3.99}$$

while the flux of thermal energy from the plant leaves to the ground surface is written as:

$$H_{pc} = \left(T_p - T_c\right)\left[\rho_g c_{p_g}\right]_{pc} \sum_{i=1}^{n_{ps}} \frac{P_{ai}^i}{\left(r_{pc}^a\right)^i} \tag{3.100}$$

and the flux from the canopy to the atmosphere as:

$$H_{ca} = \left(T_c - T_a\right)\left[\rho_g c_{p_g}\right]_{ca} \sum_{i=1}^{n_{ps}} \frac{P_{ai}^i}{\left(r_{ca}^a\right)^i} \tag{3.101}$$

where the interfacial values of the sensible thermal capacitance are harmonically averaged.

3.2.4.1 Aerodynamic Resistance for Heat Transfer

In Equations (3.92) and (3.93), the resistances are also controlled by molecular diffusion, and computation requires knowledge of the temperature profile or its parameters. As described in Section 3.1.2.1, under conditions of neutral or nearly neutral atmospheric stability, the relationship between temperature and elevation can be described by a logarithmic function. The ground surface to atmosphere aerodynamic resistance is determined by integrating the inverse of the eddy diffusion coefficient over the height range from z_{0h} to z_{ref}, giving rise to an equation similar to Equation (3.50). Above the canopy, the eddy diffusion coefficient is assumed to vary linearly with elevation and friction velocity; and below the canopy, the eddy diffusion is assumed to decrease exponentially with height following Shuttleworth and Wallace (1985). Using the assumptions of Equations (3.36) through (3.38), (3.41), and (3.42), the ground-canopy and canopy-atmosphere resistances can be determined by integrating the inverse of the eddy diffusion coefficient over the height ranges from 0 to $d_c + z_{0m}$ and $d_c + z_{0h}$ to z_{ref}, respectively.

The roughness lengths are essentially integration constants in the logarithmic profile, and it is assumed that $d_c = d_{0m} = d_{0h}$. Developments similar to those in Sections 3.1.2.1 and 3.2.1 are then used to estimate

the appropriate resistances. Because heat and moisture is transferred towards the atmosphere by molecular diffusion, the roughness lengths for momentum and heat transfer can differ by up to an order of magnitude or so over natural homogenous surfaces and even more over non-homogenous surfaces like sparse canopies. In the limit of very small roughness density, as can be expected in sparse canopies, z_{0m} tends to the value of the underlying surface (much smaller roughness), and $z_h \approx z_m/6.4 \cdot 10^3$ (Beljaars and Holstag 1991). At high densities, the ratio should return to its value and is estimated as $\ln(z_m/z_h) = 2$, or approximately 0.1, i.e., $z_h \approx z_m/10$ (Garratt and Hicks 1973).

3.2.5 Plant-Leaves Thermal-Energy Balance

Energy conservation at the plant leaves is a transient equation that includes the enthalpy of water mass stored on the plant leaves from intercepted precipitation and condensation. Transpiration, however, is considered a steady-flow process. Thus, transpiration is assumed not to contribute to water stored on the plant leaves. The energy balance for plants considers radiation, convection, and diffusion exchanges with the ground surface and atmosphere and is written as:

$$R_p^n + R_p^{nl} - L_{pa}\left[\omega_l^w \rho_l h_l\right]_{pa} - E_{pc}\left[h_g^w\right]_{pc} - F_{pc}\left[h_g^w\right]_{pc} - H_{pc} = \frac{\Delta\left(m^w h_l\right)_p}{\Delta t} - L_{sp}\left[\omega_l^w \rho_l h_l\right]_{sp} - F_{pc}\left[h_l^w\right]_{np} \tag{3.102}$$

The net radiation into the plant includes short- and long-wave radiation. Short-wave radiation arrives at the plant from the atmosphere and from reflections from the ground surface. Short-wave radiation arriving at the plant is absorbed, reflected, or transmitted. The net short-wave radiation equals the arriving radiation less the amount reflected and transmitted through the plant,

$$R_p^{sn} = \left(R_a^{sd} + R_s^{su}\right)\left(\sum_{i=1}^{n_{ps}}\left(1-\alpha^i\right)P_{ai}^i \exp\left\{-C^i L_{ai}^i\right\}\right) \tag{3.103}$$

where the upward short-wave radiation from the ground includes contributions from inside and outside the areal plant distribution.

$$R_s^{su} = \alpha_s R_a^{sd}\left[\left(1 - \sum_{i=1}^{n_{ps}} P_{ai}^i\right) + \left(\sum_{i=1}^{n_{ps}} P_{ai}^i \exp\left\{-C^i L_{ai}^i\right\}\right)\right] \tag{3.104}$$

Long-wave radiation arrives at the plant from the atmosphere (sky) and ground surface. The ground-surface component includes that which is emitted from the ground and reflected from the atmosphere (sky). Long-wave radiation arriving at the plant can be absorbed, reflected, or transmitted. In computing the radiation exchange between the plants and atmosphere and plants and ground surface, we assume a view factor of one from the plant to atmosphere and from plant to ground surface. The net long-wave radiation equals the arriving radiation less the amount reflected and transmitted, plus the amount emitted by the plants,

$$R_p^{ln} = \left(R_a^{ld} + R_s^{lu}\right)\left(\sum_{i=1}^{n_{ps}} \varepsilon^i P_{ai}^i \left[1 - \exp\left\{-C^i L_{ai}^i\right\}\right]\right)$$
$$-\left(\sum_{i=1}^{n_{ps}} 2\varepsilon^i P_{ai}^i \sigma T_p{}^4 \left[1 - \exp\left\{-C^i L_{ai}^i\right\}\right]\right) \tag{3.105}$$

where long-wave emission from the plant occurs toward the ground surface and atmosphere (sky). Long-wave radiation arriving at the plant from the atmosphere (sky) is computed according Equation (3.76), adjusted for the areal plant distribution

$$R_a^{ld} = \left[\varepsilon_a^0 \left(1 - 0.84 c_a\right) \sigma T_a + 0.84 c_a \sigma T_a{}^4\right]\left(\sum_{i=1}^{n_{ps}} P_{ai}^i\right) \tag{3.106}$$

Long-wave radiation arriving at the plant from the ground surface is a combination of reflected long-wave radiation from the atmosphere (sky) and that emitted from the ground surface:

$$R_s^{lu} = R_a^{ld}\left(1 - \varepsilon_s\right)\left(\left(1 - \sum_{i=1}^{n_{ps}} P_{ai}^i\right) + \left(\sum_{i=1}^{n_{ps}} P_{ai}^i \exp\left\{-C_e{}^i L_{ai}^i\right\}\right)\right) + \varepsilon_s \sigma T_s{}^4 \tag{3.107}$$

where the amount reflected from the ground includes radiation outside and within the areal plant distribution.

It should be noted that there are two transpiration flux terms in Equation (3.63); one from the plant to canopy, using water-vapor enthalpy; and the other from the subsurface to the plant, using liquid-water enthalpy. The latent heat of evaporation for the transpired water occurs at the plant leaves. The interfacial average values for the transpiration terms, which represent the enthalpy transport associated with transpiration and root-water uptake, depend on the direction of transpiration and are computed as:

$$\left[h_g^w\right]_{pc} = \begin{cases} \left(h_g^w\right)_p & for\ F_{pc} \geq 0 \\ \left(h_g^w\right)_c & for\ F_{pc} < 0 \end{cases} \tag{3.108}$$

$$\left[h_l^w\right]_{np} = \begin{cases} \left(h_l^w\right)_n & for\ F_{pc} \geq 0 \\ \left(h_l^w\right)_p & for\ F_{pc} < 0 \end{cases} \tag{3.109}$$

where $F_{pc} \geq 0$ is transpiration, with water being supplied from the roots, and $F_{pc} < 0$ is stomatal condensation on the plant surfaces, with water also being supplied to the roots.

The amount of water removed from a subsurface cell by transpiration therefore depends on the overall root stress factor, a normalized vertical root spatial distribution, and a plant-limiting function integrated over the node depth as follows:

$$R_{wu}^{n} = F_{pc} \frac{\int_{\zeta_t^n}^{\zeta_b^n} \gamma^i \left[h_c(\zeta)\right] S_d^i(\zeta)\, d\zeta}{\int_{0}^{\zeta^*} \gamma^i \left[h_c(\zeta)\right] S_d^i(\zeta)\, d\zeta} \tag{3.110}$$

Root water uptake transported through the plant carries the enthalpy of the node just beneath the boundary surface. Root water passing through deeper nodes is assumed to be in equilibrium with the local node temperature.

3.2.6 Numerical Solution Scheme

The entire system depicted in Figure 2.1 is represented mathematically by invoking the conservation equations for component liquid water, water vapor, gas, and thermal energy (White and Ward 2004). These equations encompass the detailed physics of water mass, vapor, and energy flow in the soil-vegetation-atmosphere-transfer scheme. Hourly or daily averages of climate data, including solar radiation, temperature, humidity, atmospheric pressure, wind speed, and precipitation, are used to define the upper flux boundary conditions and to allow parameterization of the mode for evapotranspiration. The discretized mass and energy transport equations are solved using an integral volume finite-difference approach with the nonlinearities in the discretized equations being resolved through Newton-Raphson iteration. The iteration component of the program flow path contains a pair of nested loops. The outer loop increments time and represents a single time step whereas the inner loop increments iterations of the Newton-Raphson linearization technique. During a single time step both the flow and transport governing equation sets are solved. The Newton-Raphson linearization loop is applicable only to the solution of the mass and heat flow governing equations. The solute transport governing equations are solved directly (without iteration) after convergence of the flow solution. The next procedure involves loading the previous time step arrays for field variables. Field variables from the array location for the current field variable value are loaded into the array location for the previous time step field variable value.

Coefficients of the Jacobian matrix and solution vector are computed in a three-stage approach. In the first stage, all of the previous coefficient arrays are set to zero. In the second stage, the Jacobian matrix and solution vector are calculated. The Jacobian matrix is loaded according to governing partial differential equations to be solved. Coefficients for the water mass conservation equation are loaded first, followed by the air mass, and finally the energy conservation equations. The resulting system of equations represents the discretized and linearized system of governing flow equations with zero flux boundary conditions imposed, where the source contributions have been incorporated. The final stage modifies this linear system according to the active user imposed boundary conditions. Boundary conditions alter both the coefficient matrix and solution vector. With the Jacobian matrix and solution vector elements computed, the next step is to solve the linear system of equations. The linear system is solved either with a direct banded matrix solver or an iterative conjugate gradient solver. Corrections to the primary variables, computed from the linear system solvers, are used to update the primary variables and determine convergence. The Newton-Raphson procedure computes corrections to the primary variable set with each iteration. The starting values for primary variables for each new time step are the previous time step values of the primary variables, as these values represent reasonable estimates of the future values. For a convergent iteration scheme, each successive iteration yields diminishing corrections to the primary variables. Convergence occurs if the normalized values of the primary variable corrections for all unknowns falls below a user-defined value (typically 1×10^{-6}). Further details of the solution scheme are discussed in the STOMP Theory Guide (White and Oostrom, 2000).

Simulation results are written to the “Reference Node Output Record,” the standard input/output device (screen), a “*plot*” file, and/or a “*restart*” file, depending on the directives made by the user on the “Output Control” card. The user has the option of requesting output of the water balance components, temperature, moisture, and solute profiles as well as mass and energy transfer from the soil to the atmosphere and from the soil surface to the subsurface. In the following sections, we provide instructions for compiling and executing the code, describe the modifications to the input requirements, and summarize the results of several example simulations, including benchmark problems based on the observations and model predictions of the water balance components at Hanford’s 300 Area grass site described by Gee and Kirkham (1984) and a monofill barrier in Idaho as reported by Scanlon et al. (2002).

4.0 Compilation and Execution

The user is referred to Chapter 5 of the User's Guide (White and Oostrom 2003) for detailed information on execution of the STOMP simulator. Information on the code execution and a compendium of example problems are included in the Introductory Short Course Manual (Oostrom et al. 2003). In its native form, the STOMP simulator is a collection of files that contain either global routines or those specific to a particular operational mode. For users outside of the Pacific Northwest National Laboratory, the STOMP simulator is distributed as an assembled source coding for a particular operational mode, with associated files, modules, example input files, and required external libraries (e.g., SPLIB). For external distribution, the source code of the desired mode is assembled into a single file that includes the appropriate solvers using the make utility (Talbott 1988). For users within the laboratory, the make utility can be used to directly create an executable. Except for external libraries, the STOMP simulator is coded in Fortran.

While distributing the code as open source allows qualified users to modify the simulator and perhaps promote the exchange of ideas, one disadvantage is that the user is solely responsible for compiling and linking the source code to create an executable appropriate to the problem to be solved. Such a requirement assumes a qualified user who has the appropriate software (e.g., a Fortran compiler), hardware (workstation with adequate memory), and is familiar with their use for generating useable code. Advanced users interested in modifying the code should additionally be familiar, if not skilled, with using a symbolic debugger (often provided with the Fortran compiler). The unassembled STOMP source is coded in a combination of Fortran 77 and Fortran 90. With respect to memory allocation, the assembled source code can be configured in two forms: static and dynamic memory.

Potential users with access only to a Fortran 77 compiler, (e.g., g77, f77, pgf77) will need to have the code configured in static memory form. In this form, the source code includes a *parameters* and a *commons* file. As Fortran 77 is unable to dynamically allocate memory, the user is responsible for editing the *parameters* file to define array dimensions to statically allocate memory during compilation. For users with access to a Fortran 90 compiler (e.g., f90, pgf90, ifc), the source code can be configured for dynamic memory allocation. In the dynamic memory form, both the *parameters* and *commons* files are replaced with a series of Fortran 90 modules in the file *allo.f*. This module must be compiled before compiling the source code. When configured under the dynamic memory option, a utility named *step* is included in the source code. When incorporated, the *step* utility becomes the first subroutine called and reads the STOMP input file to determine dimensioned array requirements. These values (i.e., parameters) are then used to allocate memory for the dimensioned arrays via a call to the subroutine *alloc.f*. This subroutine makes a series of memory allocations and memory checks. If STOMP attempts to allocate more memory than available on the computer, the simulation stops and an error message are printed. Memory allocation under the dynamic memory option only occurs during the execution startup (i.e., memory is never deallocated until the execution stops). The dynamic memory option is generally preferred as it allows the user to execute problems without having to create a parameters file and recompile the code with changes in the input file. Memory allocation options are summarized in Table 4.1.

Table 4.1. STOMP Memory Allocation Options

Memory Option	Fortran Compiler	Include Files	Module File	Comments
Static	f77	commons parameters	NA	• user generated parameters • recompilation w/input change
Dynamic	f90		allo.f	• no recompilation w/input change • greater 1 GB memory on Linux

Compiling the source code into an executable differs between operating systems, compilers, and memory options. This section describes the differences between memory options, using the UNIX operating system. For the static memory option, the following files will be provided with the assembled source coding: stomp#_[sp,bd].f, commons, and parameters where the # in the filename stomp#_[sp,bd].f refers to the operational mode number and the solver options *sp* and *bd* refer to the conjugate gradient or banded solvers, respectively (e.g., stomp3_bd.f is the source code for the Water-Air-Energy-Barrier operation mode with the banded solver; stomp3_sp.f is the source code for the Water-Air-Energy-Barrier operation mode with the conjugate gradient solver). To create an executable on a UNIX or LINUX system, assuming the commons and parameters files were in the same directory as the source code, the user would issue the following command:

```
f77 -I .  -o stomp3_bd.e stomp3_bd.f
```

For the conjugate gradient solver, the compiler must link to the splib library, and the corresponding compilation command would be:

```
f77 -I .  -o stomp3_sp.e stomp3_sp.f $SPLIB_PATH/splib.a
```

where $SPLIB_PATH is the path to the splib library. For the dynamic memory option, the following files will be provided with the assembled source coding: stomp#_[sp,bd].f, and allo.f. To create an executable on a UNIX or LINUX system, assuming the commons and parameters files were in the same directory as the source code, the user would issue the following command:

```
f90 -c allo.f
f90 -c stomp3_bd.f
f90 -o stomp3_bd.e allo.o stomp3_bd.o
```

For the conjugate gradient solver, the compiler must link to the *splib* library, and the compilation command would be:

```
f90 -c allo.f
f90 -c stomp3_bd.f
f90 -o stomp3_bd.e allo.o stomp4_bd.o $SPLIB_PATH/splib.a
```

where $SPLIB_PATH is the path to the splib library.

For the static memory option, the user is responsible for creating a parameters file. A parameters file is used by the FORTRAN programming language and compilers to statically allocate memory for storage of variables. The FORTRAN 77 language is unable to allocate memory dynamically; therefore, all memory storage requirements must be defined at compilation time. No execution errors will occur if the memory allocated is greater than that required by the simulation, unless the memory requirements exceed the computer's capabilities. Unless necessary, the user should avoid executing simulations that require the use of virtual memory. The time required to swap data between the virtual memory storage device and the active memory typically yields poor execution speeds. The STOMP simulator requires two types of parameters (declared and computed) to be defined before compilation. The user is responsible for properly assigning all of the declared parameters. Declared parameters are assigned by modifying the parameters file supplied with the STOMP simulator using a text editor (word processor) or by creating a new parameters file. The equations for the computed parameters must be included in each parameter file after the declared parameters. The parameter definitions given in this manual represent minimum acceptable values. All declared parameters, except for switch type parameters, must have minimum values of 1. Undersized parameters will generally yield execution errors, which may or may not be detected by the system. Oversized parameters are permissible, but can result in excessive memory allocation.

Executing the simulator is straight forward and only requires that the executable version of the code and an input file named input reside in the current directory. For restart simulations, a restart file named restart must also reside in the current directory. Because restart files are created with an extension that corresponds with the generating time step, the user must rename the appropriate restart file to restart. For a UNIX or LINUX operating system, execution is started by typing in the name of the executable file. Execution will be indicated by the printing of a STOMP title banner and program disclaimer to the standard input/output device (e.g., screen). Two types of error messages may be generated during a STOMP execution. The first type is a system-generated message that typically indicates a memory, FORTRAN, or other system error identified by the system. The second type of error messages refers to those generated by the STOMP code, which typically refer to input, parameter, or convergence failure type messages. STOMP-generated messages are divided into three categories according to severity. The most severe are ERROR messages that abort the program execution. Undersized parameters are typical of errors that yield ERROR messages because execution of the simulator with undersized parameters may yield gross errors or even worse subtle errors that may pass undetected in the results. Next on the severity level are the WARNING messages that generally warrant notice by the user that a problem with the input file probably exists. The least severe are NOTE messages, which are used to record events like the absence of an optional input card.

5.0 Input File Structure

As with previous versions of STOMP, the simulator is controlled through a text file, which must be entitled "*input*" for proper execution. This input file has a structured format composed of cards that contain associated groups of input data. Depending on the operational mode, input cards maybe required, optional, or unused. Required cards must be present in an input file. Optional cards are not strictly required to execute the simulator, but may be required to execute a particular problem. Unused cards are treated as additional text that is unrecognized by the simulator but will not hinder a proper execution. Cards may appear in any order within the input file. However, the data structure within a card is critical and must follow the formatting directives described in the Users Guide (White and Oostrom 2003).

5.1 Input File Structure

A STOMP input file is composed of cards, some of which are required and others that are optional or unused. The number of required cards depends on the operational mode. If an attempt is made to execute the simulator on an "*input*" file with an incomplete set of required cards, an error message will be generated, and the code execution will stop. Optional cards are used to specify STOMP capabilities that may be required to execute a particular problem or generate desired output data. These cards are considered optional because the capabilities accessed through these cards are not necessarily required to execute the code. Execution of the simulator on input files with an incomplete set of optional cards yields messages that will note the missing optional cards but allow the execution to continue.

Table 5.1 summarizes the required and optional cards that comprise the input requirements for STOMP-WAE-B. Input specific to this mode are four input cards that include (1) *Atmospheric Conditions Card* used to input local atmospheric conditions, (2) the *Plant Properties Card*, used to input time-invariant plant species data, (3) the *Boundary Conditions Card*, used to input time varying plant species data and the traditional boundary condition data, and (4) the *Thermal Properties Card*, used to enter traditional thermal properties data as well as parameters used to describe the bare surface albedo of rock/soil types used in the simulation.

Each card begins with a header that must contain a tilde symbol (~) in the first column followed by the card name (e.g., ~*Simulation Title Card*). Cards may be arranged in any order within an input file; however, the input format within a card is structured. Blank lines or additional comment lines (preceded by #) may be included in the input file outside of the card structures. Modifications have been made to read in the new cards required for the SVAT scheme that has been developed for evapotranspiration from sparse canopies. In addition, the *Boundary Condition Card* has been modified to plant canopy characteristics, namely the time-varying leaf area index and plant water index. To run STOMP with the SVAT scheme, the term "Water-Air-Energy-Barrier" is needed in the *Simulation Card*. Table 5.1 summarizes the required cards specific to this operational mode.

Table 5.1. Required and Optional Input Cards for STOMP-WAE-B

Required Cards	**Card Status**
Simulation Title	Required
Solution Control	Required
Grid	Required
Rock/Soil Zonation	Required
Mechanical Properties	Required
Hydraulic Properties	Required
Thermal Properties	Required
Saturation Function	Required
Aqueous Relative Permeability	Required
Function	Required
Gas Relative Permeability Function	Required
Boundary Conditions	Required
Atmospheric Conditions	
Optional Cards	Card Status
Inactive Nodes	Optional
Fixed Nodes	Optional
Fixed Nodes Conditions	Optional
Initial Conditions	Optional
Source	Optional
Output Control	Optional
Surface Flux	Optional
Solute/Fluid Interactions	Optional
Solute/Porous Media Interactions	Optional
Plant Properties	Optional
X-Direction Permeability	Optional
Y-Direction Permeability	Optional
Z-Direction Permeability	Optional

5.2 Card Descriptions

The reader is referred to the SOMP User's Guide (White and Oostrom 2003) for detailed information on the format and data requirements for STOMP input cards. Input cards are listed in alphabetical order in the Appendix of the User's manual (White and Oostrom 2003). This section provides a brief synopsis of each of new input card added for the SVAT scheme with emphasis on its purpose and application. Detailed formatting instructions for the new input cards are provided in Appendix A.

5.2.1 Atmospheric Conditions Card

This card allows the user to specify time-varying atmospheric conditions for temperature, pressure, relative humidity, net solar radiation, and wind speed. At present, data from this card are only used in conjunction with the *Plant Card* and the *Water-Air-Energy-Barrier* operational mode. This card comprises two input sections: (1) reference data and (2) time-varying atmospheric conditions data. The reference data inputs include atmospheric conditions start time; wind speed; air temperature and relative humidity measurement heights, local longitude; local latitude; meridian, and roughness parameters. The

Atmospheric Start Time, *Local Longitude*, and *Local Meridian* inputs are used to split total horizontal solar radiation into direct-beam and indirect components. The *Atmospheric Start Time* is also used as the reference time for specifying the plant growth cycle and the time-dependent albedo. Regardless of the start time of a simulation as specified in the *Solution Control* Card, definitions of the plant growth cycle and other time-dependent plant variables are all defined relative to the *Atmospheric Start Time*. *Local Longitude* The *Wind Speed Measurement Height* input is used to convert wind speed at the measurement height to wind speed near the ground surface and plant canopy heights using the classical logarithmic from of the wind profile. As with the wind speed, the *Air Temperature* and *Relative Humidity Measurement Height* inputs are used to convert their respective values at the ground surface and plant canopy heights. The surface of a barrier is rough at multiple scales from the roughness associated with soil particles to grass and shrubs protruding into the air. Therefore, as the wind flows over the surface, it produces turbulence on a similar horizontal scale to the obstacle. The bulk aerodynamic relationship relates the heat flux to the difference between the aerodynamic temperature at the thermal roughness height and the temperature in the surface layer. Therefore, the *Aerodynamic Roughness Length* and *Thermal* Roughness Lengths are required parameters. In general, the *Thermal Roughness Length* is smaller than the *Aerodynamic Roughness Length*. The default value for both roughness parameters in STOMP-WAE is $1.3 \cdot 10^{-3}$ m, which is based on measurements obtained at the 200-BP-1 prototype Hanford barrier (Ward et al. 1997).

The time-varying inputs are read in tabular form in which each line of input represents the atmospheric conditions at that point in time. The *Atmospheric Condition Time* input is the first entry in each time-varying input line and is relative to the *Atmospheric Start Time* declared in the reference data input section. The time entry is followed in succession by the *Atmospheric Condition Temperature*, *Atmospheric Condition Pressure*, *Atmospheric Conditions Relative Humidity*, *Atmospheric Conditions Net Solar Radiation*, and *Atmospheric Conditions Wind Speed* inputs. The *Net Solar Radiation* input should be total solar radiation incident on a horizontal ground surface. The time-varying inputs can be read directly from the input file or from an external file. Weather data are read as hourly or average daily measurements, which for Hanford-specific simulations can be obtained from the HMS. In cases where required atmospheric data are not available, the missing data can be calculated from available data using published theoretical relationships.

5.2.2 Boundary Conditions Card

This card allows the user to control the simulation by defining time varying boundary conditions. Although this card is optional, it is generally necessary to simulate a particular problem. White and Oostrom (2003) provide detailed discussions of the Boundary Conditions Card. Briefly, boundary conditions may be applied to any boundary surface or surface dividing active and inactive nodes. By default, all undeclared boundary surfaces have zero flux boundary conditions for both flow and transport. Boundary conditions may be applied only to surfaces of active nodes. To apply a boundary condition to a boundary surface, the surface is referenced by the adjacent active node and a direction with respect to the adjacent node. To apply a boundary condition to a surface dividing an active and inactive node, the surface is referenced by the active node and the direction to the inactive node with respect to the active node. Boundary conditions are time varying. The user is not allowed to assign multiple boundary conditions to a boundary surface during the same time period, but multiple boundary conditions can be applied to a boundary surface over different time periods. The simulator controls time steps to agree with time transitions in boundary conditions.

An error-free *Boundary Conditions Card* does not guarantee that a solution as an ill-posed problem could lead to non-convergence. For example, a mistake frequently made by users is to specify infiltration rates at the top of a column with positive fluxes. While this input would be perfectly acceptable to the boundary condition input reader, the specified condition would actually withdraw flux from the top of the column because the z-axis and z-direction flux are positive in the upward direction. Regardless of the boundary type, the boundary condition inputs are used to compute phase saturations, phase relative permeabilities, and physical properties at the boundary surfaces. Because STOMP-WAE-B involves three-phase conditions, it is critical that the user specify boundary conditions that yield appropriate secondary field variables at the boundary surface.

Correct application of boundary conditions requires an appropriate conceptualization of the physical problem and translation of that conceptualization into boundary condition form. The variety of boundary condition types available in the simulator should afford the user with the flexibility to solve most subsurface flow and transport problems. The boundary condition card reader within the simulator performs limited error checking on the boundary condition inputs. This section focuses on the requirements for the SVET scheme in STOMP-WAE-B. It is through this card that time-varying atmospheric conditions are read.

Generally, the number of boundary types that must be declared for each boundary equals the number of solved equations governing flow and transport. In STOMP-WAE-B, the *Dirichlet* boundary type is used to specify values of pressure, temperature, or solute concentration at the boundary surface. The *Neumann* boundary type allows the user to specify a flux (e.g., liquid phase flux, heat flux, or solute flux) at the boundary surface. The *Zero Flux boundary* type is used to impose no flow and/or transport conditions across the boundary. The *Saturated* boundary type is available only for two-phase conditions and imposes total-liquid saturation conditions (e.g., water table) at the boundary surface. The *Unit Gradient* boundary type imposes hydrostatic conditions across the boundary surface for the specified phase. The *Hydraulic Gradient* boundary type should be applied only to a column or plane of vertical surfaces. With this boundary type, the user specifies a fluid phase pressure at the lowest surfaces of a column or row, and the simulator then computes fluid phase pressure for the remaining boundary surfaces assuming hydrostatic conditions for the fluid phase. The *Seepage Face* boundary type is similar to a *Hydraulic Gradient* boundary, but is limited to pressure boundaries of the local gas pressure. This boundary type is designed to model an exposed vertical face that “seeps” liquids. Liquid can enter a seepage face only for phase pressures that exceed the local gas pressure. The *Initial Conditions* boundary type fixes the boundary field variables (e.g., pressure, temperature, or solute concentration) to the initial value of the field variables of the node adjacent to the boundary surface. This boundary type is invariant with time. *Inflow* and *Outflow* boundary types are applicable only to solute and energy boundary conditions. These boundary types consider only solute or energy transported by advection; diffusion transport across the boundary surface is neglected. The solute concentration boundary types (e.g., *Volumetric Concentration*, *Aqueous Conc.*, and *Gas Conc.*) are equivalent to Dirichlet boundary types for solute transport. These boundary types differ by their definitions of solute concentration.

Unique to the SVAT scheme of STOMP-WAE-B is the *Bare Shuttleworth-Wallace* and *Shuttleworth-Wallace* boundary types that may be imposed as an energy boundary on the upper surfaces of boundary nodes. The *Bare Shuttleworth-Wallace* is used to calculate potential evaporation from the bare soil surfaces whereas the *Shuttleworth-Wallace* boundary is used to calculate the PET from the canopy and

surface. In the SVAT scheme, evapotranspiration is the sum of three components: (1) evaporation of intercepted precipitation, (2) soil evaporation, and (3) transpiration. The SVAT scheme uses the model of Shuttleworth and Wallace (1985) to separate these components of evapotranspiration in sparse canopies. This boundary type provides a potential transpiration estimate based primarily on canopy resistance. For potential transpiration, canopy resistance depends on maximum leaf conductance, corrected for humidity, temperature, and light penetration. Aerodynamic resistances depend on leaf area index and plant area index, both of which are allowed to vary with time, and on canopy height. In STOMP-WAE-B, the boundary condition time is followed by *Volumetric Aqueous Flux, Leaf Area Index,* and *Plant Area Index* inputs for plant species. These plant parameters can remain constant for the duration of the simulation, or they can be varied over time to reflect changes in canopy characteristics. Even though STOMP-WAE-B does not include a feedback mechanism for including the effects of plant growth, the capability to vary canopy characteristics and ground cover over time provides a relatively simple way to evaluate the effects of changes that typically occur because of plant growth. In STOMP-W, one option available for simulating flow with evapotranspiration at the surface is the *Potential Evapotranspiration Aqueous* boundary condition. This condition requires calculating the PET values externally. This is typically done by applying the Penman equation as reported by Doorenbos and Pruitt (1977) to meteorological data from the HMS.

Actual transpiration is reduced below the potential transpiration when the water supply to the plant becomes limiting. Water uptake may become limited by plant resistance, resistance in the root zone, or the achievement of the critical leaf water potential. Actual transpiration is the lesser of potential transpiration and a soil water supply rate determined by the resistance to liquid water flow in the plants and on root distribution and soil water potential in the soil layers. Evaporation of intercepted precipitation is calculated with a canopy resistance of zero and aerodynamic resistances based on canopy height, coupled with a canopy capacity and an average duration of a precipitation event. Evaporation from the soil and the transpiration from the canopy are derived from a modification of the Penman-Monteith combination equations. For evaporation, the theory assumes a bare soil under a canopy that is uniformly distributed vertically and horizontally. Evaporation from a bare soil is invoked using the *Bare Shuttleworth-Wallace* boundary type. Soil evaporation resistance depends on soil water potential in the top soil layer and the bare soil albedo.

The *Boundary Surface Direction* is specified with respect to the active node adjacent to a boundary surface. For the Cartesian coordinate system, the terms west, south, and bottom refer to the negative *x*-, *y*-, and *z*-directions, respectively, and the terms east, north, and top refer to the positive *x*-, *y*-, and *z*-directions, respectively. For the cylindrical coordinate system, the terms west, south, and bottom refer to the negative *r*-, θ-, and *z*-directions, respectively, and the terms east, north, and top refer to the positive *r*-, θ-, and *z*-directions, respectively. In the current version of STOMP, the *Bare Shuttleworth-Wallace* and the *Shuttleworth-Wallace* boundary types can be applied only to the top surfaces of the boundary. By default, vertical faces are treated as zero flux boundaries. Alternatively, the *Dirichlet* boundary type can be used to specify values of pressure, temperature, or solute concentration on these faces.

Time variations of the boundary conditions, including variation in plant parameters for the *Shuttleworth-Wallace* boundary types, are controlled by declaring multiple boundary times. These boundary times can be read in from a linked file external to the input file. All *Boundary Time* inputs are referenced against the *Initial Time* specified in the *Solution Control* card or obtained from a "*restart*" file. A boundary condition declared with a single *Boundary Time* implies that the boundary condition is time invariant and

the specified *Boundary Time* represents the start time for the boundary condition. Before the start time, the boundary surface will be assumed to be of type *Zero Flux*. The specified boundary condition will remain in effect from the start time until the execution completion. If a boundary condition is declared with multiple *Boundary Times*, then the first time listed equals the start time, the last time listed equals the stop time, and the intermediate times are transition points. For simulation times outside of the start and stop time limits, *Zero Flux* boundary conditions apply. For simulation times between two *Boundary Times*, the linear interpolation of the boundary conditions is applied. Step boundary condition changes can be simulated by defining duplicate *Boundary Times*. The first time would indicate the completion of the previous boundary condition, and the second time would indicate the start of the new boundary condition. At the completion of the step boundary condition, another set of duplicate *Boundary Time* declarations would be used. Step boundary conditions are convenient methods for introducing slugs of fluids, heat, or solute in conjunction with the *Neumann* boundary type.

5.2.3 Observed Data Card

Parameter estimation with the STOMP simulator is executed using inverse modeling techniques in conjunction with UCODE (Poeter and Hill 1998), a computer code for universal inverse modeling. Inverse modeling involves repetitive forward modeling where each forward realization differs by increments in the parameters of interest. Simulation results are compared against observed data to compute error. This card is divided into two sections, one for specifying observed data parameters and the other for entering field (laboratory) observation data. Observed data can be field parameters (i.e., aqueous pressure, aqueous saturation, aqueous moisture content, surface or soil temperature), flux rate parameters (i.e., aqueous volumetric flux, solute flux, gas advective heat flux, surface latent heat flux), or flux integral parameters (i.e., aqueous volumetric flux integral, gas volumetric flux integral, heat flux integral). Observed data are defined by the parameter type, physical location, statistical index, and time and space weighting factors. Physical locations for field parameters can be specified as x, y, z (r, θ, z) coordinates or an i, j, k node index where the node indexing refers to the centroid of the grid cell. Flux rate and integral parameters can only be specified by defining surfaces as with the *Surface Flux Card* (i.e., a surface direction and a domain of i, j, k indexed nodes). As with the *Surface Flux Card*, surfaces can span over a range of nodes, and the reported surface flux values will be the summed quantity (i.e., the flux rate or integral across the entire surface). In the first section of the card, observed data parameters are defined and located within the computational domain. In the second section of the card, experimental data for the defined parameter are read, either directly from the input file or from an external file. The observed experimental data include a time and observed data value where the time corresponds with the simulation time. STOMP-WAE-B does not compute or assess the error between the computed observed data and the experimental observed data; it simply records these data to a file. For reference observed data specified according to x, y, z (r, θ, z) coordinates, tri-linear interpolation is used to compute the observed data parameter at the specified physical location.

5.2.4 Plant Card

This card is used to specify properties for each plant species growing on the ground surface, their time-invariant characteristics, and how the canopy microclimate is handled. At present, this card is unique to STOMP-WAE-B and is used in conjunction with the *Atmospheric Conditions Card*. Time varying plant species data are specified through the *Boundary Conditions* Card. With this card, the user defines the number of plant species and their characteristics with respect to the canopy structure and its rainfall interception characteristics, the root distribution and its stress functions, and albedo for each plant species.

The SVAT scheme in STOMP-WAE-B provides three options for describing the canopy structure and simulating the effects of plants: 1) *Bare Surface*, 2) *Single Plant Temperature*, and 3) *Multiple Plant Temperature*. The option selected determines the nature of the equations to be solved. The *bare-surface* option considers water, air, and energy exchange between the atmosphere and subsurface, without plants. Conservation equations for water mass, air mass, and thermal energy are solved at the ground surface. The *single-plant-temperature* option considers water, air, and thermal energy exchange between the atmosphere and subsurface, assuming single temperatures at the plant leaves and mean canopy height, and a single water-vapor density at the canopy. This option requires the solution of five coupled nonlinear equations: water mass and thermal energy at the ground surface, thermal energy at the plant leaves, and water mass and thermal energy at the canopy. The *multiple-plant-temperature* option is similar to the *single-plant-temperature*, except that three additional equations are needed for each plant species: a water-mass conservation equation at the canopy for the plant species and a thermal-energy conservation equation at the plant leaves and canopy for each plant species.

Rainfall that strikes the plants is either intercepted or travels directly to the soil surface. There are two options for simulating how precipitation is handled: 1) no *Rainfall Interception* in the canopy, the default, and 2) *Rainfall Interception*. The *Rainfall Interception* option allows the simulation to account for the interception of rainfall by the canopy and the subsequent evaporation or condensation of water on plant surfaces. The *Rainfall Interception* option can be invoked with the M*ultiple Plant Temperatur*e option and allows for routing intercepted rainfall and condensate on the plant. Shed rainfall or condensate is only possible when the *Rainfall Interception* option is invoked, and the water stored on the plant leaves exceeds the storage capacitance. Rainfall or condensate water is shed from the plant when the stored water exceeds a maximum specified by the *Maximum Condensate Depth*. The *Maximum Condensate Depth* depends only on the vegetative characteristics of the canopy and constitutes an upper limit to the interception capacity. The spatial location and ground-coverage density of plants is defined through the *Boundary Conditions Card* using the *Shuttleworth-Wallace* boundary condition. The *Shuttleworth-Wallace* boundary condition computes transpiration and evaporation losses from the ground surface and plant canopy in response to atmospheric conditions, specified in the *Atmospheric Conditions Card*.

In the *Plant Card*, species names must be unique and contain no more than 64 characters. For each defined *Plant Species*, the user must specify characteristics about the plant, including the vertical root extent, canopy height, stress characteristics, and crop coefficients. For each *Plant species*, the root stress function must first be specified. At present, there are two options: 1) The *Vrugt Root Stress* model and (2) the *Jarvis Root Stress* model. The extent and spatial distribution of plant roots in the vertical direction is defined through three input parameters: *Max. Root Depth*, *Null Root Depth*, *Root Depth Fit Parameter*. The *Max. Root Depth* input represents the maximum rooting depth, and the *Null Root Depth* and *Root Depth Fit Parameter* inputs are empirical parameters derived from the regression of root distribution data on the model of Vrugt et al. (2002). These parameters provide for zero root water uptake at the maximum rooting depth, account for asymmetrical root water uptake with depth, and allow for maximum root water uptake at any depth from the ground surface to the maximum rooting depth.
The *Short-wave Albedo* input is required for calculating the amount of incoming radiation that is reflected by the surface vegetation. The *Short-wave Albedo* is the proportion (from 0, zero reflection, to 1, perfect reflector) of short-wave radiation that is reflected by the plant leaves. In mixed canopies, *Short-wave Albedo* can be lower than that of individual leaves because light reflected by one leaf may be absorbed by another. The higher the albedo of a surface, the less energy it absorbs, and the cooler a temperature it

maintains. In the *bare-surface* option, albedo is essentially a measure of reflectivity of the bare surface and is specified in the *Thermal Properties Card*. With the *single-plant-temperature* and *multiple-plant-temperature* options, albedo is a measure of reflectivity of the plant canopy and is entered in the *Plant Card*. There are two options for specifying the albedo: 1) constant albedo or 2) a temporally variable albedo. With the constant albedo option, a single value of the plant short-wave albedo is entered followed by the canopy characteristics, including the *Plant Canopy Height* and the *Maximum Condensate Depth*. With the variable albedo option, the plant albedo is assumed to vary with the plant phenophases and is as described by developmental stages used to describe the crop coefficient stages. In this case, the keyword *Temporal* is required, followed by the albedo for five time points that define the start of each developmental stage and the end of the growth cycle. The first time point is defined relative to the start time in the *Atmospheric Conditions* Card. The input requirements therefore include (1) the plant albedo at the start of the simulation, α_1, (2) the minimum albedo that typically occurs between the initial and developmental stages, α_2, (3) the albedo at the end of the developmental stage (start of the mid-season), α_3, (4) the albedo at the start of the late-season stage, α_4, and (5) the albedo at the end of the late-season stage, α_5. All of these times are defined relative to the *Atmospheric Start Time*, regardless of the simulation start time defined in the *Solution Control* Card. This input is then followed by the canopy characteristics, including the *Plant Canopy Height* input, which is necessary for calculating energy flux in the plant canopy. The percentage of ground shaded by the plant is required to calculate the differentiate soil thermal flux from plant thermal flux. It is also needed for computing shading effects of taller plants on shorter plants and to compute canopy height wind speed and temperature.

A plant limiting or stress function is available to reduce the root water uptake as a function of capillary pressure and uses four coefficient inputs: *Water Stress Point 1* (h_1), *Water Stress Point 2* (h_2), *Water Stress Point 3* (h_3), and *Water Stress Point 4* (h_4). These matric potential stress points can be calculated from the aqueous saturations using an appropriate water retention function (e.g., van Genuchten [1980] or Brooks and Corey [1964]). The stress factor accounts for conditions that are either too dry or too wet. Under conditions wetter than h_1 (oxygen deficiency), and drier than h_4 (wilting point), water uptake is zero. Limit h_3 also depends on the evaporative demand of the atmosphere and therefore varies with the potential transpiration. Between h_1 and h_2, and between h_3 and h_4, the stress function varies linearly. The matric potential at which uptake is reduced by 50 percent is also required. Simulating the actual plant transpiration requires specification of the crop coefficients and leaf area index. The crop coefficient is the ratio between actual evapotranspiration of a particular plant species at a certain growth stage and the PET. The crop coefficient is therefore used to scale actual transpiration to the potential transpiration for the plant species of interest. Variations in the transpiration rate, root water uptake, and foliage on a yearly basis are handled via a crop-coefficient function, which requires four crop coefficients and associated times: *Crop Coefficient (Start)*, *Crop Coefficient (Development Stage)*, *Crop Coefficient (Mid-season Stage)*, and *Crop Coefficient (Late-season Stage)*. Linear interpolation based on the time of year is used to interpolate the crop coefficient specified times.. The crop coefficient is defined on a Julian day cycle with day 1 being January 1.

5.2.5 Thermal Properties Card

This card allows the user to assign values to the thermal conductivity, specific heat, and short-wave albedo for each defined rock/soil type. Every rock/soil type defined on the Rock/Soil Zonation Card must be referenced. With the *IJK Indexing* option, node-dependent parameters are entered via external files, and node-independent parameters are entered directly on the card. This card is required only for

simulations involving the solution of the energy conservation equation. Declaration of the thermal conductivity depends on the operational mode and function option. Refer to the STOMP Theory Guide (White and Oostrom 2000) for a description of thermal conductivity functions. The *Constant* option fixes the thermal conductivity to a constant value, independent of temperature or saturation. The *Parallel* option requires the thermal conductivity of the soil grains and models thermal conductivity with an equivalent parallel path model dependent on porosity, phase saturations, and temperature. The *Linear* and *Somerton* options scale the thermal conductivity between the unsaturated and saturated values, depending on phase saturation. Both the *Campbell* and *Cass* options describe the thermal conductivity as a function of saturation using a polynomial function. However, the *Cass* option allows the additional specification of non-isothermal flow enhancement factors. A primary assumption with the simulator is that principal components of the thermal conductivity tensor are aligned with the principal coordinate directions. For cylindrical coordinate systems, the radial, azimuthal, and vertical permeabilities correspond with the x-, y-,and z-direction values, respectively.

Short-wave *Albedo* input is required for calculating the amount of incoming radiation that is reflected by the bare soil. The *Albedo* is the proportion (from 0, zero reflection, to 1, perfect reflector) of short-wave radiation that is reflected by the soil surface. The higher the albedo of a surface, the less energy it absorbs, and the cooler a temperature it maintains. *Albedo* is known to be a function of the solar altitude and aqueous water saturation. There are four options for specifying how the ground surface albedo is calculated: 1) *Plum and Xiu Albedo,* 2) *Wang Albedo,* 3) *Briegleb Albedo,* and 4) *Constant Albedo*. With the *Plum and Xiu Albedo* option, required input parameters are dry-soil albedo, wet-soil albedo, and the albedo attenuation factor. The *Wang Albedo* option requires identical input parameters along with a reference albedo at a solar zenith of 60^{o}. Input requirements of the *Briegleb Albedo* option are identical to those of the *Wang Albedo,* with an additional requirement for an empirical *C* parameter whose values vary from 0.4 for arable grass, grassland, and desert to 0.1 for all other surfaces. The only input requirements for the *Constant Albedo* option is a mean value of albedo for the soil type of interest.

5.2.6 UCODE Control Card

This card allows users to control UCODE executions through the STOMP input file. Parameters and options read from this card are written to external files that are then read and used by UCODE. This card is offered as a convenience to users executing UCODE in conjunction with STOMP, but is not required if the user prefers to create the control files externally. As with other STOMP input, this card uses comma delimited fields. The *UCODE Control Card* includes five lines of comma-delimited input data. The first line of the card includes seven parameters used to control the regression program, printing, and observation data. These include the options for (1) *Phase,* (2) *Time differencing,* (3) *Tolerance,* (4) *Tolerance for SOSR,* (5) *Quasi-Newton Updating,* (6) *Maximum Number of Iterations,* and (7) *Maximum Fractional Parameter Change.* The second line of input is the path of the inverse code, in this case the path of *mrdrive,* which must be written in a format consistent with the operating system (..*mrdrive.exe* for the Microsoft Windows operating system; ../*mrdrive* for the Linux and Unix operating systems). The third line contains a single entry that specifies the number of application models while the fourth line contains the execution commands for the application model. The fifth line of input includes four parameters that specify options for (1) *Scale-sensitivities,* (2) *Intermediate Printing,* (3) *Graph Printing,* and (4) *Number of Residual Sets.* The control parameters read in from this card are written to the external universal file *out_uc.uni*. For successful execution, UCODE requires the universal file (*out_uc.uni*), the prepare file (*out_uc.pre*), the extract file (*out_uc.ext*), and one or more template files (Table 5.2) along with the STOMP input file. The function file (*out_uc.fnc*) is optional, depending on the parameter

substitution method. Four additional input files are needed when PHASE = 44 or 45. These files are created automatically at PHASE 3, but the user needs to rename the files. The universal and extract files can be constructed automatically by running STOMP once with an input file containing the *w/inverse* option in the *Solution Control Card* before the start of the inverse modeling. If produced this way, the files will have the names of *out_uc1.uni* and *out_uc1.ext*, respectively. Note that STOMP does not overwrite any existing universal or extract files. Hence, the two files must be removed manually if they need to be re-constructed. The file, *out_uc1.pre*, and an optional function file, *out_uc1.fnc*, need to be constructed manually. The template file, *input.tpl*, is also constructed manually by replacing the parameters to be estimated by corresponding substitution strings that appeared in the *out_uc1.pre* file. For detailed descriptions of constructing the files, please refer to Poeter and Hill (1998). Zhang et al. (2002) presents a detailed description and example applications of the STOMP-UCODE for variably saturated flow in homogeneous and layered porous media.

Table 5.2. Required Input Files for STOMP-UCODE

File Name	Format	Functions	Notes
Universal File	fn[(a)].uni	Contains control parameters for regression and printing, and observation information.	Required
Prepare File	fn.pre	Names the template file(s) and the application model input file(s). Provides the starting parameter values. Defines prior information on the parameters.	Required
Extract File	fn.ext	Describes how to extract values from the output and defines how to calculate simulated equivalents of the observations.	Required
Template File(s)	input.tpl	A copy of application model input file, edited such that search strings replace values derived from the defined parameters.	Required
Function File	fn.fnc	Allows functions of the parameter values to be used as input to the application model.	Optional
Temp files	temp.xxx[(b)]	Needed to calculate prediction linear confidence and prediction intervals.	Required for PHASE 44, 45

(a) fn in the file name is to be replaced by a user-defined prefix; with STOMP, fn = out_uc1.
(b) temp can be u44, p44, f44, e44, u45, p45, f45, and e45.

6.0 Example Simulations

The value of a simulation model partly depends on its capability to realistically generate an observation of response variables of interest. It is not unusual for initially parameterized simulation models to fail in their capability to accurately fit observed data. Thus, the situation is often corrected by adjusting the input parameters within reasonable limits and again comparing the output with observations. The process of comparing model output with observations is known as model verification. Validation, in contrast, compares output from a verified model with independent data and includes statistical analyses to quantify the goodness of fit. Verification is therefore an important step in a statistically rigorous validation, which is required before a model can be certified as being capable of capturing responses for the major input variables and meteorological forcings.

As part of the process to verify the theory, input file formatting, and the applicability of the sparse vegetation evapotranspiration model, STOMP-WAE-B was used to simulate a series of test problems. To simplify the process, the problems selected for this exercise are those simulated in the verification of the UNSAT-H code (Fayer 2000). The first three UNSAT-H examples were verification tests of infiltration, drainage, and heat flow. The remaining four examples were simulations of water flow in a layered soil system, water and heat flow in a layered system, plant transpiration, and a multiyear simulation. For a variety of reasons, not all of these simulations are repeated here. The verification problems include those of infiltration, drainage, and heat flow in a homogeneous and layered system from the UNSAT-H problem set. In addition to these problems, the barrier simulations reported in the intercode comparison by Scanlon et al. (2002) are included both for verification and to establish a benchmark for users of STOMP-WAE-B. For this verification, the focus is limited to the prototype barrier at the Idaho site, as this cold desert environment is perhaps more similar to Hanford conditions that the Texas simulation. Because the intercode comparison did not include plants, verification was essentially limited to the water balance components without transpiration. To verify the transpiration component of the soil-vegetation-atmosphere-transfer scheme, a simulation problem was designed based on the work of Gee and Kirkham (1984) and Link et al. (1990), who reported on the measured water balance components of a cheatgrass-Sandberg ecosystem on the Hanford site. The selected problems are important to demonstrating the capability of the model to simulate the various processes that control the performance of a typical engineered barrier.

6.1 Verification of Infiltration

Infiltration of water into unsaturated soil has been studied intensively over the years, and diverse mathematical approaches based on variety of simplifying assumptions have been applied to predict the process. Perhaps two of the most common assumptions are those of the isothermal process in a homogeneous porous medium. For the infiltration verification, the problem of isothermal infiltration into Yolo light clay and sand, as reported by Haverkamp et al. (1977), was selected. In that report, Haverkamp et al. (1977) performed several infiltration simulations using different approaches to solve the nonlinear flow equation. To allow direct comparison of STOMP predictions with those of UNSAT-H, the head-based implicit solution (No. 4 in the Haverkamp paper) was chosen. This solution is essentially the same as that used in UNSAT-H (Fayer 2000). In addition, the approximate analytical solution to the flow equation derived by Philip and Smiles (1969) was used in the comparison. There is precedent in the use of this simulation as a verification test problem as it has been used previously by Fayer and Jones (1990).

6.1.1 Problem Description

This example is based on the simulation of ponded and non-ponded isothermal infiltration into Yolo light clay as reported by Haverkamp et al. (1977). Haverkamp et al. (1977) simulated infiltration into two soils: 1) a 250-cm deep column of Yolo light clay and 2) a 90-cm profile of an unidentified sand. For both simulations, the domain was divided into a uniform grid with 1.0-cm cells. The infiltration process was simulated with both STOMP-W (water mode) and STOMP-WAE (water-air-energy). In the STOMP-W simulations, a Dirichlet Aqueous boundary was used at the top with aqueous pressures of 0.0 cm for the Yolo light clay and 20.73 cm for the sand. The lower boundary condition was a Dirichlet boundary specified at 600 cm for the clay and 61.4 cm for the sand in the STOMP-W simulations. In addition to aqueous boundary conditions, simulations with STOMP-WAE also required specification of boundary conditions for the energy and gas phase. Both the top and bottom boundaries were specified as Dirichlet Energy, Dirichlet Aqueous, and Dirichlet Gas. An initial time step of 0.00125 hr with a maximum of 10 hrs was used in the clay and sand simulations with STOMP-W and the clay simulation with STOMP-WAE. An initial time step of 0.0000125 hr and a maximum of 0.01 hr were used in the sand simulation with STOMP-WAE. All solutions used a time acceleration factor of 1.25. Identical boundary conditions were used in UNSAT-H; however, time discretization was somewhat different. In UNSAT-H, an initial time step of 0.0125 hr and a maximum of 0.15 hr were used in the Yolo light clay simulation. For the sand simulation, minimum and maximum values of 10^{-5} and 0.0025 hr, respectively, were used. Haverkamp et al. (1977) allowed the time step to vary between 40 and 500 s (0.0111 to 0.139 hr) for the clay and used a constant time step of 5 s (1.39×10^{-3} hr) for the sand. In the nonisothermal simulations, the Somerton (1992) method was used to compute the thermal conductivity from the unsaturated and saturated thermal conductivities. The thermal properties were assumed to be identical for the sand and clay: an unsaturated thermal conductivity of 0.582 W/m K, a saturated thermal conductivity of 1.13 W/m K, and a specific heat of 700 J/kg K. Hydraulic properties were described by the Haverkamp model. Table 6.1 summarizes the coefficients used to parameterize the model for hydraulic properties.

Table 6.1. Parameters Used in the Infiltration Simulations

Parameter	Clay	Sand
θ_s ($cm^3\ cm^{-3}$)	0.495	0.287
θ_r ($cm^3\ cm^{-3}$)	0.124	0.075
α (cm^{-1})	739.0	1.611×10^6
β (unitless)	4.0	3.96
h_e (cm)	1.0	1.0
K_s ($cm\ hr^{-1}$)	4.428×10^{-2}	34.0
A (cm^{-1})	124.6	1.175×10^6
B (unitless)	1.77	4.74
h_e (cm), for the conductivity function	0.0	1.0

6.1.2 Results

Figure 6.1 and Figure 6.2 compare the results of the STOMP-W and STOMP-WAE simulations with those of UNSAT-H. Haverkamp et al. (1977) reported that convergence of the series solution requires at least 600 hr of simulation time for the Yolo light clay soil and about 0.29 hr for the sand. Figure 6.1

shows that like UNSAT-H and the analytical solutions, infiltration reaches steady state around 600 hr for the Yolo light clay. As shown in Figure 6.2, steady infiltration becomes steady at around state 0.30 hr for the sand. Thus, the STOMP converged to the established solutions for the two soils in comparable times. The results show that UNSAT-H tends to predict an initially faster approach to steady state than STOMP with the discrepancy being higher in the sand. This early arrival of water predicted by UNSAT-H is consistent with an over estimation of the unsaturated hydraulic conductivity relative to STOMP. In general, the agreement between the results of UNSAT-H (Fayer 2000) and the STOMP simulator (STOMP-W and STOMP-WAE) is quite good. This agreement essentially validates the infiltration component of STOMP-W and STOMP-WAE. The input files for this verification problem are given in Appendices C1 through C4. The associated output files are given in Appendices D1 through D4.

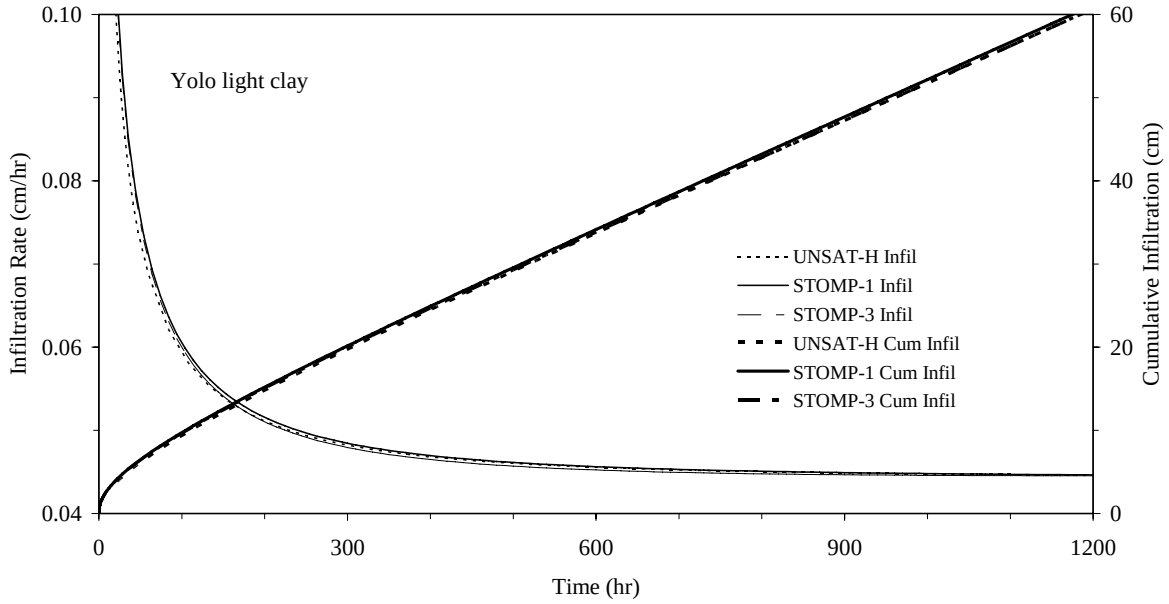

Figure 6.1. Infiltration Rate and Cumulative Infiltration Versus Time in Yolo Clay Soil as Determined Using STOMP-W (Mode 1), STOMP-WAE (Mode 3) and UNSAT-H

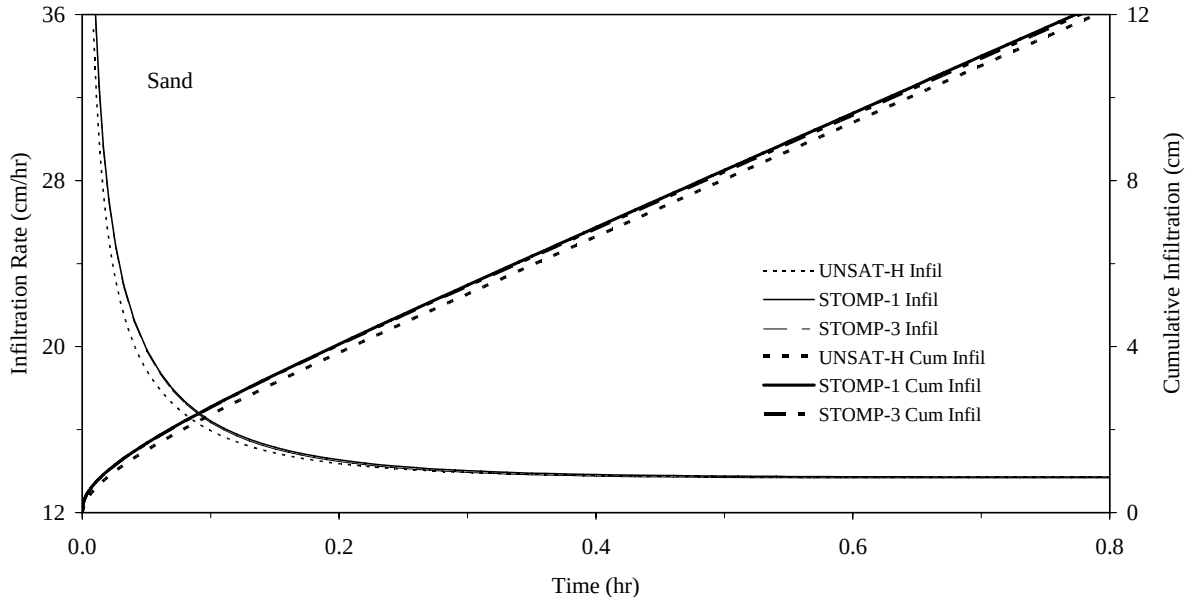

Figure 6.2. Infiltration Rate and Cumulative Infiltration Versus Time in a Sandy Soil as Determined Using STOMP-W (Mode 1), STOMP-WAE (Mode 3) and UNSAT-H

6.2 Verification of Drainage

With the introduction of more efficient techniques like the one-step (Kool et al. 1985) and multi-step (van Dam et al. 1994) outflow methods for characterizing the unsaturated hydraulic properties of soils and sediments, there is a question of the validity of these measurement techniques. Part of this concern may be because inverse flow models are used to derive the hydraulic properties from cumulative outflow (drainage) as a function of time and soil water matric potential head measured with a tensiometer at a point inside the sample. The underlying assumption of course is that flow models based on the Richards (1931) flow equation can adequately describe flow in unsaturated porous media. Kool et al. (1985) used the finite-element based parameter estimation program, ONESTEP, to fit cumulative outflow data from a one-step outflow experiment. The program estimated values for three parameters of the van Genuchten (1980) water retention function. For the purpose of drainage verification, the one-step outflow experiment was simulated with UNSAT-H,STOMP-W and STOMP-WAE using the fitted parameters reported by Kool et al. (1985).

6.2.1 Problem Description

In the experiment of Kool et al. (1985), an undisturbed core (3.95 cm long and 5.4 cm diameter) of a silt loam was obtained from a field in Virginia. The core was incorporated into a Tempe cell fitted with a ceramic plate (0.57 cm thick) at the bottom and saturated with water. After a complete cycle of drying and wetting, the core was subjected to an air pressure of 1000 cm. The drainage that resulted was monitored until it nearly ceased. Kool et al. (1985) measured the parameters θ_s and K_s in the laboratory. Three parameters, α, n, and θ_r, were inverted to obtain the best fit to the outflow data. Kool et al. (1985) simulated the ceramic plate using a constant K_s and a specific capacity of zero. For the UNSAT-H simulation, all materials must be described using the same hydraulic property model. However, this is not a limitation with STOMP as different models can be used for each soil type. To facilitate comparison

with UNSAT-H, the van Genuchten model was selected and a set of parameters derived for the ceramic that would allow the simulated plate to remain nearly saturated at suction heads up to 1000 cm (Fayer 2000).

For the STOMP simulations, the simulation domain was discretized into 89 cells with variable size. The first 10 nodes from the bottom were spaced at 0.057 cm whereas the remaining 79 were spaced at 0.05 cm. Table 6.2 summarizes the parameters for both materials. At the start of the simulation, the suction at the base of the ceramic plate was increased to 1000 cm. The Mualem (1976) conductivity model was used to describe the relative permeability. Interfacial averaging of the relative permeability was based on the geometric average. The *Solution Control Card* was used to split the simulation into three stages. The first stage simulated the first 0.5 hrs of the test and used an initial time step of 2×10^{-7} hr with a maximum allowed of 2×10^{-3} hrs. The second stage covered the period 0.5 hrs to 16 hrs with a time step that varied from 2×10^{-3} to 0.1 hr while the third stage covered the period 16 hrs to 1000 hrs with time step varying from 0.1 to 24 hrs. In the STOMP-W simulations, the top boundary was a no-flow boundary whereas the bottom was a Dirichlet aqueous. For the non-isothermal simulations, thermal properties for the ceramic and soil were described by the Somerton (1992) method. The thermal properties were assumed to be identical for the sand and clay, an unsaturated thermal conductivity of 0.582 W/m K, a saturated thermal conductivity of 1.13 W/m K, and a specific heat of 700 J/kg K. The bottom boundary was specified as Dirichlet for water and energy and zero flux for gas. The top boundary was specified as Dirichlet for water, energy, and gas. The input files for the drainage verification using STOMP-W and STOMP-WAE are presented in Appendix C5 and Appendix C6, respectively.

Table 6.2. Hydraulic Property Parameters for Silt Loam Soil and Ceramic Plate

Parameter	Silt Loam	Ceramic Plate
θ_s ($cm^3\ cm^{-3}$)	0.388	0.388
θ_r ($cm^3\ cm^{-3}$)	0.17321	0.387
α (cm^{-1})	0.04705	4.705×10^{-6}
n	1.46097	3.0
K_s ($cm\ hr^{-1}$)	5.4	0.003

6.2.2 Results

Figure 6.3 compares the cumulative outflow predicted by UNSAT-H and STOMP with the laboratory measurements and predictions from Kool et al. (1985). Neither STOMP nor UNSAT-H was able to duplicate the approximation used by Kool et al. (1985) to describe flow in portions of the core that remained saturated during the very early times of drainage. However, this difference between the models should not significantly affect the comparison because saturated conditions in the simulated core disappeared after less than 0.01 hr. There was a small discrepancy between the drainage predicted by STOMP-W in the early part of the simulation relative to the other models and the observations. The lower rate of drainage is indicative of hydraulic conductivity values in the model being too small in the early stages. This could be related to the interfacial averaging. A smaller relative hydraulic conductivity during the initial stage would restrict water redistribution. In the current conceptual model, it is assumed

that the water content is dependent only on the matric potential. However, water content is also affected by outflow rate; such an effect would need to be considered when estimating the soil hydraulic properties. The predictions could very likely be improved by using the UCODE-STOMP-W inverse model to optimize the parameters from the outflow data. Predictions with STOMP-WAE show a much better agreement with UNSAT-H and the measured data. Overall, the agreement between STOMP predictions, the observed data, and UNSAT-H is quite good. The results clearly show that STOMP is equally accurate in simulating drainage. The output files for the drainage verification using STOMP-W and STOMP-WAE are presented in Appendix D5 and Appendix D6, respectively.

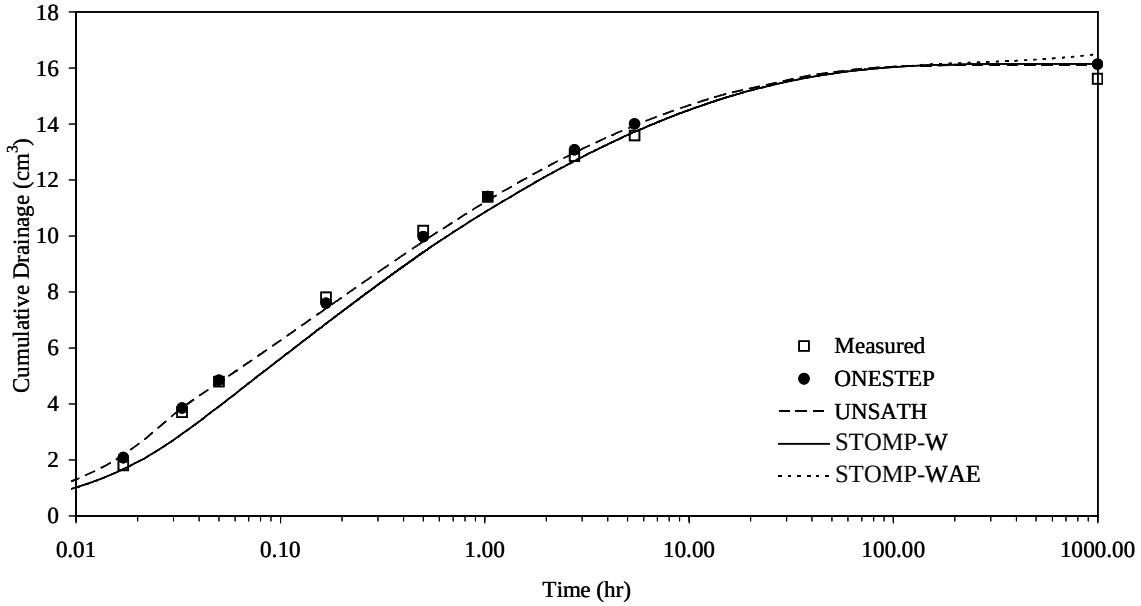

Figure 6.3. Cumulative Drainage Versus Time as Measured by Kool et al. (1985) and Versus Time Compared to Predictions of STOMP-W, STOMP-WAE and UNSAT-H. STOMP-W and STOMP-WAE are mostly indistinguishable

6.3 Verification of Heat Flow

Perhaps one of the most common assumptions made in the simulation of infiltration is that infiltration is an isothermal process. In reality, infiltration is accompanied by transformations of thermal energy that may be reflected in temperature changes. Thermal effects can be quite substantial during infiltration into very dry, fine textured soils like clays. The effects are typically smaller in coarser soils. There are essentially two thermodynamic state changes that contribute to the thermal effects, 1) a liquid–vapor phase transition and 2) a change in the potential energy and enthalpy state of liquid water that comes into close proximity to soil particle surfaces. A number of models have been developed to predict the simultaneous transfer of water and energy based on the theory developed by de Vries (1958). In unsaturated soils, water vapor flow is an important heat transport mechanism; thus, the capability to accurately simulate heat transport is a prerequisite for modeling flow in non-isothermal systems.

In this test problem, STOMP-WAE was used to simulate the diurnal variation in soil temperatures caused by a sinusoidal variation in temperature at the soil surface. This problem has been discussed previously

by Fayer and Jones (1990) and Fayer (2000). An analytical solution for this type of heat conduction problem has been reported by Campbell (1977). In that report, an analytical solution is provided for the heat-conduction problem in which the surface temperature varies according to:

$$T(0,t) = \overline{T} + A(0)\sin(\omega t) \tag{6.1}$$

where $\overline{T}$ = mean soil surface temperature, K

$A(0)$ = amplitude of soil surface temperature, K

ω = angular frequency of the soil surface temperature oscillation, hr^{-1}

t = time, hr.

Assuming a uniform soil profile of infinite thickness, the solution for a temperature wave is then given by:

$$T(z,t) = \overline{T} + A(0)e^{-z/z_d}\sin\left[\omega(t-6) - z/z_d\right] \tag{6.2}$$

where

$$\omega = 2\pi/24 \tag{6.3}$$

and

$$z_d = \sqrt{\frac{2k_h}{\omega C_h}} \tag{6.4}$$

In Equation (6.4), z_d is the damping depth, the depth at which the temperature fluctuation is reduced to 37 percent (e^{-1}) of its surface value. For this case, the angular frequency yields a complete surface temperature cycle in 24 hr. For this analysis, Equation (6.2) was adjusted such that the peak temperature occurs at noon by setting $t = t$ - 6 hr.

6.3.1 Problem Description

For the heat verification problem, a 1-m-deep soil profile consisting of loamy sand is considered. This soil type is representative of many of the near surfaced sediments at Hanford, is present in the 300 N Vadose Zone Lysimeter Facility, and is sometimes referred to as the L-soil (Rockhold et al. 1988). Following Fayer (2000), a horizontal profile is simulated to minimize water movement. Vapor flow is not included so that water contents and thermal conductivities remain constant during the simulation. The horizontal profile was discretized into a grid of 101 nodes, 1 node with a 0.5 cm spacing, 99 with a spacing of 1 cm, and one 100-cm node. The hydraulic properties for the simulation are based on the Brooks-Corey functions, the parameters of which are summarized in Table 6.3.

Table 6.3. Brooks-Corey Hydraulic Property Parameters for L-Soil

Parameter	Ceramic Plate
θ_s (cm^3 cm^{-3})	0.4326
θ_r (cm^3 cm^{-3})	0.0381
h_e (cm)	9.4
b	1.2486
K_s (cm hr^{-1})	35.3

The Burdine model was used for the relative permeability whereas a constant relative permeability was chosen for the gas phase relative permeability. The thermal properties are described by the thermal conductivity model of Cass et al. (1984). The parameters chosen were those for the lysimeter sand at 22.5°C; Table 6.4 summarizes the coefficients for the thermal conductivity model with enhanced isothermal and thermal vapor diffusion.

Table 6.4. Soil Thermal Properties used as Input in the STOMP-WAE-B Simulations

Layer	Specific Heat (kJ/kg C)	A	B	C	D	E	α_{dry}	α_{dry}	κ
1	793.1	0.60	0.80	4.5	0.22	6.0	0.267	0.160	3.585
Enhancement		9.50	3.00	3.50	1.00	3.00			
2,3,4	730.6	0.60	0.70	8.0	0.26	3.0	0.402	0.275	3.585
Enhancement		9.50	3.00	3.50	1.00	4.00			

Parameters A, B, and D have units of W/m K. The initial temperature at all nodes was set to 288K; the initial suction was set to 91531 Pa for all nodes while the gas phase pressure was fixed at 101325 Pa. The time-varying boundary conditions were applied to the west boundary. Dirichlet conditions were used for energy and water whereas a zero flux condition was used for gas. Equation (6.1) was used to predict $T(t)$, values of which were then used to create a time-varying Dirichlet condition. The boundary was subjected to a temperature variation of 10K from a mean surface temperature of 288K occurring at noon. The simulation was run for 240 hr with an initial time step of 0.01 hr and a maximum allowable time step at 0.1 hr with an acceleration factor of 1.25. The parameters used in the analytical solution are those reported by Fayer (2000), i.e., k_h = 27.448 J cm^{-1} $mole^{-1}$ K^{-1}, C_h = 1.1927 J cm^{-3} K^{-1}, and z_d = 13.26 cm. The input file for the heat flow verification using STOMP-WAE is presented in Appendix C7.

6.3.2 Results

Figure 6.4 shows the soil temperature simulated using the analytic solution and STOMP-WAE. STOMP predicted all of the features quite well; temperature increased at each depth to its maximum followed by a sharp drop to a plateau. The plateau temperatures increased with distance from the entry surface, and at the deeper locations (27 cm, 40 cm), the plateau hovered around the initial temperature. Peak temperatures also agreed well with the analytical solution.

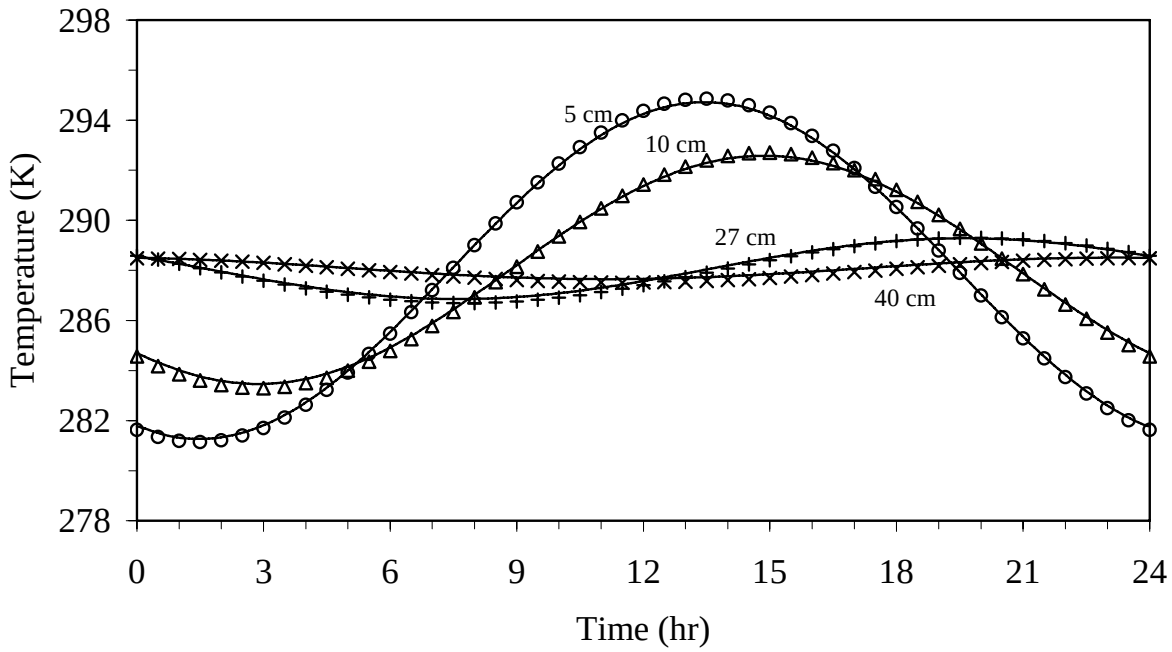

Figure 6.4. STOMP Simulated Soil Temperature (lines) as a Function of Time Compared to Predictions Using an Analytic Solution (symbols)

Figure 6.5 compares the STOMP-WAE predicted temperature profiles with those predicted by the analytical solution. The agreement between the analytical solution and the simulated temperatures at all depths and times indicates that STOMP-WAE correctly solves the heat conduction equation. More importantly, these results suggest that the use of representative physical, hydraulic, and thermal properties of Hanford sediments should allow accurate prediction of the temperature changes as saturation changes. When coupled with the inverse modeling capabilities of STOMP-WAE, thermal data and hydraulic property data from laboratory or field measurements could be jointly inverted to optimize thermal as well as hydraulic properties. The output file for the heat flow verification using STOMP-WAE is presented in Appendix D7.

6.4 Layered Soil Simulation

The rate of water flow and the distribution of water potentials in a one-dimensional soil column under steady-state conditions can be obtained by solving the Darcy-Buckingham (Darcy 1856; Buckingham 1907) flow equation. The solution for homogeneous soils at saturation is relatively straightforward. However, the problem becomes considerably more difficult for unsaturated flow in heterogeneous soils. Layering is perhaps the most common form of heterogeneity in natural and engineered systems like barriers, and numerical methods are needed to calculate the flow in soils that consist of more than one layer. Engineered barriers are being considered as a remedy for sites with buried waste. One barrier design that has been shown to work well under arid and semi-arid conditions is the capillary barrier.

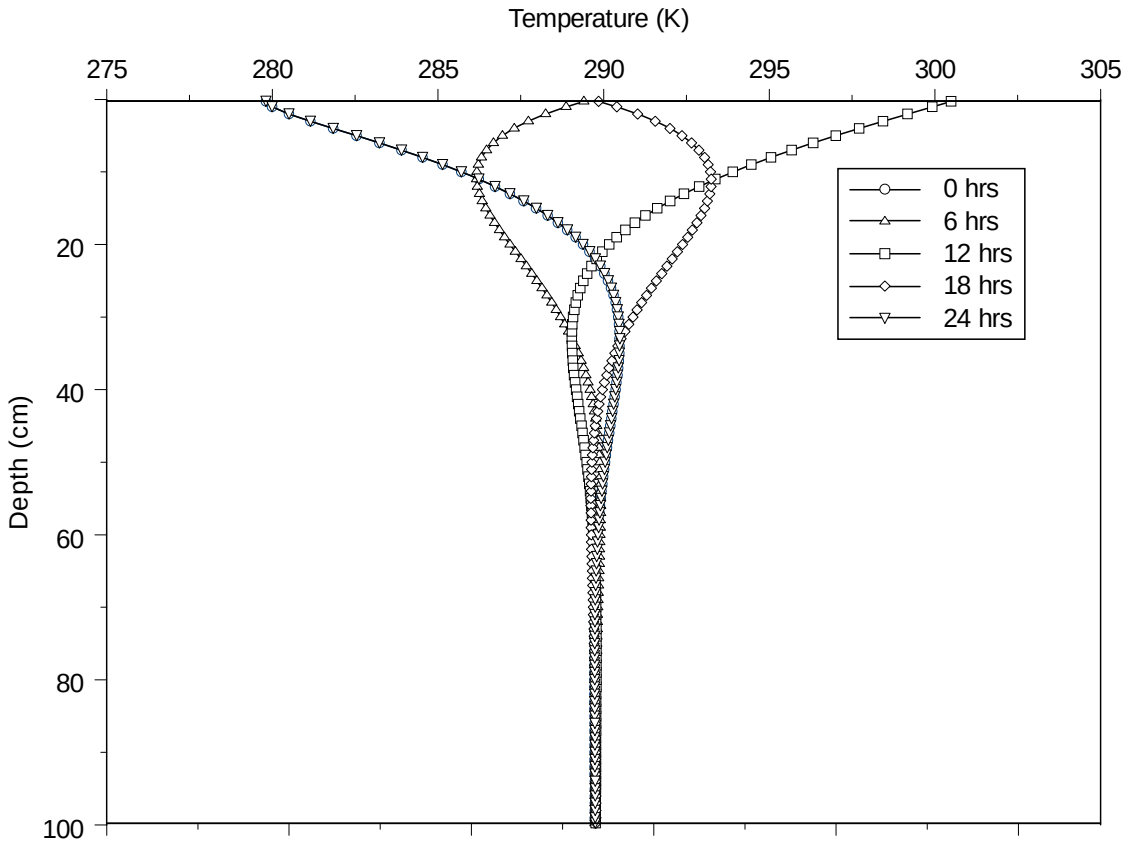

Figure 6.5. Soil Temperature as a Function of Depth as Determined by the Analytical Solution (symbols) and STOMP-WAE (lines)

Capillary barriers limit deep percolation through the difference in hydraulic unsaturated conductivity between a fine-textured layer and an underlying coarse-textured layer. Such systems are essentially layered systems, and in this example, STOMP is used to simulate flow in a hypothetical barrier using weather data from 1962 to provide the meteorological forcings at the surface.

6.4.1 Problem Description

The hypothetical barrier is a 1.5-m deep profile comprised of a 0.3-m surface layer of the Composite soil containing 15 percent by weight of gravel with a grain diameter of 0.5 to 1.0 cm (Fayer 2000). The Composite/gravel soil layer was underlain by a 1.2-m-thick layer of Composite soil. A layer of gravel with a diameter ranging from 0.6 to 1.3 cm occurred below the 1.5-m depth extending down to a depth of 5.5 m. The domain was discretized into 74 nodes with a variable spacing. The node spacing ranged from 0.1 cm at the surface and near the interfaces to 10 cm in the lower 5.1 m. The hydraulic properties of all three materials were represented using the polynomial functions described by Fayer (2000). Because these polynomials were not included in STOMP, the code was first modified to allow description of hydraulic properties via polynomial functions. The polynomial for the water retention curve, θ(h), is written as (Fayer 2000):

$$\theta = a + b\log(h) + c\log^2(h) + d\log^3(h) + e\log^4(h) \tag{6.5}$$

The hydraulic conductivity takes a similar from and is written as

$$Log\,(K_L) = a + b\log(h) + c\log^2(h) + d\log^3(h) + e\log^4(h) \qquad (6.6)$$

As noted by Fayer (2000), there is no relation between the coefficients in Equation (6.5) and 6.6). However, the polynomials are equal at each matching point. For the water retention polynomial, the derivatives must also be equivalent at each matching point.

A *Potential Evaporation Aqueous* boundary condition option was also included in STOMP-W to allow direct comparison with UNSAT-H. Use of this boundary condition requires specification of the potential evaporation rate and associated units [L/T] as well as the maximum allowed capillary pressure head and associated units. Initial head values for each node were obtained from the output of a simulation done for the year 1961. At the top boundary, a *Potential Evaporation Aqueous* boundary was imposed. Values of the potential evaporation rates for the upper boundary were calculated on a 12-hr interval using the Penman equation as described by Doorenbos and Pruitt (1977) and meteorological data from the HMS using a 12-hr time step. Following Fayer (2000), the maximum capillary head was fixed at 1×10^5 cm. Using this condition, however, precluded applying precipitation on the surface boundary. Precipitation was therefore applied as a source along the surface nodes using STOMP's *Source Card*. Hourly precipitation data were obtained from the HMS for 1962 and converted to a volumetric rate (cm^3/hr) based on the surface area of the node over which the infiltration occurred. A unit hydraulic gradient was chosen as the lower boundary condition. The unit gradient is a reasonable choice given the distance of the lower boundary. At 5.5 m, this boundary was outside the range where upward migration of water could influence the water balance.

6.4.2 Results

An important consideration in modeling infiltration and redistribution in layered sediments is the selection of an effective saturated hydraulic conductivity at cell boundaries. In STOMP, the relative hydraulic conductivity at cell boundaries is calculated through use of full upstream weighting of the arithmetic, geometric, or harmonic means of values from adjacent cells. In layered sediments in which flow is parallel to layering, the recommended average is the arithmetic mean. For flow perpendicular to layers, the harmonic mean is the recommended averaging procedure. If the hydraulic conductivity varies smoothly, the geometric mean is the recommended average. The arithmetic mean gives the highest value of relative conductivity, the harmonic mean gives the lowest and the geometric mean yields a value intermediate to arithmetic and harmonic means.

Figure 6.6 compares the distribution of water content within the barrier and underlying layers as predicted by STOMP-W using two different approaches to calculating the cell conductivities at the boundary. Figure 6.6a shows the predicted water content profiles calculated using geometric averaging of the hydraulic conductivity whereas Figure 6.6b shows results obtained with harmonic averaging. Both profiles show a discontinuity in the water content at the layer interfaces with an increase in moisture at the 150-cm depth with a sharp decrease below this depth. Figure 6.6a and Figure 6.6b also highlight differences due to the averaging method used for the hydraulic conductivity at the cell boundaries. Geometric averaging led to

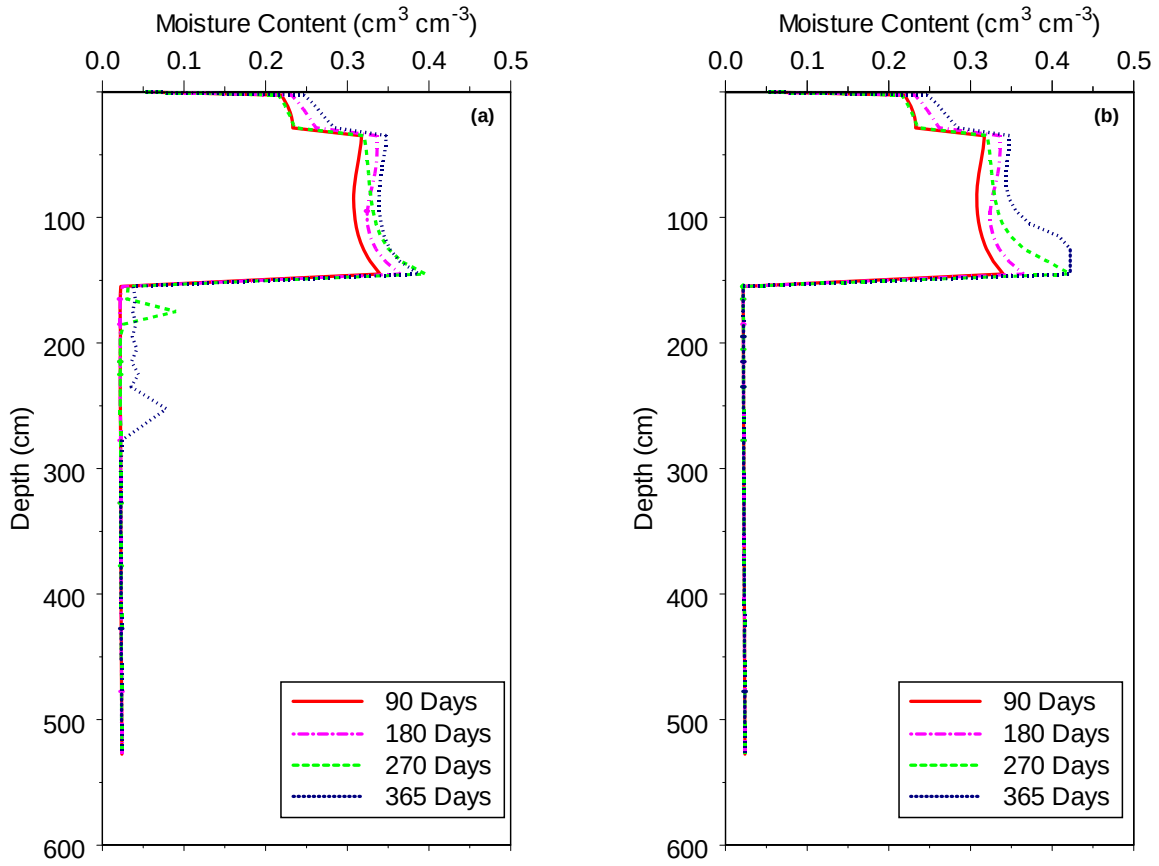

Figure 6.6. STOMP Simulated Water Content Profiles within a Layered Soil with the Effective Saturated Hydraulic Conductivity at the Cell Boundaries Determined by (a) Geometric Averaging, and (b) Harmonic Averaging

dispersive errors that manifest as sharp spikes in moisture in the 150 to 275-m depth interval (Figure 6.6a). Use of the harmonic average does not give rise to these features (Figure 6.6b).

The capillary break causes water to be retained within the fine-textured layer. It has been shown by analytical methods that the lateral diversion of water over a capillary barrier interface is maximized as the soil-particle size contrast becomes infinitely large. However, practical limitations affecting interface integrity and slope stability may restrict the contrast in particle size. In a layered soil system such as the one described here, the conductivity will be non-uniform throughout even if the soil is saturated. Just below the capillary break that separates the high and the low permeable layers, a regime with hydrostatic capillary pressures develops and downward movement of water is restricted. In a sloped, two-dimensional, layered system, the majority of flow would occur along the layer of higher hydraulic conductivity with less flow taken by the layers with lower hydraulic conductivity. The increase in storage capacity in the fine textured layer and the reduction of downward movement of water is the coarse layer is the fundamental basis of capillary breaks and the rationale behind their use in surface barrier designs.

Such a configuration impacts the overall performance of an engineered cover and the potential for remobilization of buried contaminants in real systems. In a study of chloride transport in two-layered combinations of loamy sand, sandy loam, and silt loam soils, Ghuman and Prihar (1998) found that the depth of migration was less with a fine-over-coarse sequence of layering than in a coarse-over-fine after the same amount of water was applied. This is attributed to the high water retention capacity of the fine top layer and less complete and slower redistribution of water because of smaller suction in the lower coarse layer. Layering of soil profiles can therefore be expected to reduce deep drainage and ultimately recharge rates relative to those for monolithic profiles. Figure 6.7 shows the measured precipitation and predicted drainage for the layered soil resulting from the STOMP-W simulation.

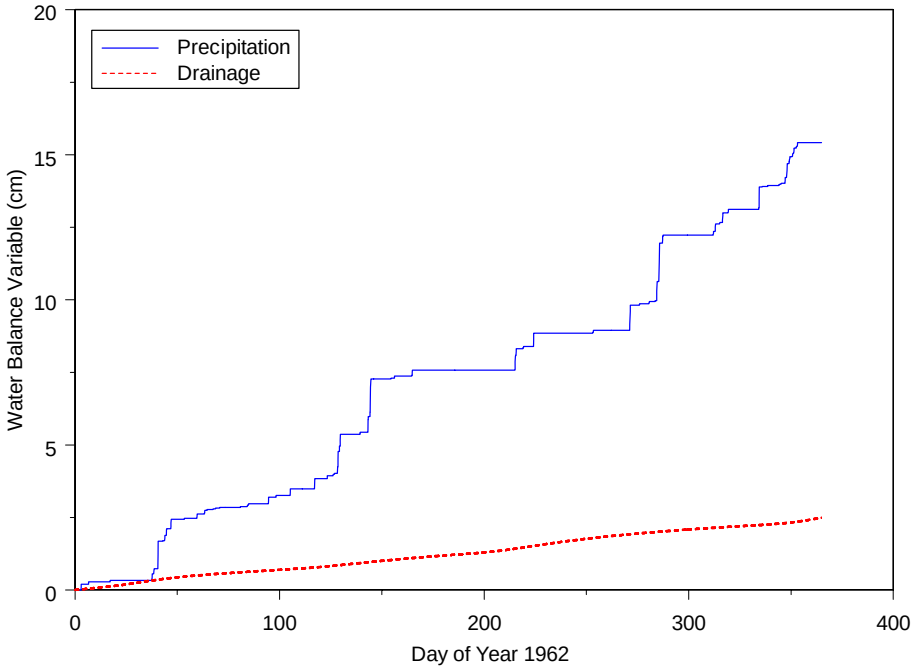

Figure 6.7. Water Balance Components for the Layered Soil Profile

Although the *Potential Evapotranspiration* boundary condition was incorporated into STOMP-W, no attempt has been made to predict evaporation as conceptualized in UNSAT-H. Thus, comparisons are limited to the predicted water content profile (Figure 6.6) and drainage. Total precipitation intercepted by the soil surface was 15.41 cm while the cumulative drainage was 2.49 cm, or 16.15 percent of precipitation. In contrast, Fayer (2000) reported a total precipitation of 15.39 cm, evaporation of 12.85 cm, and drainage of 1.662 cm, or 10.8 percent of precipitation. Actual evaporation was about 12.8 cm, or 8 percent of the annual potential evaporation of 161.1 cm (Fayer 2000). Because evaporation is not included in the STOMP-W water balance, predicted drainage is about 1.5 times that of UNSAT-H and the storage change is somewhat smaller. These results highlight the importance of choosing the correct conceptual model. On the Hanford site, potential evapotranspiration typically exceeds precipitation whereas actual evapotranspiration equals precipitation (Gee and Hillel 1988). Although this suggest that most of the water stored in the soil will eventually be evaporated or transpired, it is difficult to predict the actual rates of water loss. Potential evaporation rates are therefore not the best indicators of actual evaporation. In the next verification problem, STOMP-WAE-B is used to simulate water balance in the same profile while considering evaporation.

6.5 Infiltration and Heat Flow in a Layered Soil

As discussed previously, natural soils and sediments are typically layered, and infiltration is accompanied by transformations of thermal energy that is often reflected in temperature changes and changes in flow behavior. Several models have been developed to predict the simultaneous transfer of water and energy based on the theory developed by de Vries (1958). However, most differ in the extent to which the de Vries (1958) theory is incorporated and how well the flow and thermal transport equations are coupled. In this example problem, STOMP-WAE, which is enthalpy based with tightly coupled mass and energy equations, is compared to UNSAT-H. The layered soil flow simulation from Section 6.4 was repeated with coupled heat flow to demonstrate the simultaneous flow of water and heat. Recall that this simulation focused on the response of a hypothetical protective barrier under a PET surface boundary condition. The PET values were calculated using the Penman equation modified by Doorenbos and Pruitt (1977) and meteorological data from the HMS using a 12-hr time step.

6.5.1 Problem Description

The input file used in Section 6.4 was modified for this example to include soil thermal properties, momentum and thermal roughness lengths, initial conditions (soil water suction and temperatures) derived from the end of Day 143, and atmospheric data. The only precipitation for the simulation period occurred on Day 144 on which 13.0 mm was recorded. Thermal conductivity parameters and enhancement factors for the barrier materials are based on the work of Cass et al. (1984). The parameters for Portneuf silt loam at 32.5°C were used for the composite-gravel mix (compgrav) whereas the parameters for the lysimeter sand at 22.5°C were used for the composite soil (compos1) and the gravel layer. Enhancement of non-isothermal vapor flow was ignored. The measurement heights for temperature and wind speed were 0.914 and 15.24 m, respectively. There is much theoretical and experimental evidence that the momentum and thermal roughness lengths differ by at least one order of magnitude; however, to simplify the problem and allow comparison with the UNSAT-H results, the two roughness lengths were assumed equal with a value of 4.9×10^{-4} m. Soil water suction simulated at the end of Day 143 with STOMP-W was used to initialize the model. Soil temperatures were initialized using data from the end of Day 143. The historical average at the 91.4-cm depth for May (15.9°C) was applied to all nodes (Fayer 2000).

6.5.2 Results

Figure 6.8 shows the surface energy balance for the 3-day period. The temporal pattern in the heat flux densities has been shown in Section 3 to be dependent on a number of factors. For a bare surface, these factors include precipitation, wind speed, time of year, and near-surface soil moisture content. Figure 6.8 shows considerable variability even for the short 3-day period. The net radiation, calculated from the sum of net long-wave and short-wave radiation showed a range of over one order of magnitude, vary from -43 W m^{-2} to 405 W m^{-2}. Cloud cover and precipitation in the early part of the simulation resulted in low net radiation and other energy fluxes. Up until noon of day 143, most of the net radiation was partitioned as latent-heat flux. It is known that high winds can produce large latent-heat fluxes even after only light to

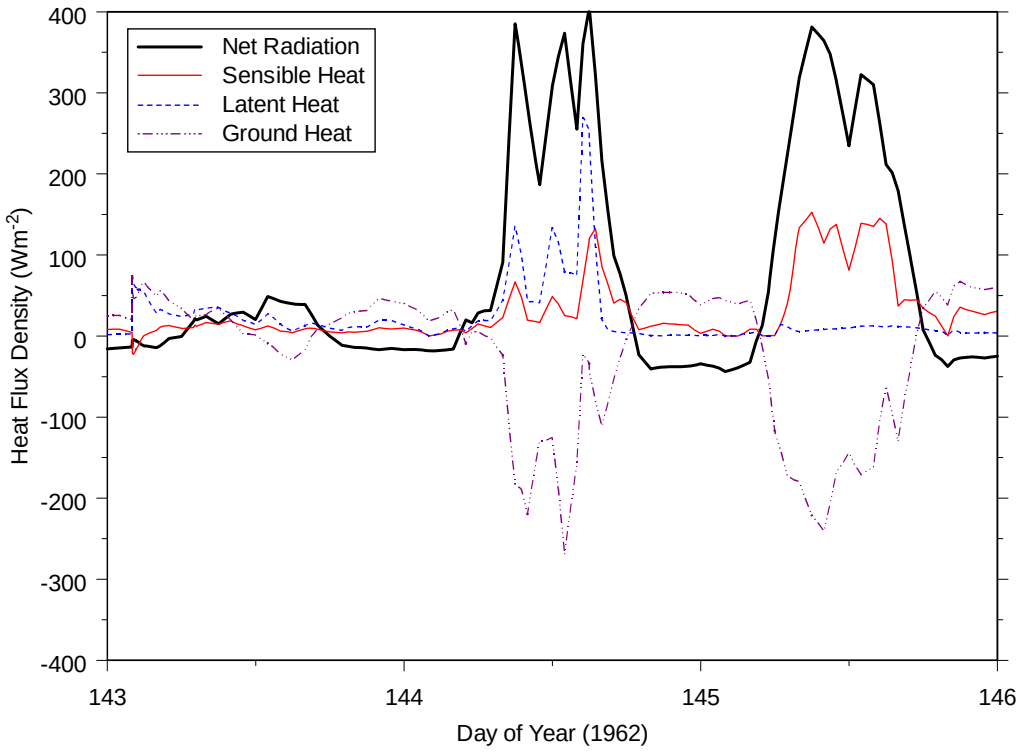

Figure 6.8. Predicted Energy Fluxes at the Surface of a Layered Soil with Heat Flow

moderate rainfall events, such as occurred on Day 143. Shortly after the start of the simulation on Day 143 and on a few other occasions, latent heat also exceeded net radiation. This means that essentially all of the incoming radiation was converted to evaporation. In order for the latent heat to exceed net radiation, additional energy is required and would have come from either soil heat flux or advected sensible heat. These results show that on occasional increases in latent-heat flux above the net radiation were accompanied by negative values of sensible heat flux, which is indicative of surface cooling. Subsequent clear dry days (144, 145) led to increased net radiation with the peak occurring around noon, as expected. Around day 144.3 all of the components of the energy balance showed sharp changes with latent heat, sensible heat, and net radiation being almost equal. Increases in latent-heat flux can occur as result of wind-induced evaporation from the soil surface even without precipitation. Sensible-heat flux increased because of surface heating, which in turn caused a downward flux of heat through the soil surface. As time progressed and radiation increased, there was a significant shift in the partitioning of energy with most of the net radiation being converted to latent-heat flux. Sensible-heat flux was mostly positive during the day and negative during the night because of surface cooling. In contrast, ground-heat flux was mostly negative during the day because of surface heating and positive at night as heat moved upward to the cooler surface. The results are consistent with theoretical predictions and are also qualitatively similar to those of UNSAT-H. The higher temporal variability in the STOMP predictions relative to those from UNSAT-H are due to the use of hourly and a fixed time step of 0.5 hrs. Slight differences in absolute values of the energy balance components between and STOMP and UNSAT-H are also evident. These differences can be expected given that the complete thermal balance equation is solved in STOMP-WAE (White and Ward 2004). For example, latent-heat flux includes the contribution of evaporation and condensation whereas in UNSAT-H it does not; relative air permeability in UNSAT-H

is always 1.0 whereas in STOMP-WAE, it varies with aqueous saturation. Similarly, calculating ground heat flux includes the contribution of energy transport by water in the vapor phase while the sensible heat accounts for energy transfer by radiation, all mechanisms that are ignored in UNSAT-H.

Figure 6.9 and Figure 6.10 show the time series of soil water suction and water content at the surface. Sharp decreases in soil water suction and accompanying increases in water content occurred with precipitation events. Sharp increases in suction and decreases in water content occurred at or shortly after increases in latent-heat flux. The largest water contents and lowest suctions occurred between day 143 and day 144 in response to the precipitation events. Water content at the surface increased to over 0.40 $m^3\ m^{-3}$ and suction decreased to around 1 cm. Evaporation resulted in gradual reduction in water content and an increase in suction until around day 144.5 when the rate of decline increased dramatically. This change in the rate of drying occurred in response to the increase in net radiation and the concomitant increase in the evaporation rate (Figure 6.8).

The largest increase in suction and decrease in moisture at the surface occurred in the afternoon of day 144 when net radiation and temperature peaked. Desiccation of the surface node resulted in a suction of about 1.9×10^6 cm just after noon on day 144 (Figure 6.9) whereas water content decreased to around 0.02 $m^3\ m^{-3}$ (Figure 6.10). These dry surface conditions caused a significant shift in the energy balance. Shortly after noon on day 144, the latent heat decreased and sensible-heat flux increased considerably. Latent-heat flux is strongly influenced by soil moisture conditions and as the surface node dried out, evaporation essentially ceased. Drying out of the surface node resulted in the net radiation being partitioned mostly between sensible-heat flux and ground-heat flux. This result is significantly different from UNSAT-H. Qualitatively, these results are similar to those of UNSAT-H, but again the absolute values are quite different. For example, the UNSAT-H simulations showed a steady increase in the latent-heat flux on day 145 until around until 1400 hr. By that time, the surface node has dried to a suction head of 6.2×10^5 cm.

Nevertheless, STOMP is able to simulate the energy balance quite well, and the responses are physically consistent with expectations. On overcast days and days with precipitation, soil heat flux and net radiation provided very little surface warming, so soil- and sensible-heat fluxes remained quite low (less than 50 $W\ m^{-2}$). Drying of the surface nodes resulted in most of the net radiation being partitioned as sensible-heat flux and to a lesser extent, soil-heat flux. Under these conditions, sensible-heat flux approached the net radiation while latent heat flux went to zero. At night, sensible heat became positive and net radiation became negative as energy moved upward from the warm soil to the cool air.

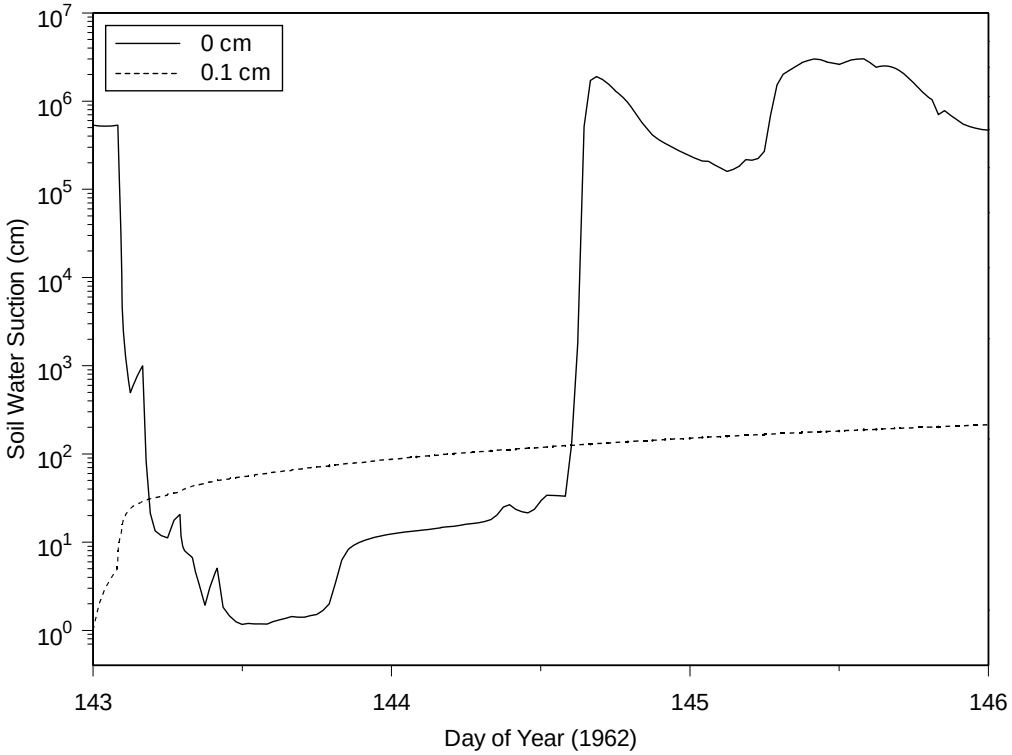

Figure 6.9. Predicted Soil Water Suction at the 0.0 and 0.1 cm Depths in a Layered Soil with Heat Flow

Suction at the surface continued to increase, reaching a maximum of about 1.6×10^6 cm by noon of day 144 and another by noon of day 145. Continued drying of the surface node led to a decline in latent-heat flux and a repartioning of net radiation, mostly into sensible-heat flux as shown in Figure 6.8. Near-surface moisture showed a steady decline until the sharp increase in incoming solar radiation occurred just after day 144. In general, the predicted trends and values of suction and water content are quite similar to those predicted in UNSAT-H. The biggest difference is in the late afternoon predictions of suction by STOMP on day 144. STOMP showed a much smaller increase in suction than UNSAT-H. Furthermore, the surface and subsurface node at 0.1 cm did not become equal as in UNSAT-H. The generally larger suctions and lower water contents at the surface are indicative of increased vapor diffusion compared to the UNSAT-H simulations. At high diffusion rates, the flow of vapor to the surface would cause an over estimation of simulated evaporation regardless of the lowest value of hydraulic conductivity. Conversely, low diffusion rates would result in lower evaporation rates because of the limited amount of soil water that could be transmitted to the surface.

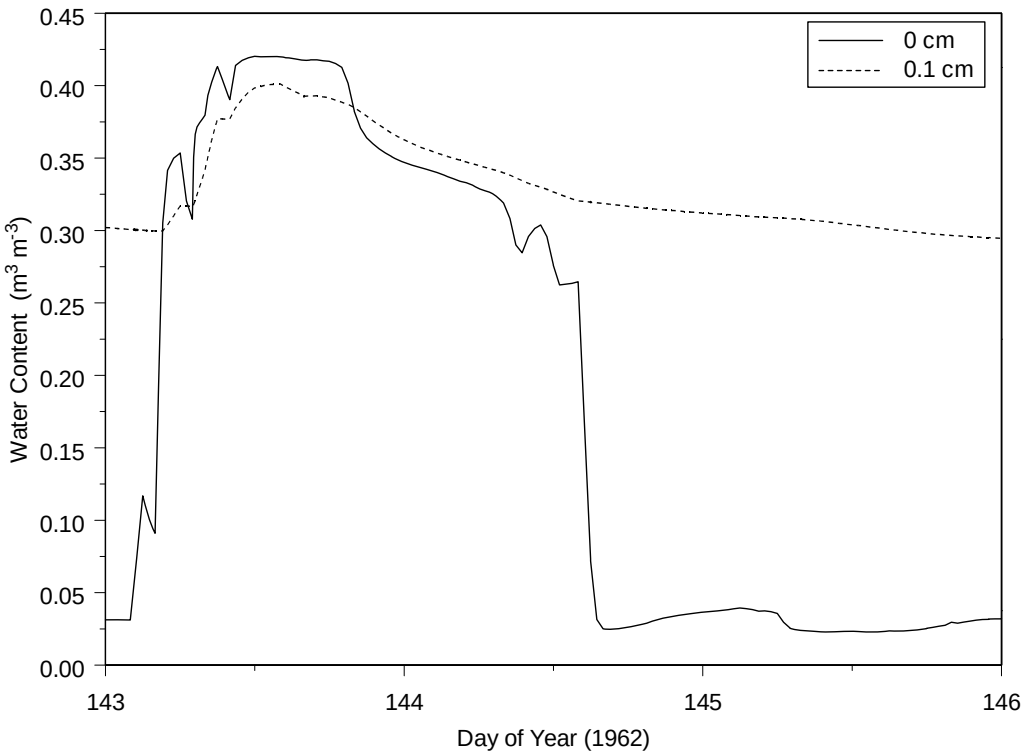

Figure 6.10. Predicted Volumetric Soil Water Suction at the 0.0 and 0.1 cm Depths in a Layered Soil with Heat Flow

Figure 6.11 shows the temporal development of temperature in the air and at the soil surface. The temperature peaks show a relatively even spacing over time occurring between the noon peak of net radiation and the 1500-hr peak in air temperature. In general, the surface temperature remained higher than the air temperature throughout the 3-day period. Large differences between ground surface temperature and air temperature were usually accompanied by positive values of ground-heat flux. This observation is consistent with heat moving up towards the surface because of lower surface temperatures. Such an occurrence would result in a decline in soil temperature. Surface temperatures in the afternoon of days 145 and 146 exceeded the air temperature by between 15 ^{o}C and 25 ^{o}C, with the difference increasing with net radiation. Simulation of the layered soil profile in which fine-textured sediment overlaid coarser sediment has been shown to reduce recharge rates relative to those for monolithic profiles. As shown in Figure 6.11, simulations with STOMP-W predicted 2.49 cm of drainage through the hypothetical barrier whereas potential evapotranspiration was 161.1 cm. Figure 6.12 compares the precipitation and actual evaporation for the 3-day period simulated with the nonisothermal STOMP-WAE. For the simulation period, total precipitation was 1.32 cm; the predicted potential evaporation was 1.4 cm whereas the predicted actual evaporation was 0.234 cm. Evaporation in this case was only 18 percent of the precipitation amount and 17 percent of the potential rate. Clearly, potential evaporation rates are inappropriate as indicators of actual evaporation as the two are only equal under very specific conditions.

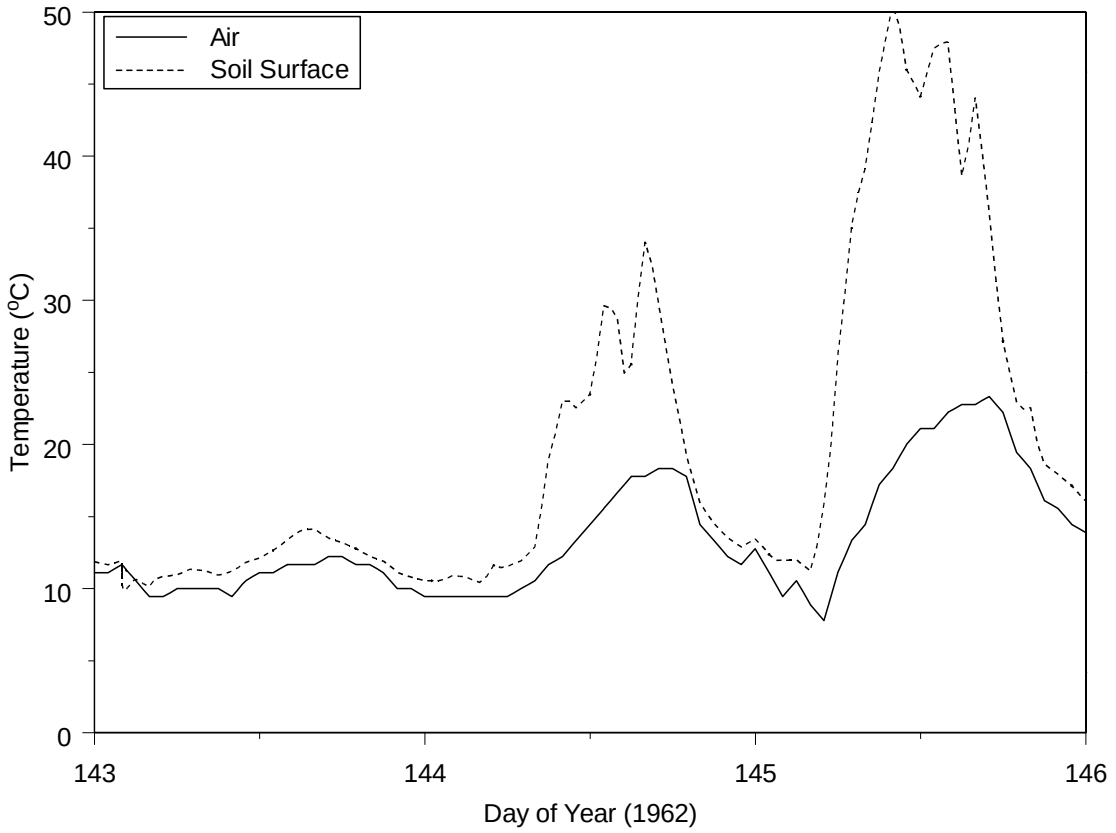

Figure 6.11. Predicted Air and Soil Surface Temperatures in a Layered Soil with Heat Flow

On several occasions, potential and actual evaporation rates were equal. Around this same time, increase solar radiation and latent-heat flux led to desiccation of the surface node and a sharp increase in soil water suction. This increase in suction essentially curtailed latent-heat flux and evaporation. At this point, actual evaporation became less than the potential rate. In the UNSAT-H simulation of this problem, Fayer (2000) reported actual evaporation of 5.57 mm for the 3-day period, compared to 3.75 mm or the same period in the isothermal simulation of the layered soil with similar time step control. Recall that in the simulation of drainage from the layered soil without heat flow, total drainage was about 18 percent of the total precipitation. In the simulation with heat flow, drainage amounted to 0.191 mm.

The larger evaporation amount predicted by UNSAT-H is due mostly to the different surface conditions predicted by the two models. UNSAT-H predicted a decline in soil water suction of about 4 orders of magnitude between day 145 and 145.5 whereas STOMP-WAE showed a decrease of less than one order of magnitude. Such a large decrease in suction would have been sufficient to keep actual and potential evaporation rates very similar in UNSAT-H while the rates diverged in STOMP-WAE. Accurate simulation of these processes therefore requires an appropriately coupled model.

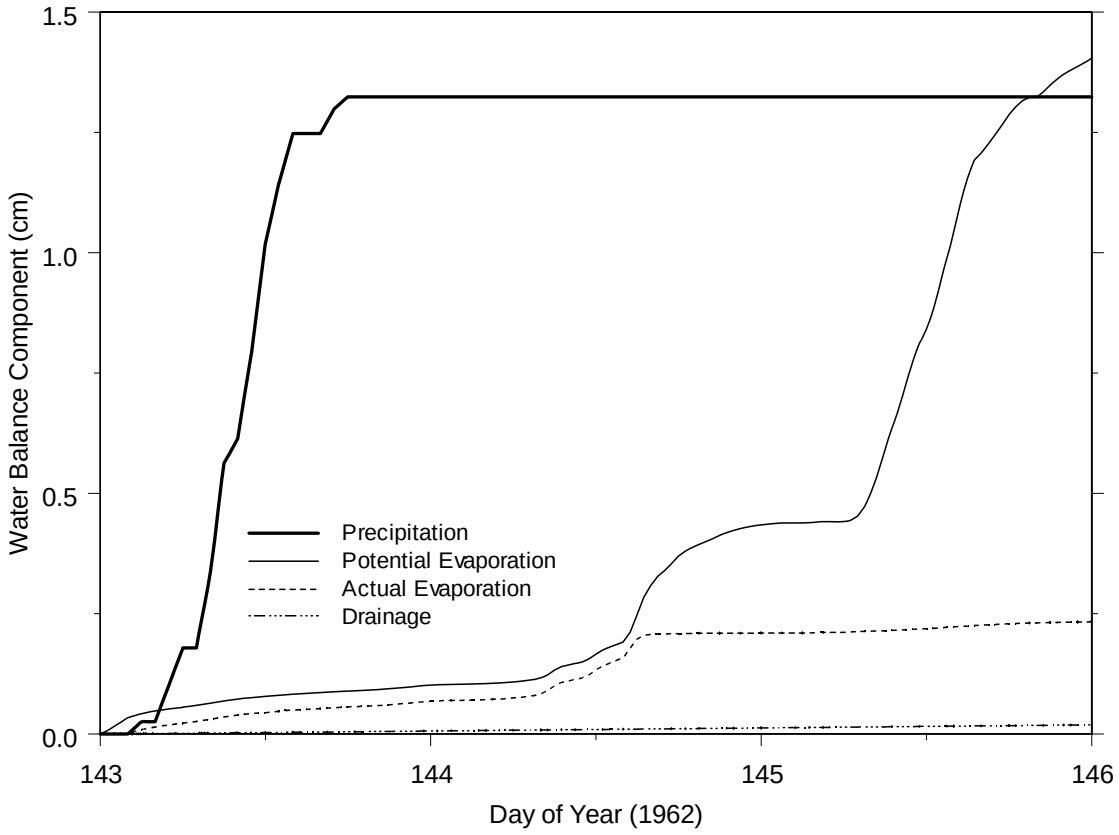

Figure 6.12. Water Balance Components for the Layered Soil

These results clearly show that STOMP-WAE is capable of simulating the coupled flow of mass and energy in physically complex systems. In this test problem, the code calculated the energy balance quite well and generated responses to the meteorological forcings that were consistent with expectations and results from UNSAT-H to the extent that they could be compared. The model is also capable of partitioning intercepted rainfall into infiltration and evaporation. An important difference between STOMP-WAE and other commonly used codes is its capability to predict actual evaporation as a function of the soil water energy status rather than relying on soil water content, drying time, or other empirical functions. As described in the theory section, actual evaporation is calculated as a function of the water energy state using the Shuttleworth and Wallace (1985) model and is currently the only fully coupled model capable of such calculations in multiple dimensional domains.

6.6 Simulation of Evapotranspiration at the 300 Area Grass Site

As part of a study to quantify recharge rates at arid waste sites, Gee and Kirkham (1984) conducted a field study to measure and predict water movement at a grass-covered field site located on the DOE's Hanford site near Richland, Washington. The grass site is located 2 km south of the 300 North Lysimeter site, formerly known as the Buried Waste Test Facility (BWTF). Both direct measurements of actual drainage and indirect measurements of changes in moisture profiles confirmed that water moved below the root zone and is lost to deep drainage during periods of low evapotranspiration (Gee and Kirkham 1984). Although the average annual rainfall at the Hanford site is 160 mm, precipitation in the 1983 test year exceeded 280 mm with nearly 75 percent occurring during the winter months (January, February, March,

November, and December). Comparative field studies of cheatgrass with Sandberg's bluegrass were also conducted at this site to gain insight into the plant characteristics that contribute to success in water-limited habitats (Link et al. 1990). Measurements of plant phenological development, stomatal conductance, xylem pressure potential of these grasses, and soil water contents were also made in 1986 and 1987. Measurements of the water balance components during two wet years, 1983 and 1984, indicated a drainage rate of over 5 cm/yr from the site vegetated with cheatgrass (*Bromus tectorum L.*) and Sandberg's bluegrass *(Poa sandbergii Vasey)*. Stomata1 conductance, transpiration, and xylem pressure potential measurements made during 1986 indicated that water stress developed earlier and to a greater degree in Sandberg's bluegrass than in cheatgrass. Instantaneous profile measurements conducted at the grass site were inverted using STOMP-UCODE to obtain field-scale hydraulic properties. These parameters along with measured phenological data were used as input to STOMP-WAE-B to simulate infiltration and redistribution for the year 1983. Measured water balance data and canopy resistances were used for validating model predictions.

6.6.1 Problem Description

The vegetated area, known as the grass site, used in the water balance study by Gee and Kirkham (1984) was selected for simulation. The grass site is located in a slight depression about 900 m wide and several thousand meters long. The vegetation is typical of disturbed areas on the Hanford site where natural revegetation has occurred and consisted of cheatgrass (*Bromus tectorum L.*) and Sandberg's bluegrass *(Poa sandbergii Vasey)*, which comprised 35 and 27 percent of the total cover, respectively. Both grasses are winter annuals with growth confined to the late fall and early spring. The soil at the site is well drained and nearly uniform to a depth of 3.5 m. The top 0.6 m is classified as loamy sand with 79 percent sand, 17 percent silt, and 4 percent clay whereas the 0.6 m to 3.5 m depth is classified as sand. A rock/gravel layer, estimated to be several m thick based on adjacent outcrops, lies below the 3.5-m depth. The water table is below 10 m. Meteorological data, including precipitation, air temperature, humidity, and wind speed, were collected at the site. Incoming solar radiation data were obtained from the HMS, approximately 27 km northwest of the grass site. Soil water content profiles were measured to determine storage whereas evapotranspiration was determined from the weighing lysimeters at the nearby 300 N lysimeters. Soil water contents were measured by neutron probe at 15-cm intervals to a depth of 165 cm and 30-cm intervals down to 345 cm; measurements were made at approximately 2-week intervals at 25 locations on a 6-m by 6-m grid.

Figure 6.13 shows the conceptual model for the problem in which the governing equations for water, energy, and air are to be solved. Details on the governing partial differential equations and the accompanying solution schemes are provided in White and Oostrom (2000). The site was simulated with a one-dimensional soil domain assumed to be comprised of four layers. This configuration is based on the analysis of Zhang et al. (2004) in which field-scale hydraulic properties for the site were obtained using inverse modeling with the STOMP-UCODE combination. The domain was discretized into 150 nodes with variable spacing. A node spacing of 2.5 cm was used from the surface to a depth of 3.5 m whereas a variable spacing with nodes ranging from 0.25 m to 30.0 m was applied from 3.5 m down to the water table at 10.0 m.

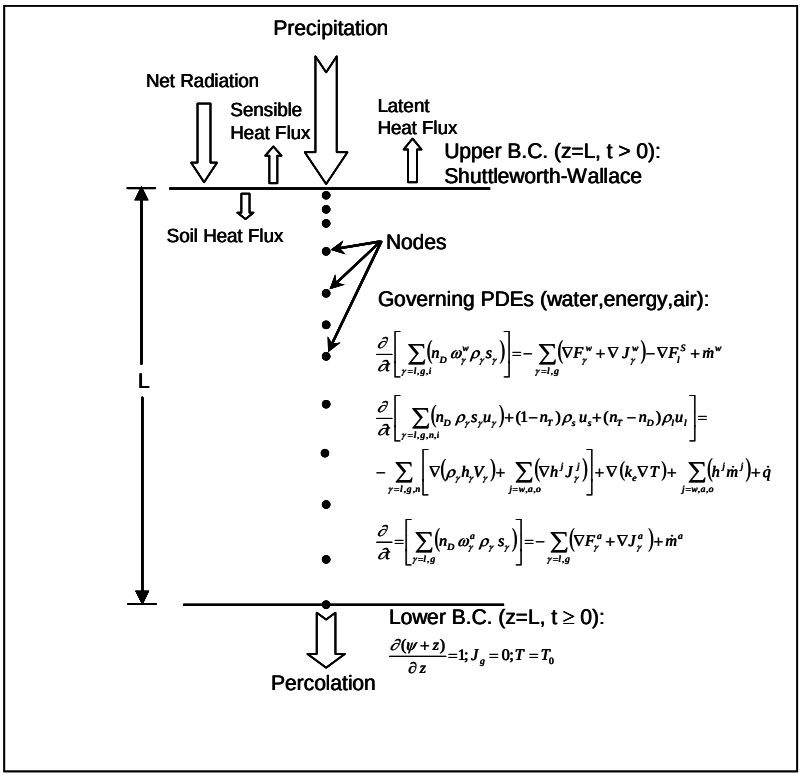

Figure 6.13. Conceptual Model for the Grass Site Used in STOMP-WAE-B

The hydraulic functions were described by the van Genuchten (1980) model for water retention:

$$\theta(\psi) = \begin{cases} \theta_r + (\theta_s - \theta_r)\left[1 + (\alpha|\psi|)^n\right]^{-m} & if \quad \psi < 0 \\ \theta_s & if \quad \psi \geq 0 \end{cases} \tag{6.7}$$

where θ_s and θ_r are the saturated and residual water content, α and n are fitting parameters, and m is a constant that is commonly approximated by $m = 1\text{-}1/n$. Combining Equation (6.7) with the Mualem (1976) model yields the hydraulic conductivity function as

$$K(\theta) = K_s\left(\frac{\theta - \theta_r}{\theta_s - \theta_r}\right)^{0.5}\left\{1 - \left[1 - \left(\frac{\theta - \theta_r}{\theta_s - \theta_r}\right)^{1/m}\right]^m\right\}^2, \quad \theta_r \leq \theta \leq \theta_s \tag{6.8}$$

or

$$K(\psi) = \begin{cases} K_s \dfrac{\left\{1 - (\alpha|\psi|)^{n-1}\left[1 + (\alpha|\psi|)^n\right]^{-m}\right\}^2}{\left[1 + (\alpha|\psi|)^n\right]^{0.5m}} & if \quad \psi < 0 \\ K_s & if \quad \psi \geq 0 \end{cases} \tag{6.9}$$

where K_s is the saturated hydraulic conductivity. Table 6.5 summarizes the soil hydraulic properties used as input. It should be noted that these parameters were derived from the inverse analysis of data collected during an instantaneous profile infiltration experiment conducted at the site (Zhang et al., 2004). The Corey function was chosen for the relative gas permeability function. An irreducible gas saturation of 0.1 was assumed for each layer while the residual water saturations were assumed equal to those used in the *Saturation Function* card.

Table 6.5. Soil Hydraulic Properties used as Input in the STOMP-WAE-B Simulations

Layer	Soil Depth (m)	K_s ($m\ s^{-1}$)	α (m^{-1})	n (-)	θ_s ($m^3\ m^{-3}$)	S_r (-)	$\theta_r^{\dagger}$ ($m^3\ m^{-3}$)
1	0–0.225	2.79×10^{-3}	11.3	1.214	0.258	0.213	0.055
2	0.225–0.375	1.20×10^{-4}	10.5	1.218	0.195	0.145	0.028
3	0.375–0.525	7.13×10^{-5}	17.0	1.336	0.150	0.145	0.022
4	0.525–3.500	2.93×10^{-5}	17.6	2.024	0.143	0.277	0.040

Solution of the problem also requires soil thermal properties. Thermal properties were not measured for the specific site but were estimated using particle size distributions and the water retention function based on the method of Johansen (1975). Soil albedo information is also required for input in the *Thermal Properties Card*. No Albedo measurements were made for the site; they were estimated using the soil Munsell color approach (Post et al. 2000). Ground-surface albedo is known to be a function of the solar altitude and aqueous water saturation (Pleim and Xiu 1995). For this simulation, the variation of ground surface albedo with solar angle was simulated using the model of Briegleb et al. (1986), as described in Equation (3.29). For this simulation, the parameter *C* was set to 0.4, the default value for arable grass, grassland, and desert. The variation of soil albedo with soil type and moisture was modeled according to Equation (3.30) using literature values (Post et al. 2000; Muller and Décamps 2000) to define α_{wet} (the soil albedo when the surface is near saturation); α_{dry} (the dry soil albedo, maximum albedo); and the albedo attenuation factor, κ, which controls the rate of decreased albedo with moisture, and θ, which is the moisture content at the surface. Table 6.6 summarizes the soil thermal properties used in the simulation. For this simulation, the Cass et al. (1984) thermal conductivity model with enhanced isothermal and thermal vapor diffusion was used.

Required vegetative input for the simulation includes parameters describing the phenological cycle, the root distribution, the leaf area index, the plant area index, the crop coefficient, and albedo. Link et al. (1990) recorded the phenological cycle for the two grass species. These data were used to determine the input information for the simulation. The root length density functions for the two grasses were not measured. However Link et al. (1990) reported that roots of the large cheatgrass plants extended to a maximum depth of between 0.45 m and 0.50 m, reaching into the coarse sand zone. The maximum root depth observed on large Sandberg's bluegrass individuals was 0.35 m. For both species, the maximum root mass was observed at about 0.10 m. To obtain the required input parameters, measured root distribution profiles for cheatgrass and a bunchgrass reported by Cline et al. (1977) were used to fit the Vrugt (2002) model after normalizing the distributions to a probability density function. Leaf area indices were estimated from the plant area index as 3.6 × PAI (Williamson et al. 1987). The resulting estimates of LAI based on PAI are in good agreement with the value of 1.1 reported for grassland by Baldocchi et al. (2004). Table 6.7 summarizes the plant parameters.

Table 6.6. Soil Thermal Properties used as Input in the STOMP-WAE-B Simulations

Specific Heat (kJ/kg C)	A†	B	C	D	E
793.1	0.60	0.70	8.0	0.26	3.0
Enhancement	9.50	3.00	3.50	1.00	3.0
† Parameters A, B, and D have units of W/m°C					

Table 6.7. Plant Parameters Used as Input in the STOMP-WAE-B Simulations

Parameter	Cheatgrass	Sandberg's Bluegrass
Plant Height (m)	0.30	0.10
Leaf Area Index	1.26	0.972
Plant Area Index	0.35	0.27
Maximum Condensate Depth (m)	1.984×10^{-3}	1.984×10^{-3}
Phenological Stages (DOY)	55, 104, 147, 160	55, 112, 148, 159
Root Density Parameters (z_m, p_z, z^*)	0.5, 4.875, 0.10	0.35, 2.620, 0.10
Albedo (α_1,α_2,α_3,α_4)	0.05,0.06,0.15,0.19,0.05	0.05,0.06,0.15,0.19,0.05
Root Stress Points (h_1,h_2,h_3,h_4)	0.03 m, 0.1 m, 1.0 m, 15 m	0.03 m, 0.1 m, 1.0 m, 15 m

Required meteorological input to STOMP-WAE-B includes hourly measurements of precipitation, air temperatures, solar radiation, relative humidity, and wind speed. The current version of STOMP-WAE-B does not include simulation of snowmelt so precipitation in the form of snow was treated as an equivalent rainfall amount and treated as rainfall. Meteorological data were obtained from the HMS and hourly data for the period 1983 through 1986 were used to generate the *Boundary Conditions* and *Atmospheric Conditions* cards.

The simulation was initialized by running STOMP-W over several loops to achieve steady flow conditions in the soil profile using precipitation data for year 1982. The resulting restart file was used to initialize STOMP-WAE-B with the "overwrite" option to incorporate temperature and gas pressure data thereby assuring compatibility across the two operational modes. STOMP offers several options for specifying the lower boundary condition for water, heat, and gas transport. If the maximum depth of the domain is assumed to be 3.5 m, a Dirichlet Aqueous condition would be inappropriate. The Dirichlet condition is be best suited to a simulation in which the bottom boundary was located at the water table (10 m). A Neumann or specified flux boundary would be inappropriate as temporal variations in drainage from the base of the domain and the conditions under which drainage occur would be unknown *a priori*. A unit downward gradient condition, although not strictly mathematically correct because of the layered sediments, is another option, particularly if one wants to limit the size of the domain to the 3.5-m depth considered in the field experiment. With this condition, it should be recognized that water can flow in either direction across the boundary, depending on the potential gradient. To avoid any potential problems with the unit gradient condition, the domain was extended to the water table (10 m) and a Dirichlet condition applied to the bottom boundary. A Dirichlet boundary was also used for heat flow whereas a zero flux condition was assumed for gas. STOMP-WAE-B simulations that include plants require consideration of the temporally variable precipitation and evaporation that occur in response to

meteorological forcings. Thus, the Shuttleworth-Wallace boundary condition was chosen. A 1-yr simulation for the year 1984 was conducted and the results analyzed using a water balance approach (Equation 2.1). Because of the relatively level surface at the site, runoff/run-on was assumed to be zero. This assumption is quite reasonable as no runoff was observed during the study period.

6.6.2 Results

6.6.2.1 Thermal Energy Balance

Predicted daily mean values of the energy balance components for the first five days of the plant growth cycle are depicted in Figure 6.14. Net radiation is not an output variable in STOMP-WAE but is obtained from the summation of net long-wave and short-wave radiation flux densities, both of which are output variables. As expected, net radiation was periodic with considerable temporally variability. Fluxes ranged from -50 W m^{-2} to over 200 W m^{-2} over the 5-day period shown. Large daytime differences over the course of the simulation were usually associated with increased cloud cover and precipitation events. Of the energy sinks, latent heat flux was the most important for the period shown. During the 5-day period, most of the net radiation was partitioned as latent-heat flux and to a lesser extent sensible-heat flux. Thus, most of the incoming radiation was converted to evaporation. Latent-heat flux exceeded net radiation on a few occasions. Such an occurrence requires an additional source of energy, and as shown in Figure 6.14, this additional energy was supplied by ground-heat flux or advected sensible heat. For example, latent-heat flux exceeded the net radiation for most of day 56. For the same period, sensible-heat flux was negative, which is indicative of cooling of the soil surface. Ground-heat flux was also negative, suggesting that energy was moving down through the surface. As expected, ground-heat flux was mostly positive during the night, which is indicative of heat moving up towards the surface, and negative during the day, which is indicative of surface heating. Ground-heat flux was also strongly correlated with net radiation with larger downward fluxes occurring during periods of highest net radiation. Both air and surface temperatures were positively correlated with net radiation, and this is illustrated for the 10-day period of interest (Figure 6.15). The small differences between air and ground surface temperature are not unusual for the period depicted as the wetter soil surface would have a higher albedo and therefore reflect more energy. In general, the ground-surface exceeded the air temperature with differences of almost 20 ^{o}C by mid year.

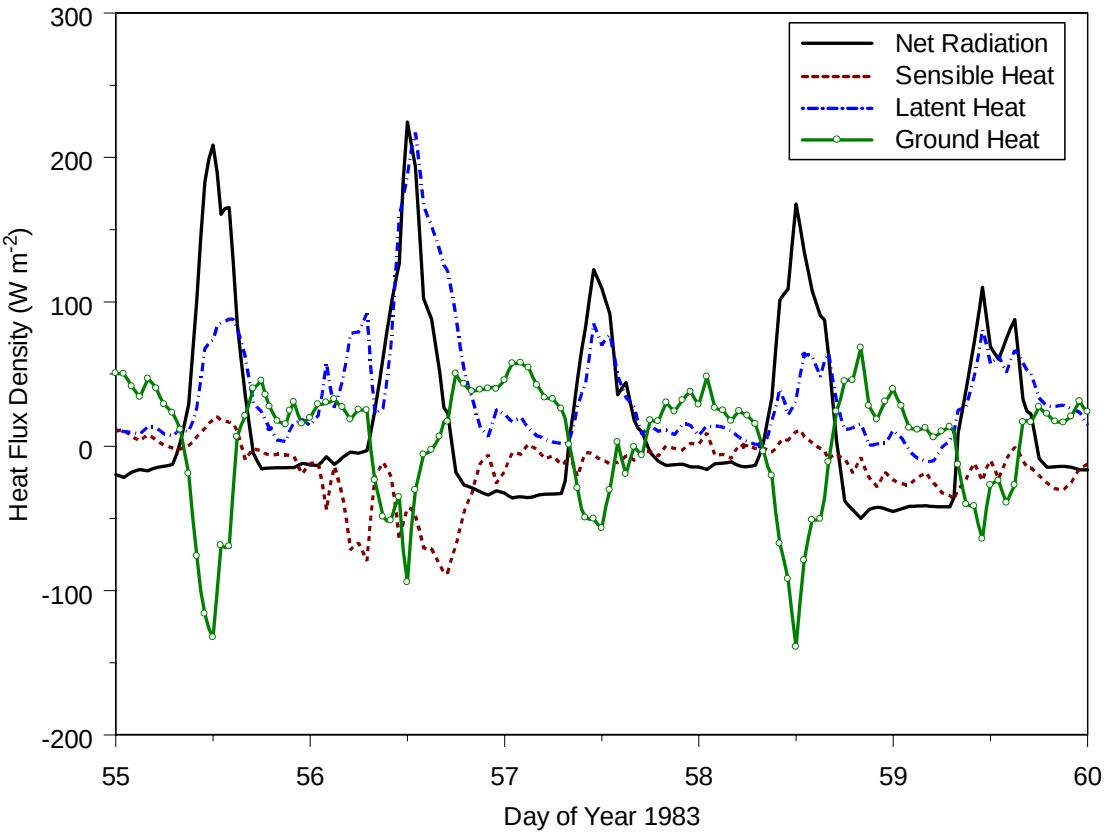

Figure 6.14. Daily Mean Values of the Energy Flux Components for the Grass Site for the first Five days Following Plant Emergence

6.6.2.2 Soil Water Storage

Gee and Kirkham (1984) reported vertical volumetric soil water content measurements during the course of the year using neutron probe. These data were integrated over depth to calculate soil water storage. Simulated water content profiles on the days of field measurements were integrated over a 1-m depth to obtain the simulated storage values. The observed and predicted water storages in this depth interval are compared in Figure 6.16. Two cases, 1 and 2 are used to illustrate the impact of the moment and thermal roughness length parameters on the water balance. In Case 1, we assumed a momentum roughness length of 40 mm derived from cheatgrass height according to Equation 3.53 and a thermal roughness of 4 mm. In Case 2, we assumed a momentum roughness length of 30 mm and a thermal roughness of 3 mm. Observed water storage started at a high of 14.91 cm (day 1) and showed a gradual decrease until around day 83 after which the rate of decreases almost doubled in rate. Water storage continued to decrease through the summer months reaching a minimum of 5.03 cm by day 279 (October 6). The onset of fall and winter precipitation coupled with the lack of water uptake by the now dormant grasses led to an increase in water storage. The data show a significant increase in rate of water accumulation occurring around day 294 (October 21) consistent with increasing precipitation, reduced evaporation, and the cessation of transpiration.

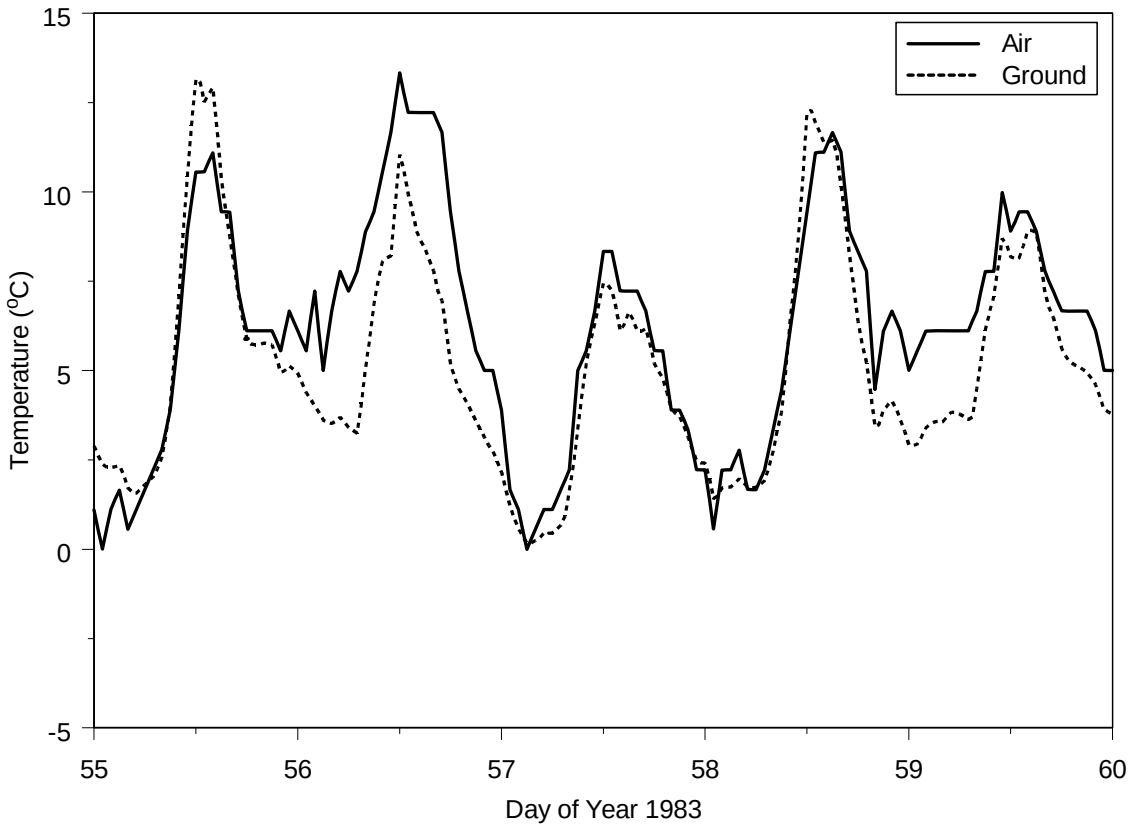

Figure 6.15. Daily Mean Values of Predicted Air and Ground Surface Temperatures for the first Five Days Following Plant Emergence

Predicted water storage shows very good agreement with the field observations in terms of the temporal distribution and the absolute values (Figure 6.16). Observed water storage started at a high of 12.94 cm, somewhat lower than the field observation, remaining relatively constant around that value until day 49 when a sharp decrease was initiated. The discrepancy between the predicted and observed results during the first 50 days or so of the simulation is perhaps due to the lack of a tightly coupled feed back mechanism between atmospheric and hydrologic conditions and plant growth. The underestimation of the start of the rapid decline in storage by 30 days in the model predictions could be due to a combination of factors. These include higher predicted evaporation rates and a more gradual start to plant water uptake. For this simulation, we specified the beginning of plant activity to be day 55 with water uptake being controlled partly through the stomatal conductance. In the stomatal conductance model, if the ambient temperature is outside of some optimal temperature range, conductance approaches zero and water uptake ceases. Qualitatively, it appears that a later start in the plant developmental cycle coupled with a gradual increase in the leaf area index rather than the currently assumed step increase would eliminate the discrepancy during the first 130 days for both cases 1 and 2 (Figure 6.16).

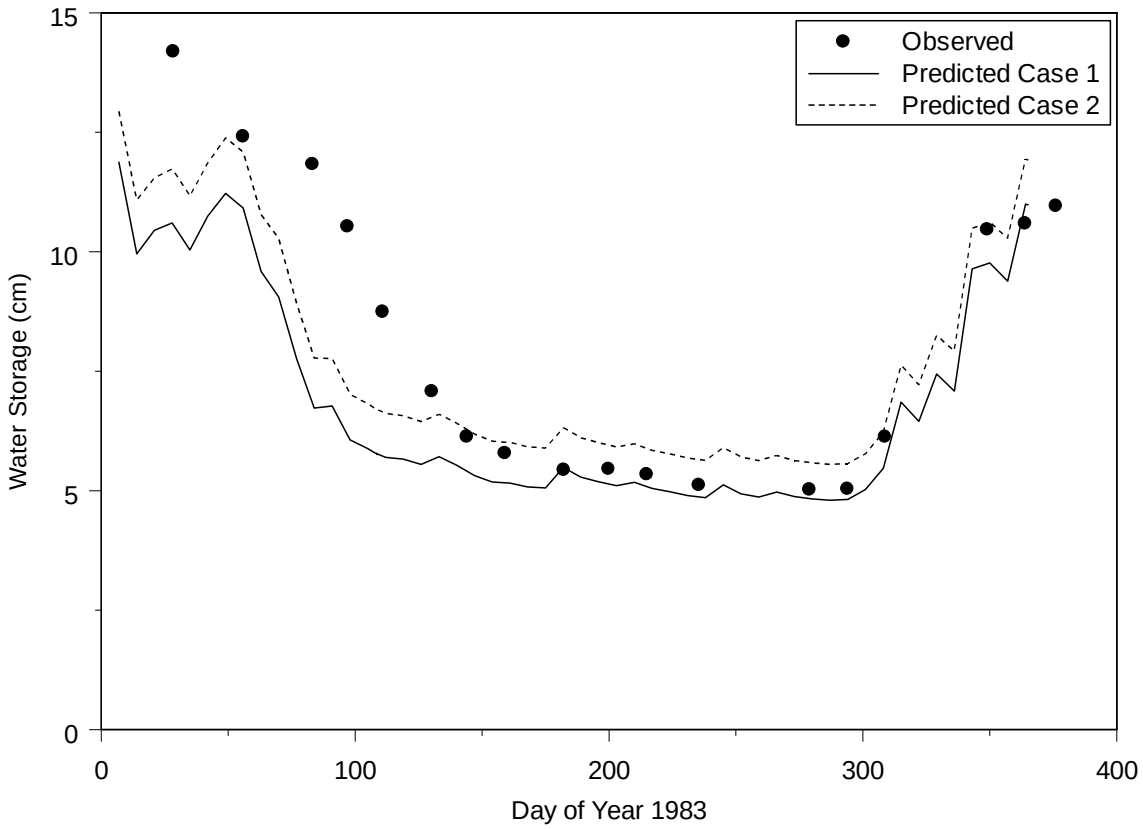

Figure 6.16. Temporal Response of Soil Water Storage in the 0-1 m Depth

Cheatgrass and Sandberg's bluegrass completed their growth cycles around day 160 with the plants going into flowering-induced dormancy. This decline continued over the course of the year, except for small increases caused by precipitation events. Evaporation and some deep percolation resulted in continued removal of water from the 0-1 m layer with the total amount of water stored in the profile reaching a minimum of about around day 287. The decline in storage was similar to that of the field observations reaching a minimum of 5.55 cm by day 287 (October 14) in Case 1 and 4.8 cm in Case 2. Both the values and their timing agree well with the observed change in water accumulation which occurred around day 294 (October 21) when the storage was 5.04 cm. The onset of fall and winter precipitation coupled with the lack of water uptake led to a sharp increase in water storage. This increase is consistent with increasing precipitation, reduced evaporation, and the cessation of transpiration by plants forced into dormancy by flowering.

Given the lack of precise data on the root distributions and canopy structure, the agreement between the measured and predicted water storage is quite remarkable. Note also that the field scale hydraulic properties were derived from inverse modeling of an instantaneous profile experiment with out consideration for plant water uptake. Thus, it is very likely that a better fit of the data could be obtained with parameters derived from the simultaneous inversion of hydraulic properties and root distribution parameters.

Figure 6.17 show the distribution of moisture at the surface node and at a depth of 14.5 cm. As can be expected, the short-term surface moisture trends were controlled by precipitation events while the long-

term behavior was dominated by evaporation and transpiration processes. The time series of the long-term water content showed a similar pattern to that shown by the soil water storage. Surface moisture showed a sharp decline following emergence of the grasses from their dormant period and continued throughout the season, reaching values of less than 0.05 m^3 m^{-3} at surface and around 0.05 m^3 m^{-3} at the 14.5-cm depth by late summer.

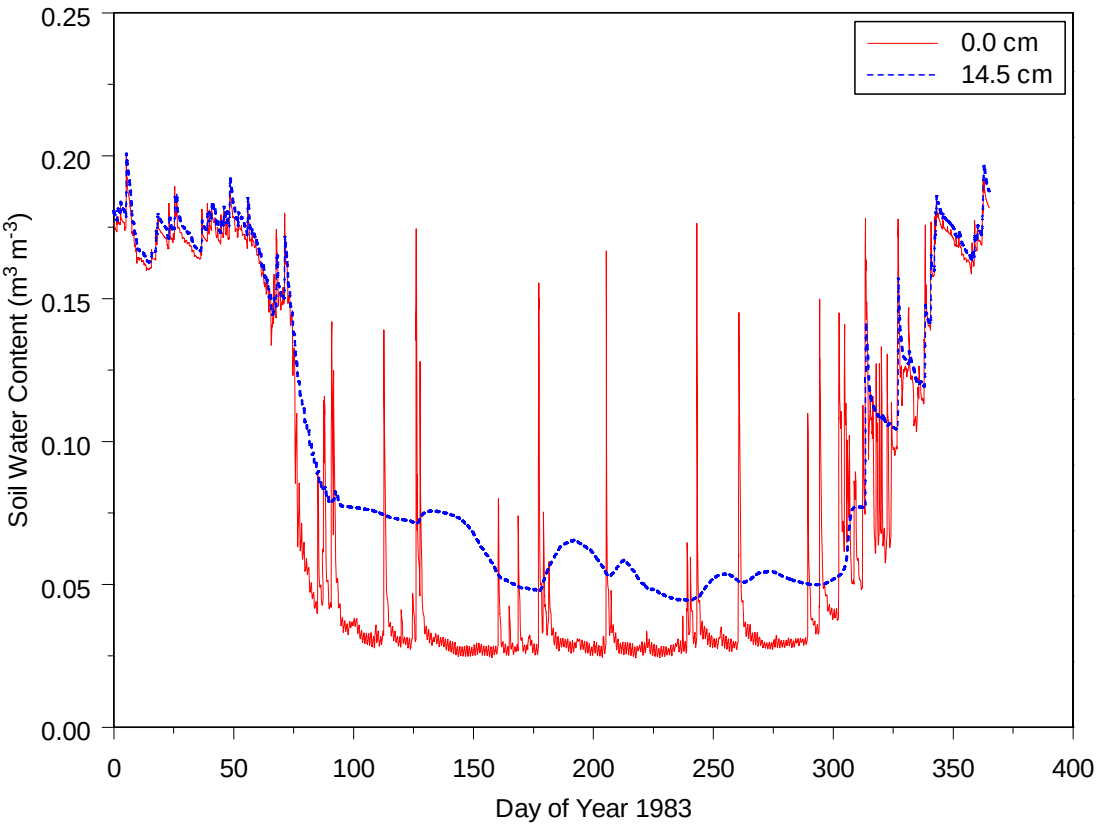

Figure 6.17. Simulated Temporal Response of Soil Water Content in 1983 on a 0.5-hr Interval

Precipitation events resulted in sharp spikes in moisture content at the surface. These effects were translated through to the 14.5-cm depth but only when the plants were dormant. During the period of active water uptake by the plants, moisture content changes at the surface did not always translate downward. In fact after day 60, it was not until late October that precipitation events began to influence the water content deeper in the profile. This is because the water status at the surface node is also strongly influenced by the energy balance at the surface. Increased net radiation and latent-heat flux coupled with water uptake after day 55 resulted in increased evapotranspiration. This combination of processes resulted in increased suction and decreased moisture.

6.6.2.3 Evapotranspiration

Transpiration rates are regulated by stomatal opening and closing functions that are controlled to some extent by temperature. In the current stomatal resistance model, there is a species-dependent minimum temperature for stomatal opening, an optimum temperature at which resistance is minimum and a maximum temperature at which the resistances reaches a species-specific maximum as the stomata close.

Stomatal resistance can therefore be expected to vary with time of day as the temperature and other atmospheric conditions change. Link et al. (1990) reported stomatal conductance and transpiration data for the two grass species from at least three sampling campaigns. In general, stomatal conductance of cheatgrass was generally higher than Sandburg's bluegrass but limited species-specific data prevented a detailed comparison between predicted and observed values. To test the capability of the stomatal resistance model, resistances were calculated using parameters for winter grasses were compared with the April 18, 1986 measurements reported by Link et al. (1990). Figure 6.18 compares the diurnal pattern in measured and predicted stomatal conductance (inverse of resistance) on April 18, 1986, for cheatgrass.

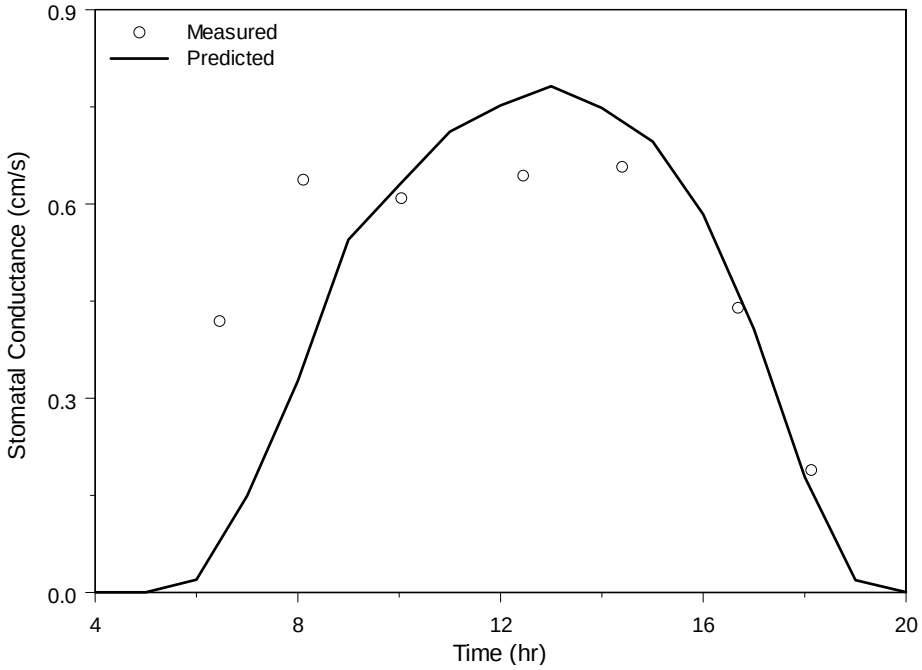

Figure 6.18. Diurnal Response of Cheatgrass Stomatal Conductance on 18 April 1986

Link et al. (1990) reported that April 18 was a hazy, warm day with the vapor pressure deficit rising to about 22 mb. Measured stomatal conductance increased with time of day, reaching a maximum of 0.68 cm/s around 1400 hours. The predicted stomatal conductance is in good agreement with the measured response, although the peak of 0.78 cm/s occurred somewhat earlier around 1300 hrs. Link et al. (1990) reported maximum stomatal conductances of 0.78, 0.68, and 0.62 cm/s on April 11, 18, and May 1, respectively with a strong positive correlation between conductance and transpiration. Nevertheless, the predicted and observed stomatal conductances show very good agreement. Furthermore, the data reported by Link et al. (1990) may be useful for fitting the parameters of the stomatal conductance model using the observed meteorological data.

Figure 6.19 shows predicted evapotranspiration along with the other water balance components. For the first 55 days or so, water was recycled to the atmosphere, primarily by evaporation. This is expected given the phenology of the two grasses (Link et al. 1990). Following emergence from the winter dormancy and the expansion of the first leaves, transpiration started and quickly became a larger component of the water loss. Transpiration peaked around day 150 by which time the plants had entered

a flowering-induced dormancy. All transpiration ceased after day 160, and further water loss from the near surface was again dominated by evaporation.

6.6.2.4 Water Balance

The total precipitation for the year was 278.4 mm, but the other balance components were dependent on the values of the momentum and thermal roughness parameters. In Case 1 (z_m = 40 mm, z_h = 4 mm), predicted drainage was 69.38, transpiration was 33.72 mm, and evaporation was 234.94 mm. In Case 2 (z_m = 30 mm, z_h = 3 mm) drainage was 53.19 mm, transpiration was 34.54 mm, and evaporation was 229.4 mm. There were insufficient data to allow calculation of the water balance for the test site with the temporal resolution depicted in Figure 6.19. However, Gee and Kirkham (1984) reported drainage of over 50 mm derived from changes in water storage, a value very similar to the 53 mm predicted in the Case 2 simulation. The cumulative water balance components are compared in Figure 6.19 for Case 2 (z_m = 30 mm, z_h = 3 mm). Cumulative actual evaporation was 229.5 mm, or 82 percent, while cumulative actual transpiration accounted for 34.5 mm or 12.4 percent. Drainage out of the profile accounted for only 53.19 mm or 19 percent of total precipitation. These results show that even though precipitation was almost 70 percent over normal, only a small fraction penetrated beyond the root zone to become percolation. It should be noted that these simulations were conducted without any calibration beyond that in which hydraulic properties were estimated from field measurements.

None of the plant parameters were optimized, so this may offer an opportunity for reducing the uncertainty in these results. In that analysis, data collected during an instantaneous profile infiltration experiment conducted at the site were inverted using a parameter-scaling approach to obtain unique hydraulic properties for each of four layers down to a depth of 2 m (Zhang et al. 2004). The inversion was performed using STOMP-W and therefore did not consider nonisothermal effects or evapotranspiration. It is now known that estimates of parameters controlling vertical unsaturated water flows can be improved if root-water uptake parameters are simultaneously optimized in the inversion (Hupet et al, 2003).

Nevertheless, these results indicate that STOMP-WAE adequately incorporates the mechanisms and constitutive theory to allow simulation of the field water balance from basic meteorological, soil, and plant data. These results highlight the importance of having site specific plant and hydraulic property data in order to accurately represent site water balance. Cheatgrass and Sandberg's blue grass were most active when available water was highest and the structure of the root systems allowed them to maximize water uptake following precipitation events. The grasses were limited in their ability to extract water from deep in the profile and as a result there was deep drainage from the root zone. There is considerable evidence from the 200-BP-1 prototype Hanford barrier (Ward et al. 2005a,b) that a combination of shallow-rooted grasses and deep-rooted shrubs are effective in minimizing percolation.

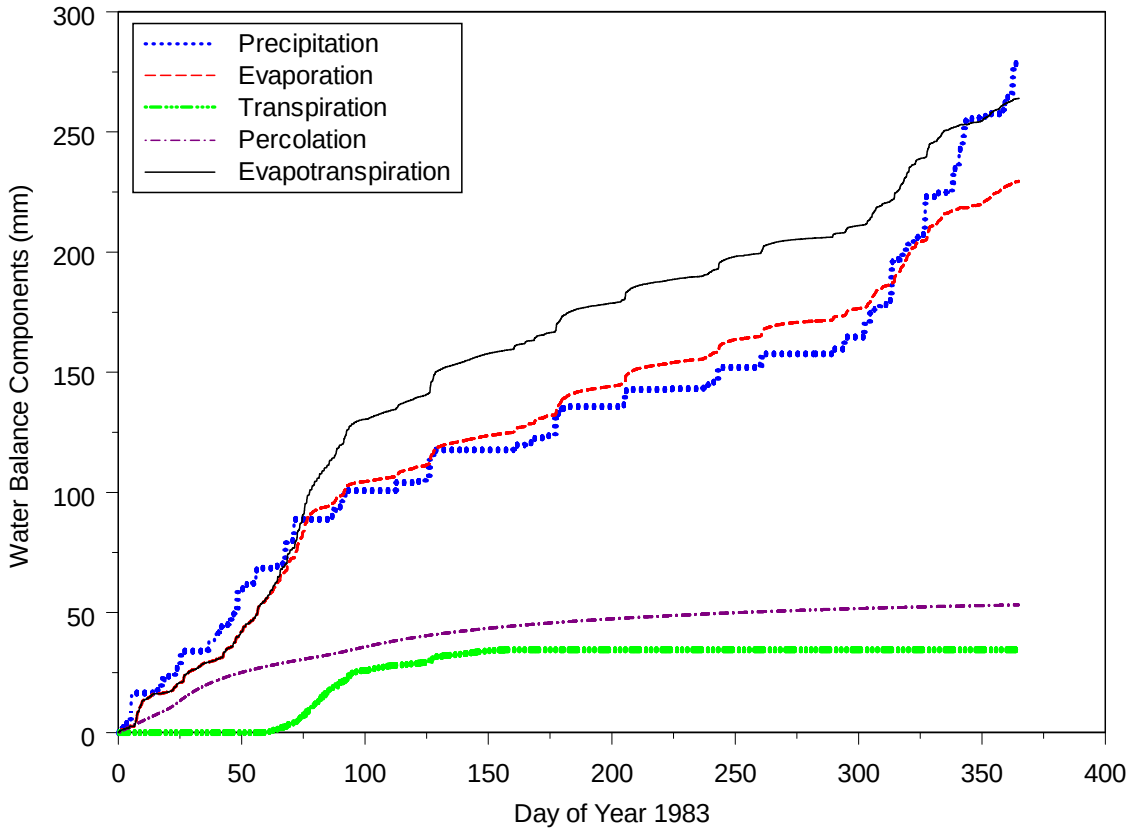

Figure 6.19. Predicted Water Balance Components

6.7 Intercode Comparison

Scanlon et al. (2002) reported on an intercode comparison study aimed at comparing the water balance simulation results from seven different codes, including HELP, HYDRUS-1D, SHAW, SoilCover, SWIM, UNSAT-H, and VS2DTI. The comparison was based on 1–3 year water balance monitoring data from bare surface engineered covers in Texas and Idaho. This problem was chosen as a benchmark problem for STOMP-WAE-B and as a means of investigating parameter sensitivity in simulations of bare-surface evaporation.

6.7.1 Problem Description

The site and soil information can be found in Scanlon et al. (2002) and is briefly described below. The site is located at the Idaho National Engineering and Environmental Laboratory in southeastern Idaho. The long-term (40-year) mean annual precipitation is 221 mm. Water balance data from a concrete structure of 3×3×3 m (four walls and a floor) were used in the study of Scanlon et al. (2002) and this study. The texture of the soil is silt loam, and the upper 0.15 m of the profile has 25 percent gravel by volume mixed with the silt loam soil to reduce wind erosion. Table 6.8 lists the hydraulic parameters for the soils. The relative permeabilities were described using the Mualem model for the aqueous phase and the Corey model for the gas phase. All the parameters except gas residual saturation were from Scanlon et al. (2002). Gas residual saturations for both layers were assumed to be 0.1.

Soil thermal conductivities under dry and wet conditions (Table 6.9) were estimated using pedotransfer functions based on the particle size distribution data given in Table 2 of Scanlon et al. (2002). It assumed that the quartz contents were 40 percent for gravel and 30 percent for silt soils. A linear relationship between thermal conductivity and water content (θ) was assumed to be when $\theta \leq 0.1$. Soil-specific heat was estimated to be 730 J kg K^{-1} (Ward and Keller, 2005). Soil albedo was calculated using the Wang et al. (2005) model with albedo under dry and wet conditions being 0.25 and 0.10, respectively. The albedo attenuation factor was 0.076, and the reference albedo for solar zenith angle adjustment at solar zenith of 60 degree was 0.04 (Wang et al. 2005).

Table 6.8. Soil Hydraulic Parameters for the Idaho Soils

Layer	Lab K_s [(a)] ($cm\ d^{-1}$)	Optimized K_s [(b)] ($cm\ d^{-1}$)	θ_s ($cm^3 cm^{-3}$)	θ_r ($cm^3 cm^{-3}$)	α (cm^{-1})	N (-)	S_{gr} (-)
1	5.9	94	0.36	0.035	0.036	1.601	0.10
2	8.9	43	0.47	0.015	0.005	2.090	0.10

(a) Measured in the laboratory (Scanlon et al. 2002).
(b) Optimized values using the trial-and-error method (Scanlon 2002)/

Hourly meteorological data were from the CFA station (latitude 43.532598 °N, longitude 112.947757 W, elevation 4950 ft), which is at the CFA Building 690 at Idaho National Laboratory. For the STOMP-WAE-B simulations, the soil profile (3.0 m) was divided into two layers. A total of 113 nodes were used to represent the profile. The node spacing was the same as that used in Scanlon et al. (2002) and was 0.2 cm at the soil surface, 2 cm at material interface, and a maximum of 24 cm within materials. The initial soil water condition was set the same as that shown by the Figure 2b of Scanlon et al. (2002). The initial soil temperature on July 21, 1997, was 30°C at the soil surface and linearly decreased to 15°C at 3 m below the surface. The top aqueous boundary condition was the time-variable Neumann condition, which was the hourly precipitation. The hourly atmospheric condition was used for the gas and heat transport. The seepage face condition was used for the aqueous phase for the lower boundary condition. A constant temperature of 15°C and a constant gas pressure were applied at the lower boundary. Based on the use of different values for K_s and aerodynamic roughness length, four cases (Table 6.10) were designed and simulated.

Table 6.9. Thermal Parameters for the Idaho Soils

Layer	K_{wet} ($W\ m^{-1}$)	K_{dry} ($W\ m^{-1}$)	λ ($J\ kg\ K^{-1}$)
1	0.272	1.752	730
2	0.188	1.374	730

Table 6.10. STOMP-WAE-B Simulation Cases

Cases	K_s	Soil Roughness (mm)
STOMP-a	Op. K_s[(a)]	0.1
STOMP-b	Lab K_s[(b)]	0.1
STOMP-c	Op. K_s	0.01
STOMP-d	Lab K_s	0.01
(a) Optimized values using the trial-and-error method (Scanlon 2002). (b) Measured in the laboratory (Scanlon et al. 2002).		

6.7.2 Results

In a fashion similar Scanlon et al. (2002), measured and simulated water balances for the Idaho site were compared for the initial period (2 July 1997 through 30 September 1997; Pre-WY98) and water years 1998 and 1999 (WY98, WY99). Table 6.11 summarizes the measured and simulated annual water balance components. Note that the simulation results from Scanlon et al. (2002) are also included for the purposes of comparison.

6.7.2.1 Drainage

Most drainage from the profile occurred in July and August 1997 in response to irrigation in July. Drainage also occurred in March/April each year (5 to 6 cm) in response to spring snowmelt. A additional drainage (2 to 3 cm) occurred in May/June each year in response to long periods of high precipitation. Uncertainties in the drainage measurements are considered to be less than 1 percent based on uncertainties in the tipping bucket and pressure transducer data. Figure 6.20 through Figure 6.22 show the difference between simulated drainage (D_{sim}) and the measured drainage (D_{mea}).

A positive value indicates over-predication while a negative value indicates an under-prediction. For all the 22 simulations, these differences vary from -7.4 to 59.3 cm for Pre-WY98 whereas the results of the four STOMP simulations were within -5.1 to -3.8 cm. For WY98 (Figure 6.21), the range of the drainage differences was between -6.0 and 17.3 cm (vs. -3.8 to -1.0 for STOMP simulations). For WY99 (Figure 6.22), the range of the drainage differences was between -8.3 and 9.6 cm (vs. -1.5 to 1.1 for STOMP simulations). For the whole simulation period (Figure 6.23), the range of the drainage differences was between -16.2 and 86.2 cm (vs. -9.7 to -4.4 for STOMP simulations). The simulation errors of drainage for the whole simulation period ranged -40.6~216.0 percent (vs. -24.4 ~ -11.0 percent for STOMP simulations).

Figure 6.24 shows the times series of drainage. Results other than those of the STOMP simulations were from Figure 5 of Scanlon et al. 2002. Note that an error in Figure 5 of Scanlon et al. 2002 was corrected for this comparison. The measured drainage for WY99 should have been 8.9 cm, as given in Table 4 of Scanlon et al. 2002, not their plotted 8.2 cm. As observed by Scanlon et al. (2002), simulated drainage generally occurred much earlier than the measured drainage each year. The difference in the timing between the simulated and measured drainage is attributed to inability of the codes to simulate reduction in infiltration and in hydraulic conductivity caused by soil freezing.

Table 6.11. Measured and Simulated Annual Water Balance Components

	Pre-98			WY98			WY99		
	E	**ΔS**	**D**	**E**	**ΔS**	**D**	**E**	**ΔS**	**D**
Measured	**5.2**	**48**	**22.7**	**15.4**	**0.5**	**8.3**	**11.7**	**-0.8**	**8.9**
1. UNSAT-H (UG, G), VG, Mualem	5.2	48.7	22.1	13.1	0.8	10.3	10.1	-2.6	12.3
2. HYDRUS-1D (S), VG, Mualem	10.2	48	17.7	18.7	-0.8	6.3	13.5	-1.3	7.7
3. SHAW (UG, G), BC, $\theta_r = 0$, Burdine	9.3	48.5	18.1	19.9	-0.7	5	22.8	-3.6	0.6
4. SoilCover (const h), (Fredlund)	9.9	49.7	16.2	16.8	-1.2	8.7	11.2	-1.3	10
5. SWIM (S), VG, Mualem	9.5	51.1	15.3	16.1	0.2	7.9	10.4	-1.3	10.8
6. VS2DTI (S), VG, Mualem	3.5	51.3	21.2	10	0.7	13.6	9	-2.8	13.7
7. HELP (UG), BC	10	7.3	58.7	15.4	1.9	7	13.6	-2.6	8.8
8. HYDRUS-1D (UG, G)	10.3	47.9	17.7	19	-1	6.3	13.7	-1.2	7.3
9. HYDRUS-1D (UG)	9.3	-11.7	78.3	14.3	-13.4	23.4	8.9	-1.3	12.3
10. HYDRUS-1D (hysteresis)	10.2	46.6	19.1	18.5	-0.7	6.5	13.3	-3.2	9.7
11. UNSAT-H (UG)	4.3	-10.4	82	9.8	-11.1	25.6	6.7	-5.3	18.5
12. UNSAT-H (BC, Burdine, $\theta_r = 0$)	6.8	48.5	20.6	19.8	-1.4	5.9	16.4	-5.1	8.5
13. UNSAT-H (BC, Burdine, $\theta_r \neq 0$)	6.6	46.9	22.4	19.4	-1.3	6.1	16.2	-5.1	8.8
14. UNSAT-H (BC, Mualem, $\theta_r \neq 0$)	9.2	44.5	22.3	26.7	-4.7	2.3	23.7	-7.1	3.2
15. UNSAT-H (VS2DTI)	3.4	48.9	23.6	8.3	0.9	15	7.9	-2.8	14.7
16. UNSAT-H (HYDRUS-1D)	9.8	48.5	17.7	16.9	-0.5	7.8	11.7	-2.3	10.5
17. UNSAT-H (1) (vapor)	5.2	48.7	22.1	13.4	0.7	10.1	10.4	-2.7	12.1
18. UNSAT-H (1) (hysteresis)	5	40.8	30.1	12	-0.2	12.5	9.7	-3	13.2
19. STOMP-a	9.9	47.8	18.3	19.4	0.4	4.5	14.6	-2.2	7.4
20. STOMP-b	9.7	48.7	17.6	16.8	0.5	7.0	12.2	-1.3	8.9
21. STOMP-c	9.3	47.7	18.9	18.9	0.3	5.1	13.9	-2.3	9.0
22. STOMP-d	9.1	48.6	18.2	16.6	0.4	7.3	11.6	-1.9	10.0

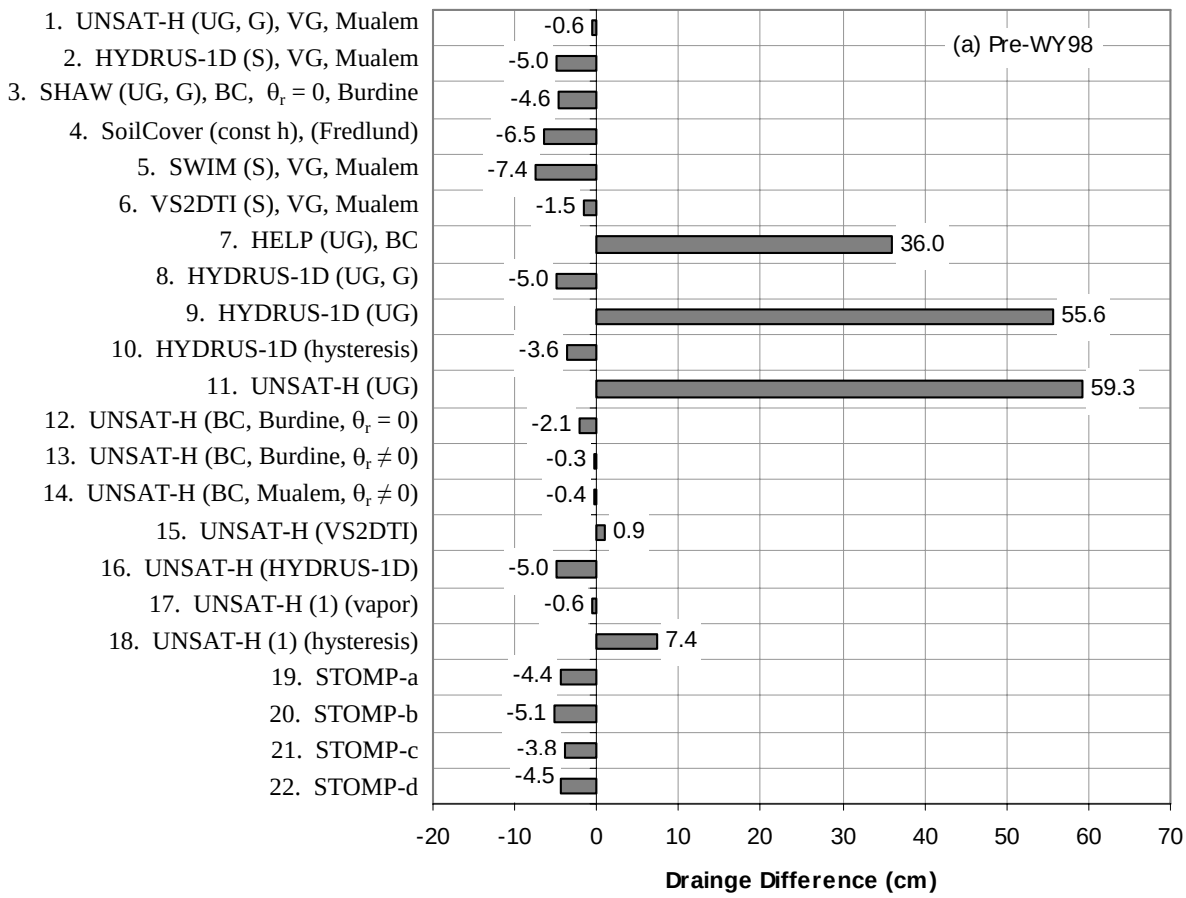

Figure 6.20. Differences Between Simulated Drainage and the Measured Values (cm) for Pre-WY98

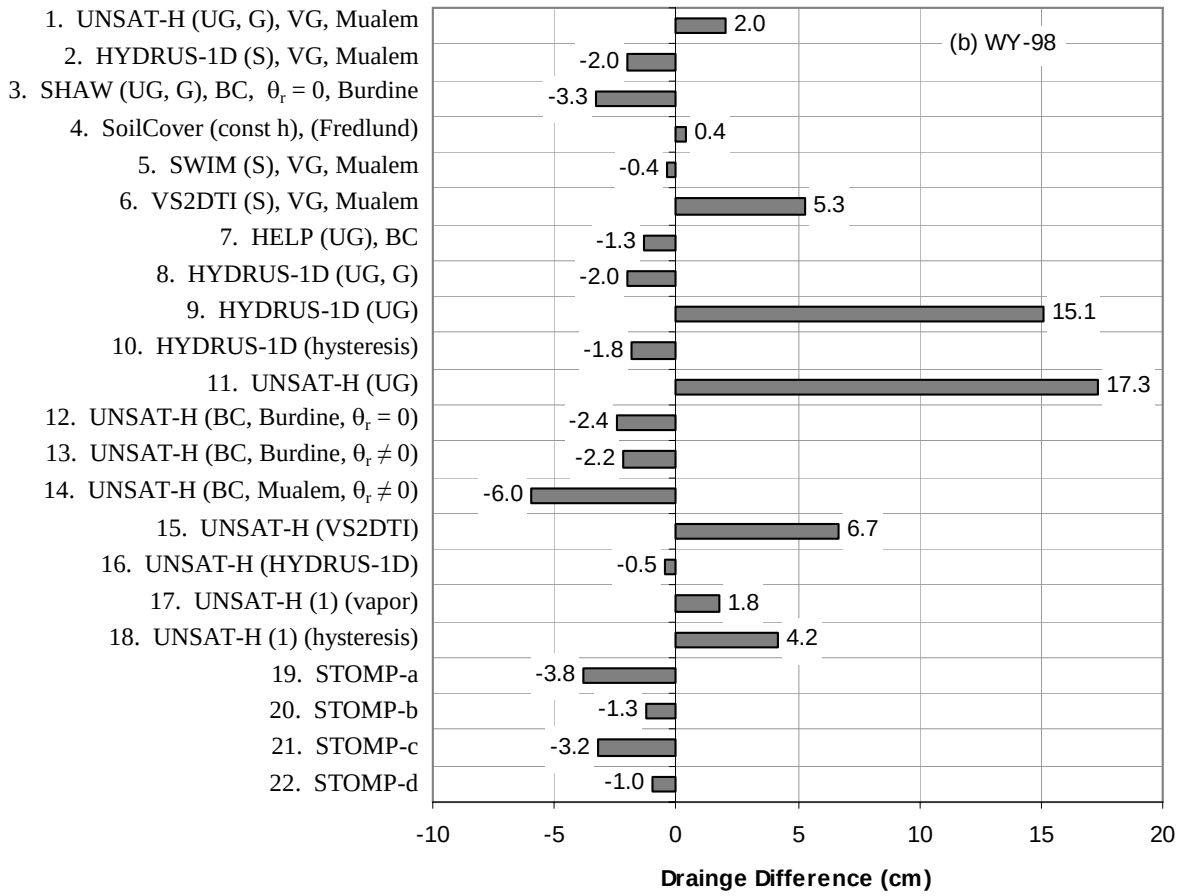

Figure 6.21. Differences Between Simulated Drainage and the Measured Values (cm) for WY98

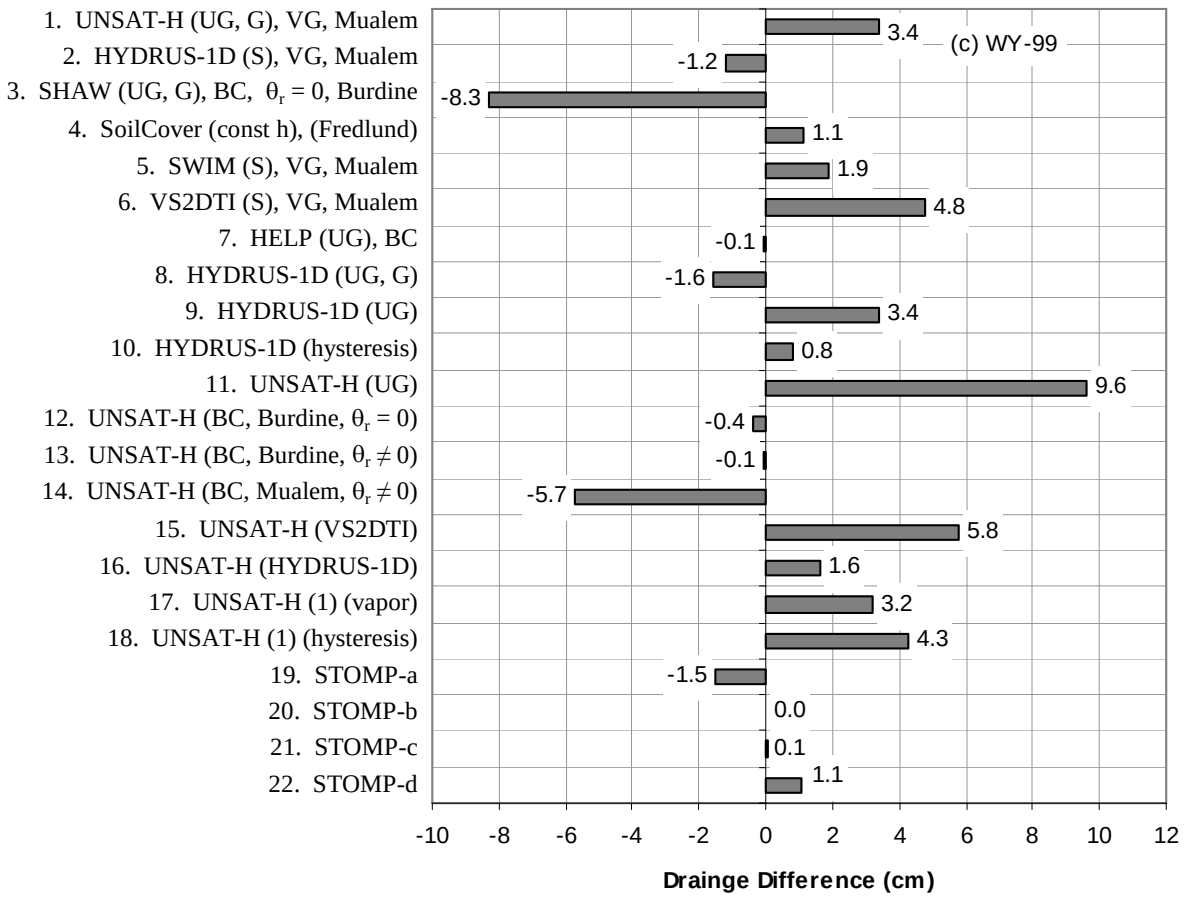

Figure 6.22. Differences Between Simulated Drainage and the Measured Values (cm) for WY99

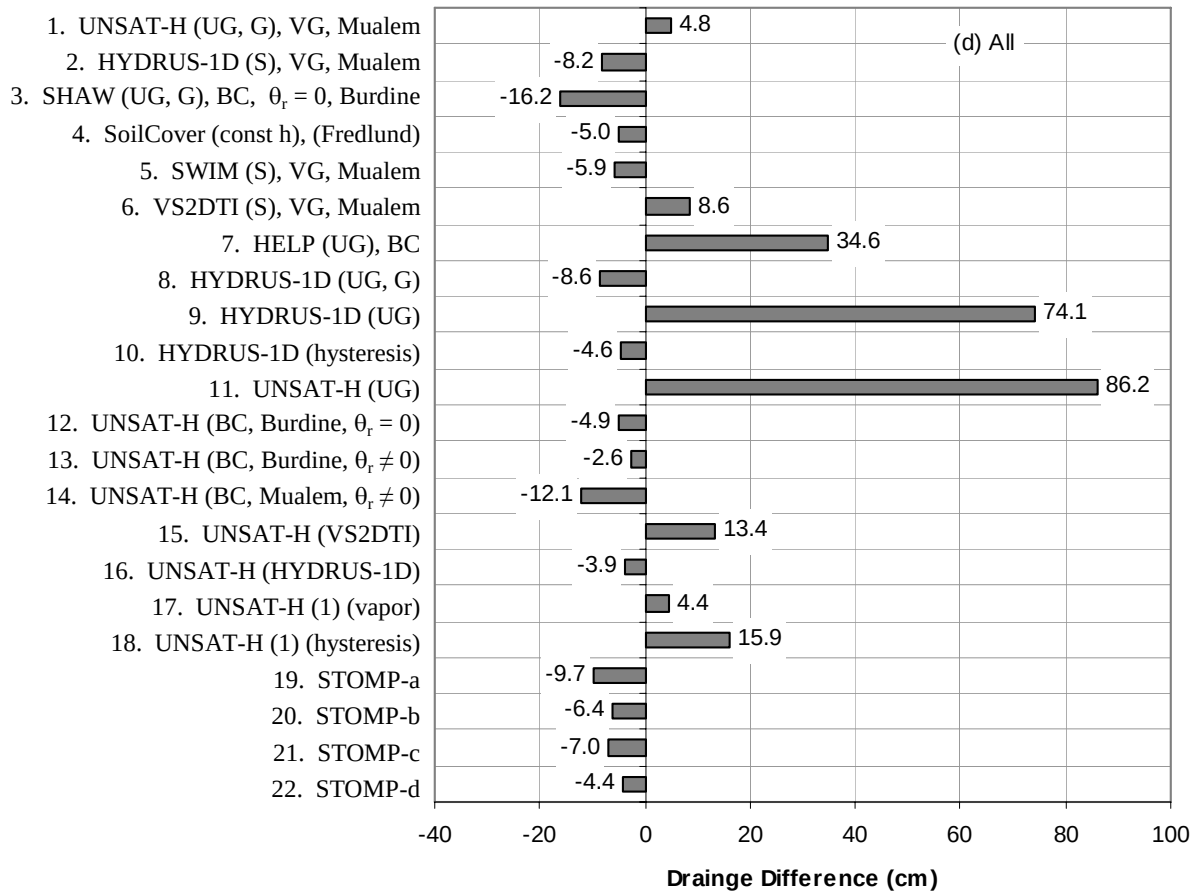

Figure 6.23. Differences Between Simulated Drainage and the Measured Values (cm) for WY87 to WY99

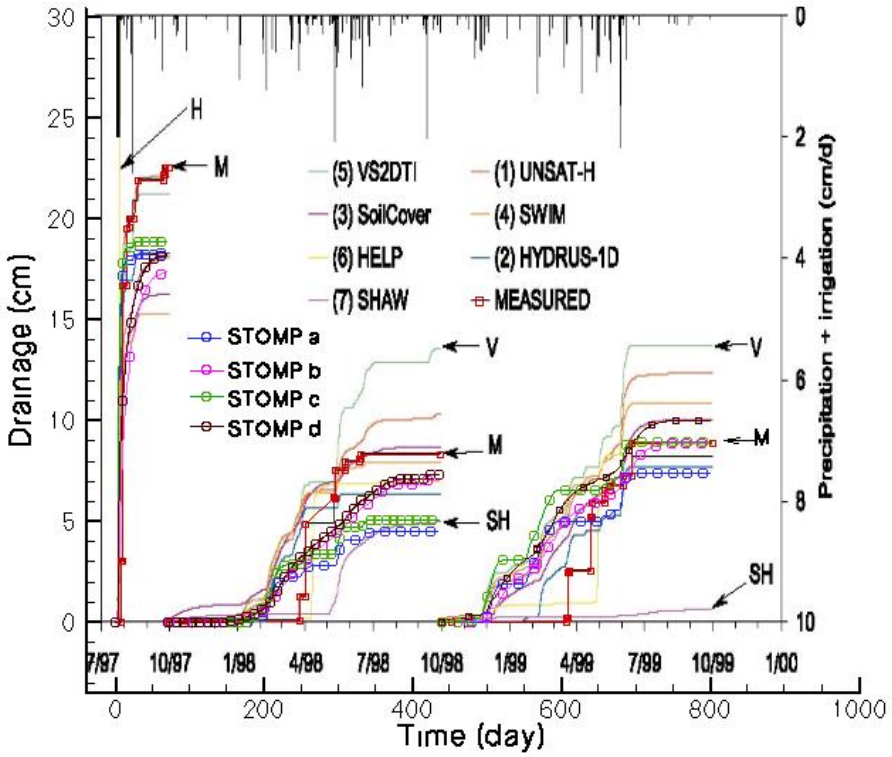

Figure 6.24. Time Series of Daily Precipitation and Applied Irrigation and Measured and Simulated Drainage at the Idaho Site

6.7.2.2 Soil Water Storage Change (ΔS)

Figure 6.25 through Figure 6.28 show the difference between simulated soil water storage change (ΔS_{sim}) and the measured water storage change (ΔS_{mea}). Results other than those of the STOMP simulations were taken from Table 4 of Scanlon et al. (2002). For all the 22 simulations, these differences vary from -59.7 to 3.3 cm for Pre-WY98 whereas the results of the four STOMP simulations were within -0.3 to -0.7 cm (Figure 6.25). For WY98 (Figure 6.26), the range of the storage differences was between -13.9 and 1.4 cm (vs. -0.2 to 0.0 for STOMP simulations). For WY99 (Figure 6.27), the range of the storage differences was between -6.3 and -0.4 cm (vs. -1.5 to -0.5 for STOMP simulations). For the whole simulation period (Figure 6.28), the range of the storage differences was between -74.5 and 2.3 cm (vs. -2.0 to 0.1 for STOMP simulations). The simulation errors of ΔS for the whole simulation period ranged from -156.2 to ~4.8 percent (vs. -4.2 to ~0.3 percent for STOMP simulations).

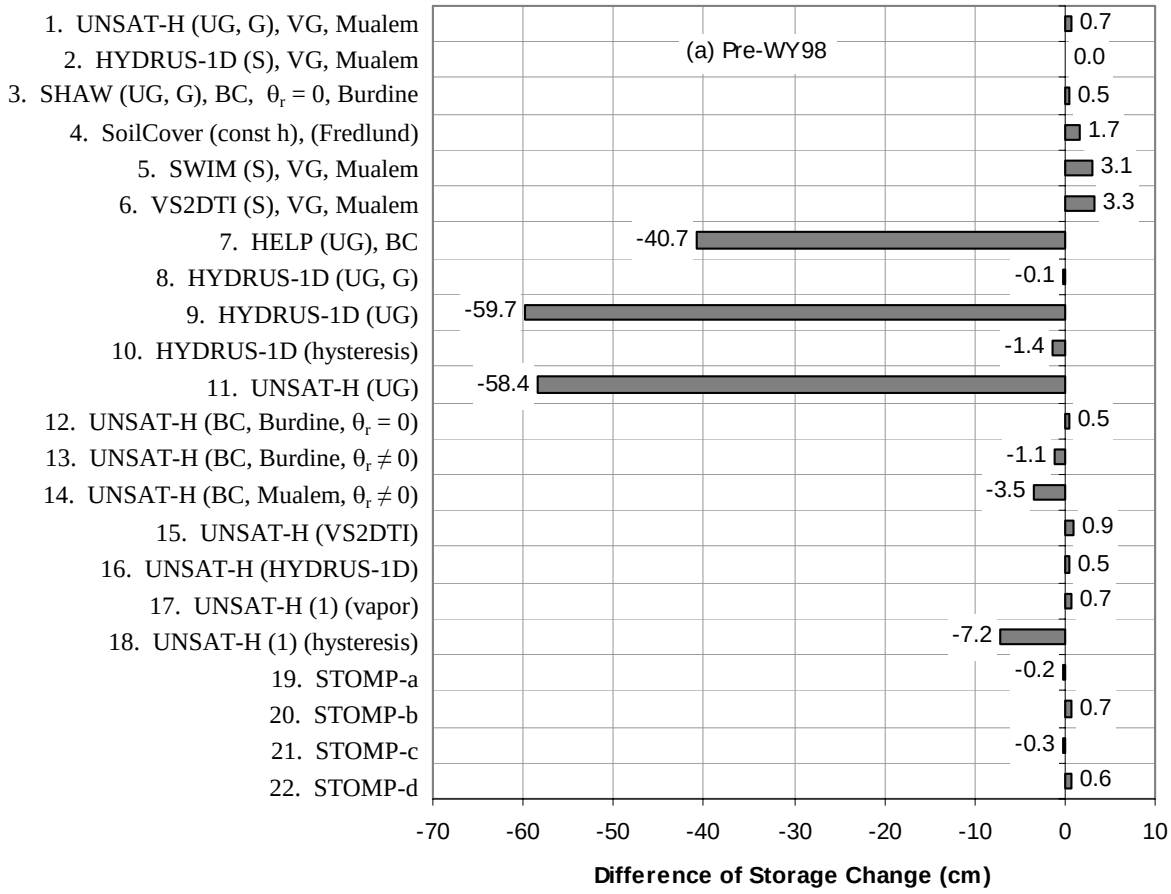

Figure 6.25. Differences Between Simulated Soil Water Storage Change and the Measured Values (cm) for Pre-WY98

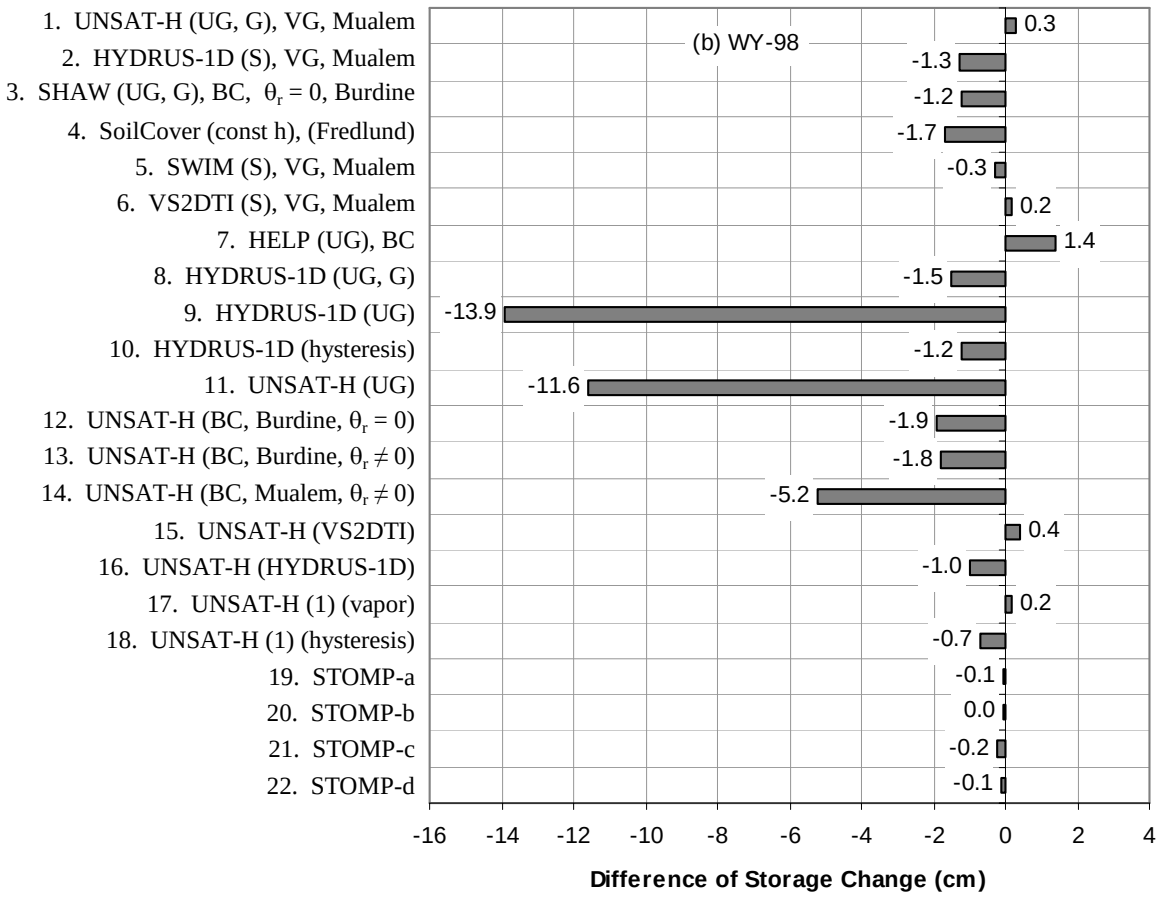

Figure 6.26. Differences Between Simulated Soil Water Storage Change and the Measured Values (cm) for WY98

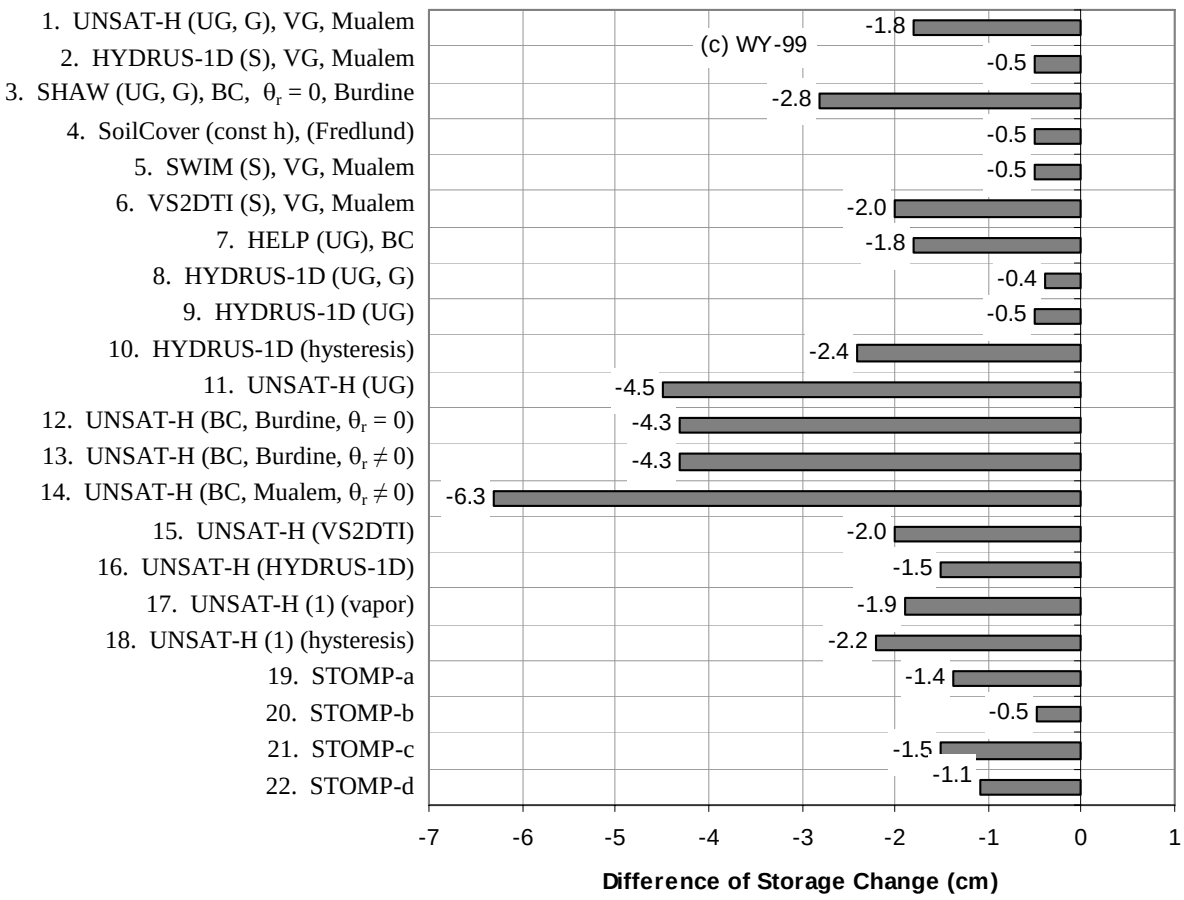

Figure 6.27. Differences Between Simulated Soil Water Storage Change and the Measured Values (cm) for WY99

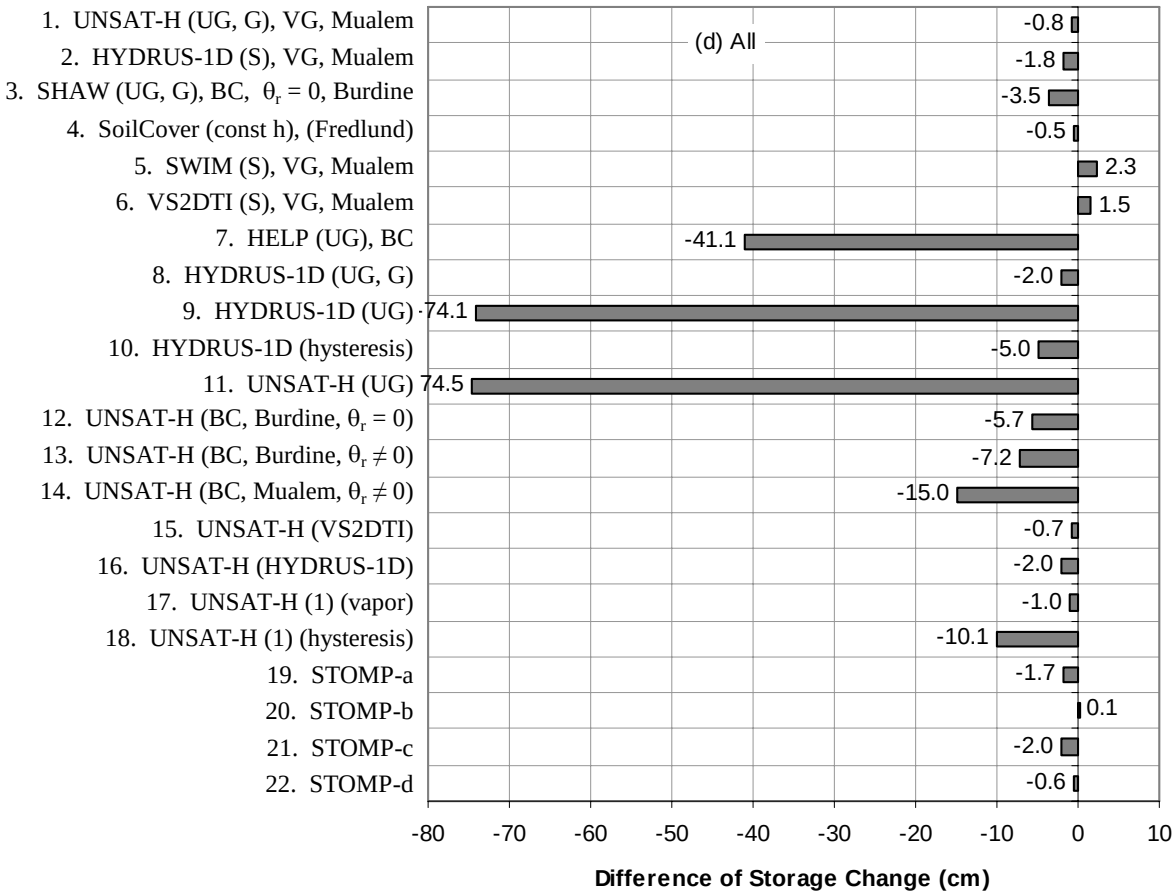

Figure 6.28. Differences Between Simulated Soil Water Storage Change and the Measured Values (cm) for WY97-99

6.7.2.3 Soil Evaporation (E)

Figure 6.29 through Figure 6.32 show the difference between simulated soil evaporation (E_{sim}) and the measured evaporation (E_{mea}). Results other than those of the STOMP simulations were taken from Table 4 of Scanlon et al. (2002). For all the 22 simulations, these differences vary from -1.8 to 5.1 cm for Pre-WY98 whereas the results of the four STOMP simulations were within 3.9 to 4.7 cm (Figure 6.29). For WY98 (Figure 6.30), the range of the evaporation differences was between -7.1 and 11.3 cm (vs. 1.2 to 4.0 cm for STOMP simulations). For WY99 (Figure 6.31), the range of the evaporation differences was between -5.0 and 12.0 cm (vs. -0.1 to 2.9 cm for STOMP simulations). For the whole simulation period (Figure 6.32), the range of the evaporation differences was between -12.7 and 27.3 cm (vs. 4.9 to 11.5 cm for STOMP simulations). The simulation errors of E for the whole simulation period ranged from -39.3 to ~84.5 percent (vs. 15.3 to ~35.7 percent for STOMP simulations).

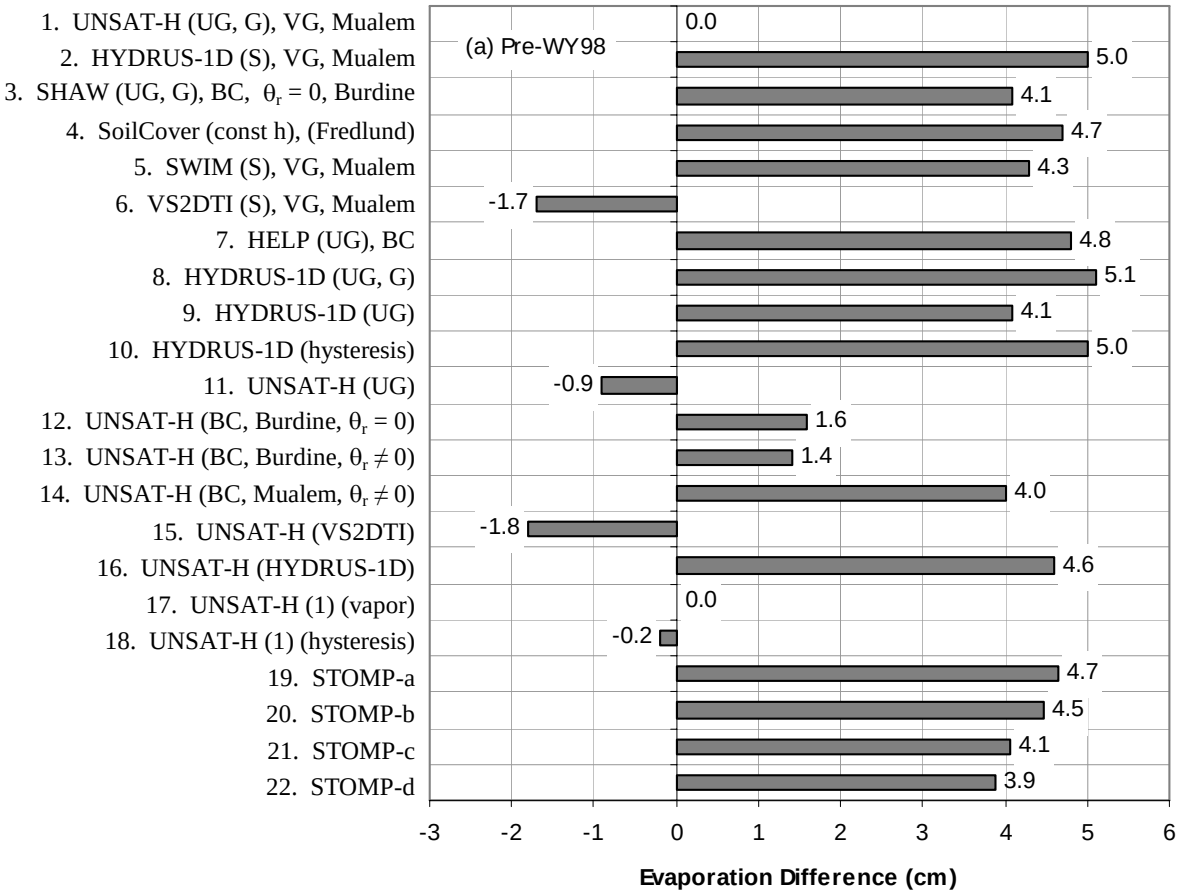

Figure 6.29. Differences Between Simulated Soil Evaporation and the Measured Values (cm) for Pre-WY98

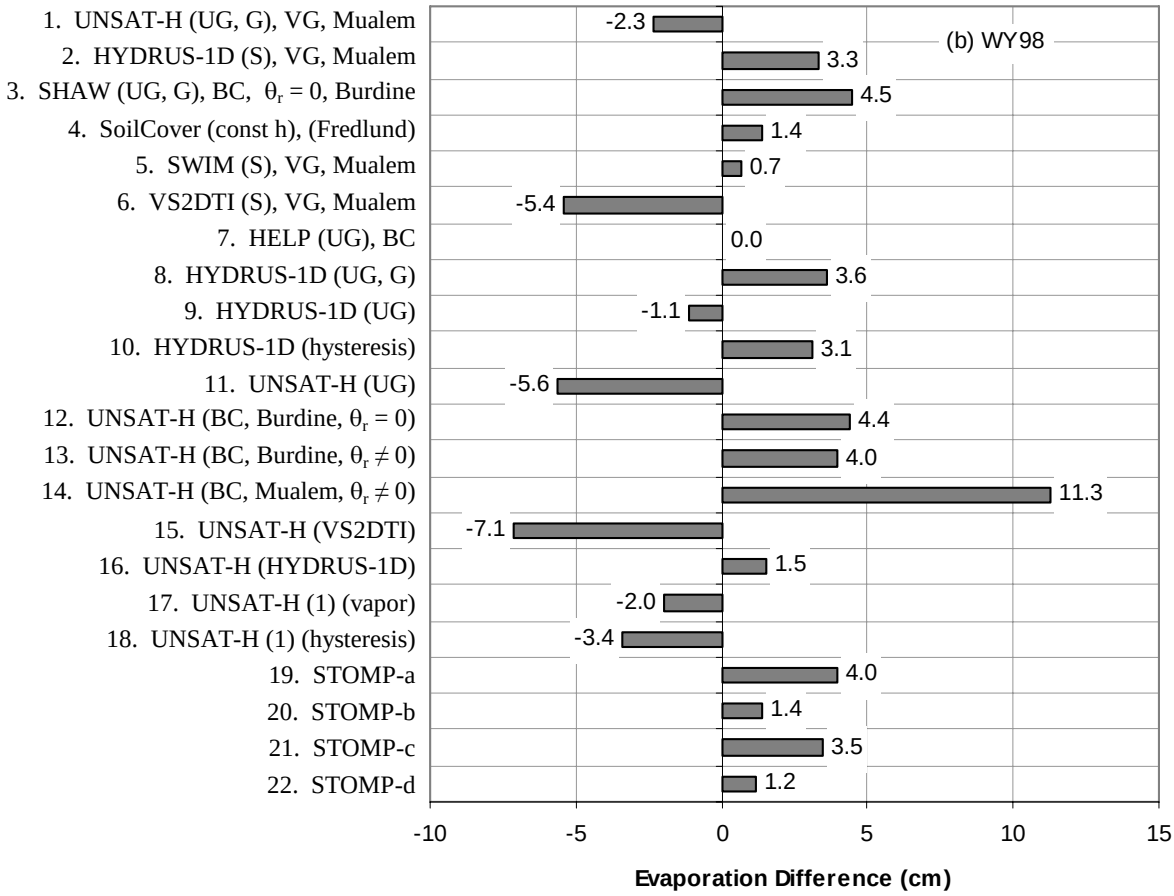

Figure 6.30. Differences Between Simulated Soil Evaporation and the Measured Values (cm) for WY-98

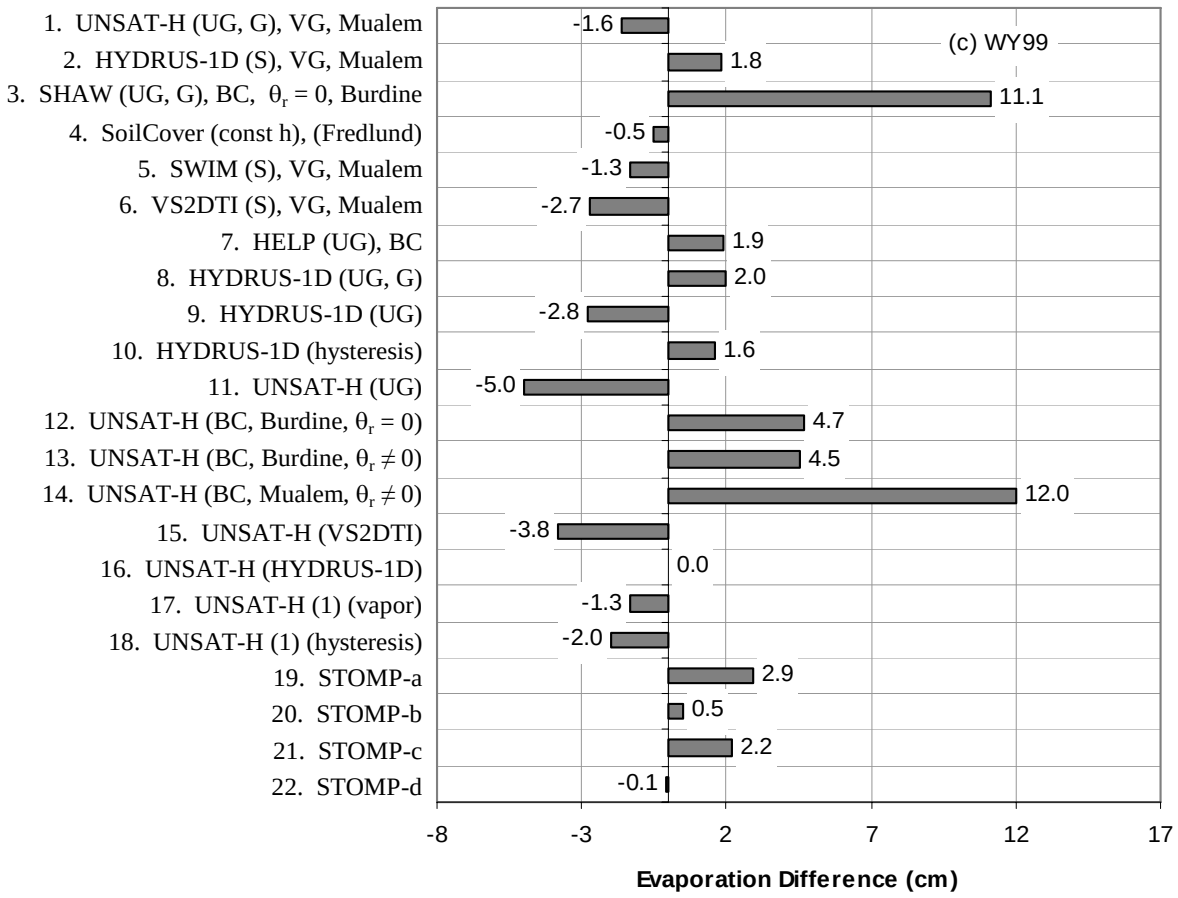

Figure 6.31. Differences Between Simulated Soil Evaporation and the Measured Values (cm) for WY-99

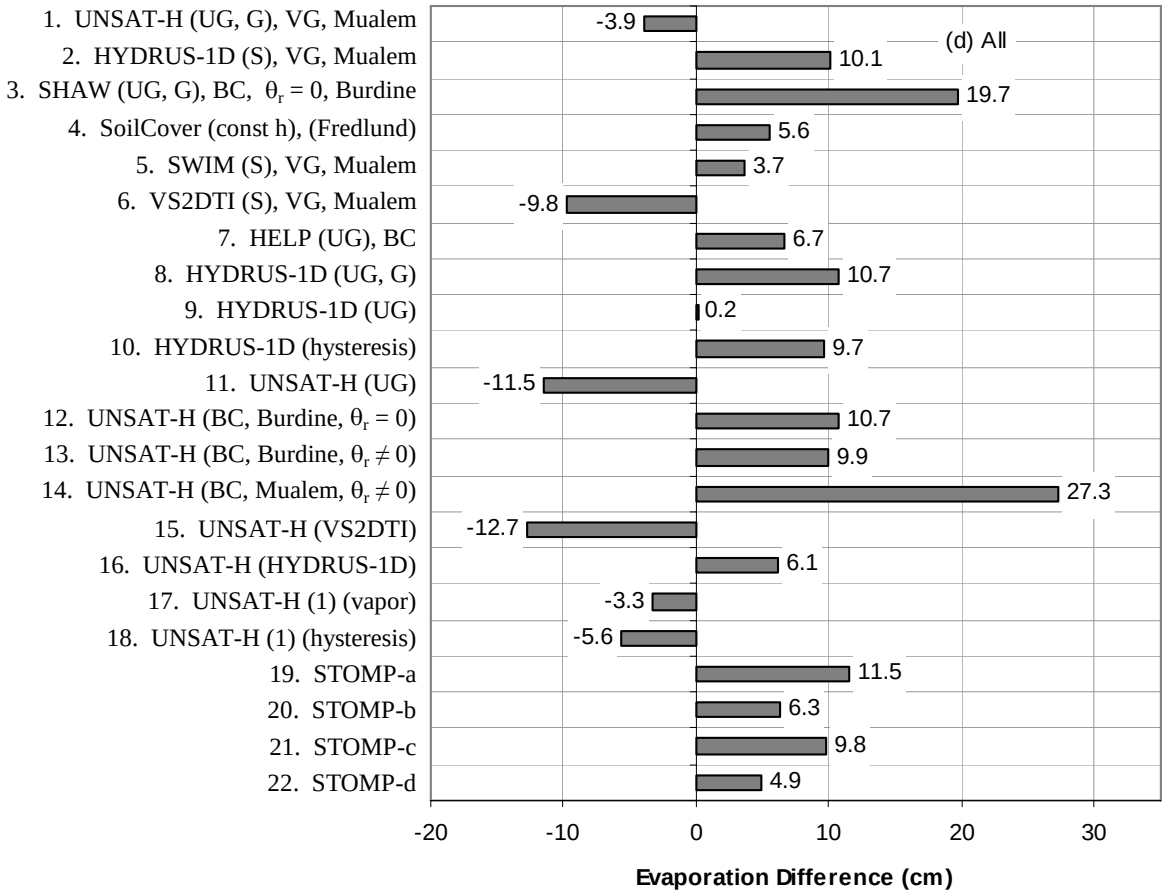

Figure 6.32. Differences Between Simulated Soil Evaporation and the Measured Values (cm) for WY97-99

6.7.3 Summary and Conclusions

A near-surface water balance is the most comprehensive way to evaluate the performance of engineered barriers. Numerical modeling of the water balance provides the means of evaluating candidate barriers before construction to identify potential shortcomings while addressing regulatory concerns and optimizing design. Scanlon et al. (2002) reported on an intercode comparison study in which they compared water balance simulation results from seven different codes, HELP, HYDRUS- 1D, SHAW, SoilCover, SWIM, UNSAT-H, and VS2DTI, using 1- to 3-year water balance monitoring data from non-vegetated engineered covers in warm (Texas) and cold (Idaho) desert regions. Simulation results from most codes were similar and reasonably approximated measured water balance components. The simulation of infiltration excess or runoff was a problem for all codes. Annual drainage was estimated to be within ± 64 percent by most codes. Scanlon et al. (2002) concluded that outliers were most likely caused by a combination of factors including, but not limited to, differences in the modeling approach (storage routing versus Richards' equation), upper boundary condition during precipitation, lower boundary condition (seepage face versus unit gradient), and the water-retention function (van Genuchten versus Brooks and Corey). The code comparison study identified important factors for simulating the near-surface water balance.

For the STOMP-WAE-B benchmark study, the Idaho barrier was chosen for simulation as the conditions are more similar to those at Hanford. In a fashion similar to Scanlon et al. (2002), measured and simulated water balances for the Idaho site were compared for the initial period (2 July 1997 through 30 September 1997; Pre-WY98) and water years 1998 and 1999 (WY98, WY99). Unlike Scanlon et al. (2002), however, the measured hydraulic properties, rather than optimized properties, were used in all the simulations.

As has been pointed out by Scanlon et al. (2002), simulated drainage generally occurred much earlier than measured drainage each year. The difference in the timing between the simulated and measured drainage is attributed to the inability of the codes to simulate reduction in infiltration and in hydraulic conductivity due to soil freezing. In a comparison of 22 simulations, errors in drainage for the whole simulation period ranged from -40.6 to 216.0 percent compared to -24.4 to -11.0 percent for STOMP simulations. In the prediction of water storage changes over the entire simulation period, differences ranged from -74.5 to 2.3 cm, compared to a range of -2.0 to 0.1 with STOMP-WAE-B. The simulation errors of water storage change for the whole simulation period ranged from -156.2 to ~4.8 percent compared to -4.2 to 0.3 percent with STOMP-WAE-B. For the whole simulation period, the range of the evaporation differences was between -12.7 and 27.3 cm compared to a range of 4.9 to 11.5 cm with STOMP-WAE-B. For the same period, the simulation errors for evaporation ranged from -39.3 to 84.5 percent compared to 15.3 to 35.7 percent with STOMP-WAE-B. Not only was the STOMP simulator capable of matching the field observations, but in all cases, it produced superior results.

7.0 References

American Society of Mechanical Engineers (ASME). 1967. *Thermodynamic and Transport Properties of Steam*. United Engineering Center, New York, NY.

Aston, A.R. 1979. "Rainfall interception by eight small trees". *J. Hydrol*., 42:383-396.

Baldocchi, D.D., L. Xu, and N. King. 2004. "How plant functional-type, weather, seasonal drought, and soil physical properties alter water and energy fluxes of an oak-savannah and an annual grassland.". *Agric. Forest Meteorol*. 123:13-39.

Battye W, and R Barrows. 2004. "Review of Ammonia Emission Modeling Techniques for Natural Landscapes and Fertilized Soils." EPA Contract No. 68-D-02-064.

Beljaars ACM, and AAM Holtslag. 1991. "Flux parameterization over land surfaces for atmospheric models." *J. App. Meterol.* 30:327-341.

Berdahl P, and R Fromberg. 1982. "The thermal radiance of clear skies." *Solar Energy* 29(4):299-314.

Briegleb BP, P Minnis, V Ramanathan, and E Harrison. 1986. "Comparison of regional clear sky albedos inferred from satellite observations and model calculations." *J. Clim. Appl. Meteorol.* 25:214-226.

Brooks RH, and AT Corey. 1964. "Hydraulic properties of porous media." Hydrol. Paper 3. Colorado State University, Fort Collins, CO.

Brutsaert W. 1979. "Heat and mass transfer to and from surfaces with dense vegetation or similar permeable roughness." *Bound.-Layer Meteor*. 16:365-388.

Buckingham E. 1907. "Studies on the movement of soil moisture." U.S. Department of Agriculture Bureau of Soils, Government Printing Office, Bulletin 38, Washington, D.C.

Bultot F, GL Dupriez, and A Bodeux. 1972. "Interception de la pluie par la ve´ge´tation forestie`re: Estimation de l'interception journalie`re a` l'aide d'un mode`le mathe´matique." *J. Hydrol.* 17:193-223.

Calder IR. 1977. "The model of transpiration and interception loss from a spruce forest in Plynlimon, central Wales." *J. Hydrol.* 33:247-265.

Campbell GS. 1977. *An introduction to environmental biophysics*. Springer-Verlag, New York, NY.

Campbell GS. 1985. "Soil Physics with Basic, Transport Models for Soil-Plant Systems." *Developments in Soil Science 14*, Elsevier, Amsterdam.

Carroll JJ. 1985. "Global transmissivity and diffuse fraction of solar radiation for clear and cloudy skies as measured and as predicted by bulk transmissivity models." *Solar Energy* 35:105-118.

Cass A, GS Campbell, and TL Jones. 1984. "Enhancement of thermal water vapor diffusion in soil." *Soil Sci. Soc. Am. J.* 48:25-32.

Cline JF, DW Uresk, and WH Rickard. 1977. "Comparison of soils water used by a sagebrush-bunchgrass and a cheatgrass community." *J. Range Manage.* 30:199-201.

Clothier BE, KL Clawson, PJ Pinter, Jr., MS Moran, RJ Reginato, and RD Jackson. 1986. "Estimation of soil heat flux from net radiation during the growth of alfalfa." *Agric. Forest Metorol.* 37:319-29.

Darcy H. 1856. *Les Fontaines Publiques de la Ville de Dijon.* Dalmont, Paris.

de Vries DA. 1958. "Simultaneous transfer of heat and moisture in porous media." *Trans. Amer. Geophys. Union* 39:909-916.

Deardorff J. 1978. "Efficient prediction of ground temperature and moisture with inclusion of a layer of vegetation." *J. Geophys. Res.* 83:1889-1903.

Dickinson, RE., and A. Henderson-Sellers. 1988. "Modeling tropical deforestation: A study of GCM land-surface parameterizations". *Quart. J. Roy. Meteor. Soc*., 114, 439–462.

Dirmhirn I, and GH Belt. 1971. "Variation of albedo of selected sagebrush range in the intermountain region." *Agr. Meteorol.* 951-961.

Doorenbos J, and WO Pruitt. 1977. "Guidelines for predicting crop water requirements." *FAO Irrigation Paper No. 24, 2nd ed.*, Food and Agriculture Organization of the United Nations, Rome, Italy, pp. 1-107.

Driese KL, and WA Reiners. 1997. "Aerodynamic roughness parameters for semiarid natural shrub communities of Wyoming, USA." *Agricultural and Forest Meteorology* 88(1-4):1-14.

Duffie, J. A., and W. A. Beckman, 1974. *Solar Energy Thermal Processes*. A Wiley-Interscience Publication, John Wiley & Sons, New York.

Dunkerley DL. 2000. "Measuring interception loss and canopy storage in dryland vegetation: a brief review and evaluation of available research strategies." *Hydrological Processes* 14:669-678.

Duynkerke PG. 1992. "The roughness length for heat and other vegetation parameters for a surface of short grass." *J. App. Meteorol.* 31: 579-586.

Evett S.R. 1999. "Energy and Water Balances at Soil-Plant-Atmosphere Interfaces." *CRC Handbook of Soil Science*. Chapter 5 in ME Summer (Ed.) A-129-A-184, CRC Press.

Fayer MJ, and TL Jones. 1990. *UNSAT-H Version 2.0: Unsaturated soil water and heat flow model*. PNL-6779, Pacific Northwest Laboratory, Richland, WA.

Fayer MJ. 2000. *UNSAT-H Version 3.0: Unsaturated soil water and heat flow model—Theory, user manual, and examples*. PNNL-13249, Pacific Northwest National Laboratory, Richland, WA.

Feddes RA, PJ Kowalik, and H. Zaradny. 1978. *Simulation of field water use and crop yield*. John Wiley and Sons, Inc., New York.

Flerchinger GN. 2000. *The Simultaneous Heat and Water (SHAW) Model: Technical Documentation*. NWRC 2000-09, Northwest Watershed Research Center, USDA Agricultural Research Service, Boise, ID.

Garratt JR, and BB Hicks. 1973. "Momentum, heat and vapour transfer from to and from natural and artificial surfaces." *Quart. J. Roy. Meteor. Soc.* 99:680-687.

Garratt JR, BB Hicks, and RA Valigura. 1993. "Comment on the "The roughness length for heat and other vegetation parameters for a surface of short grass." *J. App. Meteor.* 32:1301-1303.

Gee G, and D Hillel. 1988. ''Groundwater recharge in arid regions: Review and critique of estimation methods.'' *J. Hydrol. Processes* 2:255-266.

Gee GW, AL Ward, and MJ Fayer. 1997. ''Surface barrier research at the Hanford site.'' In: *Proc., Intl. Contain. Tech. Conf.,* U.S. Dept. of Energy, Germantown, Md., 305-311.

Gee GW, and RR Kirkham. 1984. "Arid site water balance: Evapotranspiration modeling and measurements." PNL-5177, Pacific Northwest Laboratory, Richland, WA.

Ghuman BS, and SS Prihar. 1998. "Chloride displacement by water in layered soil columns." *Australian Journal of Soil Research* 18(2):207-214.

Goudriann J. 1988. "The bare bones of leaf-angle distribution in radiation models for canopy photosynthesis and energy exchange." *Agric. and Forest Meteorology* 43:155-169.

Hanson, CL. 2001. "Clear-sky albedo measured at seven rangeland sites in southwest Idaho". *J. Hydrologic Eng*. 6(6):532-534.

Haverkamp R, M Vauclin, J Touma, PJ Wierenga, and G Vachaud. 1977. "A comparison of simulation models for one-dimensional infiltration." *Soil Sci. Soc. Am. J.* 41:285-294.

Hicks BB, DD Baldocchi, TP Meyers, RP Hosker Jr., and DR Matt. 1987. A preliminary multiple resistance routine for deriving dry deposition velocities from measured quantities. *Water,Air, Soil Pollut.* 36:311–330.

Hoitink DJ, KW Burk, and JV Ramsdell. 1999. "Hanford Site climatological data summary 1998 with historical data". PNNL-12087, Pacific Northwest National Laboratory, Richland, Washington.

Hull AC, Jr., and GI Klomp. 1974. "Yield of crested wheatgrass under four densities of big sagebrush in southern Idaho." *U.S. Dep. Agr. Tech. Bull.* 1483. 38 p.

Hupet F, S Lambot, RA Feddes, JC van Dam, and M Vanclooster. 2003. "Estimation of root water uptake parameters by inverse modeling with soil water content data." *Water Resour. Res.* 39(11): Art. No. 1312.

Idso SB, RD Jackson, RJ Reginato, BA Kimball, and FS Nakayama. 1975. "The dependence of bare soil albedo on soil water content." *J. Appl. Meteorol.* 14:109-113.

Jarvis NJ. 1989. "A simple empirical model of root water uptake." *Journal of Hydrology* 107:57-72.

Jarvis P. 1976. "The interpretation of leaf water potential and stomatal conductance found in canopies in the field." *Philos. Trans. Roy. Soc. London,* 273B:593-610.

Johansen O. 1975. *Thermal conductivity of soils*. Ph.D. Thesis (CRREL Draft Translation 637, 1977), Trondheim, Norway.

Kasten F, and G Czeplak. 1980. "Solar and terrestrial radiation dependence on the amount and type of cloud." *Solar Energy* 24:177-189.

Kool JB, JC Parker, and MTh van Genuchten. 1985. "Determining soil hydraulic properties from one-step outflow experiments by parameter estimation: 1. Theory and numerical studies." *Soil Sci. Soc. Am. J.* 49:1348-1354.

Kremer RG, ER Hunt, Jr, SW Running, and JC Coughlan. 1996. "Simulating vegetational and hydrologic responses to natural climatic variation and GCM-predicted climate change in a semi-arid ecosystem in Washington, USA." *Journal of Arid Environments* 33:23-38.

Kustas WP, and CST Daughtry. 1990. "Estimation of the soil heat flux/net radiation ratio from multispectral data." *Agric. For. Meteorol.* 49:205-223.

Link SO, GW Gee, and JL Downs. 1990. "The effect of water stress on phenological and ecophysiological characteristics of cheatgrass and Sandberg's bluegrass." *J. Range Manage.* 43:506-513.

Llasat MC, and RL Snyder. 1998. "Data error effects on net radiation and evapotranspiration estimation." *Agricultural and Forest Meteorology* 91:209-221.

Lobell DB, and GP Asner. 2002. "Moisture Effects on Soil Reflectance." *Soil Sci. Soc. Am. J.* 66:722-727.

Massman WJ. 1980. "Water storage on forest foliage: A general model." *Water Resour. Res.* 16:210-216.

McCaughey JH, and WL Saxton. 1988. "Energy balance storage terms in a mixed forest." *Agr. Forest Meteor.* 44:1-18.

Mitchell JFB. 1989. "The greenhouse effect and climate change." *Reviews of Geophysics* 27:115-139.

Monteith JL. 1965. "Evaporation and environment." p. 205-234. In: *State and Movement of Water in Living Organisms.* 19th Symposium of the Society for Experimental Biology. Cambridge University 111:839-855. Cambridge University Press, Cambridge.

Monteith JL. 1973. *Principles of environmental physics.* American Elsevier, New York. 241 pp.

Monteith JL, and MH Unsworth. 1990. *Principles of Environmental Physics*. Edward Arnold, London, UK.

Mualem Y. 1976. "Hysteretical models for prediction of the hydraulic conductivity of unsaturated porous Media." *Water Resour. Res.* 12:1248-1254.

Muller E, and H Décamps. 2001. "Modeling soil moisture-reflectance." *Remote Sens. Environ.* 76:173-180.

Oldenburg CM, and K Pruess. 1993. "On numerical modeling of capillary barriers." *Water Resour. Res.* 29:1045-1056.

Oostrom, M., DH. Meck and MD. White. 2003. *STOMP Subsurface Transport Over Multiple Phases,* Version 3.0, An introductory short course. PNNL-14440, Pacific Northwest National Laboratory, Richland, WA.

Penman HL. 1948. "Natural evaporation from open water, bare soil, and grass." *Proc. Royal Soc. London* A193:120-146.

Philip JR, and DE Smiles. 1969. "Kinetics of sorption and volume change in three-component systems" *Aust. J. Soil Res.* 7:1-19.

Philip JR, and DA de Vries. 1957. "Moisture movement in porous materials under temperature gradients." *Eos. Trans. AGU.* 38:222-232.

Pleim JE, and A Xiu. 1995. "Development and Testing of a surface flux and planetary boundary layer model for application in mesoscale models." *J. App. Meteorol.* 34:16-32.

Poeter EP, and MC Hill. 1998. "Documentation of UCODE, A Computer Code for Universal Inverse Modeling." U.S. Geological Survey, Water-Resources Investigation Report, 98-4080, Denver, CO.

Post DF, A Fimbres, AD Matthias, EE Sano, L Accioly, AK Batchily, and LG Ferreira. 2000. "Predicting Soil Albedo from Soil Color and Spectral Reflectance Data." *Soil Sci. Soc. Am. J.* 64:1027-1034.

Ramirez JA, and S Senarath. 2000. "A Statistical–Dynamical Parameterization of Interception and Land Surface–Atmosphere Interactions." *J. Climate* 13:4050-4063.

Reifsnyder WE. 1988. "Evaporation and Environment." In: *Forests, Climate and Hydrology.* RC Reynolds and FB Thompson (Eds.). The United Nations University, Tokyo, pp. 117-127.

Richards LA. 1931. "Capillary conduction of liquids through porous media." *Physics* 1:318-333.

Rockhold ML, MJ Fayer, and GW Gee. 1988. "Characterization of unsaturated hydraulic conductivity at the Hanford Site". PNL-6488, Pacific Northwest Laboratory, Richland, Washington.

Rosenberg NJ, BL Blad, and SB Verma. 1983. Microclimate: The biological environment.

Rosenburg NJ. 1974. *Microclimnate: The Biological Environment.* John Wiley & Sons, New York.

Rowntree PR. 1988. "Review of general circulation models as a basis for predicting the effects of vegetation change on climate." In: *Forest, Climate and Hydrology: Regional Impacts.* ERC Reynolds and FB Thompson (Eds), pp.162-203. Kefford Press, Singapore.

Samson R, and R. Lemeur. 2001. "Energy balance storage terms and big-leaf evapotranspiration in a mixed deciduous forest." *Ann. For. Sci.* 58:529-541.

Scanlon BR, M Christmans, RC Reedy, I Porro, and J Simunek, and GN Flerchinger. 2002. "Intercode comparisons for simulating water balance of surfacial sediments in semiarid regions." *Water Resour. Res.* 38(2):1323.

Sellers PJ, WJ Shuttleworth, JL Dorman, A Dalcher, and JM Roberts. 1989. "Calibrating the Simple Biosphere model for Amazonian tropical forest using field and remote sensing data. Part I: Average calibrating with field data." *J. Appl. Meteor.* 28:727-759.

Shuttleworth WJ. 1994. "Evaporation." In: *Handbook of hydrology*. DR Maidment (Ed.), Mcgraw-Hill, New York, pp. 4.1-4.53.

Shuttleworth JW, and JS Wallace. 1985. "Evaporation from sparse crops-an energy combination theory." *Quart. J. R. Met. Soc.* 111:839-855.

Somerton WH. 1992. *Thermal Properties and Temperature Related Behavior of Rock/Fluid Systems.* Elsevier, New York, NY.

Stanhill G. 1969. "A simple instrument for field measurement of turbulent diffusion flux." *J. Appl. Meteorol.* 8:509-513.

Stannard DI. 1993. "Comparison of Penman-Monteith, Shuttleworth-Wallace, and Modified Priestly-Taylor evapotranspiration models for wildland vegetation in semiarid rangeland." *Water Resources Research* 29(5):1379-1392.

Stone WA, JM Thorp, OP Gifford, and DJ Hoitink. 1983. *Climatological summary for the Hanford area*. PNL-4622, Pacific Northwest Laboratory, Richland, WA.

Sun J. 1999. "Diurnal Variations of Thermal Roughness Height Over a Grassland Boundary-Layer. *Meteorology* 92:407-427.

Suter GW, RJ Luxmoore, and ED Smith. 1993. "Compacted soil barriers at abandoned landfill sites are likely to fail in the long term." *J. Environ. Qual.* 22(2):217-226.

Szeicz G, G Endrodi, and S Tajchman. 1969. "Aerodynamic and surface factors in evaporation." *Water Resour. Res.* 5:380-394.

Talbott S. 1988. *Managing Projects with Make*, O'Reilly and Associates, Inc., Newton, Massachusetts.

U.S. Department of Energy-Richland Operations (DOE-RL). 1999. *200-BP-1 prototype barrier treatability test report*. DOE/RL-99-11 Rev.0, U.S. Department of Energy.

van Bavel CHM, and DI Hillel. 1976. "Calculating potential and actual evaporation from a bare soil surface by simulation of concurrent flow of water and heat." *Agric. Meteorol.* 17:453-476.

van Dam JC, JNM Stricker, and P Droogers. 1994. "Inverse method to determine soil hydraulic functions from multistep outflow experiments". *Soil Sci. Soc. Am. J.* 58:647–652.

van Genuchten MT. 1980. "A closed-form equation for predicting the hydraulic conductivity of unsaturated soils." *Soil Sci. Soc. Am. J.* 44: 892-898.

van Genuchten MTA. 1987. *A numerical model for water and solute movement in and below the root zone*. Research Report 121, U.S. Salinity Laboratory, Agricultural Research Service, U.S. Department of Agriculture, Riverside, CA.

van Genuchten MTA, and SK Gupta. 1993. "A reassessment of the crop tolerance response function." *Bulletin of the Indian Society of Soil Science* 4:730-737.

Vrugt JA, MT van Wijk, JW Hopmans, and J Simunek. 2001. "One-, two-, and three-dimensional root water uptake functions for transient modeling." *Water Resources Research* 37(10):2457-2470.

Wang Z, M Barlage, X Zeng, RE Dickinson, and CB Schaaf. 2005. "The solar zenith angle dependence of desert albedo." *Geophys. Res. Lett.* 32 (5): Art. No. L05403, Mar 8, 2005.

Ward AL, GW Gee, and SO Link. 1997. *Hanford Prototype Barrier Status Report: FY 1997*. PNNL-11789, Pacific Northwest National Laboratory, Richland, WA.

Ward AL, JK Linville, JM Keller, and GH Seedahmed. 2005a. *200-BP-1 Prototype Hanford Barrier Annual Monitoring Report for Fiscal Year 2004*. PNNL-14960, Pacific Northwest National Laboratory, Richland, WA.

Ward AL, JK Linville, and CD Wittreich. 2005b. *200-BP-1 Prototype Hanford Barrier Annual Monitoring Report for Fiscal Year 2003*. PNNL-14960, Pacific Northwest National Laboratory, Richland, WA.

Ward, A.L, and JM Keller. 2005. *Hydrology and Vegetation Data Package for 200-UW-1 Waste Site Engineered Surface Barrier Design*. PNNL-15464, Pacific Northwest National Laboratory, Richland, WA.

Ward A, and G Gee. 1997. ''Performance evaluation of a field-scale surface barrier.'' *J. Envir. Quality*. 26:694-705.

Wells LP, and GJ Blake. 1972." "Interception characteristics of some central North Island vegetation and their geographical significance." In: *Proc. Seventh New Zealand Geogr. Conf.* Hamilton, New Zealand, 217-224.

West NE. 1983. "Western Intermountain sagebrush steppe." *In: Temperate deserts and semi-deserts, Ecosystems of the World,* 5th Edition, NE West, editor. Elsevier, Amsterdam, Pages 351-374.

West NE, and GF Gifford. 1976. "Rainfall Interception by Cool-Desert Shrubs." *J. Range Manag.* 29:171-172.

White MD, and AL Ward. 2005. "Numerical simulation of surface barriers for shrub-steppe ecoregions." *Hydrology Days* 25:224-236.

White MD, and M Oostrom. 2000. *STOMP Subsurface Transport Over Multiple Phases*, Version 2.0, Theory Guide. PNNL-12030, Pacific Northwest National Laboratory, Richland, WA.

White MD, and M Oostrom. 2003. *STOMP Subsurface Transport Over Multiple Phases: User's Guide.* PNNL-14286, Pacific Northwest National Laboratory, Richland, WA.

Wilcox BP, DD Breshears, and MS Seyfried. 2003. "Water Balance on Rangelands." *Encyclopedia of Water Science*, pp. 791-794.

Williamson, S. C., J. K. Detling, J. L. Dood, and M. I. Dyer, Nondestructive estimation of shortgrass aerial biomass, J. Range Manage., 40, 254–256, 1987.

Zhang ZF, AL Ward, and GW Gee. 2002. *Estimating Field-Scale Hydraulic Parameters of Heterogeneous Soils Using A Combination of Parameter Scaling and Inverse Methods*. PNNL-14109, Pacific Northwest National Laboratory, Richland, WA.

Zhang ZF, AL Ward, and GW Gee. 2004. "A parameter scaling concept for estimating field-scale hydraulic functions of layered soils." *J. Hydraulic Res.* 42:93-103.

Appendix A

Input Format Notation Guide

Appendix A: Input Format Notation Guide

Notation	Description
{ Option }	Character string options are indicated by enclosing braces. Options are chosen by entering word(s) within the braces, exactly as shown. Only one option should be chosen for each data entry.
[Optional]	Enclosing brackets indicate optional characters or words. These characters can be entered to include the input file to improve its readability or to specify optional features.
{{ Contains }}	Indicates the option contains a particular word. For example “Fractured Tuff” contains the word “Fractured” thus indicating a dual-porosity type rock/soil.
< *Data Types* >	Indicates repeated formatting.
Char[a]	Character string data type, referenced by superscript “a”.
Integer[a]	Integer data type (no character data or decimal points) reference by superscript “a”.
Real[a]	Real data type (decimal points and exponential notation are acceptable), reference by superscript “a”.
#	A pound symbol in the first column indicates a comment line and will be ignored during execution. Comment lines may be placed inside or outside card structures. All lines outside of the card structures are ignored during execution.
~ Card Name	A tilde symbol in the first column indicates the start of a new card.
,	Data entries are comma delimited. Commas shown in the line format structures must be entered as shown, including a closing comma at the end of each line. Characters following the last comma of a data line are ignored during execution.

Units[a] (m)	Indicates the SI unit for the input data item referenced by superscript “a”.
|	Indicates a choice between more than one options
Format:	Indicates line formatting instructions and the beginning of a new input line. Each format statement requires a new input line.
Endcard:	Indicates end of a card.
For: Integer Instructions **Endfor:** Integer	Indicates instruction looping.
If: Name: Card = { Opt_1 } Instructions1 **Elseif:** Name: Card = { Opt_2 } Instructions2 **Elseif:** Instructions3 **Endif:**	Indicates decision logic.
IfDef: Opt_1 Instructions1 **ElseifDef:** Opt_2 Instructions2 **ElseDef:** Instructions3 **EndifDef:**	Indicates C preprocessor options and logic.
Note:	Indicates formatting information.

Appendix B

STOMP Input Control Card Formats

Appendix B: STOMP Input Control Card Formats

Atmospheric Conditions Card

Card Title[a] { ~Atmospheric [Conditions Card] }
Format: *Char*[a]

If: Operational Mode Option Card = { **Water-Air-Energy** }

Atmospheric Start Time: Month[a], Atmospheric Start Time: Day[b],
Atmospheric Start Time: Year[c], Atmospheric Start Time: Time (military format)[d],
Wind Speed Measurement Height[e], Units[f] (m),
Air Temperature/Relative Humidity Measurement Height[g], Units[h] (m),
Local Longitude[i], Units[j] (deg),
Local Meridian[k], Units[l] (deg),
Momentum Roughness Lengthm[m], Units[n] (m),
Thermal Roughness Length[o], Units[p] (m),
Format: *Char*[a], *Integer*[b], *Integer*[c], *Char*[d], *Real*[e], *Char*[f], *Real*[g], *Char*[h], *Real*[i], *Char*[j], *Real*[k], *Char*[l], *Real*[m], *Char*[n], *Real*[o], *Char*[p],

If: Atmospheric Conditions Read From External File

External File with Atmospheric Conditions[a],
Format: *Char*[a],

Elseif: Atmospheric Conditions Read From Input File

Number of Atmospheric Condition Times[a],
Format: *Integer*[a],

For: Number of Atmospheric Condition Times
Atmospheric Condition Time[a], Units[b] (s),
Atmospheric Condition Temperature[c], Units[d] (K),
Atmospheric Condition Pressure[e], Units[f] (kg/(m s^2)),
Atmospheric Condition Water-vapor Relative Humidity[g],
Atmospheric Condition Net Solar Radiation[h], Units[i] (kg/m^3),
Atmospheric Condition Wind Speed[j], Units[k] (m/s),
Format: *Real*[a], *Char*[b], *Real*[c], *Char*[d], *Real*[e], *Char*[f], *Real*[g], *Real*[h], *Char*[i], *Real*[j], *Char*[k],
Endfor:

Endif:

Endif:

Endcard: Atmospheric Conditions Card

B.1.1 Atmospheric Conditions Card Examples

Extracted from a STOMP3 (Water-Air-Energy) input file:

```
#-------------------------------------------------------
~Atmospheric Conditions Card
#-------------------------------------------------------
June,29,2000,00:00:00,2.0,m,2.0,m,119.627,deg,120.0,deg,
file,hms2july,
```

Extracted from a STOMP3 (Water-Air-Energy) input file:

```
#-------------------------------------------------------
~Atmospheric Conditions Card
#-------------------------------------------------------
December,31,1993,00:00:00,15.24,m,0.914,m,120.0,deg,46.57,deg,120.0,deg,0.002,m,0.0004,m,
35068,
file,HMS-hrly94-97,
```

Extracted from a STOMP3 (Water-Air-Energy-Barrier) input file:

```
#-------------------------------------------------------
~Atmospheric Conditions Card
#-------------------------------------------------------
May,23,2003,00:00:00,0.914,m,15.24,m,120.0,deg,46.57,deg,120.0,deg, 0.07,m,0.007,m,
11,
0,hr,52.02512734,F,101325,Pa,0.782656604,0,W/m^2,5.3,mi/hr,
1,hr,51.46891179,F,101325,Pa,0.804277766,0,W/m^2,5.3,mi/hr,
2,hr,51.11925995,F,101325,Pa,0.81821885,0,W/m^2,5.3,mi/hr,
3,hr,51,F,101325,Pa,0.823036934,0,W/m^2,5.3,mi/hr,
4,hr,51.11925932,F,101325,Pa,0.818218876,0,W/m^2,5.3,mi/hr,
5,hr,51.46891058,F,101325,Pa,0.804277814,24.09701458,W/m^2,5.3,mi/hr,
6,hr,52.02512562,F,101325,Pa,0.78265667,70.35707722,W/m^2,5.3,mi/hr,
7,hr,52.7499993,F,101325,Pa,0.75546981,116.6171399,W/m^2,5.3,mi/hr,
8,hr,53.59413266,F,101325,Pa,0.725161674,159.7246557,W/m^2,5.3,mi/hr,
9,hr,54.49999939,F,101325,Pa,0.694174266,196.7419187,W/m^2,5.3,mi/hr,
10,hr,55.40586617,F,101325,Pa,0.664693788,225.1462636,W/m^2,5.3,mi/hr,
11,hr,56.24999965,F,101325,Pa,0.638507033,243.0019813,W/m^2,5.3,mi/hr,
12,hr,56.97487352,F,101325,Pa,0.616960438,249.0922341,W/m^2,5.3,mi/hr,
13,hr,57.53108881,F,101325,Pa,0.600991532,243.0019813,W/m^2,5.3,mi/hr,
14,hr,57.88074037,F,101325,Pa,0.591195796,225.1462636,W/m^2,5.3,mi/hr,
15,hr,58,F,101325,Pa,0.587896633,196.7419187,W/m^2,5.3,mi/hr,
16,hr,57.84666618,F,101325,Pa,0.592142311,159.7246557,W/m^2,5.3,mi/hr,
17,hr,57.39711419,F,101325,Pa,0.60479416,116.6171399,W/m^2,5.3,mi/hr,
18,hr,56.68198024,F,101325,Pa,0.625564639,70.35707722,W/m^2,5.3,mi/hr,
19,hr,55.74999955,F,101325,Pa,0.653872216,24.09701458,W/m^2,5.3,mi/hr,
20,hr,54.66468508,F,101325,Pa,0.68870512,0,W/m^2,5.3,mi/hr,
21,hr,53.49999922,F,101325,Pa,0.728471608,0,W/m^2,5.3,mi/hr,
22,hr,52.33531342,F,101325,Pa,0.770888154,0,W/m^2,5.3,mi/hr,
23,hr,51.2499991,F,101325,Pa,0.812974017,0,W/m^2,5.3,mi/hr,
```

B.2 Boundary Conditions Card

Card Title[a] {~Boundary [Conditions Card] }
Format: *Char*[a]

Number of Boundary Condition Domains[a],
Format: *Integer*[a],

For: Number of Boundary Condition Domains

Boundary Surface Direction Option[a],
{ Bottom } { South } { West } { East } { North } { Top } { File }

If: Operational Mode Option = { **Water-Air-Energy** }
Energy Boundary Type Option[b],
{ Dirichlet | Neumann | Zero Flux |
| Outflow | Initial Condition | Ground | Convective | Convective-Radiative |
Bare Shuttleworth-Wallace | Shuttleworth-Wallace }
Aqueous-Phase Boundary Type Option[c],
{ Dirichlet | Neumann | Zero Flux | Saturated | Outflow |
Unit Gradient | Hydraulic Gradient | Initial Condition | Seepage Face }
Gas-Phase Boundary Type Option[d],
{ Dirichlet | Neumann | Zero Flux |
Hydraulic Gradient | Initial Condition }
For: Number of Solutes
Solute Transport Boundary Type Option[e],
{ Volumetric Conc. | Aqueous Conc. | Gas Conc. |
Zero Flux | Outflow | Initial Condition }
Endfor: Number of Solutes
Format: *Char*[a], *Char*[b], *Char*[c], *Char*[d], <*Char*[e],>
Endif:

If: Operational Mode Option = { **Water-Air-Energy** }
For: Number of Boundary Times
Boundary Time[a], Units[b] (s),

If: Energy Boundary Type Option = { Bare Shuttleworth-Wallace }
Volumetric Aqueous Flux[c], Units[d] (C),
Elseif: Energy Boundary Type Option = { Shuttleworth-Wallace }
Volumetric Aqueous Flux[c], Units[d] (C),
For: Number of Plant Species
Leaf Area Index[e],
Plant Area Index[f],

Endfor:

If: Aqueous-Phase Boundary Type Option = { Dirichlet } { Zero Flux }

Boundary Conditions Card (cont'd)

Aqueous Pressure[g], Units[h] (Pa),
Elseif: Aqueous-Phase Boundary Type Option = { Neumann }
Aqueous Volumetric Flux[g], Units[h] (m/s),
Elseif: Aqueous-Phase Boundary Type Option = { Hydraulic Gradient }
{ Seepage Face }
Base Aqueous Pressure[g], Units[h] (Pa),
Else:
Null[g], Null[h],
Endif:
Aqueous Dissolved-Air Relative Saturation[i],
If: Gas-Phase Boundary Type Option = { Dirichlet } { Zero Flux }
Gas Pressure[j], Units[k] (Pa),
Elseif: Gas-Phase Boundary Type Option = { Neumann }
Gas Volumetric Flux[j], Units[k] (m/s),
Elseif: Gas-Phase Boundary Type Option = { Hydraulic Gradient }
Base Gas Pressure[j], Units[k] (Pa),
Else:
Null[j], Null[k],
Endif:
Water-Vapor Relative Humidity[l],
For: Number of Solutes
If: Solute Transport Boundary Type Option = { Volumetric Conc. }
Solute Volumetric Conc[m], Units[n] (1/m^3),
Elseif: Solute Transport Boundary Type Option = { Aqueous Conc. }
Solute Aqueous-Phase Volumetric Conc[m], Units[n] (1/m^3),
Elseif: Solute Transport Boundary Type Option = { Gas Conc. }
Solute Gas Volumetric Conc[m], Units[n] (1/m^3),
Else:
Null[m], Null[n],
Endif:
Endfor: Number of Solutes
Format: *Real[a], Char[b], Real[c], Char[d],< Real[e],> Real[f], Char[g], Real[h], Real[i], Char[j], Real[k], < Real[l], Char[m], >*

Elseif: Energy Boundary Type Option = { Convective } { Convective-Radiative }
If: Energy Boundary Type Option = { Convective }
Conv. Temperature[c], Units[d] (C), Conv. Heat Transfer Coeff.[e], Units[r] (kg/C s^3),
Elseif: Energy Boundary Type Option = { Convective-Radiative }
Conv. Temperature[c], Units[d] (C), Rad. Temperature[e], Units[r] (C),
Endif:
If: Aqueous-Phase Boundary Type Option = { Dirichlet } { Zero Flux }
Aqueous Pressure[g], Units[h] (Pa),
Elseif: Aqueous-Phase Boundary Type Option = { Neumann }
Aqueous Volumetric Flux[g], Units[h] (m/s),
Elseif: Aqueous-Phase Boundary Type Option = { Hydraulic Gradient }
{ Seepage Face }

Boundary Conditions Card (cont'd)

Base Aqueous Pressure[g], Units[h] (Pa),
Else:
Null[g], Null[h],
Endif:
Aqueous Dissolved-Air Relative Saturation[i],
If: Gas-Phase Boundary Type Option = { Dirichlet } { Zero Flux }
Gas Pressure[j], Units[k] (Pa),
Elseif: Gas-Phase Boundary Type Option = { Neumann }
Gas Volumetric Flux[j], Units[k] (m/s),
Elseif: Gas-Phase Boundary Type Option = { Hydraulic Gradient }
Base Gas Pressure[j], Units[k] (Pa),
Else:
Null[j], Null[k],
Endif:
Water-Vapor Relative Humidity[l],
For: Number of Solutes
If: Solute Transport Boundary Type Option = { Volumetric Conc. }
Solute Volumetric Conc[m], Units[n] (1/m^3),
Elseif: Solute Transport Boundary Type Option = { Aqueous Conc. }
Solute Aqueous-Phase Volumetric Conc[m], Units[n] (1/m^3),
Elseif: Solute Transport Boundary Type Option = { Gas Conc. }
Solute Gas Volumetric Conc[m], Units[n] (1/m^3),
Else:
Null[m], Null[n],
Endif:
Endfor: Number of Solutes
Format: *Real[a], Char[b], Real[c], Char[d], Real[e], Char[f], Real[g], Char[h], Real[i], Real[j], Char[k], Real[l], < Real[m], Char[n], >*
Else:
If: Energy Boundary Type Option = { Dirichlet }
Temperature[c], Units[d] (C),
Elseif: Energy Boundary Type Option = { Neumann }
Energy Flux[c], Units[d] (W/m^2),

Elseif: Energy Boundary Type Option = { Ground }
Air Temperature[c], Units[d] (C),
Else:
Null[c], Null[d],
Endif:
If: Aqueous-Phase Boundary Type Option = { Dirichlet } { Zero Flux }
Aqueous Pressure[e], Units[f] (Pa),
Elseif: Aqueous-Phase Boundary Type Option = { Neumann }
Aqueous Volumetric Flux[e], Units[f] (m/s),
Elseif: Aqueous-Phase Boundary Type Option = { Hydraulic Gradient }
{ Seepage Face }

Boundary Conditions Card (cont'd)

Base Aqueous Pressure[e], Units[f] (Pa),
Else:
Null[e], Null[f],
Endif:
Aqueous Dissolved-Air Relative Saturation[g],
If: Gas-Phase Boundary Type Option = { Dirichlet } { Zero Flux }
Gas Pressure[h], Units[i] (Pa),
Elseif: Gas-Phase Boundary Type Option = { Neumann }
Gas Volumetric Flux[h], Units[i] (m/s),
Elseif: Gas-Phase Boundary Type Option = { Hydraulic Gradient }
Base Gas Pressure[i], Units[i] (Pa),
Else:
Null[h], Null[i],
Endif:
Water-Vapor Relative Humidity[j],
For: Number of Solutes
If: Solute Transport Boundary Type Option = { Volumetric Conc. }
Solute Volumetric Conc[k], Units[l] (1/m^3),
Elseif: Solute Transport Boundary Type Option = { Aqueous Conc. }
Solute Aqueous-Phase Volumetric Conc[k], Units[l] (1/m^3),
Elseif: Solute Transport Boundary Type Option = { Gas Conc. }
Solute Gas Volumetric Conc[k], Units[l] (1/m^3),
Else:
Null[k], Null[l],
Endif:
Endfor: Number of Solutes
Format: *Real[a], Char[b], Real[c], Char[d], Real[e], Char[f], Real[g], Real[h], Char[i], Real[j],* < *Real[k], Char[l],* >
Endif:
Endfor: Number of Boundary Times
Endif:

Endfor: Number of Boundary Condition Domains

Endcard: Boundary Conditions Card

B.2.1 Boundary Conditions Card Examples

Extracted from a STOMP3 (Water-Air-Energy) input file:

```
#-------------------------------------------------
~Boundary Conditions Card
#-------------------------------------------------
2,
West,Dirichlet Energy,Dirichlet Aqueous,Dirichlet Gas,
1,1,1,1,1,1,1,
0,day,70,C,101330,Pa,0,101330,Pa,1,
East,Neumann Energy,Zero Flux Aqueous,Zero Flux Gas,
50,50,1,1,1,1,1,
0,Day,-100,W/m^2,,,,,,,
```

Extracted from a STOMP3 (Water-Air-Energy) input file:

```
#-------------------------------------------------
~Boundary Conditions Card
#-------------------------------------------------
2,
Top,Zero Flux,Dirichlet,
1,1,1,1,91,91,2,
0,hr,-1.e9,Pa,1.,101758.43,Pa,
25,d,-1.e9,Pa,1.,101758.43,Pa,
Bottom,Dirichlet,Zero Flux,
1,1,1,1,1,1,2,
0,s,110629,Pa,1.0,,,
10,min,109595.22,Pa,1.0,,,
```

Extracted from STOMP-WAE-B (Water-Air-Energy-Barrier) input file:

```
#-------------------------------------------------
~Boundary Conditions Card
#-------------------------------------------------
2,
Top,Bare Shuttleworth-Wallace,,,
1,1,1,1,113,113,1700,
file,idaho_precip.dat,
Bottom,dirichlet Energy,Seepage Face Aqueous,Dirichlet Gas,
1,1,1,1,1,1,2,
0,day,15.0,C,101325,pa,1.0,101365,pa,1.0,
803,day,15.0,C,101325,pa,1.0,101365,pa,1.0,
```

Extracted from a STOMP-WAE-B (Water-Air-Energy-Barrier) input file:

```
#-------------------------------------------------
~Boundary Conditions Card
#-------------------------------------------------
5,
Bottom,Dirichlet Energy,Dirichlet Aqueous,Zero Flux Gas,
1,233,1,1,1,1,1,
0,day,20.0,C,101325,Pa,1.0,,,1.0,
```

Boundary Conditions Card (cont'd)

file,hanford_toeslope_top_bc,Bare Shuttleworth-Wallace,,,
2624,
file,94-97top_bc.dat,
file,hanford_slope_top_bc,Bare Shuttleworth-Wallace,,,
2624,
file,94-97top_bc.dat,
file,hanford_soil_top_bc,Bare Shuttleworth-Wallace,,,
2624,
file,94-97top_bc.dat,
file,hanford_slope_west_bc,Dirichlet Energy,Zero Flux Aqueous,Hydraulic Gradient Gas,
35067,
file,94-97west_bc.dat,

B.3 Gas Relative Permeability Card

Card Title[a] { ~Gas Rel [ative Permeability Card] }
Format: *Char[a]*

For: Number of Rock/Soil Types

If: Rock/Soil Name = { IJK | JKI | KIJ } Indexing

Note: A parameter value input can be replaced with an external file using the following formatting for ASCII files:

file: *filename*

or the following formattings for binary files:

binary file: *filename*

where; the external file will contain unique parameter values for each node (active or inactive) arranged according to the indexing scheme (i.e., IJK, JKI, or KIJ). Applicable units will be applied to all parameter values in the external file. An example input card is included in section B.6.1

Endif:

For: Number of Rock/Soil Types

If: Operational Mode ={ **Water-Air-Energy** }
Rock/Soil Name[a],
Permeability Function Option[b],
{ Constant | Mualem | Burdine | Fatt and Klikoff | Corey |
Tabular [Linear | Spline] [Water Content | Saturation] }
If: Permeability Function Option = { Constant }
If: Rock/Soil Name = {{ Fractured }} {{ DP }}
Matrix Gas Relative Permeability[c],
Fracture Gas Relative Permeability[d],
Format: *Char[a], Char[b], Real[c], Real[d],*
Else:
Gas Relative Permeability[c]
Format: *Char[a], Char[b], Real[c],*
Endif:
Elseif: Permeability Function Option = { Mualem } { Burdine }
If: Saturation Function Option = {{ van Genuchten }}
and Rock/Soil Name = {{ Fractured }} {{ DP }}
Matrix van Genuchten m parameter[c],
Fracture van Genuchten m parameter[d],

Gas Permeability Card (cont'd)

Format: *Char[a], Char[b], Real[c], Real[d],*

Elseif: Saturation Function Option = {{ Brooks and Corey }}
and Rock/Soil Type Name = {{ Fractured }} {{ DP }}
Matrix Brooks and Corey λ parameter[c],
Fracture Brooks and Corey λ parameter[d],
Format: *Char[a], Char[b], Real[c], Real[d],*
Elseif: Saturation Function Option = {{ van Genuchten }}
van Genuchten m parameter[c],
Format: *Char[a], Char[b], Real[c],*
Elseif: Saturation Function Option = {{ Brooks and Corey }}
Brooks and Corey λ parameter[c],
Format: *Char[a], Char[b], Real[c],*
Endif:
Elseif: Permeability Function Option = { Corey }
Irreducible Gas Saturation[c], Irreducible Aqueous Saturation[d],
Format: *Char[a], Char[b], Real[c], Real[d],*
Elseif: Permeability Function Option = { Fatt and Klikoff }
Format: *Char[a], Char[b],*
Elseif: Permeability Function Option = { Tabular Water Content [Linear | Spline] }
Number of Table Entries[c],
Format: *Char[a],Char[b],Integer[c],*
For: Number of Table Entries
Water Content[a], Gas Relative Permeability[b],
Format: *Real[a], Real[b],*
Endfor:
Elseif: Permeability Function Option = { Tabular [Saturation] [Linear | Spline] }
Number of Table Entries[c],
Format: *Char[a],Char[b],Integer[c],*
For: Number of Table Entries
Saturation[a], Gas Relative Permeability[b],
Format: *Real[a], Real[b],*
Endfor:
Endif:

Endfor: Number of Rock/Soil Types

Endcard: Gas Relative Permeability Card

Gas Permeability Card (cont'd)

B.3.1 Gas Relative Permeability Examples

Extracted from a STOMP3 (Water-Air-Energy) input file:

```
#-------------------------------------------------------
~Gas Relative Permeability Card
#-------------------------------------------------------
Sand,Mualem,,
```

Extracted from a STOMP (Water-Air-Energy) input file:

```
#-------------------------------------------------------
~Gas Relative Permeability Card
#-------------------------------------------------------
Sand,Corey,0.1,0.213,
```

Extracted from a STOMP3 (Water-Air-Energy) input file:

```
#-------------------------------------------------------
~Gas Relative Permeability Card
#-------------------------------------------------------
IJK Indexing,Constant,file:rel_g_x.dat,
```

Extracted from a STOMP3 (Water-Air-Energy) input file:

```
#-------------------------------------------------------
~Gas Rel
#-------------------------------------------------------
20/30 Ottawa Sand,Mualem,0.56,
```

Extracted from a STOMP3 (Water-Air-Energy) input file:

```
#-------------------------------------------------------
~Gas Relative Permeability Card
#-------------------------------------------------------
Sand,Fatt and Klikoff,
```

Extracted from a STOMP3 (Water-Air-Energy) input file:

```
#-------------------------------------------------------
~Gas Relative Permeability
#-------------------------------------------------------
SM-ML1,Burdine,,
SW1,Burdine,,
# Tabular Input
SP3,Tabular,6,
1.0, 1.0,
0.8, 0.64,
0.6, 0.36,
0.4, 0.16,
0.2, 0.04,
0.0, 0.0,
SM-SP1,Mualem,0.5,
SP2,Burdine,,
SP1,Burdine,,
```

B.4 Initial Conditions Card

Card Title[a] { ~Initial [Conditions Card] }
Format: *Char[a]*

If: Operational Mode Option: { **Water-Air-Energy** }
Initial Saturation Option[a], Initial Saturation Option[b],
{ Gas Pressure, Aqueous Pressure |
Gas Pressure, Aqueous Saturation |
Aqueous Pressure, Aqueous Saturation }
Format: *Char[a], Char[b],*
Endif:

Number of Initial Conditions Domains[a]
Format: *Integer[a],*

For: Number of Initial Conditions Domains

Note: The [Overwrite] option is used in conjunction with Restart simulations.

If: Operational Mode Option = { **Water-Air-Energy** }
Variable Name Option[a],
{ File [Binary] | Rock | Zonation |
Temperature [Overwrite] | Aqueous Pressure [Overwrite]
Gas Pressure [Overwrite] |
Aqueous Saturation | Trapped Gas Saturation [Overwrite] |
Aqueous Dissolved Air Mole frac[tion] [Overwrite] |
Aqueous Dissolved Air Mass Fraction [Overwrite] |
Aqueous Dissolved Air Relative Saturation [Overwrite] |
Solute [Volumetric Conc.] [Overwrite], Solute Name |
Solute Aqueous [Volumetric Conc.] [Overwrite], Solute Name |
Solute Gas [Volumetric Conc.] [Overwrite], Solute Name }
Endif:

If: Variable Name Option = { Pressure }
Pressure[b], Units[c] (Pa),
If: Variable Name Option = { File [Binary] }
File Name[d], File Units[e] (Pa),
Note: File contains pressure values for every node.
Format: *Char[a], Real[b], Char[c], Char[d], Char[e],*
Elseif: Variable Name Option = { Zonation | Rock }
Rock/Soil or Scaling Group Name[d],
Format: *Char[a], Real[b], Char[c], Char[d],*
Else:
X-Dir. Gradient[d], Units[e] (1/m),
Y-Dir. Gradient[f], Units[g] (1/m),

Z-Dir. Gradient[h], Units[i] (1/m),
I-Start Index[j], I-End Index[k],
J-Start Index[l], J-End Index[m],
K-Start Index[n], K-End Index[o],
Format: *Char[a], Real[b], Char[c], Real[d], Char[e], Real[f], Char[g], Real[h],*
Char[i], Integer[j], Integer[k], Integer[l], Integer[m], Integer[n], Integer[o],
Endif:

Elseif: Variable Name Option = { Temperature }
Temperature[b], Units[c] (C),
If: Variable Name Option = { File [Binary] }
File Name[d], File Units[e] (C),
Note: File contains temperature values for every node.
Format: *Char[a], Real[b], Char[c], Char[d], Char[e],*
Elseif: Variable Name Option = { Zonation | Rock }
Rock/Soil or Scaling Group Name[d],
Format: *Char[a], Real[b], Char[c], Char[d],*
Else:
X-Dir. Gradient[d], Units[e] (1/m),
Y-Dir. Gradient[f], Units[g] (1/m),
Z-Dir. Gradient[h], Units[i] (1/m),
I-Start Index[j], I-End Index[k],
J-Start Index[l], J-End Index[m],
K-Start Index[n], K-End Index[o],
Format: *Char[a], Real[b], Char[c], Real[d], Char[e], Real[f], Char[g], Real[h],*
Char[i], Integer[j], Integer[k], Integer[l], Integer[m], Integer[n], Integer[o],
Endif:
Elseif: Variable Name Option = { Saturation }
Saturation[b], Null[c],
If: Variable Name Option = { File [Binary] }
Note: File contains saturation values for every node.
Filename[d],
Format: *Char[a], Real[b], Char[c], Char[d],*
Elseif: Variable Name Option = { Zonation | Rock }
Rock/Soil or Scaling Group Name[d],
Format: *Char[a], Real[b], Char[c], Char[d],*
Else:
X-Dir. Gradient[d], Units[e] (1/m),
Y-Dir. Gradient[f], Units[g] (1/m),
Z-Dir. Gradient[h], Units[i] (1/m),
I-Start Index[j], I-End Index[k],
J-Start Index[l], J-End Index[m],
K-Start Index[n], K-End Index[o],
Format: *Char[a], Real[b],Null[c], Real[d], Char[e], Real[f], Char[g], Real[h],*
Char[i], Integer[j], Integer[k], Integer[l], Integer[m], Integer[n], Integer[o],

Endif:

Elseif: Variable Name Option = { Mass Fraction }
Mass Fraction[b], Null[c],
If: Variable Name Option = { File [Binary] }
File Name[d], Null[e] ,
Note: File contains mass fraction values for every node.
Format: *Char[a], Real[b], Char[c], Char[d], Char[e],*
Elseif: Variable Name Option = { Zonation | Rock }
Rock/Soil or Scaling Group Name[d],
Format: *Char[a], Real[b], Char[c], Char[d],*
Else:
X-Dir. Gradient[d], Units[e] (1/m),
Y-Dir. Gradient[f], Units[g] (1/m),
Z-Dir. Gradient[h], Units[i] (1/m),
I-Start Index[j], I-End Index[k],
J-Start Index[l], J-End Index[m],
K-Start Index[n], K-End Index[o],
Format: *Char[a], Real[b],Null[c], Real[d], Char[e], Real[f], Char[g], Real[h],*
Char[i], Integer[j], Integer[k], Integer[l], Integer[m], Integer[n], Integer[o],
Endif:

Elseif: Variable Name Option = { Mole frac[tion] }
Mole frac[tion][b],Null[c],
If: Variable Name Option = { File [Binary] }
File Name[d], Null[e] ,
Note: File contains mole frac[tion] values for every node.
Format: *Char[a], Real[b], Char[c], Char[d], Char[e],*
Elseif: Variable Name Option = { Zonation | Rock }
Rock/Soil or Scaling Group Name[d],
Format: *Char[a], Real[b], Char[c], Char[d],*
Else:
X-Dir. Gradient[d], Units[e] (1/m),
Y-Dir. Gradient[f], Units[g] (1/m),
Z-Dir. Gradient[h], Units[i] (1/m),
I-Start Index[j], I-End Index[k],
J-Start Index[l], J-End Index[m],
K-Start Index[n], K-End Index[o],
Format: *Char[a], Real[b], Null[c], Real[d], Char[e], Real[f], Char[g], Real[h],*
Char[i], Integer[j], Integer[k], Integer[l], Integer[m], Integer[n], Integer[o],
Endif:

Elseif: Variable Name Option = { Salt }
Volumetric Conc[b], Units[c] (kg/m^3[3]),
If: Variable Name Option = { File [Binary] }

Initial Conditions Card (cont'd)

File Name[d], Units[e] (kg/m^3),
Note: File contains salt Conc values for every node.
Format: *Char[a], Real[b], Char[c], Char[d], Char[e],*
Elseif: Variable Name Option = { Zonation | Rock }
Rock/Soil or Scaling Group Name[d],
Format: *Char[a], Real[b], Char[c], Char[d],*
Else:
X-Dir. Gradient[d], Units[e] (1/m),
Y-Dir. Gradient[f], Units[g] (1/m),
Z-Dir. Gradient[h], Units[i] (1/m),
I-Start Index[j], I-End Index[k],
J-Start Index[l], J-End Index[m],
K-Start Index[n], K-End Index[o],
Format: *Char[a], Real[b], Null[c], Real[d], Char[e], Real[f], Char[g], Real[h], Char[i], Integer[j], Integer[k], Integer[l], Integer[m], Integer[n], Integer[o],*
Endif:

Elseif: Variable Name Option = { Solute }
Solute Name[b], Volumetric Conc[c], Units[d] (1/m^3),
If: Variable Name Option = { File [Binary] }
File Name[d], Units[e] (1/m^3),
Note: File contains solute Conc values for every node.
Format: *Char[a], Real[b], Char[c], Char[d], Char[e],*
Elseif: Variable Name Option = { Zonation | Rock }
Rock/Soil or Scaling Group Name[d],
Format: *Char[a], Real[b], Char[c], Char[d],*
Else:
X-Dir. Gradient[d], Units[e] (1/m), Y-Dir. Gradient[f], Units[g] (1/m),
Z-Dir. Gradient[h], Units[i] (1/m),
I-Start Index[j], I-End Index[k],
J-Start Index[l], J-End Index[m],
K-Start Index[n], K-End Index[o],
Format: *Char[a], Char[b], Real[c], Char[d], Real[e], Char[f], Reals[g], Char[h], Real[i], Char[j], Integer[k], Integer[l], Integer[m], Integer[n], Integer[o], Integer[p],*
Endif:
Endif:

Endfor: Number of Initial Conditions Domains

Endcard: Initial Conditions Card

Initial Conditions Card (cont'd)

B.4.1 Initial Conditions Card Examples

Extracted from a STOMP3 (Water) input file:

```
#-------------------------------------------------------
~Initial Conditions Card
#-------------------------------------------------------
Gas Pressure,Aaqueous Pressure,
2,
Gas Pressure,101325,Pa,,,,,,,1,80,1,1,1,66,
Aqueous Pressure,91534.848,Pa,,,,,-9793.519,1/m,1,80,1,1,1,66,
```

Extracted from a STOMP1 (Water) input file:

```
#-------------------------------------------------------
~Initial Conditions Card
#-------------------------------------------------------
Gas Pressure,Aqueous Pressure,
17,
Aqueous Pressure Zonation,9.8614e+4,Pa,bf,
Aqueous Pressure Zonation,9.5260e+4,Pa,ss2,
Aqueous Pressure Zonation,9.7295e+4,Pa,ps2,
Aqueous Pressure Zonation,9.5272e+4,Pa,ss7,
Aqueous Pressure Zonation,9.2080e+4,Pa,ep3,
Aqueous Pressure Zonation,9.8334e+4,Pa,ur,
Aqueous Pressure Zonation,9.7191e+4,Pa,mr,
Aqueous Pressure Zonation,9.5260e+4,Pa,ss1,
Aqueous Pressure Zonation,9.7295e+4,Pa,ps1,
Aqueous Pressure Zonation,9.5260e+4,Pa,ss6,
Aqueous Pressure Zonation,9.2080e+4,Pa,ep1,
Aqueous Pressure Zonation,9.5260e+4,Pa,ss3,
Aqueous Pressure Zonation,9.5260e+4,Pa,ss4,
Aqueous Pressure Zonation,9.2080e+4,Pa,ep2,
Aqueous Pressure Zonation,9.5260e+4,Pa,ss5,
Gas Pressure,102130.86,Pa,,,,,-12.6549,1/m,1,50,1,50,1,50,
Temperature,16.979,C,,,,,-0.065625,1/m,1,50,1,50,1,50,
```

Extracted from a STOMP3 (Water-Air-Energy) input file:

```
#-------------------------------------------------------
~Initial Conditions Card
#-------------------------------------------------------
Gas Pressure,Aqueous Pressure,
4,
Temperature,20.0,C,,,,,,1,60,1,1,1,20,
Aqueous Pressure,106173.84,Pa,-1.7554,1/cm,,,-97.9352,1/cm,1,60,1,1,1,20,
Gas Pressure,101331.852,Pa,,,,,-0.11713,1/cm,1,60,1,1,1,20,
Overwrite Solute Aqueous Conc,NaNO3,200,1/l,,,,,,28,32,1,1,10,13,
```

Extracted from a STOMP3 (Water-Air-Energy) input file:

```
#-------------------------------------------------------
~Initial Conditions Card
#-------------------------------------------------------
Gas Pressure,Aqueous Pressure,
```

3,
Gas Pressure,138.0,Bar,,,,,,,1,100,1,1,1,50,
Aqueous Pressure,138.0,Bar,,,,,,,1,100,1,1,1,50,
Temperature,25.0,C,,,,,,,1,100,1,1,1,50,

Extracted from a STOMP3 (Water-Air-Energy-Barrier) input file:

```
#-------------------------------------------------------
~Initial Conditions Card
#-------------------------------------------------------
# Restart with Mode 1 Conditions #
Aqueous Saturation,Gas Pressure,
2,
Gas Pressure Overwrite,101325,Pa,,,,,,,1,1,1,1,1,141,
Temperature Overwrite,15.0,C,,,,,-1.3,1/m,1,1,1,1,1,141,
```

B.5 Observed Data Card

Card Title[a] { ~Observed Data [Card] }
Format: *Char*[a]

If: Operational Mode Option Card = { **Water-Air-Energy** }

Number of Observed Data Types[a],
Format: *Integer*[a],
If: Execution Mode Option = { Normal w/ Inverse } { Restart w/ Inverse }

Observed Data Type[a], { Field } { Reference } { Surface Flux } { Surface Rate }
{ Surface Integral }
If: Observed Data Type = { Field }
Field Observation Variable[b],
{ Aqueous Pressure | Aqueous Saturation | Aqueous Moisture Content |
Aqueous Hydraulic Head | X Aqueous Volumetric Flux |
Y Aqueous Volumetric Flux | Z Aqueous Volumetric Flux |
Matric Potential | Solute Volumetric Conc | Solute Aqueous Conc |
Solute Aqueous Mole frac[tion] | X Solute Flux | Y Solute Flux | Z Solute Flux|
Atmospheric Temperature |Atmospheric Relative Humidity |
Atmospheric Solar Radiation |Atmospheric Wind Speed |
Ground Surface Temperature |Ground Surface Water-Vapor Pressure |
Actual Evaporation Rate |Potential Evaporation Rate |Actual Transpiration Rate |
Potential Transpiration Rate |Aqueous Pressure|Gas Pressure |Aqueous Saturation |
Gas Saturation |Aqueous Moisture Content |Water Gas Mass Fraction|
Air Gas Mass Fraction |Water Aqueous Mass Fraction |Air Aqueous Mass Fraction|
Aqueous Hydrualic Head| Gas Hydrualic Head|Aqueous Relative Permeability|
Gas Relative Permeability |Aqueous Density|Gas Density|
X-Dir. Effective Thermal Conductivity |Y-Dir. Effective Thermal Conductivity|
Z-Dir. Effective Thermal Conductivity |X-Dir. Aqueous Volumetric Flux |
Y-Dir. Aqueous Volumetric Flux |Z-Dir. Aqueous Volumetric Flux |
X-Dir. Gas Volumetric Flux |Y-Dir. Gas Volumetric Flux| Z-Dir. Gas Volumetric Flux
X-Dir. Heat Flux |Y-Dir. Heat Flux|Z-Dir. Heat Flux| Matric Potential|
Water Gas Concentration |Air Gas Concentration|Water Aqueous Concentration |
Air Aqueous Concentration |Solute Volumetric Concentration|
Solute Aqueous Concentration |Solute Gas Concentration|
Solute Aqueous Mole Fracton |Solute Gas Mole Fracton |X Solute Flux |
Y Solute Flux |Z Solute Flux|}

If: Field Observation Variable = { Solute Volumetric Conc }
{ Solute Aqueous Conc } { Solute Aqueous Mole frac[tion] }
{ X Solute Flux } { Y Solute Flux } { Z Solute Flux }
Solute Name[c], Field Observation Output Units[d],
Field Observation X-Dir Coordinate[e], Field Observation X-Dir Coordinate Units[f],
Field Observation Y-Dir Coordinate[g], Field Observation X-Dir Coordinate Units[h],

Field Observation Z-Dir Coordinate[i], Field Observation X-Dir Coordinate Units[j]
Observed Data Statistical Index[k], Observed Data Statistic[l],
Observed Data Time Weighting Factor[m], Observed Data Space Weighting Factor[n],
Format: *Char[a], Char[b], Char[c],Char[d], Real[e], Char[f], Reals[g], Char[h], Real[i], Char[j], Integer[k], Real[l], Real[m], Real[n],*

Else:
Field Observation Output Units[c],
Field Observation X-Dir Coordinate[d], Field Observation X-Dir Coordinate Units[e],
Field Observation Y-Dir Coordinate[f], Field Observation X-Dir Coordinate Units[g],
Field Observation Z-Dir Coordinate[h], Field Observation X-Dir Coordinate Units[i],
Observed Data Statistical Index[j], Observed Data Statistic[k],
Observed Data Time Weighting Factor[l], Observed Data Space Weighting Factor[m],
Format: *Char[a], Char[b], Char[c], Real[d], Char[e], Real[f], Char[g], Real[h], Char[i], Integer[j], Real[k], Real[l], Real[m],*

Endif:

Elseif: Observed Data Type = { Reference }
Reference Observation Variable[b],
{ Aqueous Pressure | Aqueous Saturation | Aqueous Moisture Content |
Aqueous Hydraulic Head | X Aqueous Volumetric Flux |
Y Aqueous Volumetric Flux | Z Aqueous Volumetric Flux |
Matric Potential | Solute Volumetric Conc | Solute Aqueous Conc |
Solute Aqueous Mole frac[tion] | X Solute Flux | Y Solute Flux | Z Solute Flux|
Atmospheric Temperature |Atmospheric Relative Humidity |
Atmospheric Solar Radiation |Atmospheric Wind Speed |
Ground Surface Temperature |Ground Surface Water-Vapor Pressure |
Actual Evaporation Rate |Potential Evaporation Rate |Actual Transpiration Rate |
Potential Transpiration Rate |Aqueous Pressure|Gas Pressure |Aqueous Saturation |
Gas Saturation |Aqueous Moisture Content |Water Gas Mass Fraction|
Air Gas Mass Fraction |Water Aqueous Mass Fraction |Air Aqueous Mass Fraction|
Aqueous Hydrualic Head| Gas Hydrualic Head|Aqueous Relative Permeability|
Gas Relative Permeability |Aqueous Density|Gas Density|
X-Dir. Effective Thermal Conductivity |Y-Dir. Effective Thermal Conductivity|
Z-Dir. Effective Thermal Conductivity |X-Dir. Aqueous Volumetric Flux |
Y-Dir. Aqueous Volumetric Flux |Z-Dir. Aqueous Volumetric Flux |
X-Dir. Gas Volumetric Flux |Y-Dir. Gas Volumetric Flux| Z-Dir. Gas Volumetric Flux
X-Dir. Heat Flux |Y-Dir. Heat Flux|Z-Dir. Heat Flux| Matric Potential|
Water Gas Concentration |Air Gas Concentration|Water Aqueous Concentration |
Air Aqueous Concentration |Solute Volumetric Concentration|
Solute Aqueous Concentration |Solute Gas Concentration|
Solute Aqueous Mole Fracton |Solute Gas Mole Fracton |X Solute Flux |
Y Solute Flux |Z Solute Flux|}

If: Reference Observation Variable = { Solute Volumetric Conc }
{ Solute Aqueous Conc } { Solute Aqueous Mole frac[tion] }
{ X Solute Flux } { Y Solute Flux } { Z Solute Flux }

Observed Data Card (cont'd)

Solute Name[c], Reference Observation Output Units[d],
IJK Index 1[e], IJK Index 2[f], IJK Index 3[g],
Observed Data Statistical Index[h], Observed Data Statistic[i],
Observed Data Time Weighting Factor[j], Observed Data Space Weighting Factor[i],
Format: *Char[a], Char[b], Char[c], Integer[d], Integer[e], Integer[f], Integer[g], Real[h], Real[i], Real[j],*

Else:
Reference Observation Output Units[c],
IJK Index 1[c], IJK Index 2[d], IJK Index 3[e],
Observed Data Statistical Index[f], Observed Data Statistic[g],
Observed Data Time Weighting Factor[h], Observed Data Space Weighting Factor[i],
Format: *Char[a], Char[b], Integer[c], Integer[d], Integer[e], Integer[f], Real[g], Real[h], Real[i],*
Endif:

Elseif: Observed Data Type = { Surface Flux | Surface Rate }
Surface Rate Observation Variable[b],
{ Aqueous Volumetric Flux | Aqueous Mass Flux | Solute Flux | Heat Flux }
If: Surface Rate Observation Variable = { Solute Flux }
Solute Name[c], Surface Rate Observation Output Units[d],
Surface Rate Observation Orientation[d],
I-Start Domain Index[f], I-End Domain Index[g],
J-Start Domain Index[h], J-End Domain Index[i],
K-Start Domain Index[j], K-End Domain Index[k],
Observed Data Statistical Index[l], Observed Data Statistic[m],
Observed Data Time Weighting Factor[n], Observed Data Space Weighting Factor[o],
Format: *Char[a], Char[b], Char[c], Char[d], Char[e], Integer[f], Integer[g], Integer[h], Integer[i], Integer[j], Integer[k], Integer[l], Real[m], Real[n], Real[o],*
Else:
Surface Rate Observation Output Units[c],
Surface Rate Observation Orientation[d],
I-Start Domain Index[e], I-End Domain Index[f],
J-Start Domain Index[g], J-End Domain Index[h],
K-Start Domain Index[i], K-End Domain Index[j],
Observed Data Statistical Index[k], Observed Data Statistic[l],
Observed Data Time Weighting Factor[m], Observed Data Space Weighting Factor[n],
Format: *Char[a], Char[b], Char[c], Char[d], Integer[e], Integer[f], Integer[g], Integer[h], Integer[i], Integer[j], Integer[k], Real[l], Real[m], Real[n],*
Endif:

Else: Observed Data Type = { Surface Integral }
{ Aqueous Volumetric Flux Integral | Aqueous Mass Flux Integral | Gas Volumetric Flux Integral | Solute Flux Integral | Heat Flux Integral}
If: Surface Rate Observation Variable = { Solute Integral }
Solute Name[c], Surface Integral Observation Output Units[d],
Surface Integral Observation Orientation[d],

Observed Data Card (cont'd)

I-Start Domain Index[f], I-End Domain Index[g],
J-Start Domain Index[h], J-End Domain Index[i],
K-Start Domain Index[j], K-End Domain Index[k],
Observed Data Statistical Index[l], Observed Data Statistic[m],
Observed Data Time Weighting Factor[n], Observed Data Space Weighting Factor[o],
Format: *Char[a], Char[b], Char[c], Char[d], Char[e], Integer[f], Integer[g], Integer[h], Integer[i], Integer[j], Integer[k], Integer[l], Real[m], Real[n], Real[o],*

Else:

Surface Integral Observation Output Units[c],
Surface Integral Observation Orientation[d],
I-Start Domain Index[e], I-End Domain Index[f],
J-Start Domain Index[g], J-End Domain Index[h],
K-Start Domain Index[i], K-End Domain Index[j],
Observed Data Statistical Index[k], Observed Data Statistic[l],
Observed Data Time Weighting Factor[m], Observed Data Space Weighting Factor[n],
Format: *Char[a], Char[b], Char[c], Char[d], Integer[e], Integer[f], Integer[g], Integer[h], Integer[i], Integer[j], Integer[k], Real[l], Real[m], Real[n],*

Endif:

Endif:

If: Observed Data Read in from External File

File[a] (File), Filename[b], External File Time Units[c], External File Variable Units[d],
Format: *Char[a], Char[b], Char[c], Char[d],*

Elseif: Observed Data Read in from Input file

Number of Observed Data Samples[a],
Format: Integer[a],
Time[a], Time Units[b], Value[c], Value Units[d],
Format: *Real[a], Char[b], Real[c], Char[d],*

Endif:

Endif:

Endif:

Endcard: Observed Data Card

B.5.1 Observed Data Card Examples

Extracted from a STOMP3 (Water-Air-Energy) input file:

```
#-------------------------------------------------------
~Observed Data Card
#-------------------------------------------------------
3,
field,aqueous moisture content,,0.5,cm,0.5,cm,165.5,cm,1,0.01,0.8,0.95,
21,
0,s,0.218,,
484,s,0.213,,
1080,s,0.213,,
1680,s,0.204,,
2880,s,0.204,,
4080,s,0.205,,
5280,s,0.207,,
7080,s,0.204,,
8880,s,0.209,,
13100,s,0.201,,
16700,s,0.201,,
19700,s,0.205,,
68900,s,0.2,,
99300,s,0.196,,
187000,s,0.191,,
427000,s,0.174,,
618000,s,0.164,,
767000,s,0.159,,
1030000,s,0.151,,
1380000,s,0.143,,
1980000,s,0.136,,
field,matric potential,cm,0.5,cm,0.5,cm,60.5,cm,1,4.0,0.8,0.8,
21,
0,s,-1,cm,
484,s,-1,cm,
1080,s,-2,cm,
1680,s,-3,cm,
2880,s,-5,cm,
4080,s,-7,cm,
5280,s,-9,cm,
7080,s,-10,cm,
8880,s,-11,cm,
13100,s,-14,cm,
16700,s,-16,cm,
19700,s,-16,cm,
68900,s,-20,cm,
99300,s,-20,cm,
187000,s,-23,cm,
427000,s,-24,cm,
618000,s,-26,cm,
```

Observed Data Card (cont'd)

767000,s,-27,cm,
1030000,s,-28,cm,
1380000,s,-31,cm,
1980000,s,-33,cm,

field,temperature,F,0.5,cm,0.5,cm,60.5,cm,1,4.0,0.8,0.8,
21,
0,s,-1,cm,
484,s,-1,cm,
1080,s,-2,cm,
1680,s,-3,cm,
2880,s,-5,cm,
4080,s,-7,cm,
5280,s,-9,cm,
7080,s,-10,cm,
8880,s,-11,cm,
13100,s,-14,cm,
16700,s,-16,cm,
19700,s,-16,cm,
68900,s,-20,cm,
99300,s,-20,cm,
187000,s,-23,cm,
427000,s,-24,cm,
618000,s,-26,cm,
767000,s,-27,cm,
1030000,s,-28,cm,
1380000,s,-31,cm,
1980000,s,-33,cm,

B.6 Output Control Card

Card Title[a] { ~Output [Control Card] }
Format: *Char[a]*

Number of Reference Nodes[a],
Format: *Integer[a],*

For: Number of Reference Nodes
I Index[a], J Index[b], K Index[c],
Endfor: Number of Reference Nodes
Format: *Integer[a], Integer[b], Integer[c],*

Reference Node Screen Output Frequency[a],
Reference Node Output File Frequency[b],
Output Time Units[c] (s),
Output Length Units[d] (m),
Screen Significant Digits[e],
Output File Significant Digits[f],
Plot File Significant Digits[g]
Format: *Integer[a], Integer[b], Char[c], Char[d], Integer[e], Integer[f], Integer[g],*

Number of Reference Node Variables[a],
Format: *Integer[a],*

For: Number of Reference Node Variables
Reference Node Variable Option[a], Reference Node Variable Units[b],
Format: *Real[a], Char[b],*
Endfor: Number of Reference Node Variables

Note: Refer to following pages for Reference Node Variable Options and Units.

Number of Plot File Times[a]
Format: *Integer[a],*

For: Number of Plot File Times
Plot File Output Time[a], Units[b] (s)
Format: *Real[a], Char[b],*
Endfor: Number of Plot File Times

Number of Plot File Variables[a]
Format: *Integer[a],*

For: Number of Plot File Variables
Plot File Variable Option[a], Plot File Variable Units[b],
Format: *Char[a], Char[b],*

Output Control Card (cont'd)

Endfor: Number of Plot File Variables

Note: Refer to the following pages for Plot File Variable Options and Units.

Endcard: Output Control Card

Reference Node Variable and Plot File Variable Options

If: Operational Mode Option = { **Water-Air-Energy** }
{ actual evaporation rate | actual transpiration rate |
air aqueous conc[entration] | air aqueous mass frac[tion] | air gas conc[entration] |
air gas mass frac[tion] | air gas mole frac[tion] | air mass source int[egral] |
air mass source rate | air partial pressure |apparent aqueous saturation |
aqueous courant [number] | aqueous density |aqueous fracture saturation |
aqueous gauge pressure | aqueous hydraulic head | Aqueous matric potential |
aqueous moisture cont[ent] | aqueous pressure |aqueous relative perm[eability] | aqueous
saturation | aqueous viscosity | atmospheric pressure |atmospheric relative humidity |
atmospheric solar radiation | atmospheric temperature | atmospheric wind speed |
axial aquous flux | axial gas flux| bare-soil aerodynamic resistance|diffusive porosity |
dissolved air saturation | effective trapped air | energy source int[egral] | energy source rate |
gas courant [number] |gas density | gas fracture saturation |gas gauge pressure |
gas hydraulic head | gas matrix saturation | gas pressure | gas relative perm[eability] |
gas saturation | integrated air mass* | integrated aqueous air [mass]* |
integrated aqueous water [mass]* | integrated gas air [mass]* | integrated gas water [mass]* |
integrated trapped gas air* | integrated water mass* | phase condition |
potential evaporation rate | potential transpiration rate | rock/soil type |
solute aqueous conc[entration] | solute aqueous mole fra[ction] |solute gas conc[entration] |
solute gas mole fra[ction] | solute source int[egral] |solute volumetric conc[entration] |
stomatal resistance |surface aqueous pressure | surface aqueous saturation |
surface gas pressure|surface latent heat flux | surface mass precipitation |
surface net long-wave radiation |surface net short-wave radiation |
surface net total radiation|surface sensible heat flux|surface volumetric precipitation|
surface temperature|surface vapor pressure|surface water mass balance|
temperature |total air mass frac[tion] |total water mass frac[tion] | vertical aqueous flux |
vertical gas flux |water aqueous conc[entration] | water aqueous mass frac[tion] |
water gas conc[entration] | water gas mass frac[tion] | water gas mole frac[tion] |
water mass source int[egral] | water mass source rate | water vapor partial pressure |
x aqueous vol[umetric flux] | x gas vol[umetric flux] | x heat flux | x solute flux |
x thermal cond[uctivity] |xnc aqueous vol[umetric flux (node centered)] |
xnc gas vol[umetric flux (node centered)] | xnc heat flux (node centered) |
y aqueous vol[umetric flux] | y gas vol[umetric flux] | y heat flux |y solute flux |
y thermal cond[uctivity] | ync aqueous vol[umetric flux (node centered)] |
ync gas vol[umetric flux (node centered)] | ync heat flux (node centered) |
z aqueous vol[umetric flux] | z gas vol[umetric flux] | z heat flux |z solute flux |
z thermal cond[uctivity] | znc aqueous vol[umetric flux (node centered)] |
znc gas vol[umetric flux (node centered)] | znc heat flux (node centered) }

* Reference Node Variable Only

Output Control Card (cont'd)

Default Units for the Reference Node and Plot File Variables

Actual Evaporation (g/day)	Moisture Content (null)
Actual Evaporation,g/day,	Mole frac[tion] (null)
Actual Transpiration (g/day)	Phase Condition (null)
Air Conc (kg/m^3)	Potential Evaporation (g/day)
Air Mass Source Integral (kg)	Potential Transpiration (g/day
Aqueous matric potential (cm)	Pressure (Pa)
Aqueous moisture content (null)	Relative Permeability (null)
Aqueous Relative Permeability (null)	Salt Aqueous Conc. (kg/m^3)
Aqueous Relative permeability (null)	Salt Conc. (kg/m^3)
Aqueous Saturation (null)	Salt Flux (kg/ m^3 s)
Aqueous Volumetric Flux (m/s)	Saturation (null)
Atmospheric Pressure (Pa)	Solute Conc. (1/m^3)
Atmospheric Pressure,Pa,	Solute Flux (1/m^2 s)
Atmospheric Relative Humidity (null)	Solute Mole frac[tion] (null)
Atmospheric Relative Humidity,,	Surface Aqueous Pressure (Pa)
Atmospheric Solar Radiation (W/m^2)	Surface Aqueous Saturation (null)
Atmospheric Solar Radiation (W/m^2)	Surface Aqueous Saturation,,
Atmospheric Solar Radiation,W/m^2,	Surface Gas Pressure (Pa)
Atmospheric Solar Radiation,W/m^2,	Surface Gas Pressure,Pa,
Atmospheric Temperature,C,	Surface Ground Heat Flux,W/m^2,
Atmospheric Wind Speed (mi/hr)	Surface Latent Heat Flux (W/m^2)
Bare-Soil Aerodynamic Resistance,s/m,	Surface Mass Precipitation (g/day)
CO_2 Conc (kg/m^3)	Surface Net Long-Wave Radiation,W/m^2,
CO_2 Mass Source Integral (kg)	Surface Net Short-Wave Radiation,W/m^2,
Density (kg/m^3)	Surface Sensible Heat Flux (W/m^2),
Energy Source Integral (J)	Surface Temperature (C)
Gas Relative Permeability (null)	Surface Temperature,C,
Gas Saturation (null)	Surface Temperature,C,
Gas Volumetric Flux (m/s)	Surface Volumetric Precipitation (cm^3/day)
Gauge Pressure (Pa)	Surface Water Mass Balance (g/day)
Head (m)	Temperature (C)
Heat Flux (W/ m^2)	Thermal Conductivity (W/m K)
Mass (kg)	Water Conc (kg/m^3)
Mass Fraction (null)	Water Mass Source Integral (kg)

B.6.1 Output Control Card Examples

Extracted from STOMP3 (Water-Air-Energy) input file:

```
#-------------------------------------------------------
~Output Options Card
#-------------------------------------------------------
1,
1,1,10,
1,1,day,m,6,6,6,
12,
Aqueous Saturation,,
Temperature,C,
Surface Temperature,C,
Surface Vapor Pressure,Pa,
Atmospheric Temperature,C,
Atmospheric Solar Radiation,W/m^2,
Atmospheric Wind Speed,m/s,
Atmospheric Relative Humidity,,
Potential Evaporation,gm/s,
Actual Evaporation,gm/s,
Potential Transpiration,gm/s,
Actual Transpiration,gm/s,
0,
6,
Aqueous Saturation,,
Aqueous Pressure,Pa,
Gas Pressure,Pa,
Temperature,C,
Surface Temperature,C,
Surface Vapor Pressure,Pa,
```

Extracted from STOMP3 (Water-Air-Energy-Barriers) input file:

```
#-------------------------------------------------------
~Output Options Card
#-------------------------------------------------------
4,
1,1,54,
66,1,84,
112,1,100,
233,1,100,
1,1,day,m,5,5,5,
14,
Temperature,C,
Aqueous Pressure,Pa,
Gas Pressure,Pa,
Aqueous Saturation,,
Surface Net Total Radiation,W/m^2,
Surface Latent Heat Flux,W/m^2,
Surface Sensible Heat Flux,W/m^2,
```

Atmospheric Temperature,C,

Output Control Card (cont'd)

Surface Temperature,C,
Aqueous Moisture Content,,
Potential Evaporation,kg/s,
Actual Evaporation,kg/s,
Potential Transpiration,kg/s,
Actual Transpiration,kg/s,
10,
10,day,
20,day,
30,day,
40,day,
50,day,
60,day,
70,day,
80,day,
90,day,
100,day,
9,
Rock/Soil Type,,
Aqueous pressure,Pa,
Aqueous saturation,,
Aqueous Moisture Content,,
Temperature,C,
xnc aqueous vol,cm/hr,
znc aqueous vol,cm/hr,
xnc gas vol,cm/hr,
znc gas vol,cm/hr,

Extracted from STOMP3 (Water-Air-Energy-Barriers) input file:

```
#-------------------------------------------------------
~Output Options Card
#-------------------------------------------------------
3,
1,1,113,# 0.1 cm
1,1,93, #14.87 cm deep
1,1,92, #15.13 cm deep
1,1,1,
24,1,day,m,3,6,6,
27,
Atmospheric Temperature,C,
Atmospheric Pressure,Pa,
Atmospheric Relative Humidity,,
Atmospheric Solar Radiation,W/m^2,
Atmospheric Wind Speed,mi/hr,
Surface Temperature,C,
Surface Aqueous Pressure,Pa,
Surface Gas Pressure,Pa,
Surface Aqueous Saturation,,
Surface Water Mass Balance,g/day,
```

Output Control Card (cont'd)

Potential Evaporation,g/day,
Actual Evaporation,g/day,
Potential Transpiration,g/day,
Actual Transpiration,g/day,
Bare-Soil Aerodynamic Resistance,s/m,
Surface Latent Heat Flux,W/m^2,
Surface Sensible Heat Flux,W/m^2,
Surface Net Long-Wave Radiation,W/m^2,
Surface Net Short-Wave Radiation,W/m^2,
Surface Net Total Radiation,W/m^2,
Surface Volumetric Precipitation,cm^3/day,
Surface Mass Precipitation,g/day,
Temperature,C,
Aqueous matric potential,cm,
Aqueous moisture content,,
Aqueous saturation,,
Aqueous relative permeability,,
10,
0.0,day,
72.0,day,
164.0,day,
254.0,day,
345.0,day,
437.0,day,
529.0,day,
619.0,day,
710.0,day,
803.0,day,
5,
Temperature,C,
Aqueous pressure,pa,
Aqueous matric potential,cm,
Aqueous moisture content,,
Aqueous relative permeability,,

B.7 Plant Card

Card Title[a] { ~Plant [Card] }
Format: *Char*[a]

If: Operational Mode Option Card = { **Water-Air-Energy** }

Number of Plant Species[a], [Plant Temperature Option[b]], [Rainfall Interception Option[c]]
Format: *Integer*[a], *Char*[a], *Char*[b]

For: Number of Plant Species
Plant Name[a], [Plant Root Stress Option[b]], [Stomatal Resistance[c]] { Stress }
Format: *Char*[a], *Char*[b], *Char*[c]
Max. Root Depth[a], Units[b] (m),
Null Root Depth[c] (z^*), Units[d] (m),
Root Depth Fit Parameter[e] (p_z),
Format: *Real*[a], *Char*[b], *Real*[c], *Char*[d], *Real*[e],
If: Plant Albedo = {Temporal[a]}
Plant Albedo Initial Stage Start[b], Plant Albedo Crop Development Start[c],
Plant Albedo Mid-Season Start[d], Plant Albedo Late-Season Start[e],
Plant Albedo Late-Season Stop[f], Plant Canopy Height[g], Units[h] (m),
Maximum Condensate Depth[i], Units (m)[j]
Format: *Char*[a] *Real*[b],*Real*[c],*Real*[d],*Real*[e],*Real*[f],*Real*[g],*Char*[h],*Real*[i],*Char*[j],
Else:
Plant Albedo[a],Plant Canopy Height[b], Units (m)[c],
Format: *Real*[a], *Real*[b],*Char*[c],
Endif:
If: Plant Stress Option = { Stress }
Water Stress Point 1[a], Units[b] (m), Water Stress Point 2[c], Units[d] (m),
Water Stress Point 3[e], Units[f] (m), Water Stress Point 4[g], Units[h] (m),
Format: *Real*[a], *Char*[b], *Real*[c], *Char*[d], *Real*[e], *Char*[f], *Real*[g], *Char*[h],
Else:
Root Uptake Reduced 50%[a], Units[b] (m),
Format: *Real*[a], *Char*[b],
Endif:
Crop Coefficient Start[a], Crop Coefficient Day of Year (Start)[b], Units (s)[c],
Crop Coefficient (Mature Stage 1)[d], Crop Coefficient Day of Year (Mature Stage 1)[e],
Units (s)[f], Crop Coefficient (Mature Stage 2)[g],
Crop Coefficient Day of Year (Mature Stage 2)[h], Units (s)[i],
Crop Coefficient (Die-off)[j], Crop Coefficient Day of Year (Die-off)[k], Units (s)[l],
Format: *Real*[a], *Real*[b], *Char*[c], *Real*[d], *Real*[e], *Char*[f], *Real*[g], *Real*[h], *Char*[i], *Real*[j], *Real*[k], *Char*[l],
Endfor: Number of Plant Species
Endif:

Endcard: Plant Card

B.7.1 Plant Card Examples

Extracted from STOMP3 (Water-Air-Energy-Barrier) input file:

```
#-------------------------------------------------------
~Plant Card
#-------------------------------------------------------
2,Single Plant Temperature Rainfall Interception,
Cheatgrass,Vrugt Root Stress Hicks,
0.50,m,0.10,m,4.875,
Temporal Albedo,0.05,0.06,0.15,0.19,0.05,0.30,m,1.984e-3,m,
0.1,m,1.0,m,10.0,m,150.,m,
0.0,0.0,day,0.0,55,day,1.0,112,day,1.0,148,day,0.0,159,day,
50,s/m,20,W/m^2,5,C,45,C,25,C,
Sandberg Bluegrass,Vrugt Root Stress Hicks,
0.35,m,0.20,m,2.62,
Temporal Albedo,0.05,0.06,0.15,0.19,0.05,0.10,m,1.984e-3,m,
0.1,m,1.0,m,10.0,m,150.,m,
0.0,0.0,day,0.0,55,day,1.0,104,day,1.0,147,day,0.0,160,day,
50,s/m,20,W/m^2,5,C,45,C,25,C,
```

Extracted from STOMP3 (Water-Air-Energy-Barrier) input file:

```
#-------------------------------------------------------
~Plant Properties Card
#-------------------------------------------------------
1,Single Plant Temperature, Rainfall Interception,
Russian Thistle,Vrugt Root Stress,
0.957,m,0.15,m,0.298,
Temporal albedo,0.15,0.12,0.15,0.17,0.15,62.9,cm,0.2e-03,m,
0.1,m,1.0,m,10.0,m,850.,m, #h1,h2,h3,h4,
0.0,121.0,day,1.0,175.0,day,1.0,250.0,day,0.0,274.0,day,0.0,365,day,
```

Extracted from STOMP-WAE-B (Water-Air-Energy-Barrier) input file:

```
#-------------------------------------------------------
~Plant Properties Card
#-------------------------------------------------------
2,Multiple Plant Temperature,Rainfall Interception,
Sagebrush,Vrugt Root Stress,
0.957,m,0.15,m,0.298,
Temporal albedo,0.15,0.12,0.15,0.17,0.15,62.9,cm,0.2e-03,m,
0.1,m,1.0,m,10.0,m,850.,m,
0.0,90,day,1.0,100,day,1.0,275,day,0.0,304,day,0.0,365,day,
Sandbergs Bluegrass,Jarvis Root Stress,
0.254,m,0.05,m,0.068,
Temporal albedo,0.12,0.06,0.15,0.18,0.05,7.5,cm,0.2e-03,m,
0.1,m,1.0,m,10.0,m,150.,m,
0.0,60,day,1.0,80,day,1.0,160,day,0.0,181,day,0.0,365,day,
```

B.8 Surface Flux Card

Card Title[a] { ~Surface [Flux Card] }
Format: *Char*[a]

Number of Surface Flux Inputs[a]
Format: Integer[a],

Note: The number of suface flux inputs may be written to one or more user specified files. For each user specified file, the following input line has to be specified. An example has been included in the Surface Flux Card Examples section. The sum of the "Number of Surface Flux Inputs in File" has to be equal to the "Number of Surface Flux Inputs".

Number of Surface Flux Inputs in File[a], Filename[b],
Format: Integer[a], Char[b],

For: Number of Surface Flux Inputs:
If: Operation Mode Option = { **Water-Air-Energy** }
Surface Flux Type Option[a],
{ Aqueous Volumetric Flux | Aqueous Mass Flux | Gas Volumetric Flux |
Gas Mass Flux | Gas Advective Heat Flux | Gas Advective Water Mass Flux |
Gas Advective Air Mass Flux | Gas Diffusive Heat Flux |
Gas Diffusive Water Mass Flux | Gas Diffusive Air Mass Flux |
Solute Flux, Solute Name | Heat Flux | Condensate Water Mass }
Endif:

If: Surface Flux Type Option = { Heat Flux }
Units[b] (W), Units[c] (J),
ElseIf: Surface Flux Type Option = { Volumetric Flux }
Units[b] (m^3/s), Units[c] (m^3),
Elseif: Surface Flux Type Option = { Mass Flux } { Dissolved Oil }
Units[b] (kg/s), Units[c] (kg),
Elseif: Surface Flux Type Option = { Solute Flux }
Units[b] (sol/s), Units[c] (sol),
Endif:

Surface Flux Orientation Option[d]
{ West } { East }
{ South } { North }
{ Top } { Bottom }
I-Start Index[e], I-End Index[f],
J-Start Index[g], J-End Index[h],
K-Start Index[i], K-End Index[j],
Format: Char[a], Char[b], Char[c], Char[d], Integer[e], Integer[f], Integer[g], Integer[h], Integer[i], Integer[j],
Endfor: Number of Surface Flux Inputs
Endcard: Surface Flux Card

B.8.1 Surface Flux Card Examples

Extracted from STOMP-WAE-B (Water-Air-Energy) input file:

```
#-------------------------------------------------------
~Surface Flux Card
#-------------------------------------------------------
5,
Aqueous Volumetric,gal/min,gal,East,2,2,1,1,14,33,
Aqueous Volumetric,gal/min,gal,East,2,2,1,1,71,100,
Aqueous Volumetric,gal/min,gal,East,52,52,1,1,1,113,
Solute Flux,KBr,1/min,,East,2,2,1,1,14,33,
Solute Flux,KBr,1/min,,East,2,2,1,1,71,100,
```

Extracted from STOMP-WAE-B (Water-Air-Energy-Barrier) input file:

```
#-------------------------------------------------------
~Surface Flux Card
#-------------------------------------------------------
4,
Actual Evaporation,kg/hr,kg,Top,1,1,1,1,167,167,
Actual Transpiration,kg/hr,kg,Top,1,1,1,1,167,167,
Aqueous Volumetric,cm^3/hr,cm^3,Top,1,1,1,1,144,144,
Aqueous Volumetric,cm^3/hr,cm^3,Top,1,1,1,1,147,147,
```

Extracted from STOMP-WAE-B (Water-Air-Energy-Barrier) input file:

```
#-------------------------------------------------------
~Surface Flux Card
#-------------------------------------------------------
3,
Aqueous Volumetric,cm^3/hr,cm^3,Top,   1,1,1,1,113,113, #0.0 cm
Heat Flux,W,J,Top,1,1,1,1,113,113, #0.0 cm
```

B.9 Thermal Properties Card

Card Title[a] { ~Thermal [Properties Card] }
Format: *Char[a]*

For: Number of Rock/Soil Types
Rock/Soil Name[a],
Thermal Conductivity Function Option[b],
{ Constant } { Parallel } { Linear } { Somerton } { Campbell } {Cass}
Ground-Surface Albedo Option[k],
{Plum and Xiu Albedo} {Wang Albedo} {Briegleb Albedo} {Constant Albedo}

If: Thermal Conductivity Function Option = { Constant }
X-Dir. Thermal Conductivity[c], Units[d] (W/m K),
Y-Dir. Thermal Conductivity[e], Units[f] (W/m K),
Z-Dir. Thermal Conductivity[g], Units[h] (W/m K), Specific Heat[i], Units[j] (J/kg K),
If: Ground-Surface Albedo Option = {Plum and Xiu Albedo[k]}
Dry-Soil Albedo[l],Wet-Soil Albedo[m], Albedo Attenuation Factor[n],
Elseif: Ground-Surface Albedo Option = {Wang Albedo[k]}
Dry-Soil Albedo[l],Wet-Soil Albedo[m], Albedo Attenuation Factor[n],
Reference Albedo @ Solar Zenith = 60 deg[o],
Elseif: Ground-Surface Albedo Option = {Briegleb Albedo[k]}
Dry-Soil Albedo[l],Wet-Soil Albedo[m], Albedo Attenuation Factor[n],
Reference Albedo @ Solar Zenith = 60 deg[o], Parameter C[p],
Elseif: Ground-Surface Albedo Option = {Constant[k]}
Mean Soil Albedo[l] (0.20),
Format: *Char[a], Char[b], Real[c], Char[d], Real[e], Char[f], Real[g], Char[h], Real[i], Char[j], Char[k],Real[l],Real[m],Real[n],Real[o],Real[p],*
E**ndif:**
Elseif: Thermal Conductivity Function Option = { Parallel }
X-Dir. Rock/Soil Grain Thermal Conductivity[c], Units[d] (W/m K),
Y-Dir. Rock/Soil Grain Thermal Conductivity[e], Units[f] (W/m K),
Z-Dir. Rock/Soil Grain Thermal Conductivity[g], Units[h] (W/m K),
Specific Heat[h], Units[i] (J/kg K),
If: Ground-Surface Albedo Option = {Plum and Xiu Albedo[k]}
Dry-Soil Albedo[l],Wet-Soil Albedo[m], Albedo Attenuation Factor[n],
Elseif: Ground-Surface Albedo Option = {Wang Albedo[k]}
Dry-Soil Albedo[l],Wet-Soil Albedo[m], Albedo Attenuation Factor[n],
Reference Albedo @ Solar Zenith = 60 deg[o],
Elseif: Ground-Surface Albedo Option = {Briegleb Albedo[k]}
Dry-Soil Albedo[l],Wet-Soil Albedo[m], Albedo Attenuation Factor[n],
Reference Albedo @ Solar Zenith = 60 deg[o], Parameter C[p],

Thermal Properties Card (cont'd)

Elseif: Ground-Surface Albedo Option = {Constant[k]}
Mean Soil Albedo[l] (0.20),
Format: *Char[a], Char[b], Real[c], Char[d], Real[e], Char[f], Real[g], Char[h], Real[i], Char[j], Char[k],Real[l],Real[m],Real[n],Real[o],Real[p],*

Elseif: Thermal Conductivity Function Option = { Linear }
X-Dir. Rock/Soil Unsaturated Thermal Conductivity[c], Units[d] (W/m K),
Y-Dir. Rock/Soil Unsaturated Thermal Conductivity[e], Units[f] (W/m K),
Z-Dir. Rock/Soil Unsaturated Thermal Conductivity[g], Units[h] (W/m K),
X-Dir. Rock/Soil Water Saturated Thermal Conductivity[i], Units[j] (W/m K),
Y-Dir. Rock/Soil Water Saturated Thermal Conductivity[k], Units[l] (W/m K),
Z-Dir. Rock/Soil Water Saturated Thermal Conductivity[m], Units[n] (W/m K),
Specific Heat[o], Units[p] (J/kg K),
If: Ground-Surface Albedo Option = {Plum and Xiu Albedo[k]}
Dry-Soil Albedo[l],Wet-Soil Albedo[m], Albedo Attenuation Factor[n],
Elseif: Ground-Surface Albedo Option = {Wang Albedo[k]}
Dry-Soil Albedo[l],Wet-Soil Albedo[m], Albedo Attenuation Factor[n],
Reference Albedo @ Solar Zenith = 60 deg[o],
Elseif: Ground-Surface Albedo Option = {Briegleb Albedo[k]}
Dry-Soil Albedo[l],Wet-Soil Albedo[m], Albedo Attenuation Factor[n],
Reference Albedo @ Solar Zenith = 60 deg[o], Parameter C[p],
Elseif: Ground-Surface Albedo Option = {Constant[k]}
Mean Soil Albedo[l] (0.20),
Format: *Char[a], Char[b], Real[c], Char[d], Real[e], Char[f], Real[g], Char[h], Real[i], Char[j], Char[k],Real[l],Real[m],Real[n],Real[o],Real[p],*
Endif:
Elseif: Thermal Conductivity Function Option = { Somerton }
X-Dir. Rock/Soil Unsaturated Thermal Conductivity[c], Units[d] (W/m K),
Y-Dir. Rock/Soil Unsaturated Thermal Conductivity[e], Units[f] (W/m K),
Z-Dir. Rock/Soil Unsaturated Thermal Conductivity[g], Units[h] (W/m K),
X-Dir. Rock/Soil Water Saturated Thermal Conductivity[i], Units[j] (W/m K),
Y-Dir. Rock/Soil Water Saturated Thermal Conductivity[k], Units[l] (W/m K),
Z-Dir. Rock/Soil Water Saturated Thermal Conductivity[m], Units[n] (W/m K),
Specific Heat[o], Units[p] (J/kg K),
If: Ground-Surface Albedo Option = {Plum and Xiu Albedo[k]}
Dry-Soil Albedo[l],Wet-Soil Albedo[m], Albedo Attenuation Factor[n],
Elseif: Ground-Surface Albedo Option = {Wang Albedo[k]}
Dry-Soil Albedo[l],Wet-Soil Albedo[m], Albedo Attenuation Factor[n],
Reference Albedo @ Solar Zenith = 60 deg[o],
Elseif: Ground-Surface Albedo Option = {Briegleb Albedo[k]}
Dry-Soil Albedo[l],Wet-Soil Albedo[m], Albedo Attenuation Factor[n],

Thermal Properties Card (cont'd)

Reference Albedo @ Solar Zenith = 60 deg[o], Parameter C[p],
Elseif: Ground-Surface Albedo Option = {Constant[k]}
Mean Soil Albedo[l] (0.20),
Format: *Char[a], Char[b], Real[c], Char[d], Real[e], Char[f], Real[g], Char[h], Real[i], Char[j], Char[k],Real[l],Real[m],Real[n],Real[o],Real[p],*
Endif:
Format: *Char[a], Char[b], Real[c], Char[d], Real[e], Char[f], Real[g], Char[h], Real[i], Char[j], Real[k], Char[l], Real[m], Char[n], Real[o], Char[p],*
Elseif: Thermal Conductivity Function Option = { Campbell }
Parameter a[c] (0.734), Units[d] (W/m K), Parameter b[e] (1.45), Units[f] (W/m K),
Parameter c[g] (2.01), Parameter d[h] (0.204), Units[i] (W/m K),
Parameter e[j] (4.0), Specific Heat[k], Units[l] (J/kg K),
If: Ground-Surface Albedo Option = {Plum and Xiu Albedo[k]}
Dry-Soil Albedo[l],Wet-Soil Albedo[m], Albedo Attenuation Factor[n],
Elseif: Ground-Surface Albedo Option = {Wang Albedo[k]}
Dry-Soil Albedo[l],Wet-Soil Albedo[m], Albedo Attenuation Factor[n],
Reference Albedo @ Solar Zenith = 60 deg[o],
Elseif: Ground-Surface Albedo Option = {Briegleb Albedo[k]}
Dry-Soil Albedo[l],Wet-Soil Albedo[m], Albedo Attenuation Factor[n],
Reference Albedo @ Solar Zenith = 60 deg[o], Parameter C[p],
Elseif: Ground-Surface Albedo Option = {Constant[k]}
Mean Soil Albedo[l] (0.20),
Format: *Char[a], Char[b], Real[c], Char[d], Real[e], Char[f], Real[g], Char[h], Real[i], Char[j], Char[k],Real[l],Real[m],Real[n],Real[o],Real[p],*
Endif:
Elseif: Thermal Conductivity Function Option = { Cass }
Parameter a[c] , Units[d] (W/m K), Parameter b[e], Units[f] (W/m K),
Parameter c[g] , Parameter d[h] , Units[i] (W/m K),
Parameter e[j] , Specific Heat[k], Units[l] (J/kg K),
If: Ground-Surface Albedo Option = {Plum and Xiu Albedo[k]}
Dry-Soil Albedo[l],Wet-Soil Albedo[m], Albedo Attenuation Factor[n],
Elseif: Ground-Surface Albedo Option = {Wang Albedo[k]}
Dry-Soil Albedo[l],Wet-Soil Albedo[m], Albedo Attenuation Factor[n],
Reference Albedo @ Solar Zenith = 60 deg[o],
Elseif: Ground-Surface Albedo Option = {Briegleb Albedo[k]}
Dry-Soil Albedo[l],Wet-Soil Albedo[m], Albedo Attenuation Factor[n],
Reference Albedo @ Solar Zenith = 60 deg[o], Parameter C[p],
Elseif: Ground-Surface Albedo Option = {Constant[k]}
Mean Soil Albedo[l] (0.20),
Format: *Char[a], Char[b], Real[c], Char[d], Real[e], Char[f], Real[g], Char[h], Real[i], Char[j], Char[k],Real[l],Real[m],Real[n],Real[o],Real[p],*

Thermal Properties Card (cont'd)

Endif:

If: { Enhanced }

Enhanced[c], Parameter a[d] , Parameter b[e], Parameter c[f], Parameter d[g], Parameter e[h],

Endif:

Endfor: Number of Rock/Soil Types

Endcard: Thermal Properties Card

B.9.1 Thermal Properties Card Examples

Extracted from STOMP-WAE-B (Water-Air-Energy-Barrier) input file:

```
#-------------------------------------------------------
~Thermal Properties Card
#-------------------------------------------------------
Soil,Constant,0.5,W/m K,0.5,W/m K,0.5,W/m K,750,J/kg K
```

Extracted from STOMP-WAE-B (Water-Air-Energy-Barrier) input file:

```
#-------------------------------------------------------
~Thermal Properties Card
#-------------------------------------------------------
Silt Loam-Gravel Admix,Somerton,0.25,W/m K,0.25,W/m K,0.25,W/m K,2.0,W/m K,2.0,W/m K,2.0,W/m
K,750,J/kg K,
Gravel Drainage,Somerton,0.25,W/m K,0.25,W/m K,0.25,W/m K,2.0,W/m K,2.0,W/m K,2.0,W/m
K,750,J/kg K,
Gravel Filter,Somerton,0.25,W/m K,0.25,W/m K,0.25,W/m K,2.0,W/m K,2.0,W/m K,2.0,W/m K,750,J/kg K,
Riprap,Somerton,0.25,W/m K,0.25,W/m K,0.25,W/m K,2.0,W/m K,2.0,W/m K,2.0,W/m K,750,J/kg K,
Compacted Silt Loam,Somerton,0.25,W/m K,0.25,W/m K,0.25,W/m K,2.0,W/m K,2.0,W/m K,2.0,W/m
K,750,J/kg K,
```

Extracted from STOMP-WAE-B (Water-Air-Energy-Barrier) input file:

```
#-------------------------------------------------------
~Thermal Properties Card
#-------------------------------------------------------
Layer1,Cass,0.60,W/m K,0.70,W/m K,8.0,0.26,W/m K,3.0,793.1,J/kg
C,enhanced,9.5,2.0,8.0,0.50,3.0,albedo,Wang,0.267,0.160,3.585,0.04,
Layer2,Cass,0.60,W/m K,0.70,W/m K,8.0,0.26,W/m K,3.0,793.1,J/kg
C,enhanced,9.5,2.0,8.0,0.50,3.0,albedo,Wang,0.402,0.275,3.585,0.04,
Layer3,Cass,0.60,W/m K,0.70,W/m K,8.0,0.26,W/m K,3.0,730.6,J/kg
C,enhanced,9.5,2.0,8.0,0.50,3.0,albedo,Wang,0.402,0.275,3.585,0.04,
Layer4,Cass,0.60,W/m K,0.70,W/m K,8.0,0.26,W/m K,3.0,730.6,J/kg
C,enhanced,9.5,2.0,8.0,0.50,3.0,albedo,Wang,0.402,0.275,3.585,0.04,
```

B.10 Ucode Control Card

Card Title[a] { ~Ucode [Control Card] }
Format: *Char[a]*

If: Operational Mode Option Card = { **Water-Air-Energy**}

If: Execution Mode Option = { Normal w/ Inverse } { Restart w/ Inverse }

Ucode Phase[a], { 1 | 2 | 3 | 11 | 22 | 33 | 44 | 45 }
Note: 1 = Forward Modeling
2 = Sensitivities at Starting Parameters
3 = Perform Regression
11 = Calculates Sum of Squares
22 = Sensitivities at Starting Parameters using Central Differences
33 = Calculate Model Linearity
44 = Calculate Prediction Intervals
45 = Calculate Differnences and Prediction Intervals

Ucode Differencing Index[b], { 1 | 2 }
Note: 1 = Forward Differencing (Recommended)
2 = Central Differencing

Ucode Tolerance[c], Ucode Sum-of-Squared Residual Factor[d],
Ucode Quasi-Newton Updating Index[e], { 0 | 1 }
0 = No Quasi-Newton Updating
1 = Quasi-Newton Updating

Maximum Change Factor[f],
Format: *Integer[a], Integer[b], Real[c], Real[d], Integer[e], Real[f],*

Ucode Path and Name of Inverse Code[a],
Format: *Char[a],*
Ucode Number of Application Models[a],
Format: *Integer[a],*
For: Number of Application Models
Ucode Application Model Execution Commands[a],
Format: *Char[a],*
Endfor:

Ucode Scale Sensitivities Index[a], { 0 | 1 | 2 | 3 }
Note: 0 = No Scaling is Applied and Unscaled Sensitivities are Printed
1 = Dimensionless Scaled Sensitivities are Printed
2 = One-Percent Scaled Sensitivities are Printed
3 = Both Dimensionless and One-Percent Scaled Sensitivities are Printed

Ucode Control Card (cont'd)

Ucode Print Intermediate Index[b], { 0 | 1 }
Note: 0 = No Printing for Intermediate Iterations
1 = Printing for Intermediate Iterations

Ucode Print Graph Index[c], { 0 | 1 }
Note: 0 = Do not Print Post-Processing Files
1 = Print Post-Processing Files

Number of Residual Sets[d],
Format: Integer[a], Integer[b], Integer[c], Integer[d],
Endif:

Endif:

Endcard: Ucode Control Card

B.10.1 UCode Control Card Examples

Extracted from a STOMP1 (Water) input file:

```
#-----------------------------------------
~UCode Control Card
#-----------------------------------------
1,1,0.01,0.01,0,20,1.0,
../bin/mrdrive,
1,
batch,
3,0,1,1,
```

Appendix C

STOMP Example Input Files

Appendix C: STOMP Example Input Files

C.1 STOMP-W Input File for Infiltration Verification in Sand

```
#-------------------------------------------------------
~Simulation Title Card
#-------------------------------------------------------
1,
UNSAT-H 7.1,
M.D. White, A.L. Ward,
PNNL,
11 July 2003,
09:05,
1,
UNSAT-H, Problem 7.1, Sand

#-------------------------------------------------------
~Solution Control Card
#-------------------------------------------------------
Normal,
Water,
1,
0,hr,0.8,hr,0.0000125,hr,0.01,hr,1.25,8,1.e-6,
10000,
0,

#-------------------------------------------------------
~Grid Card
#-------------------------------------------------------
Uniform Cartesian,
1,1,90,
1.0,cm,
1.0,cm,
1.0,cm,

#-------------------------------------------------------
~Rock/Soil Zonation Card
#-------------------------------------------------------
1,
Sand,1,1,1,1,1,90,

#-------------------------------------------------------
~Mechanical Properties Card
#-------------------------------------------------------
Sand,2650,kg/m^3,0.287,0.287,,,Constant,0.7,0.7,

#-------------------------------------------------------
~Hydraulic Properties Card
#-------------------------------------------------------
```

Sand,34.0,hc cm/hr,34.0,hc cm/hr,34.0,hc cm/hr,

#----------
~Saturation Function Card
#----------
Sand,Haverkamp,1.0,cm,1.611e+6,cm,3.96,0.261324,
#----------
~Aqueous Relative Permeability Card
#----------
Sand,Haverkamp,1.175e+6,cm,4.74,1.0,cm,

#----------
~Initial Conditions Card
#----------
Aqueous Pressure,Gas Pressure,
3,
Aqueous Pressure,95343.35,Pa,,,,,,1,1,1,1,1,90,
Gas Pressure,101356.57,Pa,,,,,,1,1,1,1,1,90,
Temperature,20.0,C,,,,,,1,1,1,1,1,90,

#----------
~Boundary Conditions Card
#----------
2,
Top,Dirichlet Aqueous,
1,1,1,1,90,90,1,
0,day,99326.37,Pa,
Bottom,Dirichlet Aqueous,
1,1,1,1,1,1,1,
0,day,95343.35,Pa,

#----------
~Output Options Card
#----------
6,
1,1,90,
1,1,75,
1,1,60,
1,1,45,
1,1,30,
1,1,1,
1,1,hr,cm,5,5,5,
2,
Aqueous saturation,,
Aqueous pressure,,
4,
1,hr,
300,hr,
600,hr,
900,hr,
2,

Aqueous saturation,,
Aqueous pressure,,
#---
~Surface Flux Card
#---
2,
Aqueous Volumetric,cm^3/hr,cm^3,Top,1,1,1,1,90,90,
Aqueous Volumetric,cm^3/hr,cm^3,Bottom,1,1,1,1,1,1,

C.2 STOMP-W Input File for Infiltration Verification in Clay

```
#-------------------------------------------------------
~Simulation Title Card
#-------------------------------------------------------
1,
UNSAT-H 7.1,
M.D. White, A.L. Ward,
PNNL,
11 July 2003,
09:05,
1,
UNSAT-H, Problem 7.1, Yolo light clay

#-------------------------------------------------------
~Solution Control Card
#-------------------------------------------------------
Normal,
Water,
1,
0,hr,1200,hr,0.00125,hr,10,hr,1.25,8,1.e-6,
10000,
0,

#-------------------------------------------------------
~Grid Card
#-------------------------------------------------------
Uniform Cartesian,
1,1,250,
1.0,cm,
1.0,cm,
1.0,cm,

#-------------------------------------------------------
~Rock/Soil Zonation Card
#-------------------------------------------------------
1,
Yolo Light Clay,1,1,1,1,1,250,

#-------------------------------------------------------
~Mechanical Properties Card
#-------------------------------------------------------
Yolo Light Clay,2650,kg/m^3,0.495,0.495,,,Constant,0.7,0.7,

#-------------------------------------------------------
~Hydraulic Properties Card
#-------------------------------------------------------
Yolo Light Clay,4.428e-2,hc cm/hr,4.428e-2,hc cm/hr,4.428e-2,hc cm/hr,

#-------------------------------------------------------
~Saturation Function Card
```

```
#-----------------------------------------------------
Yolo Light Clay,Haverkamp w/ Log,1.0,cm,739.0,cm,4.0,0.250505,

#-----------------------------------------------------
~Aqueous Relative Permeability Card
#-----------------------------------------------------
Yolo Light Clay,Haverkamp,124.6,cm,1.77,0.0,cm,

#-----------------------------------------------------
~Initial Conditions Card
#-----------------------------------------------------
Aqueous Pressure,Gas Pressure,
3,
Aqueous Pressure,42595.45,Pa,,,,,,,1,1,1,1,1,250,
Gas Pressure,101356.57,Pa,,,,,,,1,1,1,1,1,250,
Temperature,20.0,C,,,,,,,1,1,1,1,1,250,

#-----------------------------------------------------
~Boundary Conditions Card
#-----------------------------------------------------
2,
Top,Dirichlet Aqueous,
1,1,1,1,250,250,1,
0,day,101356.57,Pa,
Bottom,Dirichlet Aqueous,
1,1,1,1,1,1,1,
0,day,42595.52,Pa,

#-----------------------------------------------------
~Output Options Card
#-----------------------------------------------------
6,
1,1,250,
1,1,200,
1,1,150,
1,1,100,
1,1,50,
1,1,1,
1,1,hr,cm,5,5,5,
2,
Aqueous saturation,,
Aqueous pressure,,
4,
1,hr,
300,hr,
600,hr,
900,hr,
2,
Aqueous saturation,,
Aqueous pressure,,

#-----------------------------------------------------
```

~Surface Flux Card
#---
2,
Aqueous Volumetric,cm^3/hr,cm^3,Top,1,1,1,1,250,250,
Aqueous Volumetric,cm^3/hr,cm^3,Bottom,1,1,1,1,1,1,

C.3 STOMP-WAE Input File for Infiltration Verification in Sand

```
#-------------------------------------------------------
~Simulation Title Card
#-------------------------------------------------------
1,
UNSAT-H 7.1,
M.D. White, A.L. Ward,
PNNL,
11 July 2003,
09:05,
1,
UNSAT-H, Problem 7.1, Sand

#-------------------------------------------------------
~Solution Control Card
#-------------------------------------------------------
Normal,
Water-Air-Energy,
1,
0,hr,0.8,hr,0.0000125,hr,0.01,hr,1.25,8,1.e-6,
10000,
variable aqueous diffusion,
variable gas diffusion,
0,

#-------------------------------------------------------
~Grid Card
#-------------------------------------------------------
Uniform Cartesian,
1,1,90,
1.0,cm,
1.0,cm,
1.0,cm,

#-------------------------------------------------------
~Rock/Soil Zonation Card
#-------------------------------------------------------
1,
Sand,1,1,1,1,1,90,

#-------------------------------------------------------
~Mechanical Properties Card
#-------------------------------------------------------
Sand,2650,kg/m^3,0.287,0.287,,,Constant,0.7,0.7,

#-------------------------------------------------------
~Hydraulic Properties Card
#-------------------------------------------------------
Sand,34.0,hc cm/hr,34.0,hc cm/hr,34.0,hc cm/hr,
```

```
#-----------------------------------------------------
~Thermal Properties Card
#-----------------------------------------------------
Sand,Somerton,,,,,0.582,W/m K,,,,,1.13,W/m K,700,J/kg K,
#-----------------------------------------------------
~Saturation Function Card
#-----------------------------------------------------
Sand,Haverkamp,1.0,cm,1.611e+6,cm,3.96,0.261324,

#-----------------------------------------------------
~Aqueous Relative Permeability Card
#-----------------------------------------------------
Sand,Haverkamp,1.175e+6,cm,4.74,1.0,cm,

#-----------------------------------------------------
~Gas Relative Permeability Card
#-----------------------------------------------------
Sand,Constant,1.0,

#-----------------------------------------------------
~Initial Conditions Card
#-----------------------------------------------------
Aqueous Pressure,Gas Pressure,
3,
Aqueous Pressure,95343.35,Pa,,,,,-12.65,1/m,1,1,1,1,1,90,
Gas Pressure,101356.57,Pa,,,,,-12.65,1/m,1,1,1,1,1,90,
Temperature,20.0,C,,,,,,1,1,1,1,1,90,

#-----------------------------------------------------
~Boundary Conditions Card
#-----------------------------------------------------
2,
Top,Dirichlet Energy,Dirichlet Aqueous,Dirichlet Gas,
1,1,1,1,90,90,1,
0,day,20,C,99315.05,Pa,1.0,101345.25,Pa,1.0,
Bottom,Dirichlet Energy,Dirichlet Aqueous,Dirichlet Gas,
1,1,1,1,1,1,1,
0,day,20,C,95343.35,Pa,1.0,101356.64,Pa,1.0,

#-----------------------------------------------------
~Output Options Card
#-----------------------------------------------------
6,
1,1,90,
1,1,75,
1,1,60,
1,1,45,
1,1,30,
1,1,1,
1,1,hr,cm,5,5,5,
6,
```

Temperature,,
Aqueous saturation,,
Phase condition,,
Water gas mass frac.,,
Aqueous pressure,,
Gas pressure,,
4,
1,hr,
300,hr,
600,hr,
900,hr,
6,
Temperature,,
Aqueous saturation,,
Phase condition,,
Water gas mass frac.,,
Aqueous pressure,,
Gas pressure,,

#---
~Surface Flux Card
#---
2,
Aqueous Volumetric,cm^3/hr,cm^3,Top,1,1,1,1,90,90,
Aqueous Volumetric,cm^3/hr,cm^3,Bottom,1,1,1,1,1,1,

C.4 STOMP-WAE Input File for Infiltration Verification in Clay

```
#-------------------------------------------------------
~Simulation Title Card
#-------------------------------------------------------
1,
UNSAT-H 7.1,
M.D. White, A.L. Ward,
PNNL,
11 July 2003,
09:05,
1,
UNSAT-H, Problem 7.1, Yolo light clay

#-------------------------------------------------------
~Solution Control Card
#-------------------------------------------------------
Normal,
Water-Air-Energy,
1,
0,hr,1200,hr,0.00125,hr,10,hr,1.25,8,1.e-6,
10000,
variable aqueous diffusion,
variable gas diffusion,
0,

#-------------------------------------------------------
~Grid Card
#-------------------------------------------------------
Uniform Cartesian,
1,1,250,
1.0,cm,
1.0,cm,
1.0,cm,

#-------------------------------------------------------
~Rock/Soil Zonation Card
#-------------------------------------------------------
1,
Yolo Light Clay,1,1,1,1,1,250,

#-------------------------------------------------------
~Mechanical Properties Card
#-------------------------------------------------------
Yolo Light Clay,2650,kg/m^3,0.495,0.495,,,Constant,0.7,0.7,

#-------------------------------------------------------
~Hydraulic Properties Card
#-------------------------------------------------------
Yolo Light Clay,4.428e-2,hc cm/hr,4.428e-2,hc cm/hr,4.428e-2,hc cm/hr,
```

```
#-----------------------------------------------------
~Thermal Properties Card
#-----------------------------------------------------
Yolo Light Clay,Somerton,,,,,0.582,W/m K,,,,,1.13,W/m K,700,J/kg K,

#-----------------------------------------------------
~Saturation Function Card
#-----------------------------------------------------
Yolo Light Clay,Haverkamp w/ Log,1.0,cm,739.0,cm,4.0,0.250505,

#-----------------------------------------------------
~Aqueous Relative Permeability Card
#-----------------------------------------------------
Yolo Light Clay,Haverkamp,124.6,cm,1.77,0.0,cm,

#-----------------------------------------------------
~Gas Relative Permeability Card
#-----------------------------------------------------
Yolo Light Clay,Constant,1.0,

#-----------------------------------------------------
~Initial Conditions Card
#-----------------------------------------------------
Aqueous Pressure,Gas Pressure,
3,
Aqueous Pressure,42595.45,,,,,,-12.65,1/m,1,1,1,1,1,250,
Gas Pressure,101356.57,Pa,,,,,-12.65,1/m,1,1,1,1,1,250,
Temperature,20.0,C,,,,,,1,1,1,1,1,250,

#-----------------------------------------------------
~Boundary Conditions Card
#-----------------------------------------------------
2,
Top,Dirichlet Energy,Dirichlet Aqueous,Dirichlet Gas,
1,1,1,1,250,250,1,
0,day,20,C,101325.00,Pa,1.0,101325.00,Pa,1.0,
Bottom,Dirichlet Energy,Dirichlet Aqueous,Dirichlet Gas,
1,1,1,1,1,1,1,
0,day,20,C,42595.52,Pa,1.0,101356.64,Pa,1.0,

#-----------------------------------------------------
~Output Options Card
#-----------------------------------------------------
6,
1,1,250,
1,1,200,
1,1,150,
1,1,100,
1,1,50,
1,1,1,
1,1,hr,cm,5,5,5,
6,
```

Temperature,,
Aqueous saturation,,
Phase condition,,
Water gas mass frac.,,
Aqueous pressure,,
Gas pressure,,
4,
1,hr,
300,hr,
600,hr,
900,hr,
6,
Temperature,,
Aqueous saturation,,
Phase condition,,
Water gas mass frac.,,
Aqueous pressure,,
Gas pressure,,

#---
~Surface Flux Card
#---
2,
Aqueous Volumetric,cm^3/hr,cm^3,Top,1,1,1,1,250,250,
Aqueous Volumetric,cm^3/hr,cm^3,Bottom,1,1,1,1,1,1,

C.5 STOMP-W Input File for Drainage Verification

```
#-----------------------------------------------------
~Simulation Title Card
#-----------------------------------------------------
1,
UNSAT-H 7.2,
M.D. White, A.L. Ward,
PNNL,
11 July 2003,
09:05,
1,
UNSAT-H, Problem 7.2, Drainage Mode 1

#-----------------------------------------------------
~Solution Control Card
#-----------------------------------------------------
Normal,
Water,
3,
0,hr,0.5,hr,0.0000002,hr,0.002,hr,1.25,16,1.e-6,
0.5,hr,16.0,hr,0.002,hr,0.1,hr,1.25,8,1.e-6,
16.0,hr,1000.0,hr,0.1,hr,24.0,hr,1.25,8,1.e-6,
10000,
1,
aqueous relative permeability,geometric,

#-----------------------------------------------------
~Grid Card
#-----------------------------------------------------
Cartesian,
1,1,89,
0.0,cm,4.785625,cm,
0.0,cm,4.785625,cm,
0.0,cm,10@0.057,cm,79@0.05,cm,

#-----------------------------------------------------
~Rock/Soil Zonation Card
#-----------------------------------------------------
2,
Ceramic Plate,1,1,1,1,1,10,
Silty Loam,1,1,1,1,11,89,

#-----------------------------------------------------
~Mechanical Properties Card
#-----------------------------------------------------
Ceramic Plate,2650,kg/m^3,0.388,0.388,1.e-5,1/m,Constant,0.7,0.7,
Silty Loam,2650,kg/m^3,0.388,0.388,1.e-5,1/m,Constant,0.7,0.7,

#-----------------------------------------------------
```

```
~Hydraulic Properties Card
#-----------------------------------------------------
Ceramic Plate,0.003,hc cm/hr,0.003,hc cm/hr,0.003,hc cm/hr,
Silty Loam,5.4,hc cm/hr,5.4,hc cm/hr,5.4,hc cm/hr,
#-----------------------------------------------------
~Saturation Function Card
#-----------------------------------------------------
Ceramic Plate,van Genuchten,4.705e-6,1/cm,3.0,0.997423,,
Silty Loam,van Genuchten,0.04705,1/cm,1.46097,0.446418,,

#-----------------------------------------------------
~Aqueous Relative Permeability Card
#-----------------------------------------------------
Ceramic Plate,Mualem,,
Silty Loam,Mualem,,

#-----------------------------------------------------
~Initial Conditions Card
#-----------------------------------------------------
Aqueous Pressure,Gas Pressure,
3,
Aqueous Pressure,199700.072,Pa,,,,,-9793.52,1/m,1,1,1,1,1,89,
Gas Pressure,199260.192,Pa,,,,,,,1,1,1,1,1,89,
Temperature,15.3,C,,,,,,,1,1,1,1,1,89,

#-----------------------------------------------------
~Boundary Conditions Card
#-----------------------------------------------------
1,
Bottom,Dirichlet Aqueous,
1,1,1,1,1,1,1,
0,day,101325.0,Pa,

#-----------------------------------------------------
~Output Options Card
#-----------------------------------------------------
6,
1,1,89,
1,1,75,
1,1,60,
1,1,45,
1,1,30,
1,1,1,
1,1,hr,cm,5,5,5,
2,
Aqueous saturation,,
Aqueous pressure,,
0,
2,
Aqueous saturation,,
Aqueous pressure,,
```

#----------
~Surface Flux Card
#----------
2,
Aqueous Volumetric,cm^3/hr,cm^3,Top,1,1,1,1,89,89,
Aqueous Volumetric,cm^3/hr,cm^3,Bottom,1,1,1,1,1,1,

C.6 STOMP-WAE Input File for Drainage Verification

```
#-------------------------------------------------------
~Simulation Title Card
#-------------------------------------------------------
1,
UNSAT-H 7.2,
M.D. White, A.L. Ward,
PNNL,
11 July 2003,
09:05,
1,
UNSAT-H, Problem 7.2, Drainage Mode 3

#-------------------------------------------------------
~Solution Control Card
#-------------------------------------------------------
Normal,
Water-Air-Energy,
3,
0,hr,0.5,hr,0.0000002,hr,0.002,hr,1.25,16,1.e-6,
0.5,hr,16.0,hr,0.002,hr,0.1,hr,1.25,8,1.e-6,
16.0,hr,1000.0,hr,0.1,hr,24.0,hr,1.25,8,1.e-6,
10000,
variable aqueous diffusion,
variable gas diffusion,
1,
aqueous relative permeability,geometric,

#-------------------------------------------------------
~Grid Card
#-------------------------------------------------------
Cartesian,
1,1,89,
0.0,cm,4.785625,cm,
0.0,cm,4.785625,cm,
0.0,cm,10@0.057,cm,79@0.05,cm,

#-------------------------------------------------------
~Rock/Soil Zonation Card
#-------------------------------------------------------
2,
Ceramic Plate,1,1,1,1,1,10,
Silty Loam,1,1,1,1,11,89,

#-------------------------------------------------------
~Mechanical Properties Card
#-------------------------------------------------------
Ceramic Plate,2650,kg/m^3,0.388,0.388,1.e-5,1/m,Constant,0.7,0.7,
Silty Loam,2650,kg/m^3,0.388,0.388,1.e-5,1/m,Constant,0.7,0.7,
```

```
#-----------------------------------------------------
~Hydraulic Properties Card
#-----------------------------------------------------
Ceramic Plate,0.003,hc cm/hr,0.003,hc cm/hr,0.003,hc cm/hr,
Silty Loam,5.4,hc cm/hr,5.4,hc cm/hr,5.4,hc cm/hr,

#-----------------------------------------------------
~Thermal Properties Card
#-----------------------------------------------------
Ceramic Plate,Somerton,,,,,0.582,W/m K,,,,,1.13,W/m K,700,J/kg K,
Silty Loam,Somerton,,,,,0.582,W/m K,,,,,1.13,W/m K,700,J/kg K,

#-----------------------------------------------------
~Saturation Function Card
#-----------------------------------------------------
Ceramic Plate,van Genuchten,4.705e-6,1/cm,3.0,0.997423,,
Silty Loam,van Genuchten,0.04705,1/cm,1.46097,0.446418,,

#-----------------------------------------------------
~Aqueous Relative Permeability Card
#-----------------------------------------------------
Ceramic Plate,Mualem,,
Silty Loam,Mualem,,

#-----------------------------------------------------
~Gas Relative Permeability Card
#-----------------------------------------------------
Ceramic Plate,Constant,1.0,
Silty Loam,Constant,1.0,

#-----------------------------------------------------
~Initial Conditions Card
#-----------------------------------------------------
Aqueous Pressure,Gas Pressure,
3,
Aqueous Pressure,199700.072,Pa,,,,,-9793.52,1/m,1,1,1,1,1,89,
Gas Pressure,199260.192,Pa,,,,,,,1,1,1,1,1,89,
Temperature,15.3,C,,,,,,,1,1,1,1,1,89,

#-----------------------------------------------------
~Boundary Conditions Card
#-----------------------------------------------------
2,
Bottom,Dirichlet Energy,Dirichlet Aqueous,Zero Flux Gas,
1,1,1,1,1,1,1,
0,day,15.3,C,101767.86,Pa,1.0,,,1.0,
Top,Dirichlet Energy,Zero Flux Aqueous,Dirichlet Gas,
1,1,1,1,89,89,1,
0,day,15.3,C,,,1.0,199260.192,Pa,1.0,

#-----------------------------------------------------
~Output Options Card
```

```
#-----------------------------------------------------
6,
1,1,89,
1,1,75,
1,1,60,
1,1,45,
1,1,30,
1,1,1,
1,1,hr,cm,5,5,5,
2,
Aqueous saturation,,
Aqueous relative permeability,,
0,
6,
Temperature,,
Aqueous saturation,,
Aqueous relative permeability,,
Water gas mass frac.,,
Aqueous pressure,,
Gas pressure,,

#-----------------------------------------------------
~Surface Flux Card
#-----------------------------------------------------
2,
Aqueous Volumetric,cm^3/hr,cm^3,Top,1,1,1,1,89,89,
Aqueous Volumetric,cm^3/hr,cm^3,Bottom,1,1,1,1,1,1,
```

C.7 STOMP-WAE Input File for Heat Flow Verification

```
#-------------------------------------------------------
~Simulation Title Card
#-------------------------------------------------------
1,
UNSAT-H 7.3,
A.L. Ward, M.D. White,
PNNL,
23 September 2004,
11:52,
1,
UNSAT-H, Problem 7.3, Verification of Heat Flow

#-------------------------------------------------------
~Solution Control Card
#-------------------------------------------------------
Normal,
Water-Air-Energy,
1,
0,hr,240,hr,0.01,hr,0.1,hr,1.25,16,1.e-6,
10000,
variable aqueous diffusion,
variable gas diffusion,
0,

#-------------------------------------------------------
~Grid Card
#-------------------------------------------------------
Cartesian,
101,1,1,
0.0,cm,101@1.0,cm,
0.0,cm,1.0,cm,
0.0,cm,1.0,cm,

#-------------------------------------------------------
~Rock/Soil Zonation Card
#-------------------------------------------------------
1,
L-soil,1,101,1,1,1,1,

#-------------------------------------------------------
~Mechanical Properties Card
#-------------------------------------------------------
L-soil,2650,kg/m^3,0.4326,0.4326,1.e-5,1/m,Constant,0.66,0.66,

#-------------------------------------------------------
~Hydraulic Properties Card
#-------------------------------------------------------
L-soil,35.3,hc cm/hr,35.3,hc cm/hr,35.3,hc cm/hr,
```

```
#-----------------------------------------------------w
~Thermal Properties Card
#-----------------------------------------------------
L-soil,Cass,0.60,W/m K,0.70,W/m K,8.0,0.26,W/m K,3.0,513.208,J/kg K,enhanced,9.5,2.0,8.0,0.50,3.0,

#-----------------------------------------------------
~Saturation Function Card
#-----------------------------------------------------
L-soil,Brooks and Corey,9.4,cm,0.778452,0.08807,,

#-----------------------------------------------------
~Aqueous Relative Permeability Card
#-----------------------------------------------------
L-soil,Burdine,,

#-----------------------------------------------------
~Gas Relative Permeability Card
#-----------------------------------------------------
L-soil,Constant,1.0,

#-----------------------------------------------------
~Initial Conditions Card
#-----------------------------------------------------
Aqueous Pressure,Gas Pressure,
3,
Aqueous Pressure,91531.48,Pa,,,,,,,1,101,1,1,1,1,
Gas Pressure,101325.0,Pa,,,,,,,1,101,1,1,1,1,
Temperature,14.85,C,,,,,,,1,101,1,1,1,1,

#-----------------------------------------------------
~Boundary Conditions Card
#-----------------------------------------------------
1,
West,Dirichlet Energy,Dirichlet Aqueous,Zero Flux Gas,
1,1,1,1,1,1,-128,
0,hr,4.85,C,91531.48,Pa,1.0,101325.0,Pa,1.0,
0.188976,hr,4.86224,C,91531.48,Pa,1.0,101325.0,Pa,1.0,
0.377953,hr,4.89891,C,91531.48,Pa,1.0,101325.0,Pa,1.0,
0.566929,hr,4.95994,C,91531.48,Pa,1.0,101325.0,Pa,1.0,
0.755906,hr,5.04518,C,91531.48,Pa,1.0,101325.0,Pa,1.0,
0.944882,hr,5.1544,C,91531.48,Pa,1.0,101325.0,Pa,1.0,
1.13386,hr,5.28735,C,91531.48,Pa,1.0,101325.0,Pa,1.0,
1.32283,hr,5.44371,C,91531.48,Pa,1.0,101325.0,Pa,1.0,
1.51181,hr,5.62308,C,91531.48,Pa,1.0,101325.0,Pa,1.0,
1.70079,hr,5.82503,C,91531.48,Pa,1.0,101325.0,Pa,1.0,
1.88976,hr,6.04907,C,91531.48,Pa,1.0,101325.0,Pa,1.0,
2.07874,hr,6.29465,C,91531.48,Pa,1.0,101325.0,Pa,1.0,
2.26772,hr,6.56116,C,91531.48,Pa,1.0,101325.0,Pa,1.0,
2.45669,hr,6.84796,C,91531.48,Pa,1.0,101325.0,Pa,1.0,
2.64567,hr,7.15434,C,91531.48,Pa,1.0,101325.0,Pa,1.0,
2.83465,hr,7.47955,C,91531.48,Pa,1.0,101325.0,Pa,1.0,
3.02362,hr,7.8228,C,91531.48,Pa,1.0,101325.0,Pa,1.0,
```

3.2126,hr,8.18324,C,91531.48,Pa,1.0,101325.0,Pa,1.0,
3.40157,hr,8.56,C,91531.48,Pa,1.0,101325.0,Pa,1.0,
3.59055,hr,8.95215,C,91531.48,Pa,1.0,101325.0,Pa,1.0,
3.77953,hr,9.35874,C,91531.48,Pa,1.0,101325.0,Pa,1.0,
3.9685,hr,9.77876,C,91531.48,Pa,1.0,101325.0,Pa,1.0,
4.15748,hr,10.2112,C,91531.48,Pa,1.0,101325.0,Pa,1.0,
4.34646,hr,10.655,C,91531.48,Pa,1.0,101325.0,Pa,1.0,
4.53543,hr,11.109,C,91531.48,Pa,1.0,101325.0,Pa,1.0,
4.72441,hr,11.5722,C,91531.48,Pa,1.0,101325.0,Pa,1.0,
4.91339,hr,12.0435,C,91531.48,Pa,1.0,101325.0,Pa,1.0,
5.10236,hr,12.5216,C,91531.48,Pa,1.0,101325.0,Pa,1.0,
5.29134,hr,13.0054,C,91531.48,Pa,1.0,101325.0,Pa,1.0,
5.48031,hr,13.4937,C,91531.48,Pa,1.0,101325.0,Pa,1.0,
5.66929,hr,13.9853,C,91531.48,Pa,1.0,101325.0,Pa,1.0,
5.85827,hr,14.479,C,91531.48,Pa,1.0,101325.0,Pa,1.0,
6.04724,hr,14.9737,C,91531.48,Pa,1.0,101325.0,Pa,1.0,
6.23622,hr,15.468,C,91531.48,Pa,1.0,101325.0,Pa,1.0,
6.4252,hr,15.9609,C,91531.48,Pa,1.0,101325.0,Pa,1.0,
6.61417,hr,16.451,C,91531.48,Pa,1.0,101325.0,Pa,1.0,
6.80315,hr,16.9372,C,91531.48,Pa,1.0,101325.0,Pa,1.0,
6.99213,hr,17.4183,C,91531.48,Pa,1.0,101325.0,Pa,1.0,
7.1811,hr,17.8931,C,91531.48,Pa,1.0,101325.0,Pa,1.0,
7.37008,hr,18.3604,C,91531.48,Pa,1.0,101325.0,Pa,1.0,
7.55906,hr,18.8192,C,91531.48,Pa,1.0,101325.0,Pa,1.0,
7.74803,hr,19.2683,C,91531.48,Pa,1.0,101325.0,Pa,1.0,
7.93701,hr,19.7065,C,91531.48,Pa,1.0,101325.0,Pa,1.0,
8.12598,hr,20.1329,C,91531.48,Pa,1.0,101325.0,Pa,1.0,
8.31496,hr,20.5463,C,91531.48,Pa,1.0,101325.0,Pa,1.0,
8.50394,hr,20.9458,C,91531.48,Pa,1.0,101325.0,Pa,1.0,
8.69291,hr,21.3304,C,91531.48,Pa,1.0,101325.0,Pa,1.0,
8.88189,hr,21.6991,C,91531.48,Pa,1.0,101325.0,Pa,1.0,
9.07087,hr,22.051,C,91531.48,Pa,1.0,101325.0,Pa,1.0,
9.25984,hr,22.3854,C,91531.48,Pa,1.0,101325.0,Pa,1.0,
9.44882,hr,22.7013,C,91531.48,Pa,1.0,101325.0,Pa,1.0,
9.6378,hr,22.9979,C,91531.48,Pa,1.0,101325.0,Pa,1.0,
9.82677,hr,23.2747,C,91531.48,Pa,1.0,101325.0,Pa,1.0,
10.0157,hr,23.5308,C,91531.48,Pa,1.0,101325.0,Pa,1.0,
10.2047,hr,23.7657,C,91531.48,Pa,1.0,101325.0,Pa,1.0,
10.3937,hr,23.9787,C,91531.48,Pa,1.0,101325.0,Pa,1.0,
10.5827,hr,24.1695,C,91531.48,Pa,1.0,101325.0,Pa,1.0,
10.7717,hr,24.3374,C,91531.48,Pa,1.0,101325.0,Pa,1.0,
10.9606,hr,24.4821,C,91531.48,Pa,1.0,101325.0,Pa,1.0,
11.1496,hr,24.6032,C,91531.48,Pa,1.0,101325.0,Pa,1.0,
11.3386,hr,24.7005,C,91531.48,Pa,1.0,101325.0,Pa,1.0,
11.5276,hr,24.7736,C,91531.48,Pa,1.0,101325.0,Pa,1.0,
11.7165,hr,24.8225,C,91531.48,Pa,1.0,101325.0,Pa,1.0,
11.9055,hr,24.8469,C,91531.48,Pa,1.0,101325.0,Pa,1.0,
12.0945,hr,24.8469,C,91531.48,Pa,1.0,101325.0,Pa,1.0,
12.2835,hr,24.8225,C,91531.48,Pa,1.0,101325.0,Pa,1.0,
12.4724,hr,24.7736,C,91531.48,Pa,1.0,101325.0,Pa,1.0,
12.6614,hr,24.7005,C,91531.48,Pa,1.0,101325.0,Pa,1.0,
12.8504,hr,24.6032,C,91531.48,Pa,1.0,101325.0,Pa,1.0,

13.0394,hr,24.4821,C,91531.48,Pa,1.0,101325.0,Pa,1.0,
13.2283,hr,24.3374,C,91531.48,Pa,1.0,101325.0,Pa,1.0,
13.4173,hr,24.1695,C,91531.48,Pa,1.0,101325.0,Pa,1.0,
13.6063,hr,23.9787,C,91531.48,Pa,1.0,101325.0,Pa,1.0,
13.7953,hr,23.7657,C,91531.48,Pa,1.0,101325.0,Pa,1.0,
13.9843,hr,23.5308,C,91531.48,Pa,1.0,101325.0,Pa,1.0,
14.1732,hr,23.2747,C,91531.48,Pa,1.0,101325.0,Pa,1.0,
14.3622,hr,22.9979,C,91531.48,Pa,1.0,101325.0,Pa,1.0,
14.5512,hr,22.7013,C,91531.48,Pa,1.0,101325.0,Pa,1.0,
14.7402,hr,22.3854,C,91531.48,Pa,1.0,101325.0,Pa,1.0,
14.9291,hr,22.051,C,91531.48,Pa,1.0,101325.0,Pa,1.0,
15.1181,hr,21.6991,C,91531.48,Pa,1.0,101325.0,Pa,1.0,
15.3071,hr,21.3304,C,91531.48,Pa,1.0,101325.0,Pa,1.0,
15.4961,hr,20.9458,C,91531.48,Pa,1.0,101325.0,Pa,1.0,
15.685,hr,20.5463,C,91531.48,Pa,1.0,101325.0,Pa,1.0,
15.874,hr,20.1329,C,91531.48,Pa,1.0,101325.0,Pa,1.0,
16.063,hr,19.7065,C,91531.48,Pa,1.0,101325.0,Pa,1.0,
16.252,hr,19.2683,C,91531.48,Pa,1.0,101325.0,Pa,1.0,
16.4409,hr,18.8192,C,91531.48,Pa,1.0,101325.0,Pa,1.0,
16.6299,hr,18.3604,C,91531.48,Pa,1.0,101325.0,Pa,1.0,
16.8189,hr,17.8931,C,91531.48,Pa,1.0,101325.0,Pa,1.0,
17.0079,hr,17.4183,C,91531.48,Pa,1.0,101325.0,Pa,1.0,
17.1969,hr,16.9372,C,91531.48,Pa,1.0,101325.0,Pa,1.0,
17.3858,hr,16.451,C,91531.48,Pa,1.0,101325.0,Pa,1.0,
17.5748,hr,15.9609,C,91531.48,Pa,1.0,101325.0,Pa,1.0,
17.7638,hr,15.468,C,91531.48,Pa,1.0,101325.0,Pa,1.0,
17.9528,hr,14.9737,C,91531.48,Pa,1.0,101325.0,Pa,1.0,
18.1417,hr,14.479,C,91531.48,Pa,1.0,101325.0,Pa,1.0,
18.3307,hr,13.9853,C,91531.48,Pa,1.0,101325.0,Pa,1.0,
18.5197,hr,13.4937,C,91531.48,Pa,1.0,101325.0,Pa,1.0,
18.7087,hr,13.0054,C,91531.48,Pa,1.0,101325.0,Pa,1.0,
18.8976,hr,12.5216,C,91531.48,Pa,1.0,101325.0,Pa,1.0,
19.0866,hr,12.0435,C,91531.48,Pa,1.0,101325.0,Pa,1.0,
19.2756,hr,11.5722,C,91531.48,Pa,1.0,101325.0,Pa,1.0,
19.4646,hr,11.109,C,91531.48,Pa,1.0,101325.0,Pa,1.0,
19.6535,hr,10.655,C,91531.48,Pa,1.0,101325.0,Pa,1.0,
19.8425,hr,10.2112,C,91531.48,Pa,1.0,101325.0,Pa,1.0,
20.0315,hr,9.77876,C,91531.48,Pa,1.0,101325.0,Pa,1.0,
20.2205,hr,9.35874,C,91531.48,Pa,1.0,101325.0,Pa,1.0,
20.4094,hr,8.95215,C,91531.48,Pa,1.0,101325.0,Pa,1.0,
20.5984,hr,8.56,C,91531.48,Pa,1.0,101325.0,Pa,1.0,
20.7874,hr,8.18324,C,91531.48,Pa,1.0,101325.0,Pa,1.0,
20.9764,hr,7.8228,C,91531.48,Pa,1.0,101325.0,Pa,1.0,
21.1654,hr,7.47955,C,91531.48,Pa,1.0,101325.0,Pa,1.0,
21.3543,hr,7.15434,C,91531.48,Pa,1.0,101325.0,Pa,1.0,
21.5433,hr,6.84796,C,91531.48,Pa,1.0,101325.0,Pa,1.0,
21.7323,hr,6.56116,C,91531.48,Pa,1.0,101325.0,Pa,1.0,
21.9213,hr,6.29465,C,91531.48,Pa,1.0,101325.0,Pa,1.0,
22.1102,hr,6.04907,C,91531.48,Pa,1.0,101325.0,Pa,1.0,
22.2992,hr,5.82503,C,91531.48,Pa,1.0,101325.0,Pa,1.0,
22.4882,hr,5.62308,C,91531.48,Pa,1.0,101325.0,Pa,1.0,
22.6772,hr,5.44371,C,91531.48,Pa,1.0,101325.0,Pa,1.0,

22.8661,hr,5.28735,C,91531.48,Pa,1.0,101325.0,Pa,1.0,
23.0551,hr,5.1544,C,91531.48,Pa,1.0,101325.0,Pa,1.0,
23.2441,hr,5.04518,C,91531.48,Pa,1.0,101325.0,Pa,1.0,
23.4331,hr,4.95994,C,91531.48,Pa,1.0,101325.0,Pa,1.0,
23.622,hr,4.89891,C,91531.48,Pa,1.0,101325.0,Pa,1.0,
23.811,hr,4.86224,C,91531.48,Pa,1.0,101325.0,Pa,1.0,
24,hr,4.85,C,91531.48,Pa,1.0,101325.0,Pa,1.0,

#---
~Output Options Card
#---
5,
1,1,1,
6,1,1,
11,1,1,
28,1,1,
41,1,1,
1,1,hr,cm,6,6,6,
6,
Temperature,K,
Aqueous saturation,,
Aqueous relative permeability,,
Water gas mass frac.,,
Aqueous pressure,,
Gas pressure,,
9,
0,hr,
6,hr,
12,hr,
18,hr,
24,hr,
216,hr,
222,hr,
228,hr,
234,hr,
6,
Temperature,K,
Aqueous saturation,,
Aqueous relative permeability,,
Water gas mass frac.,,
Aqueous pressure,,
Gas pressure,,

C.8 STOMP-W Input File for Verification of Flow in a Layered Soil

```
#-------------------------------------------------------
~Simulation Title Card
#-------------------------------------------------------
1,
UNSAT-H Problem 7.5 Layered Soil,
M.D. White, A.L. Ward,
PNNL,
August 2005,
11:52,
1,
STOMP-W
#-------------------------------------------------------
~Solution Control Card
#-------------------------------------------------------
Normal,
Water,
1,
0,hr,8760,hr,0.01,hr,1.0,hr,1.25,16,1.e-6,
100000,
1,
effective permeability,geometric,

#-------------------------------------------------------
~Grid Card
#-------------------------------------------------------
Cartesian,
1,1,74,
0.0,cm,1.0,cm,
0.0,cm,1.0,cm,
0,cm,10,cm,20,cm,30,cm,40,cm,50,cm,
60,cm,70,cm,80,cm,90,cm,100,cm,110,cm,120,cm,
130,cm,140,cm,150,cm,160,cm,170,cm,180,cm,190,cm,
200,cm,210,cm,220,cm,230,cm,240,cm,250,cm,260,cm,
270,cm,280,cm,290,cm,300,cm,310,cm,320,cm,330,cm,
340,cm,350,cm,360,cm,370,cm,380,cm,390,cm,400,cm,
410,cm,420,cm,430,cm,440,cm,450,cm,460,cm,470,cm,
480,cm,490,cm,500,cm,510,cm,515,cm,520,cm,525,cm,
530,cm,531,cm,532,cm,533,cm,534,cm,535,cm,536,cm,
537,cm,538,cm,539,cm,539.1,cm,539.2,cm,539.3,cm,
539.4,cm,539.5,cm,539.6,cm,539.7,cm,539.8,cm,539.9,cm,
540,cm,

#-------------------------------------------------------
~Rock/Soil Zonation Card
#-------------------------------------------------------
3,
COMPGRAV,1,1,1,1,52,74,
COMPOS1,1,1,1,1,40,51,
```

GRAVEL1,1,1,1,1,1,39,
#---
~Mechanical Properties Card
#---
COMPGRAV,2650,kg/m^3,0.422,0.422,1.e-5,1/m,Constant,0.66,0.66,
COMPOS1,2650,kg/m^3,0.422,0.422,1.e-5,1/m,Constant,0.66,0.66,
GRAVEL1,2650,kg/m^3,0.419,0.419,1.e-5,1/m,Constant,0.66,0.66,

#---
~Hydraulic Properties Card
#---
COMPGRAV,3.6E-01,hc cm/hr,3.6E-01,hc cm/hr,3.6E-01,hc cm/hr,
COMPOS1,1.080002E-01,hc cm/hr,1.080002E-01,hc cm/hr,1.080002E-01,hc cm/hr,
GRAVEL1,1.2600005E+03,hc cm/hr,1.2600005E+03,hc cm/hr,1.2600005E+03,hc cm/hr,

#---
~Saturation Function Card
#---
COMPGRAV,Polynomial,4,
4,1.0,12.65,4.2199999E-01,-2.7573731E-02,-2.3653656E-03,-3.2151621E-02,cm,
5,12.65,244.2,-1.38834E-01,1.5021513,-1.4785267,5.4422855E-01,-7.0263125E-02,cm,
5,244.2,7197.0,-1.7569752,2.7017555,-1.3545368,2.8460807E-01,-2.161908E-02,,cm,
5,7197.0,8.6326599e+06,-3.4936512E-01,3.145951E-01,-8.4237993E-02,9.1790808E-03,-3.5545405E-04,cm,
COMPOS1,Polynomial,4,
3,1.0,5.4290004,4.2199999E-01,-7.3107332E-03,-3.5250444E-02,cm,
3,5.4290004,5.6900012E+02,4.2632636E-01,-1.9087702E-02,-2.7235843E-02,cm,
4,5.6900012E+02,1.6770025E+04,2.4613359,-1.7952768,4.5785773E-01,-3.9381173E-02,cm,
4,1.6770025E+04,8.6326599E+06,3.6377275E-01,-1.0580593E-01,1.0616908E-02,-3.5810552E-04,cm,
GRAVEL1,Polynomial,4,
3,9.9999998E-03,7.743001E-02,2.9529411E-01,-9.5835656E-02,-1.6991356E-02,cm,
3,7.743001E-02,2.7829993E-01,-2.0774645E-01,-1.0013254,-4.2446923E-01,cm,
5,2.782999E-01,1.2920002E+01,5.8681458E-02,-1.1252354E-01,2.0134E-01,-1.705484E-01,5.2016903E-02,cm,
5,1.292000E+01,8.777789E+06,4.5875967E-02,-2.251409E-02,6.265761E-03,-7.932858E-04,3.5441328E-05,cm,

#---
~Aqueous Relative Permeability Card
#---
COMPGRAV,Polynomial,2,3.6E-01,
4,1.0,4.498E+01,-4.4369757E-01,-5.8029747E-01,-2.8344643E-01,-2.1685658E-01,cm,
3,4.498E+01,8.6326599E+06,2.4089615,-3.4391944,4.3601289E-02,cm,
COMPOS1,Polynomial,3,1.080002E-01,
4,1.0,1.3260002E+03,-9.6657562E-01,-1.0965506,5.8941185E-02,-1.2111266E-01,cm,
4,1.3260002E+03,7.1970044E+03,-6.3407219E+01,6.0421951E+01,-2.0131914E+01,2.0865219,cm,
4,7.1970044E+03,8.6326599E+06,-9.5900745,1.8411379,-6.0871047E-01,2.465306E-02,cm,
GRAVEL1,Polynomial,4,1.2600005E+03,
4,9.9999998E-03,2.7829993E-01,-2.7429957,-1.0566543E+01,-6.7793403,-1.4784553,cm,
3,2.7829993E-01,4.6420007,-1.3305095,-5.0247631,-5.5922753E-01,cm,
3,4.6420007,1.6680004E+01,1.8869209E-01,-9.5821028,2.8585794,cm,
4,1.6680004E+01,8.7777891E+06,-3.7477951,-3.1739995,2.7821976E-01,-2.2469539E-02,cm,

#---
~Initial Conditions Card

```
#-----------------------------------------------------
Aqueous Pressure,Gas Pressure,
76,
Aqueous Pressure,101070.6476,Pa,,,,,,1,1,1,1,1,1,
Aqueous Pressure,101070.2265,Pa,,,,,,1,1,1,1,2,2,
Aqueous Pressure,101069.8054,Pa,,,,,,1,1,1,1,3,3,
Aqueous Pressure,101069.3843,Pa,,,,,,1,1,1,1,4,4,
Aqueous Pressure,101068.9631,Pa,,,,,,1,1,1,1,5,5,
Aqueous Pressure,101068.542,Pa,,,,,,1,1,1,1,6,6,
Aqueous Pressure,101068.1209,Pa,,,,,,1,1,1,1,7,7,
Aqueous Pressure,101067.6998,Pa,,,,,,1,1,1,1,8,8,
Aqueous Pressure,101067.2786,Pa,,,,,,1,1,1,1,9,9,
Aqueous Pressure,101066.8575,Pa,,,,,,1,1,1,1,10,10,
Aqueous Pressure,101066.363,Pa,,,,,,1,1,1,1,11,11,
Aqueous Pressure,101065.7949,Pa,,,,,,1,1,1,1,12,12,
Aqueous Pressure,101065.2269,Pa,,,,,,1,1,1,1,13,13,
Aqueous Pressure,101064.6589,Pa,,,,,,1,1,1,1,14,14,
Aqueous Pressure,101064.0909,Pa,,,,,,1,1,1,1,15,15,
Aqueous Pressure,101063.5228,Pa,,,,,,1,1,1,1,16,16,
Aqueous Pressure,101062.9548,Pa,,,,,,1,1,1,1,17,17,
Aqueous Pressure,101062.3868,Pa,,,,,,1,1,1,1,18,18,
Aqueous Pressure,101061.8188,Pa,,,,,,1,1,1,1,19,19,
Aqueous Pressure,101061.2507,Pa,,,,,,1,1,1,1,20,20,
Aqueous Pressure,101060.6318,Pa,,,,,,1,1,1,1,21,21,
Aqueous Pressure,101059.9629,Pa,,,,,,1,1,1,1,22,22,
Aqueous Pressure,101059.294,Pa,,,,,,1,1,1,1,23,23,
Aqueous Pressure,101058.6241,Pa,,,,,,1,1,1,1,24,24,
Aqueous Pressure,101057.9552,Pa,,,,,,1,1,1,1,25,25,
Aqueous Pressure,101057.2863,Pa,,,,,,1,1,1,1,26,26,
Aqueous Pressure,101056.7555,Pa,,,,,,1,1,1,1,27,27,
Aqueous Pressure,101056.3638,Pa,,,,,,1,1,1,1,28,28,
Aqueous Pressure,101055.972,Pa,,,,,,1,1,1,1,29,29,
Aqueous Pressure,101055.5803,Pa,,,,,,1,1,1,1,30,30,
Aqueous Pressure,101055.1885,Pa,,,,,,1,1,1,1,31,31,
Aqueous Pressure,101054.7968,Pa,,,,,,1,1,1,1,32,32,
Aqueous Pressure,101054.1485,Pa,,,,,,1,1,1,1,33,33,
Aqueous Pressure,101053.2445,Pa,,,,,,1,1,1,1,34,34,
Aqueous Pressure,101052.3406,Pa,,,,,,1,1,1,1,35,35,
Aqueous Pressure,101051.4366,Pa,,,,,,1,1,1,1,36,36,
Aqueous Pressure,101050.7442,Pa,,,,,,1,1,1,1,37,37,
Aqueous Pressure,101050.1939,Pa,,,,,,1,1,1,1,38,38,
Aqueous Pressure,101049.4593,Pa,,,,,,1,1,1,1,39,39,
Aqueous Pressure,100487.5562,Pa,,,,,,1,1,1,1,40,40,
Aqueous Pressure,99548.04429,Pa,,,,,,1,1,1,1,41,41,
Aqueous Pressure,98652.29964,Pa,,,,,,1,1,1,1,42,42,
Aqueous Pressure,97808.63693,Pa,,,,,,1,1,1,1,43,43,
Aqueous Pressure,97024.76365,Pa,,,,,,1,1,1,1,44,44,
Aqueous Pressure,96298.32937,Pa,,,,,,1,1,1,1,45,45,
Aqueous Pressure,95619.19778,Pa,,,,,,1,1,1,1,46,46,
Aqueous Pressure,94970.47507,Pa,,,,,,1,1,1,1,47,47,
Aqueous Pressure,94331.10517,Pa,,,,,,1,1,1,1,48,48,
Aqueous Pressure,93685.97668,Pa,,,,,,1,1,1,1,49,49,
```

Aqueous Pressure,93056.8508,Pa,,,,,,1,1,1,1,50,50,
Aqueous Pressure,92707.63349,Pa,,,,,,1,1,1,1,51,51,
Aqueous Pressure,93495.56128,Pa,,,,,,1,1,1,1,52,52,
Aqueous Pressure,94721.847,Pa,,,,,,1,1,1,1,53,53,
Aqueous Pressure,95557.9589,Pa,,,,,,1,1,1,1,54,54,
Aqueous Pressure,95621.51884,Pa,,,,,,1,1,1,1,55,55,
Aqueous Pressure,95460.99327,Pa,,,,,,1,1,1,1,56,56,
Aqueous Pressure,95407.48148,Pa,,,,,,1,1,1,1,57,57,
Aqueous Pressure,95179.77237,Pa,,,,,,1,1,1,1,58,58,
Aqueous Pressure,94777.87572,Pa,,,,,,1,1,1,1,59,59,
Aqueous Pressure,94375.96928,Pa,,,,,,1,1,1,1,60,60,
Aqueous Pressure,93974.07263,Pa,,,,,,1,1,1,1,61,61,
Aqueous Pressure,93136.16851,Pa,,,,,,1,1,1,1,62,62,
Aqueous Pressure,91862.2765,Pa,,,,,,1,1,1,1,63,63,
Aqueous Pressure,89294.0534,Pa,,,,,,1,1,1,1,64,64,
Aqueous Pressure,86742.93959,Pa,,,,,,1,1,1,1,65,65,
Aqueous Pressure,85503.27593,Pa,,,,,,1,1,1,1,66,66,
Aqueous Pressure,84263.51433,Pa,,,,,,1,1,1,1,67,67,
Aqueous Pressure,83023.85067,Pa,,,,,,1,1,1,1,68,68,
Aqueous Pressure,81784.18701,Pa,,,,,,1,1,1,1,69,69,
Aqueous Pressure,77159.88311,Pa,,,,,,1,1,1,1,70,70,
Aqueous Pressure,69150.84105,Pa,,,,,,1,1,1,1,71,71,
Aqueous Pressure,61141.79898,Pa,,,,,,1,1,1,1,72,72,
Aqueous Pressure,-38326.66638,Pa,,,,,,1,1,1,1,73,73,
Aqueous Pressure,-1139239.664,Pa,,,,,,1,1,1,1,74,74,
Gas Pressure,101325.0,Pa,,,,,,1,1,1,1,1,74,
Temperature,288.46,K,,,,,,1,1,1,1,1,74,

#---
~Boundary Conditions Card
#---
2,
Top,Potential Evaporation Aqueous,
1,1,1,1,74,74,367,
0,day,0.04665,cm/day,1.0e+5,cm,
0.5,day,0.0087,cm/day,1.0e+5,cm,
1.5,day,0.0141,cm/day,1.0e+5,cm,
2.5,day,0.1314,cm/day,1.0e+5,cm,
3.5,day,0.1198,cm/day,1.0e+5,cm,
4.5,day,0.0273,cm/day,1.0e+5,cm,
5.5,day,0.0381,cm/day,1.0e+5,cm,
6.5,day,0.241,cm/day,1.0e+5,cm,
7.5,day,0.1452,cm/day,1.0e+5,cm,
8.5,day,0.1637,cm/day,1.0e+5,cm,
9.5,day,0.1134,cm/day,1.0e+5,cm,
10.5,day,0.1323,cm/day,1.0e+5,cm,
11.5,day,0.0568,cm/day,1.0e+5,cm,
12.5,day,0.0266,cm/day,1.0e+5,cm,
13.5,day,0.151,cm/day,1.0e+5,cm,
14.5,day,0.0815,cm/day,1.0e+5,cm,
15.5,day,0.0906,cm/day,1.0e+5,cm,
16.5,day,0.102,cm/day,1.0e+5,cm,

17.5,day,0.0961,cm/day,1.0e+5,cm,
18.5,day,0.1251,cm/day,1.0e+5,cm,
19.5,day,0.2172,cm/day,1.0e+5,cm,
20.5,day,0.071,cm/day,1.0e+5,cm,
21.5,day,0.084,cm/day,1.0e+5,cm,
22.5,day,0.0841,cm/day,1.0e+5,cm,
23.5,day,0.1251,cm/day,1.0e+5,cm,
24.5,day,0.2007,cm/day,1.0e+5,cm,
25.5,day,0.2937,cm/day,1.0e+5,cm,
26.5,day,0.2593,cm/day,1.0e+5,cm,
27.5,day,0.0991,cm/day,1.0e+5,cm,
28.5,day,0.0882,cm/day,1.0e+5,cm,
29.5,day,0.0842,cm/day,1.0e+5,cm,
30.5,day,0.1137,cm/day,1.0e+5,cm,
31.5,day,0.0958,cm/day,1.0e+5,cm,
32.5,day,0.0884,cm/day,1.0e+5,cm,
33.5,day,0.1858,cm/day,1.0e+5,cm,
34.5,day,0.2037,cm/day,1.0e+5,cm,
35.5,day,0.2551,cm/day,1.0e+5,cm,
36.5,day,0.124,cm/day,1.0e+5,cm,
37.5,day,0.0239,cm/day,1.0e+5,cm,
38.5,day,0.0551,cm/day,1.0e+5,cm,
39.5,day,0.02,cm/day,1.0e+5,cm,
40.5,day,0.1382,cm/day,1.0e+5,cm,
41.5,day,0.1122,cm/day,1.0e+5,cm,
42.5,day,0.1109,cm/day,1.0e+5,cm,
43.5,day,0.0378,cm/day,1.0e+5,cm,
44.5,day,0.3229,cm/day,1.0e+5,cm,
45.5,day,0.1245,cm/day,1.0e+5,cm,
46.5,day,0.1218,cm/day,1.0e+5,cm,
47.5,day,0.1145,cm/day,1.0e+5,cm,
48.5,day,0.0997,cm/day,1.0e+5,cm,
49.5,day,0.2021,cm/day,1.0e+5,cm,
50.5,day,0.2795,cm/day,1.0e+5,cm,
51.5,day,0.2476,cm/day,1.0e+5,cm,
52.5,day,0.2838,cm/day,1.0e+5,cm,
53.5,day,0.3072,cm/day,1.0e+5,cm,
54.5,day,0.1677,cm/day,1.0e+5,cm,
55.5,day,0.2489,cm/day,1.0e+5,cm,
56.5,day,0.1876,cm/day,1.0e+5,cm,
57.5,day,0.185,cm/day,1.0e+5,cm,
58.5,day,0.0702,cm/day,1.0e+5,cm,
59.5,day,0.1203,cm/day,1.0e+5,cm,
60.5,day,0.2653,cm/day,1.0e+5,cm,
61.5,day,0.192,cm/day,1.0e+5,cm,
62.5,day,0.1124,cm/day,1.0e+5,cm,
63.5,day,0.1072,cm/day,1.0e+5,cm,
64.5,day,0.1911,cm/day,1.0e+5,cm,
65.5,day,0.2635,cm/day,1.0e+5,cm,
66.5,day,0.3553,cm/day,1.0e+5,cm,
67.5,day,0.1938,cm/day,1.0e+5,cm,
68.5,day,0.2371,cm/day,1.0e+5,cm,

69.5,day,0.1945,cm/day,1.0e+5,cm,
70.5,day,0.2327,cm/day,1.0e+5,cm,
71.5,day,0.3027,cm/day,1.0e+5,cm,
72.5,day,0.355,cm/day,1.0e+5,cm,
73.5,day,0.3529,cm/day,1.0e+5,cm,
74.5,day,0.3609,cm/day,1.0e+5,cm,
75.5,day,0.3469,cm/day,1.0e+5,cm,
76.5,day,0.4007,cm/day,1.0e+5,cm,
77.5,day,0.308,cm/day,1.0e+5,cm,
78.5,day,0.5262,cm/day,1.0e+5,cm,
79.5,day,0.2678,cm/day,1.0e+5,cm,
80.5,day,0.4346,cm/day,1.0e+5,cm,
81.5,day,0.6619,cm/day,1.0e+5,cm,
82.5,day,0.4193,cm/day,1.0e+5,cm,
83.5,day,0.4046,cm/day,1.0e+5,cm,
84.5,day,0.222,cm/day,1.0e+5,cm,
85.5,day,0.5073,cm/day,1.0e+5,cm,
86.5,day,0.3693,cm/day,1.0e+5,cm,
87.5,day,0.4175,cm/day,1.0e+5,cm,
88.5,day,0.3949,cm/day,1.0e+5,cm,
89.5,day,0.4055,cm/day,1.0e+5,cm,
90.5,day,0.461,cm/day,1.0e+5,cm,
91.5,day,0.441,cm/day,1.0e+5,cm,
92.5,day,0.36,cm/day,1.0e+5,cm,
93.5,day,0.4694,cm/day,1.0e+5,cm,
94.5,day,0.4621,cm/day,1.0e+5,cm,
95.5,day,0.669,cm/day,1.0e+5,cm,
96.5,day,0.6968,cm/day,1.0e+5,cm,
97.5,day,0.3236,cm/day,1.0e+5,cm,
98.5,day,0.6149,cm/day,1.0e+5,cm,
99.5,day,0.577,cm/day,1.0e+5,cm,
100.5,day,0.5249,cm/day,1.0e+5,cm,
101.5,day,0.5936,cm/day,1.0e+5,cm,
102.5,day,0.5112,cm/day,1.0e+5,cm,
103.5,day,0.8737,cm/day,1.0e+5,cm,
104.5,day,0.7137,cm/day,1.0e+5,cm,
105.5,day,0.4886,cm/day,1.0e+5,cm,
106.5,day,0.6254,cm/day,1.0e+5,cm,
107.5,day,0.6081,cm/day,1.0e+5,cm,
108.5,day,0.8085,cm/day,1.0e+5,cm,
109.5,day,0.8943,cm/day,1.0e+5,cm,
110.5,day,0.5121,cm/day,1.0e+5,cm,
111.5,day,0.5811,cm/day,1.0e+5,cm,
112.5,day,0.6597,cm/day,1.0e+5,cm,
113.5,day,0.8057,cm/day,1.0e+5,cm,
114.5,day,0.4862,cm/day,1.0e+5,cm,
115.5,day,0.5826,cm/day,1.0e+5,cm,
116.5,day,0.6063,cm/day,1.0e+5,cm,
117.5,day,0.6575,cm/day,1.0e+5,cm,
118.5,day,0.5076,cm/day,1.0e+5,cm,
119.5,day,0.4987,cm/day,1.0e+5,cm,
120.5,day,0.7081,cm/day,1.0e+5,cm,

121.5,day,0.655,cm/day,1.0e+5,cm,
122.5,day,0.475,cm/day,1.0e+5,cm,
123.5,day,0.6035,cm/day,1.0e+5,cm,
124.5,day,0.6472,cm/day,1.0e+5,cm,
125.5,day,0.2371,cm/day,1.0e+5,cm,
126.5,day,0.4961,cm/day,1.0e+5,cm,
127.5,day,0.1388,cm/day,1.0e+5,cm,
128.5,day,0.3908,cm/day,1.0e+5,cm,
129.5,day,0.6124,cm/day,1.0e+5,cm,
130.5,day,0.8612,cm/day,1.0e+5,cm,
131.5,day,0.4663,cm/day,1.0e+5,cm,
132.5,day,0.6882,cm/day,1.0e+5,cm,
133.5,day,0.7202,cm/day,1.0e+5,cm,
134.5,day,0.6811,cm/day,1.0e+5,cm,
135.5,day,0.8746,cm/day,1.0e+5,cm,
136.5,day,0.7894,cm/day,1.0e+5,cm,
137.5,day,0.793,cm/day,1.0e+5,cm,
138.5,day,0.3232,cm/day,1.0e+5,cm,
139.5,day,0.7349,cm/day,1.0e+5,cm,
140.5,day,0.8545,cm/day,1.0e+5,cm,
141.5,day,0.642,cm/day,1.0e+5,cm,
142.5,day,0.2399,cm/day,1.0e+5,cm,
143.5,day,0.0604,cm/day,1.0e+5,cm,
144.5,day,0.387,cm/day,1.0e+5,cm,
145.5,day,0.4988,cm/day,1.0e+5,cm,
146.5,day,0.843,cm/day,1.0e+5,cm,
147.5,day,1.0443,cm/day,1.0e+5,cm,
148.5,day,0.8566,cm/day,1.0e+5,cm,
149.5,day,0.6601,cm/day,1.0e+5,cm,
150.5,day,0.714,cm/day,1.0e+5,cm,
151.5,day,0.773,cm/day,1.0e+5,cm,
152.5,day,0.4783,cm/day,1.0e+5,cm,
153.5,day,0.53,cm/day,1.0e+5,cm,
154.5,day,0.6966,cm/day,1.0e+5,cm,
155.5,day,0.734,cm/day,1.0e+5,cm,
156.5,day,0.7017,cm/day,1.0e+5,cm,
157.5,day,0.7129,cm/day,1.0e+5,cm,
158.5,day,0.9887,cm/day,1.0e+5,cm,
159.5,day,1.0461,cm/day,1.0e+5,cm,
160.5,day,0.9742,cm/day,1.0e+5,cm,
161.5,day,0.8162,cm/day,1.0e+5,cm,
162.5,day,0.7739,cm/day,1.0e+5,cm,
163.5,day,0.5662,cm/day,1.0e+5,cm,
164.5,day,0.6192,cm/day,1.0e+5,cm,
165.5,day,0.9868,cm/day,1.0e+5,cm,
166.5,day,1.1284,cm/day,1.0e+5,cm,
167.5,day,1.0941,cm/day,1.0e+5,cm,
168.5,day,0.7926,cm/day,1.0e+5,cm,
169.5,day,0.9205,cm/day,1.0e+5,cm,
170.5,day,1.0681,cm/day,1.0e+5,cm,
171.5,day,1.1116,cm/day,1.0e+5,cm,
172.5,day,1.0078,cm/day,1.0e+5,cm,

173.5,day,0.6856,cm/day,1.0e+5,cm,
174.5,day,1.0529,cm/day,1.0e+5,cm,
175.5,day,1.2261,cm/day,1.0e+5,cm,
176.5,day,0.9774,cm/day,1.0e+5,cm,
177.5,day,0.968,cm/day,1.0e+5,cm,
178.5,day,0.8483,cm/day,1.0e+5,cm,
179.5,day,1.2064,cm/day,1.0e+5,cm,
180.5,day,1.1217,cm/day,1.0e+5,cm,
181.5,day,0.9786,cm/day,1.0e+5,cm,
182.5,day,0.734,cm/day,1.0e+5,cm,
183.5,day,0.9531,cm/day,1.0e+5,cm,
184.5,day,0.4029,cm/day,1.0e+5,cm,
185.5,day,0.8044,cm/day,1.0e+5,cm,
186.5,day,0.7088,cm/day,1.0e+5,cm,
187.5,day,0.806,cm/day,1.0e+5,cm,
188.5,day,0.8863,cm/day,1.0e+5,cm,
189.5,day,0.9877,cm/day,1.0e+5,cm,
190.5,day,1.0531,cm/day,1.0e+5,cm,
191.5,day,0.9746,cm/day,1.0e+5,cm,
192.5,day,1.3469,cm/day,1.0e+5,cm,
193.5,day,1.1903,cm/day,1.0e+5,cm,
194.5,day,0.8928,cm/day,1.0e+5,cm,
195.5,day,1.0352,cm/day,1.0e+5,cm,
196.5,day,0.9692,cm/day,1.0e+5,cm,
197.5,day,1.142,cm/day,1.0e+5,cm,
198.5,day,0.8244,cm/day,1.0e+5,cm,
199.5,day,0.8143,cm/day,1.0e+5,cm,
200.5,day,1.0159,cm/day,1.0e+5,cm,
201.5,day,0.8786,cm/day,1.0e+5,cm,
202.5,day,0.9741,cm/day,1.0e+5,cm,
203.5,day,0.9108,cm/day,1.0e+5,cm,
204.5,day,0.9706,cm/day,1.0e+5,cm,
205.5,day,1.1875,cm/day,1.0e+5,cm,
206.5,day,0.9185,cm/day,1.0e+5,cm,
207.5,day,0.7703,cm/day,1.0e+5,cm,
208.5,day,1.2239,cm/day,1.0e+5,cm,
209.5,day,0.8933,cm/day,1.0e+5,cm,
210.5,day,0.9179,cm/day,1.0e+5,cm,
211.5,day,0.9451,cm/day,1.0e+5,cm,
212.5,day,0.9499,cm/day,1.0e+5,cm,
213.5,day,0.8839,cm/day,1.0e+5,cm,
214.5,day,0.4846,cm/day,1.0e+5,cm,
215.5,day,0.7673,cm/day,1.0e+5,cm,
216.5,day,0.6125,cm/day,1.0e+5,cm,
217.5,day,0.5935,cm/day,1.0e+5,cm,
218.5,day,0.2626,cm/day,1.0e+5,cm,
219.5,day,0.3052,cm/day,1.0e+5,cm,
220.5,day,0.6043,cm/day,1.0e+5,cm,
221.5,day,0.8002,cm/day,1.0e+5,cm,
222.5,day,0.6887,cm/day,1.0e+5,cm,
223.5,day,0.8256,cm/day,1.0e+5,cm,
224.5,day,0.672,cm/day,1.0e+5,cm,

225.5,day,0.6493,cm/day,1.0e+5,cm,
226.5,day,0.7429,cm/day,1.0e+5,cm,
227.5,day,1.0438,cm/day,1.0e+5,cm,
228.5,day,0.7649,cm/day,1.0e+5,cm,
229.5,day,0.8102,cm/day,1.0e+5,cm,
230.5,day,0.7141,cm/day,1.0e+5,cm,
231.5,day,0.7767,cm/day,1.0e+5,cm,
232.5,day,1.2115,cm/day,1.0e+5,cm,
233.5,day,0.7846,cm/day,1.0e+5,cm,
234.5,day,0.6445,cm/day,1.0e+5,cm,
235.5,day,0.6365,cm/day,1.0e+5,cm,
236.5,day,1.0513,cm/day,1.0e+5,cm,
237.5,day,0.8167,cm/day,1.0e+5,cm,
238.5,day,0.7899,cm/day,1.0e+5,cm,
239.5,day,0.7236,cm/day,1.0e+5,cm,
240.5,day,0.5612,cm/day,1.0e+5,cm,
241.5,day,0.571,cm/day,1.0e+5,cm,
242.5,day,0.6085,cm/day,1.0e+5,cm,
243.5,day,0.7288,cm/day,1.0e+5,cm,
244.5,day,0.8719,cm/day,1.0e+5,cm,
245.5,day,0.6333,cm/day,1.0e+5,cm,
246.5,day,0.6372,cm/day,1.0e+5,cm,
247.5,day,0.5823,cm/day,1.0e+5,cm,
248.5,day,0.8337,cm/day,1.0e+5,cm,
249.5,day,0.7834,cm/day,1.0e+5,cm,
250.5,day,0.457,cm/day,1.0e+5,cm,
251.5,day,0.515,cm/day,1.0e+5,cm,
252.5,day,0.3562,cm/day,1.0e+5,cm,
253.5,day,0.6782,cm/day,1.0e+5,cm,
254.5,day,0.4423,cm/day,1.0e+5,cm,
255.5,day,0.3903,cm/day,1.0e+5,cm,
256.5,day,0.6784,cm/day,1.0e+5,cm,
257.5,day,0.4838,cm/day,1.0e+5,cm,
258.5,day,0.4678,cm/day,1.0e+5,cm,
259.5,day,0.5742,cm/day,1.0e+5,cm,
260.5,day,0.7367,cm/day,1.0e+5,cm,
261.5,day,0.4864,cm/day,1.0e+5,cm,
262.5,day,0.6552,cm/day,1.0e+5,cm,
263.5,day,0.5615,cm/day,1.0e+5,cm,
264.5,day,0.4973,cm/day,1.0e+5,cm,
265.5,day,0.4155,cm/day,1.0e+5,cm,
266.5,day,0.4458,cm/day,1.0e+5,cm,
267.5,day,0.5334,cm/day,1.0e+5,cm,
268.5,day,0.5232,cm/day,1.0e+5,cm,
269.5,day,0.5716,cm/day,1.0e+5,cm,
270.5,day,0.1959,cm/day,1.0e+5,cm,
271.5,day,0.4217,cm/day,1.0e+5,cm,
272.5,day,0.4049,cm/day,1.0e+5,cm,
273.5,day,0.344,cm/day,1.0e+5,cm,
274.5,day,0.4692,cm/day,1.0e+5,cm,
275.5,day,0.3824,cm/day,1.0e+5,cm,
276.5,day,0.3799,cm/day,1.0e+5,cm,

277.5,day,0.285,cm/day,1.0e+5,cm,
278.5,day,0.3613,cm/day,1.0e+5,cm,
279.5,day,0.0745,cm/day,1.0e+5,cm,
280.5,day,0.3479,cm/day,1.0e+5,cm,
281.5,day,0.4004,cm/day,1.0e+5,cm,
282.5,day,0.0734,cm/day,1.0e+5,cm,
283.5,day,0.0337,cm/day,1.0e+5,cm,
284.5,day,0.1582,cm/day,1.0e+5,cm,
285.5,day,0.3364,cm/day,1.0e+5,cm,
286.5,day,0.1827,cm/day,1.0e+5,cm,
287.5,day,0.2706,cm/day,1.0e+5,cm,
288.5,day,0.2334,cm/day,1.0e+5,cm,
289.5,day,0.2079,cm/day,1.0e+5,cm,
290.5,day,0.1555,cm/day,1.0e+5,cm,
291.5,day,0.158,cm/day,1.0e+5,cm,
292.5,day,0.238,cm/day,1.0e+5,cm,
293.5,day,0.3065,cm/day,1.0e+5,cm,
294.5,day,0.2577,cm/day,1.0e+5,cm,
295.5,day,0.1311,cm/day,1.0e+5,cm,
296.5,day,0.1726,cm/day,1.0e+5,cm,
297.5,day,0.1312,cm/day,1.0e+5,cm,
298.5,day,0.1566,cm/day,1.0e+5,cm,
299.5,day,0.109,cm/day,1.0e+5,cm,
300.5,day,0.1287,cm/day,1.0e+5,cm,
301.5,day,0.1051,cm/day,1.0e+5,cm,
302.5,day,0.0127,cm/day,1.0e+5,cm,
303.5,day,0.0414,cm/day,1.0e+5,cm,
304.5,day,0.0729,cm/day,1.0e+5,cm,
305.5,day,0.0852,cm/day,1.0e+5,cm,
306.5,day,0.0498,cm/day,1.0e+5,cm,
307.5,day,0.052,cm/day,1.0e+5,cm,
308.5,day,0.1872,cm/day,1.0e+5,cm,
309.5,day,0.1671,cm/day,1.0e+5,cm,
310.5,day,0.1832,cm/day,1.0e+5,cm,
311.5,day,0.0491,cm/day,1.0e+5,cm,
312.5,day,0.1645,cm/day,1.0e+5,cm,
313.5,day,0.1596,cm/day,1.0e+5,cm,
314.5,day,0.1424,cm/day,1.0e+5,cm,
315.5,day,0.0436,cm/day,1.0e+5,cm,
316.5,day,0.0907,cm/day,1.0e+5,cm,
317.5,day,0.0084,cm/day,1.0e+5,cm,
318.5,day,0.0185,cm/day,1.0e+5,cm,
319.5,day,0.0692,cm/day,1.0e+5,cm,
320.5,day,0.0635,cm/day,1.0e+5,cm,
321.5,day,0.0307,cm/day,1.0e+5,cm,
322.5,day,0.434,cm/day,1.0e+5,cm,
323.5,day,0.2254,cm/day,1.0e+5,cm,
324.5,day,0.1372,cm/day,1.0e+5,cm,
325.5,day,0.1193,cm/day,1.0e+5,cm,
326.5,day,0.092,cm/day,1.0e+5,cm,
327.5,day,0.1243,cm/day,1.0e+5,cm,
328.5,day,0.456,cm/day,1.0e+5,cm,

329.5,day,0.1965,cm/day,1.0e+5,cm,
330.5,day,0.147,cm/day,1.0e+5,cm,
331.5,day,0.0705,cm/day,1.0e+5,cm,
332.5,day,0.0311,cm/day,1.0e+5,cm,
333.5,day,0.1128,cm/day,1.0e+5,cm,
334.5,day,0.0763,cm/day,1.0e+5,cm,
335.5,day,0.1169,cm/day,1.0e+5,cm,
336.5,day,0.1506,cm/day,1.0e+5,cm,
337.5,day,0.0201,cm/day,1.0e+5,cm,
338.5,day,0.0132,cm/day,1.0e+5,cm,
339.5,day,0.0777,cm/day,1.0e+5,cm,
340.5,day,0.047,cm/day,1.0e+5,cm,
341.5,day,0.0173,cm/day,1.0e+5,cm,
342.5,day,0.0197,cm/day,1.0e+5,cm,
343.5,day,0,cm/day,1.0e+5,cm,
344.5,day,0.0118,cm/day,1.0e+5,cm,
345.5,day,0.0117,cm/day,1.0e+5,cm,
346.5,day,0.0159,cm/day,1.0e+5,cm,
347.5,day,0.0307,cm/day,1.0e+5,cm,
348.5,day,0.0045,cm/day,1.0e+5,cm,
349.5,day,0.0146,cm/day,1.0e+5,cm,
350.5,day,0.008,cm/day,1.0e+5,cm,
351.5,day,0.0134,cm/day,1.0e+5,cm,
352.5,day,0.0318,cm/day,1.0e+5,cm,
353.5,day,0.0021,cm/day,1.0e+5,cm,
354.5,day,0.0575,cm/day,1.0e+5,cm,
355.5,day,0.0947,cm/day,1.0e+5,cm,
356.5,day,0.0735,cm/day,1.0e+5,cm,
357.5,day,0.0841,cm/day,1.0e+5,cm,
358.5,day,0.0848,cm/day,1.0e+5,cm,
359.5,day,0.0639,cm/day,1.0e+5,cm,
360.5,day,0.0695,cm/day,1.0e+5,cm,
361.5,day,0.2235,cm/day,1.0e+5,cm,
362.5,day,0.1272,cm/day,1.0e+5,cm,
363.5,day,0.153,cm/day,1.0e+5,cm,
364.5,day,0.0846,cm/day,1.0e+5,cm,
365,day,0.04665,cm/day,1.0e+5,cm,
Bottom,Unit Gradient Aqueous,
1,1,1,1,1,1,1,
0,day,,,

#----------
~Source Card
#----------
1,
Aqueous Volumetric,1,1,1,1,74,74,389,
0,hr,0.0,cm^3/hr,
72,hr,0.0,cm^3/hr,
72,hr,0.1016,cm^3/hr,
74,hr,0.1016,cm^3/hr,
74,hr,0.0,cm^3/hr,
158,hr,0.0,cm^3/hr,

158,hr,0.0762,cm^3/hr,
159,hr,0.0762,cm^3/hr,
159,hr,0.0,cm^3/hr,
412,hr,0.0,cm^3/hr,
412,hr,0.0508,cm^3/hr,
413,hr,0.0508,cm^3/hr,
413,hr,0.0,cm^3/hr,
902,hr,0.0,cm^3/hr,
902,hr,0.0635,cm^3/hr,
904,hr,0.0635,cm^3/hr,
904,hr,0.0,cm^3/hr,
905,hr,0.0,cm^3/hr,
905,hr,0.0508,cm^3/hr,
907,hr,0.0508,cm^3/hr,
907,hr,0.0,cm^3/hr,
924,hr,0.0,cm^3/hr,
924,hr,0.03556,cm^3/hr,
929,hr,0.03556,cm^3/hr,
929,hr,0.0,cm^3/hr,
973,hr,0.0,cm^3/hr,
973,hr,0.23495,cm^3/hr,
977,hr,0.23495,cm^3/hr,
977,hr,0.0,cm^3/hr,
1029,hr,0.0,cm^3/hr,
1029,hr,0.0254,cm^3/hr,
1030,hr,0.0254,cm^3/hr,
1030,hr,0.0,cm^3/hr,
1052,hr,0.0,cm^3/hr,
1052,hr,0.0889,cm^3/hr,
1054,hr,0.0889,cm^3/hr,
1054,hr,0.0,cm^3/hr,
1071,hr,0.0,cm^3/hr,
1071,hr,0.067733333,cm^3/hr,
1074,hr,0.067733333,cm^3/hr,
1074,hr,0.0,cm^3/hr,
1075,hr,0.0,cm^3/hr,
1075,hr,0.0254,cm^3/hr,
1076,hr,0.0254,cm^3/hr,
1076,hr,0.0,cm^3/hr,
1125,hr,0.0,cm^3/hr,
1125,hr,0.093133333,cm^3/hr,
1128,hr,0.093133333,cm^3/hr,
1128,hr,0.0,cm^3/hr,
1128,hr,0.0,cm^3/hr,
1128,hr,0.0508,cm^3/hr,
1129,hr,0.0508,cm^3/hr,
1129,hr,0.0,cm^3/hr,
1283,hr,0.0,cm^3/hr,
1283,hr,0.0254,cm^3/hr,
1284,hr,0.0254,cm^3/hr,
1284,hr,0.0,cm^3/hr,
1429,hr,0.0,cm^3/hr,

1429,hr,0.0381,cm^3/hr,
1431,hr,0.0381,cm^3/hr,
1431,hr,0.0,cm^3/hr,
1432,hr,0.0,cm^3/hr,
1432,hr,0.0254,cm^3/hr,
1433,hr,0.0254,cm^3/hr,
1433,hr,0.0,cm^3/hr,
1434,hr,0.0,cm^3/hr,
1434,hr,0.0508,cm^3/hr,
1435,hr,0.0508,cm^3/hr,
1435,hr,0.0,cm^3/hr,
1519,hr,0.0,cm^3/hr,
1519,hr,0.03175,cm^3/hr,
1523,hr,0.03175,cm^3/hr,
1523,hr,0.0,cm^3/hr,
1550,hr,0.0,cm^3/hr,
1550,hr,0.0254,cm^3/hr,
1551,hr,0.0254,cm^3/hr,
1551,hr,0.0,cm^3/hr,
1621,hr,0.0,cm^3/hr,
1621,hr,0.0254,cm^3/hr,
1622,hr,0.0254,cm^3/hr,
1622,hr,0.0,cm^3/hr,
1648,hr,0.0,cm^3/hr,
1648,hr,0.0254,cm^3/hr,
1649,hr,0.0254,cm^3/hr,
1649,hr,0.0,cm^3/hr,
1697,hr,0.0,cm^3/hr,
1697,hr,0.0254,cm^3/hr,
1698,hr,0.0254,cm^3/hr,
1698,hr,0.0,cm^3/hr,
1940,hr,0.0,cm^3/hr,
1940,hr,0.0254,cm^3/hr,
1941,hr,0.0254,cm^3/hr,
1941,hr,0.0,cm^3/hr,
2021,hr,0.0,cm^3/hr,
2021,hr,0.0508,cm^3/hr,
2022,hr,0.0508,cm^3/hr,
2022,hr,0.0,cm^3/hr,
2035,hr,0.0,cm^3/hr,
2035,hr,0.0254,cm^3/hr,
2037,hr,0.0254,cm^3/hr,
2037,hr,0.0,cm^3/hr,
2270,hr,0.0,cm^3/hr,
2270,hr,0.1143,cm^3/hr,
2272,hr,0.1143,cm^3/hr,
2272,hr,0.0,cm^3/hr,
2358,hr,0.0,cm^3/hr,
2358,hr,0.0508,cm^3/hr,
2359,hr,0.0508,cm^3/hr,
2359,hr,0.0,cm^3/hr,
2524,hr,0.0,cm^3/hr,

2524,hr,0.1143,cm^3/hr,
2526,hr,0.1143,cm^3/hr,
2526,hr,0.0,cm^3/hr,
2809,hr,0.0,cm^3/hr,
2809,hr,0.07112,cm^3/hr,
2814,hr,0.07112,cm^3/hr,
2814,hr,0.0,cm^3/hr,
2958,hr,0.0,cm^3/hr,
2958,hr,0.1016,cm^3/hr,
2959,hr,0.1016,cm^3/hr,
2959,hr,0.0,cm^3/hr,
3027,hr,0.0,cm^3/hr,
3027,hr,0.0254,cm^3/hr,
3029,hr,0.0254,cm^3/hr,
3029,hr,0.0,cm^3/hr,
3043,hr,0.0,cm^3/hr,
3043,hr,0.0254,cm^3/hr,
3044,hr,0.0254,cm^3/hr,
3044,hr,0.0,cm^3/hr,
3078,hr,0.0,cm^3/hr,
3078,hr,0.1016,cm^3/hr,
3079,hr,0.1016,cm^3/hr,
3079,hr,0.0,cm^3/hr,
3080,hr,0.0,cm^3/hr,
3080,hr,0.042333333,cm^3/hr,
3083,hr,0.042333333,cm^3/hr,
3083,hr,0.0,cm^3/hr,
3085,hr,0.0,cm^3/hr,
3085,hr,0.2667,cm^3/hr,
3087,hr,0.2667,cm^3/hr,
3087,hr,0.0,cm^3/hr,
3101,hr,0.0,cm^3/hr,
3101,hr,0.1778,cm^3/hr,
3102,hr,0.1778,cm^3/hr,
3102,hr,0.0,cm^3/hr,
3111,hr,0.0,cm^3/hr,
3111,hr,0.2032,cm^3/hr,
3113,hr,0.2032,cm^3/hr,
3113,hr,0.0,cm^3/hr,
3343,hr,0.0,cm^3/hr,
3343,hr,0.0508,cm^3/hr,
3344,hr,0.0508,cm^3/hr,
3344,hr,0.0,cm^3/hr,
3346,hr,0.0,cm^3/hr,
3346,hr,0.0254,cm^3/hr,
3347,hr,0.0254,cm^3/hr,
3347,hr,0.0,cm^3/hr,
3435,hr,0.0,cm^3/hr,
3435,hr,0.10795,cm^3/hr,
3439,hr,0.10795,cm^3/hr,
3439,hr,0.0,cm^3/hr,
3440,hr,0.0,cm^3/hr,

3440,hr,0.0508,cm^3/hr,
3442,hr,0.0508,cm^3/hr,
3442,hr,0.0,cm^3/hr,
3459,hr,0.0,cm^3/hr,
3459,hr,0.0762,cm^3/hr,
3461,hr,0.0762,cm^3/hr,
3461,hr,0.0,cm^3/hr,
3462,hr,0.0,cm^3/hr,
3462,hr,0.1524,cm^3/hr,
3469,hr,0.1524,cm^3/hr,
3469,hr,0.0,cm^3/hr,
3471,hr,0.0,cm^3/hr,
3471,hr,0.0381,cm^3/hr,
3473,hr,0.0381,cm^3/hr,
3473,hr,0.0,cm^3/hr,
3708,hr,0.0,cm^3/hr,
3708,hr,0.0254,cm^3/hr,
3709,hr,0.0254,cm^3/hr,
3709,hr,0.0,cm^3/hr,
3748,hr,0.0,cm^3/hr,
3748,hr,0.0762,cm^3/hr,
3749,hr,0.0762,cm^3/hr,
3749,hr,0.0,cm^3/hr,
3951,hr,0.0,cm^3/hr,
3951,hr,0.0254,cm^3/hr,
3952,hr,0.0254,cm^3/hr,
3952,hr,0.0,cm^3/hr,
3957,hr,0.0,cm^3/hr,
3957,hr,0.1778,cm^3/hr,
3958,hr,0.1778,cm^3/hr,
3958,hr,0.0,cm^3/hr,
5163,hr,0.0,cm^3/hr,
5163,hr,0.160866667,cm^3/hr,
5166,hr,0.160866667,cm^3/hr,
5166,hr,0.0,cm^3/hr,
5168,hr,0.0,cm^3/hr,
5168,hr,0.0254,cm^3/hr,
5169,hr,0.0254,cm^3/hr,
5169,hr,0.0,cm^3/hr,
5174,hr,0.0,cm^3/hr,
5174,hr,0.0762,cm^3/hr,
5177,hr,0.0762,cm^3/hr,
5177,hr,0.0,cm^3/hr,
5256,hr,0.0,cm^3/hr,
5256,hr,0.0254,cm^3/hr,
5257,hr,0.0254,cm^3/hr,
5257,hr,0.0,cm^3/hr,
5258,hr,0.0,cm^3/hr,
5258,hr,0.0254,cm^3/hr,
5259,hr,0.0254,cm^3/hr,
5259,hr,0.0,cm^3/hr,
5263,hr,0.0,cm^3/hr,

5263,hr,0.0254,cm^3/hr,
5264,hr,0.0254,cm^3/hr,
5264,hr,0.0,cm^3/hr,
5380,hr,0.0,cm^3/hr,
5380,hr,0.1524,cm^3/hr,
5383,hr,0.1524,cm^3/hr,
5383,hr,0.0,cm^3/hr,
6074,hr,0.0,cm^3/hr,
6074,hr,0.0254,cm^3/hr,
6075,hr,0.0254,cm^3/hr,
6075,hr,0.0,cm^3/hr,
6080,hr,0.0,cm^3/hr,
6080,hr,0.0254,cm^3/hr,
6083,hr,0.0254,cm^3/hr,
6083,hr,0.0,cm^3/hr,
6507,hr,0.0,cm^3/hr,
6507,hr,0.095955556,cm^3/hr,
6516,hr,0.095955556,cm^3/hr,
6516,hr,0.0,cm^3/hr,
6621,hr,0.0,cm^3/hr,
6621,hr,0.0254,cm^3/hr,
6622,hr,0.0254,cm^3/hr,
6622,hr,0.0,cm^3/hr,
6623,hr,0.0,cm^3/hr,
6623,hr,0.0254,cm^3/hr,
6624,hr,0.0254,cm^3/hr,
6624,hr,0.0,cm^3/hr,
6733,hr,0.0,cm^3/hr,
6733,hr,0.0254,cm^3/hr,
6734,hr,0.0254,cm^3/hr,
6734,hr,0.0,cm^3/hr,
6736,hr,0.0,cm^3/hr,
6736,hr,0.0508,cm^3/hr,
6737,hr,0.0508,cm^3/hr,
6737,hr,0.0,cm^3/hr,
6805,hr,0.0,cm^3/hr,
6805,hr,0.0254,cm^3/hr,
6806,hr,0.0254,cm^3/hr,
6806,hr,0.0,cm^3/hr,
6824,hr,0.0,cm^3/hr,
6824,hr,0.13208,cm^3/hr,
6829,hr,0.13208,cm^3/hr,
6829,hr,0.0,cm^3/hr,
6850,hr,0.0,cm^3/hr,
6850,hr,0.1651,cm^3/hr,
6856,hr,0.1651,cm^3/hr,
6856,hr,0.0,cm^3/hr,
6857,hr,0.0,cm^3/hr,
6857,hr,0.1651,cm^3/hr,
6859,hr,0.1651,cm^3/hr,
6859,hr,0.0,cm^3/hr,
6892,hr,0.0,cm^3/hr,

6892,hr,0.05715,cm^3/hr,
6896,hr,0.05715,cm^3/hr,
6896,hr,0.0,cm^3/hr,
6897,hr,0.0,cm^3/hr,
6897,hr,0.0254,cm^3/hr,
6898,hr,0.0254,cm^3/hr,
6898,hr,0.0,cm^3/hr,
6899,hr,0.0,cm^3/hr,
6899,hr,0.0254,cm^3/hr,
6900,hr,0.0254,cm^3/hr,
6900,hr,0.0,cm^3/hr,
7489,hr,0.0,cm^3/hr,
7489,hr,0.127,cm^3/hr,
7490,hr,0.127,cm^3/hr,
7490,hr,0.0,cm^3/hr,
7511,hr,0.0,cm^3/hr,
7511,hr,0.0508,cm^3/hr,
7512,hr,0.0508,cm^3/hr,
7512,hr,0.0,cm^3/hr,
7512,hr,0.0,cm^3/hr,
7512,hr,0.1016,cm^3/hr,
7514,hr,0.1016,cm^3/hr,
7514,hr,0.0,cm^3/hr,
7563,hr,0.0,cm^3/hr,
7563,hr,0.0254,cm^3/hr,
7565,hr,0.0254,cm^3/hr,
7565,hr,0.0,cm^3/hr,
7597,hr,0.0,cm^3/hr,
7597,hr,0.110066667,cm^3/hr,
7600,hr,0.110066667,cm^3/hr,
7600,hr,0.0,cm^3/hr,
7663,hr,0.0,cm^3/hr,
7663,hr,0.0635,cm^3/hr,
7665,hr,0.0635,cm^3/hr,
7665,hr,0.0,cm^3/hr,
8022,hr,0.0,cm^3/hr,
8022,hr,0.0254,cm^3/hr,
8024,hr,0.0254,cm^3/hr,
8024,hr,0.0,cm^3/hr,
8025,hr,0.0,cm^3/hr,
8025,hr,0.237066667,cm^3/hr,
8028,hr,0.237066667,cm^3/hr,
8028,hr,0.0,cm^3/hr,
8062,hr,0.0,cm^3/hr,
8062,hr,0.0254,cm^3/hr,
8063,hr,0.0254,cm^3/hr,
8063,hr,0.0,cm^3/hr,
8126,hr,0.0,cm^3/hr,
8126,hr,0.0254,cm^3/hr,
8127,hr,0.0254,cm^3/hr,
8127,hr,0.0,cm^3/hr,
8257,hr,0.0,cm^3/hr,

8257,hr,0.0254,cm^3/hr,
8258,hr,0.0254,cm^3/hr,
8258,hr,0.0,cm^3/hr,
8268,hr,0.0,cm^3/hr,
8268,hr,0.0254,cm^3/hr,
8269,hr,0.0254,cm^3/hr,
8269,hr,0.0,cm^3/hr,
8285,hr,0.0,cm^3/hr,
8285,hr,0.0254,cm^3/hr,
8286,hr,0.0254,cm^3/hr,
8286,hr,0.0,cm^3/hr,
8330,hr,0.0,cm^3/hr,
8330,hr,0.0508,cm^3/hr,
8334,hr,0.0508,cm^3/hr,
8334,hr,0.0,cm^3/hr,
8347,hr,0.0,cm^3/hr,
8347,hr,0.0381,cm^3/hr,
8349,hr,0.0381,cm^3/hr,
8349,hr,0.0,cm^3/hr,
8350,hr,0.0,cm^3/hr,
8350,hr,0.0635,cm^3/hr,
8352,hr,0.0635,cm^3/hr,
8352,hr,0.0,cm^3/hr,
8352,hr,0.0,cm^3/hr,
8352,hr,0.046566667,cm^3/hr,
8358,hr,0.046566667,cm^3/hr,
8358,hr,0.0,cm^3/hr,
8376,hr,0.0,cm^3/hr,
8376,hr,0.0508,cm^3/hr,
8377,hr,0.0508,cm^3/hr,
8377,hr,0.0,cm^3/hr,
8378,hr,0.0,cm^3/hr,
8378,hr,0.0254,cm^3/hr,
8379,hr,0.0254,cm^3/hr,
8379,hr,0.0,cm^3/hr,
8381,hr,0.0,cm^3/hr,
8381,hr,0.0381,cm^3/hr,
8383,hr,0.0381,cm^3/hr,
8383,hr,0.0,cm^3/hr,
8384,hr,0.0,cm^3/hr,
8384,hr,0.0254,cm^3/hr,
8387,hr,0.0254,cm^3/hr,
8387,hr,0.0,cm^3/hr,
8413,hr,0.0,cm^3/hr,
8413,hr,0.0254,cm^3/hr,
8414,hr,0.0254,cm^3/hr,
8414,hr,0.0,cm^3/hr,
8417,hr,0.0,cm^3/hr,
8417,hr,0.0381,cm^3/hr,
8419,hr,0.0381,cm^3/hr,
8419,hr,0.0,cm^3/hr,
8423,hr,0.0,cm^3/hr,

8423,hr,0.0254,cm^3/hr,
8424,hr,0.0254,cm^3/hr,
8424,hr,0.0,cm^3/hr,
8433,hr,0.0,cm^3/hr,
8433,hr,0.0762,cm^3/hr,
8435,hr,0.0762,cm^3/hr,
8435,hr,0.0,cm^3/hr,
8437,hr,0.0,cm^3/hr,
8437,hr,0.0254,cm^3/hr,
8438,hr,0.0254,cm^3/hr,
8438,hr,0.0,cm^3/hr,
8461,hr,0.0,cm^3/hr,
8461,hr,0.0254,cm^3/hr,
8463,hr,0.0254,cm^3/hr,
8463,hr,0.0,cm^3/hr,
8474,hr,0.0,cm^3/hr,
8474,hr,0.0635,cm^3/hr,
8476,hr,0.0635,cm^3/hr,
8476,hr,0.0,cm^3/hr,

#----------
~Output Options Card
#----------
6,
1,1,74,
1,1,52,
1,1,51,
1,1,40,
1,1,39,
1,1,1,
10,10,hr,cm,6,6,6,
3,
Aqueous saturation,,
Aqueous relative permeability,,
Water mass source integral,gm,
3,
90,day,
180,day,
270,day,
4,
Temperature,K,
Aqueous saturation,,
Aqueous relative permeability,,
Aqueous pressure,,

#----------
~Surface Flux Card
#----------
2,
Aqueous Volumetric,cm^3/hr,cm^3,Top,1,1,1,1,74,74,
Aqueous Volumetric,cm^3/hr,cm^3,Bottom,1,1,1,1,1,1,

C.9 STOMP-WAE Input File for Verification of Flow in a Layered Soil

```
#-------------------------------------------------------
~Simulation Title Card
#-------------------------------------------------------
1,
UNSAT-H 7.6,
M.D. White,
PNNL,
23 September 2003,
12:20,
1,
UNSAT-H, Problem 7.6, Layered Soil


#-------------------------------------------------------
~Solution Control Card
#-------------------------------------------------------
Restart Mode,1,
#Normal,
Water-Air-Energy,
1,
0,day,4,day,0.01,hr,0.5,hr,1.25,16,1.e-6,
100000,
variable aqueous diffusion,
variable gas diffusion,
1,
effective permeability,geometric,


#-------------------------------------------------------
~Grid Card
#-------------------------------------------------------
Cartesian,
1,1,45,
0.0,cm,1.0,cm,
0.0,cm,1.0,cm,
0,cm,25,cm,50,cm,75,cm,100,cm,125,cm,
150,cm,175,cm,200,cm,225,cm,250,cm,275,cm,
300,cm,310,cm,320,cm,330,cm,340,cm,350,cm,
360,cm,370,cm,380,cm,390,cm,400,cm,410,cm,
420,cm,430,cm,440,cm,450,cm,460,cm,470,cm,
480,cm,490,cm,500,cm,510,cm,512.5,cm,515,cm,
517.5,cm,520,cm,522.5,cm,525,cm,527.5,cm,530,cm,
532.5,cm,535,cm,539.8,cm,540,cm,

#-------------------------------------------------------
~Rock/Soil Zonation Card
#-------------------------------------------------------
3,
COMPGRAV,1,1,1,1,34,45,
```

COMPOS1,1,1,1,1,22,33,
GRAVEL1,1,1,1,1,1,21,

#----------
~Mechanical Properties Card
#----------
COMPGRAV,2650,kg/m^3,0.422,0.422,1.e-5,1/m,Constant,0.66,0.66,
COMPOS1,2650,kg/m^3,0.422,0.422,1.e-5,1/m,Constant,0.66,0.66,
GRAVEL1,2650,kg/m^3,0.419,0.419,1.e-5,1/m,Constant,0.66,0.66,

#----------
~Hydraulic Properties Card
#----------
COMPGRAV,3.6E-01,hc cm/hr,3.6E-01,hc cm/hr,3.6E-01,hc cm/hr,
COMPOS1,1.080002E-01,hc cm/hr,1.080002E-01,hc cm/hr,1.080002E-01,hc cm/hr,
GRAVEL1,1.2600005E+03,hc cm/hr,1.2600005E+03,hc cm/hr,1.2600005E+03,hc cm/hr,

#----------
~Thermal Properties Card
#----------
COMPGRAV,Cass Conductivity Model,0.6,W/m K,0.8,W/m K,4.5,0.22,W/m K,6.0,901.88,J/kg K,
COMPOS1,Cass Conductivity Model,0.6,W/m K,0.8,W/m K,4.5,0.22,W/m K,6.0,901.88,J/kg K,
GRAVEL1,Cass Conductivity Model,0.6,W/m K,0.7,W/m K,8.0,0.26,W/m K,3.0,513.21,J/kg K,

#----------
~Saturation Function Card
#----------
COMPGRAV,Polynomial,4,
4,1.0,12.65,4.2199999E-01,-2.7573731E-02,-2.3653656E-03,-3.2151621E-02,cm,
5,12.65,244.2,-1.38834E-01,1.5021513,-1.4785267,5.4422855E-01,-7.0263125E-02,cm,
5,244.2,7197.0,-1.7569752,2.7017555,-1.3545368,2.8460807E-01,-2.161908E-02,,cm,
5,7197.0,8.6326599e+06,-3.4936512E-01,3.145951E-01,-8.4237993E-02,9.1790808E-03,-3.5545405E-04,cm,
COMPOS1,Polynomial,4,
3,1.0,5.4290004,4.2199999E-01,-7.3107332E-03,-3.5250444E-02,cm,
3,5.4290004,5.6900012E+02,4.2632636E-01,-1.9087702E-02,-2.7235843E-02,cm,
4,5.6900012E+02,1.6770025E+04,2.4613359,-1.7952768,4.5785773E-01,-3.9381173E-02,cm,
4,1.6770025E+04,8.6326599E+06,3.6377275E-01,-1.0580593E-01,1.0616908E-02,-3.5810552E-04,cm,
GRAVEL1,Polynomial,4,
3,9.9999998E-03,7.743001E-02,2.9529411E-01,-9.5835656E-02,-1.6991356E-02,cm,
3,7.743001E-02,2.7829993E-01,-2.0774645E-01,-1.0013254,-4.2446923E-01,cm,
5,2.7829993E-01,1.2920002E+01,5.8681458E-02,-1.1252354E-01,2.01344E-01,-1.7054841E-01,5.2016903E-02,cm,
5,1.2920002E+01,8.7777891E+06,4.5875967E-02,-2.2514086E-02,6.2657609E-03,-7.9328578E-04,3.5441328E-05,cm,

#----------
~Aqueous Relative Permeability Card
#----------
COMPGRAV,Polynomial,2,3.6E-01,
4,1.0,4.498E+01,-4.4369757E-01,-5.8029747E-01,-2.8344643E-01,-2.1685658E-01,cm,
3,4.498E+01,8.6326599E+06,2.4089615,-3.4391944,4.3601289E-02,cm,
COMPOS1,Polynomial,3,1.080002E-01,

4,1.0,1.3260002E+03,-9.6657562E-01,-1.0965506,5.8941185E-02,-1.2111266E-01,cm,
4,1.3260002E+03,7.1970044E+03,-6.3407219E+01,6.0421951E+01,-2.0131914E+01,2.0865219,cm,
4,7.1970044E+03,8.6326599E+06,-9.5900745,1.8411379,-6.0871047E-01,2.465306E-02,cm,
GRAVEL1,Polynomial,4,1.2600005E+03,
4,9.9999998E-03,2.7829993E-01,-2.7429957,-1.0566543E+01,-6.7793403,-1.4784553,cm,
3,2.7829993E-01,4.6420007,-1.3305095,-5.0247631,-5.5922753E-01,cm,
3,4.6420007,1.6680004E+01,1.8869209E-01,-9.5821028,2.8585794,cm,
4,1.6680004E+01,8.7777891E+06,-3.7477951,-3.1739995,2.7821976E-01,-2.2469539E-02,cm,

#----------
~Gas Relative Permeability Card
#----------
COMPGRAV,Corey,,,
COMPOS1,Corey,,,
GRAVEL1,Corey,,,

#----------
~Atmospheric Conditions Card
#----------
May,23,1962,00:00:00,0.914,m,15.24,m,120.0,deg,46.57,deg,120.0,deg,4.9E-04,m,4.9E-04,m,
97,
0.000,day,58.000,F, 98199.213,Pa,0.560,0.000,langley/min,12.000,mi/hr,
0.042,day,58.000,F, 98165.444,Pa,0.560,0.000,langley/min, 5.000,mi/hr,
0.083,day,58.000,F, 98165.444,Pa,0.550,0.000,langley/min,10.000,mi/hr,
0.125,day,54.000,F, 98131.675,Pa,0.820,0.000,langley/min, 6.000,mi/hr,
0.167,day,52.000,F, 98131.675,Pa,0.910,0.000,langley/min,10.000,mi/hr,
0.208,day,52.000,F, 98131.675,Pa,0.890,0.020,langley/min,10.000,mi/hr,
0.250,day,51.000,F, 98165.444,Pa,0.970,0.070,langley/min, 6.000,mi/hr,
0.292,day,52.000,F, 98165.444,Pa,1.000,0.100,langley/min, 5.000,mi/hr,
0.333,day,52.000,F, 98165.444,Pa,1.000,0.160,langley/min,10.000,mi/hr,
0.375,day,52.000,F, 98165.444,Pa,0.950,0.230,langley/min, 8.000,mi/hr,
0.417,day,53.000,F, 98199.213,Pa,0.930,0.560,langley/min, 5.000,mi/hr,
0.458,day,56.000,F, 98199.213,Pa,0.850,0.380,langley/min, 0.000,mi/hr,
0.500,day,55.000,F, 98199.213,Pa,0.850,0.310,langley/min, 6.000,mi/hr,
0.541,day,56.000,F, 98199.213,Pa,0.830,0.600,langley/min,10.000,mi/hr,
0.583,day,57.000,F, 98199.213,Pa,0.810,0.200,langley/min,10.000,mi/hr,
0.625,day,58.000,F, 98199.213,Pa,0.680,0.260,langley/min,10.000,mi/hr,
0.666,day,58.000,F, 98165.444,Pa,0.670,0.170,langley/min,10.000,mi/hr,
0.708,day,58.000,F, 98131.675,Pa,0.660,0.130,langley/min, 8.000,mi/hr,
0.750,day,58.000,F, 98131.675,Pa,0.610,0.040,langley/min,14.000,mi/hr,
0.791,day,56.000,F, 98131.675,Pa,0.620,0.020,langley/min,11.000,mi/hr,
0.833,day,54.000,F, 98131.675,Pa,0.680,0.000,langley/min,10.000,mi/hr,
0.875,day,52.000,F, 98165.444,Pa,0.700,0.000,langley/min, 8.000,mi/hr,
0.916,day,52.000,F, 98131.675,Pa,0.680,0.000,langley/min,10.000,mi/hr,
0.958,day,53.000,F, 98097.907,Pa,0.640,0.000,langley/min,12.000,mi/hr,
1.000,day,52.000,F, 98064.138,Pa,0.690,0.000,langley/min, 8.000,mi/hr,
1.041,day,52.000,F, 98030.369,Pa,0.680,0.000,langley/min,13.000,mi/hr,
1.083,day,53.000,F, 97996.601,Pa,0.660,0.000,langley/min,14.000,mi/hr,
1.125,day,51.000,F, 97996.601,Pa,0.780,0.000,langley/min,10.000,mi/hr,
1.166,day,49.000,F, 97996.601,Pa,0.890,0.000,langley/min, 8.000,mi/hr,
1.208,day,49.000,F, 97962.832,Pa,0.940,0.030,langley/min, 6.000,mi/hr,
1.250,day,50.000,F, 97929.063,Pa,0.940,0.030,langley/min, 7.000,mi/hr,

1.291,day,50.000,F, 97929.063,Pa,0.910,0.070,langley/min, 5.000,mi/hr,
1.333,day,50.000,F, 97929.063,Pa,0.960,0.080,langley/min,10.000,mi/hr,
1.375,day,50.000,F, 97929.063,Pa,0.950,0.060,langley/min,12.000,mi/hr,
1.416,day,49.000,F, 97962.832,Pa,0.980,0.090,langley/min, 7.000,mi/hr,
1.458,day,51.000,F, 97996.601,Pa,1.000,0.090,langley/min, 7.000,mi/hr,
1.499,day,52.000,F, 97996.601,Pa,0.990,0.070,langley/min, 5.000,mi/hr,
1.541,day,52.000,F, 98030.369,Pa,0.950,0.130,langley/min, 5.000,mi/hr,
1.583,day,53.000,F, 98030.369,Pa,0.950,0.120,langley/min, 2.000,mi/hr,
1.624,day,53.000,F, 98064.138,Pa,1.000,0.120,langley/min, 1.000,mi/hr,
1.666,day,53.000,F, 98030.369,Pa,1.000,0.120,langley/min, 2.000,mi/hr,
1.708,day,54.000,F, 98030.369,Pa,0.990,0.060,langley/min, 4.000,mi/hr,
1.749,day,54.000,F, 98030.369,Pa,0.980,0.030,langley/min, 3.000,mi/hr,
1.791,day,53.000,F, 98064.138,Pa,0.980,0.010,langley/min, 2.000,mi/hr,
1.833,day,53.000,F, 98097.907,Pa,0.970,0.000,langley/min, 6.000,mi/hr,
1.874,day,52.000,F, 98097.907,Pa,0.980,0.000,langley/min, 5.000,mi/hr,
1.916,day,50.000,F, 98131.675,Pa,0.960,0.000,langley/min, 6.000,mi/hr,
1.958,day,50.000,F, 98131.675,Pa,0.960,0.000,langley/min, 8.000,mi/hr,
1.999,day,49.000,F, 98131.675,Pa,0.990,0.000,langley/min, 6.000,mi/hr,
2.041,day,49.000,F, 98131.675,Pa,1.000,0.000,langley/min, 4.000,mi/hr,
2.083,day,49.000,F, 98131.675,Pa,1.000,0.000,langley/min, 0.000,mi/hr,
2.124,day,49.000,F, 98131.675,Pa,1.000,0.000,langley/min, 1.000,mi/hr,
2.166,day,49.000,F, 98165.444,Pa,1.000,0.000,langley/min, 5.000,mi/hr,
2.208,day,49.000,F, 98199.213,Pa,0.980,0.080,langley/min, 1.000,mi/hr,
2.249,day,49.000,F, 98232.981,Pa,1.000,0.100,langley/min, 4.000,mi/hr,
2.291,day,50.000,F, 98266.750,Pa,0.950,0.100,langley/min, 3.000,mi/hr,
2.333,day,51.000,F, 98334.287,Pa,0.930,0.220,langley/min, 6.000,mi/hr,
2.374,day,53.000,F, 98334.287,Pa,0.860,0.880,langley/min, 5.000,mi/hr,
2.416,day,54.000,F, 98368.056,Pa,0.840,0.690,langley/min, 1.000,mi/hr,
2.457,day,56.000,F, 98368.056,Pa,0.770,0.480,langley/min, 1.000,mi/hr,
2.499,day,58.000,F, 98368.056,Pa,0.730,0.720,langley/min, 3.000,mi/hr,
2.541,day,60.000,F, 98368.056,Pa,0.630,0.920,langley/min, 1.000,mi/hr,
2.582,day,62.000,F, 98368.056,Pa,0.570,0.660,langley/min, 1.000,mi/hr,
2.624,day,64.000,F, 98300.519,Pa,0.550,1.000,langley/min, 9.000,mi/hr,
2.666,day,64.000,F, 98266.750,Pa,0.530,0.660,langley/min, 3.000,mi/hr,
2.707,day,65.000,F, 98232.981,Pa,0.480,0.360,langley/min, 2.000,mi/hr,
2.749,day,65.000,F, 98232.981,Pa,0.510,0.220,langley/min, 4.000,mi/hr,
2.791,day,64.000,F, 98232.981,Pa,0.510,0.040,langley/min, 3.000,mi/hr,
2.832,day,58.000,F, 98266.750,Pa,0.700,0.000,langley/min, 5.000,mi/hr,
2.874,day,56.000,F, 98300.519,Pa,0.800,0.000,langley/min,10.000,mi/hr,
2.916,day,54.000,F, 98300.519,Pa,0.840,0.000,langley/min, 8.000,mi/hr,
2.957,day,53.000,F, 98300.519,Pa,0.870,0.000,langley/min, 8.000,mi/hr,
2.999,day,55.000,F, 98300.519,Pa,0.870,0.000,langley/min, 3.000,mi/hr,
3.041,day,52.000,F, 98266.750,Pa,0.920,0.000,langley/min, 4.000,mi/hr,
3.082,day,49.000,F, 98300.519,Pa,0.920,0.000,langley/min, 0.000,mi/hr,
3.124,day,51.000,F, 98334.287,Pa,0.860,0.000,langley/min, 0.000,mi/hr,
3.166,day,48.000,F, 98334.287,Pa,0.930,0.020,langley/min, 2.000,mi/hr,
3.207,day,46.000,F, 98368.056,Pa,0.970,0.160,langley/min, 0.000,mi/hr,
3.249,day,52.000,F, 98368.056,Pa,0.920,0.500,langley/min, 0.000,mi/hr,
3.291,day,56.000,F, 98401.824,Pa,0.830,0.780,langley/min, 1.000,mi/hr,
3.332,day,58.000,F, 98435.593,Pa,0.770,1.000,langley/min, 3.000,mi/hr,
3.374,day,63.000,F, 98401.824,Pa,0.650,1.180,langley/min, 3.000,mi/hr,
3.415,day,65.000,F, 98401.824,Pa,0.620,1.200,langley/min, 2.000,mi/hr,

3.457,day,68.000,F, 98401.824,Pa,0.520,0.950,langley/min, 3.000,mi/hr,
3.499,day,70.000,F, 98368.056,Pa,0.470,0.750,langley/min, 2.000,mi/hr,
3.540,day,70.000,F, 98300.519,Pa,0.450,0.980,langley/min, 3.000,mi/hr,
3.582,day,72.000,F, 98266.750,Pa,0.400,0.960,langley/min, 3.000,mi/hr,
3.624,day,73.000,F, 98199.213,Pa,0.380,0.630,langley/min, 5.000,mi/hr,
3.665,day,73.000,F, 98165.444,Pa,0.370,0.660,langley/min, 1.000,mi/hr,
3.707,day,74.000,F, 98131.675,Pa,0.340,0.380,langley/min, 2.000,mi/hr,
3.749,day,72.000,F, 98131.675,Pa,0.360,0.100,langley/min, 4.000,mi/hr,
3.790,day,67.000,F, 98097.907,Pa,0.480,0.020,langley/min, 4.000,mi/hr,
3.832,day,65.000,F, 98131.675,Pa,0.530,0.000,langley/min, 0.000,mi/hr,
3.874,day,61.000,F, 98165.444,Pa,0.680,0.000,langley/min,10.000,mi/hr,
3.915,day,60.000,F, 98199.213,Pa,0.750,0.000,langley/min, 9.000,mi/hr,
3.957,day,58.000,F, 98199.213,Pa,0.790,0.000,langley/min, 6.000,mi/hr,
3.999,day,57.000,F, 98199.213,Pa,0.780,0.000,langley/min,10.000,mi/hr,
#---
~Initial Conditions Card
#---
Aqueous Pressure,Gas Pressure,
2,
Gas Pressure Overwrite,101325.0,Pa,,,,,,1,1,1,1,1,45,
Overwrite Temperature,289.1,K,,,,,,1,1,1,1,1,45,

#---
~Boundary Conditions Card
#---
2,
Top,Bare Shuttleworth-Wallace,,,
1,1,1,1,45,45,193,
0.000,day,0.000,in/hr,
0.042,day,0.000,in/hr,
0.042,day,0.000,in/hr,
0.083,day,0.000,in/hr,
0.083,day,0.000,in/hr,
0.125,day,0.000,in/hr,
0.125,day,0.000,in/hr,
0.167,day,0.000,in/hr,
0.167,day,0.010,in/hr,
0.208,day,0.010,in/hr,
0.208,day,0.040,in/hr,
0.250,day,0.040,in/hr,
0.250,day,0.080,in/hr,
0.292,day,0.080,in/hr,
0.292,day,0.040,in/hr,
0.333,day,0.040,in/hr,
0.333,day,0.000,in/hr,
0.375,day,0.000,in/hr,
0.375,day,0.030,in/hr,
0.417,day,0.030,in/hr,
0.417,day,0.010,in/hr,
0.458,day,0.010,in/hr,
0.458,day,0.000,in/hr,
0.500,day,0.000,in/hr,

0.500,day,0.000,in/hr,
0.541,day,0.000,in/hr,
0.541,day,0.000,in/hr,
0.583,day,0.000,in/hr,
0.583,day,0.000,in/hr,
0.625,day,0.000,in/hr,
0.625,day,0.000,in/hr,
0.666,day,0.000,in/hr,
0.666,day,0.000,in/hr,
0.708,day,0.000,in/hr,
0.708,day,0.000,in/hr,
0.750,day,0.000,in/hr,
0.750,day,0.000,in/hr,
0.791,day,0.000,in/hr,
0.791,day,0.000,in/hr,
0.833,day,0.000,in/hr,
0.833,day,0.000,in/hr,
0.875,day,0.000,in/hr,
0.875,day,0.000,in/hr,
0.916,day,0.000,in/hr,
0.916,day,0.000,in/hr,
0.958,day,0.000,in/hr,
0.958,day,0.000,in/hr,
1.000,day,0.000,in/hr,
1.000,day,0.000,in/hr,
1.041,day,0.000,in/hr,
1.041,day,0.000,in/hr,
1.083,day,0.000,in/hr,
1.083,day,0.010,in/hr,
1.125,day,0.010,in/hr,
1.125,day,0.000,in/hr,
1.166,day,0.000,in/hr,
1.166,day,0.030,in/hr,
1.208,day,0.030,in/hr,
1.208,day,0.030,in/hr,
1.250,day,0.030,in/hr,
1.250,day,0.000,in/hr,
1.291,day,0.000,in/hr,
1.291,day,0.060,in/hr,
1.333,day,0.060,in/hr,
1.333,day,0.090,in/hr,
1.375,day,0.090,in/hr,
1.375,day,0.020,in/hr,
1.416,day,0.020,in/hr,
1.416,day,0.070,in/hr,
1.458,day,0.070,in/hr,
1.458,day,0.090,in/hr,
1.499,day,0.090,in/hr,
1.499,day,0.050,in/hr,
1.541,day,0.050,in/hr,
1.541,day,0.040,in/hr,
1.583,day,0.040,in/hr,

1.583,day,0.000,in/hr,
1.624,day,0.000,in/hr,
1.624,day,0.000,in/hr,
1.666,day,0.000,in/hr,
1.666,day,0.020,in/hr,
1.708,day,0.020,in/hr,
1.708,day,0.010,in/hr,
1.749,day,0.010,in/hr,
1.749,day,0.000,in/hr,
1.791,day,0.000,in/hr,
1.791,day,0.000,in/hr,
1.833,day,0.000,in/hr,
1.833,day,0.000,in/hr,
1.874,day,0.000,in/hr,
1.874,day,0.000,in/hr,
1.916,day,0.000,in/hr,
1.916,day,0.000,in/hr,
1.958,day,0.000,in/hr,
1.958,day,0.000,in/hr,
1.999,day,0.000,in/hr,
1.999,day,0.000,in/hr,
2.041,day,0.000,in/hr,
2.041,day,0.000,in/hr,
2.083,day,0.000,in/hr,
2.083,day,0.000,in/hr,
2.124,day,0.000,in/hr,
2.124,day,0.000,in/hr,
2.166,day,0.000,in/hr,
2.166,day,0.000,in/hr,
2.208,day,0.000,in/hr,
2.208,day,0.000,in/hr,
2.249,day,0.000,in/hr,
2.249,day,0.000,in/hr,
2.291,day,0.000,in/hr,
2.291,day,0.000,in/hr,
2.333,day,0.000,in/hr,
2.333,day,0.000,in/hr,
2.374,day,0.000,in/hr,
2.374,day,0.000,in/hr,
2.416,day,0.000,in/hr,
2.416,day,0.000,in/hr,
2.457,day,0.000,in/hr,
2.457,day,0.000,in/hr,
2.499,day,0.000,in/hr,
2.499,day,0.000,in/hr,
2.541,day,0.000,in/hr,
2.541,day,0.000,in/hr,
2.582,day,0.000,in/hr,
2.582,day,0.000,in/hr,
2.624,day,0.000,in/hr,
2.624,day,0.000,in/hr,
2.666,day,0.000,in/hr,

2.666,day,0.000,in/hr,
2.707,day,0.000,in/hr,
2.707,day,0.000,in/hr,
2.749,day,0.000,in/hr,
2.749,day,0.000,in/hr,
2.791,day,0.000,in/hr,
2.791,day,0.000,in/hr,
2.832,day,0.000,in/hr,
2.832,day,0.000,in/hr,
2.874,day,0.000,in/hr,
2.874,day,0.000,in/hr,
2.916,day,0.000,in/hr,
2.916,day,0.000,in/hr,
2.957,day,0.000,in/hr,
2.957,day,0.000,in/hr,
2.999,day,0.000,in/hr,
2.999,day,0.000,in/hr,
3.041,day,0.000,in/hr,
3.041,day,0.000,in/hr,
3.082,day,0.000,in/hr,
3.082,day,0.000,in/hr,
3.124,day,0.000,in/hr,
3.124,day,0.000,in/hr,
3.166,day,0.000,in/hr,
3.166,day,0.000,in/hr,
3.207,day,0.000,in/hr,
3.207,day,0.000,in/hr,
3.249,day,0.000,in/hr,
3.249,day,0.000,in/hr,
3.291,day,0.000,in/hr,
3.291,day,0.000,in/hr,
3.332,day,0.000,in/hr,
3.332,day,0.000,in/hr,
3.374,day,0.000,in/hr,
3.374,day,0.000,in/hr,
3.415,day,0.000,in/hr,
3.415,day,0.000,in/hr,
3.457,day,0.000,in/hr,
3.457,day,0.000,in/hr,
3.499,day,0.000,in/hr,
3.499,day,0.000,in/hr,
3.540,day,0.000,in/hr,
3.540,day,0.000,in/hr,
3.582,day,0.000,in/hr,
3.582,day,0.000,in/hr,
3.624,day,0.000,in/hr,
3.624,day,0.000,in/hr,
3.665,day,0.000,in/hr,
3.665,day,0.000,in/hr,
3.707,day,0.000,in/hr,
3.707,day,0.000,in/hr,
3.749,day,0.000,in/hr,

3.749,day,0.000,in/hr,
3.790,day,0.000,in/hr,
3.790,day,0.000,in/hr,
3.832,day,0.000,in/hr,
3.832,day,0.000,in/hr,
3.874,day,0.000,in/hr,
3.874,day,0.000,in/hr,
3.915,day,0.000,in/hr,
3.915,day,0.000,in/hr,
3.957,day,0.000,in/hr,
3.957,day,0.000,in/hr,
3.999,day,0.000,in/hr,
3.999,day,0.000,in/hr,
Bottom,Dirichlet Energy,Unit Gradient Aqueous,Dirichlet Gas,
1,1,1,1,1,1,1,
0,day,288.46,K,,,1.0,101325.0,Pa,1.0,

#---
~Output Options Card
#---
6,
1,1,45,
1,1,44,
1,1,33,
1,1,22,
1,1,21,
1,1,1,
1,1,day,cm,6,6,6,
13,
Atmospheric Solar Radiation,W/m^2,
Surface Net Long-Wave Radiation,W/m^2,
Surface Net Short-Wave Radiation,W/m^2,
Surface Sensible Heat Flux,W/m^2,
Surface Latent Heat Flux,W/m^2,
Surface Ground Heat Flux,W/m^2,
Atmospheric Temperature,C,
Surface Temperature,C,
Surface Volumetric Precipitation,cm^3/day,
Potential Evaporation,kg/day,
Actual Evaporation,kg/day,
Aqueous matric potential,cm,
Aqueous moisture content,,
0,
3,
Aqueous matric potential,cm,
Aqueous moisture content,,
Temperature,C,

#---
~Surface Flux Card
#---
4,

Aqueous Volumetric,cm^3/day,cm^3,Top,1,1,1,1,45,45,
Aqueous Volumetric,cm^3/day,cm^3,Bottom,1,1,1,1,1,1,
Potential Evaporation,kg/day,kg,Top,1,1,1,1,45,45,
Actual Evaporation,kg/day,kg,Top,1,1,1,1,45,45,

C.10 STOMP-WAE-B Input File for Evapotranspiration at Hanford's Grass Site

```
#-------------------------------------------------------
~Simulation Title Card
#-------------------------------------------------------
1,
Water balance for the grass site in Hanford,
Andy L. Ward,
Hydrology Group, PNNL,
September 2005,
00:00,
2,
Extended van Genuchten
Year 1983 only
#-------------------------------------------------------
~Solution Control Card
#-------------------------------------------------------
Restart Mode,1,
Water-Air-Energy,
1,
0.0,day,365,day,0.1,hr,0.5,hr,1.25,20,1.e-6,
100000,
variable aqueous diffusion,
variable gas diffusion,
1,
effective permeability,geometric,

#-------------------------------------------------------
~Grid Card
#-------------------------------------------------------
Cartesian,
1,1,145,
0.0,cm,1@1.0,cm,
0.0,cm,1@1.0,cm,
0.0,cm,2@0.25,m,1@0.5,m,1@4.0,m,1@5.0,m,1@5.0,cm,139@2.5,cm,

#-------------------------------------------------------
~Rock/Soil Zonation Card
#-------------------------------------------------------
4,
Layer1,1,1,1,1,132,145,
Layer2,1,1,1,1,117,131,
Layer3,1,1,1,1,96,130,
Layer4,1,1,1,1,1,95,

#-------------------------------------------------------
~Mechanical Properties Card
#-------------------------------------------------------
Layer1,2720,kg/m^3,0.258,0.258,0,,Millington and Quirk,
```

Layer2,2720,kg/m^3,0.195,0.195,0,,Millington and Quirk,
Layer3,2720,kg/m^3,0.150,0.150,0,,Millington and Quirk,
Layer4,2720,kg/m^3,0.143,0.143,0,,Millington and Quirk,

#---
~Hydraulic Properties Card
#---
Layer1,2.79e-3,hc:m/s,,,2.79e-3,hc:m/s,
Layer2,1.20e-4,hc:m/s,,,1.20e-4,hc:m/s,
Layer3,7.13e-5,hc:m/s,,,7.13e-5,hc:m/s,
Layer4,2.93e-5,hc:m/s,,,2.93e-5,hc:m/s,

#---
~Saturation Function Card
#---
Layer1,extended van Genuchten,11.3,1/m,1.214,0.213,,
Layer2,extended van Genuchten,10.5,1/m,1.218,0.145,,
Layer3,extended van Genuchten,17.0,1/m,1.336,0.145,,
Layer4,extended van Genuchten,17.6,1/m,2.024,0.277,,

#---
~Aqueous Relative Permeability Card
#---
Layer1,Mualem,,
Layer2,Mualem,,
Layer3,Mualem,,
Layer4,Mualem,,

#---
~Gas Relative Permeability Card
#---
Layer1,Corey,0.1,0.213,
Layer2,Corey,0.1,0.145,
Layer3,Corey,0.1,0.145,
Layer4,Corey,0.1,0.277,

#---
~Thermal Properties Card
#---
Layer1,Cass,0.60,W/m K,0.70,W/m K,8.0,0.26,W/m K,3.0,793.1,J/kg
C,enhanced,9.5,2.0,8.0,0.50,3.0,albedo,Wang,0.267,0.160,3.585,0.04,
Layer2,Cass,0.60,W/m K,0.70,W/m K,8.0,0.26,W/m K,3.0,793.1,J/kg
C,enhanced,9.5,2.0,8.0,0.50,3.0,albedo,Wang,0.402,0.275,3.585,0.04,
Layer3,Cass,0.60,W/m K,0.70,W/m K,8.0,0.26,W/m K,3.0,730.6,J/kg
C,enhanced,9.5,2.0,8.0,0.50,3.0,albedo,Wang,0.402,0.275,3.585,0.04,
Layer4,Cass,0.60,W/m K,0.70,W/m K,8.0,0.26,W/m K,3.0,730.6,J/kg
C,enhanced,9.5,2.0,8.0,0.50,3.0,albedo,Wang,0.402,0.275,3.585,0.04,

#----------------------------------
~Plant Card
#----------------------------------
2,Single Plant Temperature Rainfall Interception,

Cheatgrass,Vrugt Root Stress Hicks,
0.50,m,0.10,m,4.875,
Temporal Albedo,0.05,0.06,0.15,0.19,0.05,0.30,m,1.984e-3,m,
0.1,m,1.0,m,10.0,m,150.,m,
0.0,0.0,day,0.0,55,day,1.0,112,day,1.0,148,day,0.0,159,day,
50,s/m,20,W/m^2,5,C,45,C,25,C,
Sandberg Bluegrass,Vrugt Root Stress Hicks,
0.35,m,0.20,m,2.62,
Temporal Albedo,0.05,0.06,0.15,0.19,0.05,0.10,m,1.984e-3,m,
0.1,m,1.0,m,10.0,m,150.,m,
0.0,0.0,day,0.0,55,day,1.0,104,day,1.0,147,day,0.0,160,day,
50,s/m,20,W/m^2,5,C,45,C,25,C,

#----------
~Atmospheric Conditions Card
#----------
January,1,1983,00:00:00,15.24,m,0.914,m,119.33,deg,46.41,deg,119.33,deg,30.0,mm,3.0,mm,
8761, # of atmospheric conditions
file,hms-at1983.dat,
#
#----------
~Initial Conditions Card
#----------
Aqueous Saturation,Gas Pressure,
2,
Gas Pressure Overwrite,101325,Pa,,,,,,1,1,1,1,1,145,
Temperature Overwrite,20.0,C,,,,,-0.5,1/m,1,1,1,1,1,145,

#----------
~Boundary Conditions Card
#----------
2,
Top,Shuttleworth-Wallace,,,
1,1,1,1,145,145,922,
file,hms-bc1983.dat,
Bottom,Dirichlet Energy,Dirichlet Aqueous,Zero Flux Gas,
1,1,1,1,1,1,1,
0,day,20.0,C,101325,Pa,1.0,,,1.0,

#----------
~Output Options Card
#----------
19,
1,1,145,
1,1,139,
1,1,133,
1,1,127,
1,1,110,
1,1,115,
1,1,109,
1,1,103,
1,1,97,

1,1,92,
1,1,85,
1,1,79,
1,1,67,
1,1,55,
1,1,43,
1,1,31,
1,1,19,
1,1,7,
1,1,2,
1,1,day,m,5,5,5,
15,
Atmospheric Solar Radiation,W/m^2,
Surface Net Long-Wave Radiation,W/m^2,
Surface Net Short-Wave Radiation,W/m^2,
Surface Sensible Heat Flux,W/m^2,
Surface Latent Heat Flux,W/m^2,
Surface Ground Heat Flux,W/m^2,
Atmospheric Temperature,C,
Surface Temperature,C,
Surface Volumetric Precipitation,cm^3/day,
Potential Evaporation,kg/day,
Actual Evaporation,kg/day,
Potential Transpiration,kg/day,
Actual Transpiration,kg/day,
Aqueous matric potential,cm,
Aqueous moisture content,,
77,
7,day,
14,day,
21,day,
28,day,
35,day,
42,day,
49,day,
56,day,
63,day,
70,day,
77,day,
84,day,
91,day,
98,day,
105,day,
108,day,
108.0417,day,
108.0833,day,
108.1250,day,
108.1667,day,
108.2083,day,
108.2500,day,
108.2917,day,
108.3333,day,

108.3750,day,
108.4167,day,
108.4583,day,
108.5000,day,
108.5417,day,
108.5833,day,
108.6250,day,
108.6667,day,
108.7083,day,
108.7500,day,
108.7917,day,
108.8333,day,
108.8750,day,
108.9167,day,
108.9583,day,
109,day,
112,day,
119,day,
126,day,
133,day,
140,day,
147,day,
154,day,
161,day,
168,day,
175,day,
182,day,
189,day,
196,day,
203,day,
210,day,
217,day,
224,day,
231,day,
238,day,
245,day,
252,day,
259,day,
266,day,
273,day,
280,day,
287,day,
294,day,
301,day,
308,day,
315,day,
322,day,
329,day,
336,day,
343,day,
350,day,
357,day,

```
364,day,
5,
Aqueous pressure,pa,
Aqueous matric potential,cm,
Aqueous moisture content,,
Aqueous relative permeability,,
Temperature,C,

#-----------------------------------------------------
~Surface Flux Card
#-----------------------------------------------------
8,
Potential Evaporation,kg/day,kg,Top,1,1,1,1,145,145,
Actual Evaporation,kg/day,kg,Top,1,1,1,1,145,145,
Potential Transpiration,kg/day,kg,Top,1,1,1,1,145,145,
Actual Transpiration,kg/day,kg,Top,1,1,1,1,145,145,
Aqueous Volumetric,cm^3/day,cm^3,Bottom,1,1,1,1,131,131,  # 35.0 cm Sandberg's bluegrass
Aqueous Volumetric,cm^3/day,cm^3,Bottom,1,1,1,1,125,125,  # 50.0 cm Cheatgrass
Aqueous Volumetric,cm^3/day,cm^3,Bottom,1,1,1,1,  6, 6,    # 350 cm
Aqueous Volumetric,cm^3/day,cm^3,Bottom,1,1,1,1,  2, 2,    # Water table
```

C.11 STOMP-WAE-B Input File for Barrier Benchmark Simulation

```
#-------------------------------------------------------
~Simulation Title Card
#-------------------------------------------------------
1,
Idaho site,
Andy L. Ward, Z. Fred Zhang, and Mark D. White
Hydrology Group, PNNL,
Sep 2005,
00:00,
6,
Scanlon, B.R., M. Christmans, R.C. Reedy, I. Porro,
and J. Simunek, and G.N. Flerchinger. 2002.
Intercode comparisons for simulating water balance
of surfacial sediments in semiarid regions.
Water Resour. Res. 38(2), 1323, doi: 10.1029/2001WR001233
Bare soil surface, Extended van Genuchten

#-------------------------------------------------------
~Solution Control Card
#-------------------------------------------------------
Normal,
Water-Air-Energy,
3,
0.0,day,72.0,day,1.0,s,0.1,hr,1.4,100,1.e-6,
72.0,day,437.0,day,1.0,s,0.1,hr,1.4,100,1.e-6,
437.0,day,803.0,day,1.0,s,0.1,hr,1.4,100,1.e-6,
400000,
variable aqueous diffusion,
variable gas diffusion,
1,
effective permeability,geometric,

#-------------------------------------------------------
~Grid Card,
#-------------------------------------------------------
Cartesian,
1,1,113,
0,cm,1,cm,
0,cm,1,cm,
-300,cm,-299,cm,-298,cm,-297,cm,-295,cm,-290,cm,-285,cm,-277,cm,-270,cm,-264,cm,
-260,cm,-257,cm,-255,cm,-253,cm,-250,cm,-246,cm,-234,cm,-224,cm,-215,cm,-207,cm,
-200,cm,-194,cm,-189,cm,-185,cm,-182,cm,-180,cm,-178,cm,-175,cm,-170,cm,-165,cm,
-160,cm,-155,cm,-151,cm,-148,cm,-145,cm,-142,cm,-140,cm,-137,cm,-134,cm,-131,cm,
-128,cm,-125,cm,-122,cm,-120,cm,-118,cm,-115,cm,-111,cm,-108,cm,-105,cm,-102,cm,
-100,cm,-98,cm,-95,cm,-91,cm,-88,cm,-85,cm,-82,cm,-80,cm,-78,cm,-76,cm,
-73,cm,-70,cm,-67,cm,-64,cm,-62,cm,-60,cm,-58,cm,-56,cm,-53,cm,-50,cm,
-47.255,cm,-44,cm,-42,cm,-40,cm,-38,cm,-36,cm,-35,cm,-33.136,cm,-29.903,cm,-27.21,cm,
-24.965,cm,-23.094,cm,-21.536,cm,-20.236,cm,-19.154,cm,-18.252,cm,-17.5,cm,-16.874,cm,-16.352,cm,-15.916,cm,
-15.554,cm,-15.252,cm,-15,cm,-14.748,cm,-14.446,cm,-14.084,cm,-13.649,cm,-13.127,cm,-12.5,cm,-11.748,cm,
-10.846,cm,-9.764,cm,-8.465,cm,-6.536,cm,-5.236,cm,-4.154,cm,-3.252,cm,-2.5,cm,-1.874,cm,-1.352,cm,
```

-0.916,cm,-0.554,cm,-0.252,cm,0,cm,

#----------
~Rock/Soil Zonation Card
#----------
2,
Admix,1,1,1,1,93,113,
Silt loam,1,1,1,1, 1, 92,

#----------
~Mechanical Properties Card
#----------
Admix,,,0.36,0.36,,,Millington and Quirk,
Silt loam,,,0.47,0.47,,,Millington and Quirk,

#----------
~Hydraulic Properties Card
#----------
Admix,,,,,5.9,hc:cm/day,
Silt loam,,,,,8.9,hc:cm/day,

#----------
~Saturation Function Card
#----------
Admix,extended van Genuchten,0.036,1/cm,1.601,0.097,,
Silt loam,extended van Genuchten,0.005,1/cm,2.090,0.032,,

#----------
~Aqueous Relative Permeability Card
#----------
Admix,Mualem,,
Silt loam,Mualem,,

#----------
~Gas Relative Permeability Card
#----------
Admix,Corey,0.1,0.097,
Silt loam,Corey,0.1,0.032,

#----------
~Thermal Properties Card
#----------
Admix,Cass,1.16,W/m K,0.922,W/m K,3.468,0.207,W/m K,2.177,712.250,J/kg
K,enhanced,9.5,2.0,8.0,0.50,3.0,albedo,Wang,0.25,0.1,3.5058,0.04,
Silt Loam,Cass,1.13,W/m K,0.943,W/m K,3.477,0.188,W/m K,2.325,793.1,J/kg
K,enhanced,9.5,2.0,8.0,0.50,3.0,albedo, Wang,0.25,0.1,3.5058,0.04,

#----------
~Plant Properties Card
#----------
0,

```
#-----------------------------------------------------
~Atmospheric Conditions Card
#-----------------------------------------------------
July,21,1997,00:00:00,15.0,m,2.0,m,112.95,deg,43.53,deg,112.95,deg,0.1,mm,0.01,mm,
19993,
file,idaho_atm.dat,
#-----------------------------------------------------
~Initial Condition Card,
#-----------------------------------------------------
Aqueous Pressure,Gas Pressure,
115,
Gas Pressure,101325,Pa,,,,,,1,1,1,1,1,113,
Temperature, 15.0,C,,,,, 5.0,1/m,1,1, 1, 1,1,113,
Aqueous Pressure,82632.48,Pa,,,,,,1,1,1,1,113,113,
Aqueous Pressure,82632.48,Pa,,,,,,1,1,1,1,112,112,
Aqueous Pressure,82632.48,Pa,,,,,,1,1,1,1,111,111,
Aqueous Pressure,82632.48,Pa,,,,,,1,1,1,1,110,110,
Aqueous Pressure,82632.48,Pa,,,,,,1,1,1,1,109,109,
Aqueous Pressure,82632.48,Pa,,,,,,1,1,1,1,108,108,
Aqueous Pressure,82632.48,Pa,,,,,,1,1,1,1,107,107,
Aqueous Pressure,82632.48,Pa,,,,,,1,1,1,1,106,106,
Aqueous Pressure,82632.48,Pa,,,,,,1,1,1,1,105,105,
Aqueous Pressure,82632.48,Pa,,,,,,1,1,1,1,104,104,
Aqueous Pressure,82632.48,Pa,,,,,,1,1,1,1,103,103,
Aqueous Pressure,82632.48,Pa,,,,,,1,1,1,1,102,102,
Aqueous Pressure,82632.48,Pa,,,,,,1,1,1,1,101,101,
Aqueous Pressure,82632.48,Pa,,,,,,1,1,1,1,100,100,
Aqueous Pressure,82632.48,Pa,,,,,,1,1,1,1,99,99,
Aqueous Pressure,82632.48,Pa,,,,,,1,1,1,1,98,98,
Aqueous Pressure,82632.48,Pa,,,,,,1,1,1,1,97,97,
Aqueous Pressure,82632.48,Pa,,,,,,1,1,1,1,96,96,
Aqueous Pressure,82632.48,Pa,,,,,,1,1,1,1,95,95,
Aqueous Pressure,82632.48,Pa,,,,,,1,1,1,1,94,94,
Aqueous Pressure,82632.48,Pa,,,,,,1,1,1,1,93,93,
Aqueous Pressure,82632.48,Pa,,,,,,1,1,1,1,92,92,
Aqueous Pressure,82632.48,Pa,,,,,,1,1,1,1,91,91,
Aqueous Pressure,82632.48,Pa,,,,,,1,1,1,1,90,90,
Aqueous Pressure,82632.48,Pa,,,,,,1,1,1,1,89,89,
Aqueous Pressure,82632.48,Pa,,,,,,1,1,1,1,88,88,
Aqueous Pressure,82632.48,Pa,,,,,,1,1,1,1,87,87,
Aqueous Pressure,82632.48,Pa,,,,,,1,1,1,1,86,86,
Aqueous Pressure,82632.48,Pa,,,,,,1,1,1,1,85,85,
Aqueous Pressure,82632.48,Pa,,,,,,1,1,1,1,84,84,
Aqueous Pressure,82632.48,Pa,,,,,,1,1,1,1,83,83,
Aqueous Pressure,82632.48,Pa,,,,,,1,1,1,1,82,82,
Aqueous Pressure,82632.48,Pa,,,,,,1,1,1,1,81,81,
Aqueous Pressure,82632.48,Pa,,,,,,1,1,1,1,80,80,
Aqueous Pressure,82632.48,Pa,,,,,,1,1,1,1,79,79,
Aqueous Pressure,82632.48,Pa,,,,,,1,1,1,1,78,78,
Aqueous Pressure,82632.48,Pa,,,,,,1,1,1,1,77,77,
Aqueous Pressure,81805.96667,Pa,,,,,,1,1,1,1,76,76,
Aqueous Pressure,80152.94,Pa,,,,,,1,1,1,1,75,75,
```

Aqueous Pressure,78499.91333,Pa,,,,,,1,1,1,1,74,74,
Aqueous Pressure,76846.88667,Pa,,,,,,1,1,1,1,73,73,
Aqueous Pressure,75193.86,Pa,,,,,,1,1,1,1,72,72,
Aqueous Pressure,72503.5591,Pa,,,,,,1,1,1,1,71,71,
Aqueous Pressure,70234.78,Pa,,,,,,1,1,1,1,70,70,
Aqueous Pressure,67755.24,Pa,,,,,,1,1,1,1,69,69,
Aqueous Pressure,65275.7,Pa,,,,,,1,1,1,1,68,68,
Aqueous Pressure,65089.5,Pa,,,,,,1,1,1,1,67,67,
Aqueous Pressure,64903.3,Pa,,,,,,1,1,1,1,66,66,
Aqueous Pressure,64717.1,Pa,,,,,,1,1,1,1,65,65,
Aqueous Pressure,64530.9,Pa,,,,,,1,1,1,1,64,64,
Aqueous Pressure,64251.6,Pa,,,,,,1,1,1,1,63,63,
Aqueous Pressure,63972.3,Pa,,,,,,1,1,1,1,62,62,
Aqueous Pressure,63693,Pa,,,,,,1,1,1,1,61,61,
Aqueous Pressure,63693,Pa,,,,,,1,1,1,1,60,60,
Aqueous Pressure,63693,Pa,,,,,,1,1,1,1,59,59,
Aqueous Pressure,63693,Pa,,,,,,1,1,1,1,58,58,
Aqueous Pressure,63693,Pa,,,,,,1,1,1,1,57,57,
Aqueous Pressure,64299.375,Pa,,,,,,1,1,1,1,56,56,
Aqueous Pressure,64905.75,Pa,,,,,,1,1,1,1,55,55,
Aqueous Pressure,65512.125,Pa,,,,,,1,1,1,1,54,54,
Aqueous Pressure,66320.625,Pa,,,,,,1,1,1,1,53,53,
Aqueous Pressure,66927,Pa,,,,,,1,1,1,1,52,52,
Aqueous Pressure,66613.4,Pa,,,,,,1,1,1,1,51,51,
Aqueous Pressure,66299.8,Pa,,,,,,1,1,1,1,50,50,
Aqueous Pressure,65829.4,Pa,,,,,,1,1,1,1,49,49,
Aqueous Pressure,65359,Pa,,,,,,1,1,1,1,48,48,
Aqueous Pressure,64888.6,Pa,,,,,,1,1,1,1,47,47,
Aqueous Pressure,64321.09091,Pa,,,,,,1,1,1,1,46,46,
Aqueous Pressure,63940.22727,Pa,,,,,,1,1,1,1,45,45,
Aqueous Pressure,63686.31818,Pa,,,,,,1,1,1,1,44,44,
Aqueous Pressure,63432.40909,Pa,,,,,,1,1,1,1,43,43,
Aqueous Pressure,63051.54545,Pa,,,,,,1,1,1,1,42,42,
Aqueous Pressure,62670.68182,Pa,,,,,,1,1,1,1,41,41,
Aqueous Pressure,62289.81818,Pa,,,,,,1,1,1,1,40,40,
Aqueous Pressure,61908.95455,Pa,,,,,,1,1,1,1,39,39,
Aqueous Pressure,61528.09091,Pa,,,,,,1,1,1,1,38,38,
Aqueous Pressure,61147.22727,Pa,,,,,,1,1,1,1,37,37,
Aqueous Pressure,60893.31818,Pa,,,,,,1,1,1,1,36,36,
Aqueous Pressure,60512.45455,Pa,,,,,,1,1,1,1,35,35,
Aqueous Pressure,60131.59091,Pa,,,,,,1,1,1,1,34,34,
Aqueous Pressure,59750.72727,Pa,,,,,,1,1,1,1,33,33,
Aqueous Pressure,59242.90909,Pa,,,,,,1,1,1,1,32,32,
Aqueous Pressure,59258.5,Pa,,,,,,1,1,1,1,31,31,
Aqueous Pressure,59707.66667,Pa,,,,,,1,1,1,1,30,30,
Aqueous Pressure,60156.83333,Pa,,,,,,1,1,1,1,29,29,
Aqueous Pressure,60606,Pa,,,,,,1,1,1,1,28,28,
Aqueous Pressure,60875.5,Pa,,,,,,1,1,1,1,27,27,
Aqueous Pressure,61055.16667,Pa,,,,,,1,1,1,1,26,26,
Aqueous Pressure,60682.93,Pa,,,,,,1,1,1,1,25,25,
Aqueous Pressure,59296.72,Pa,,,,,,1,1,1,1,24,24,
Aqueous Pressure,57448.44,Pa,,,,,,1,1,1,1,23,23,

Aqueous Pressure,55138.09,Pa,,,,,,1,1,1,1,22,22,
Aqueous Pressure,52365.67,Pa,,,,,,1,1,1,1,21,21,
Aqueous Pressure,48129.47247,Pa,,,,,,1,1,1,1,20,20,
Aqueous Pressure,43097.30243,Pa,,,,,,1,1,1,1,19,19,
Aqueous Pressure,39918.10401,Pa,,,,,,1,1,1,1,18,18,
Aqueous Pressure,37668.44835,Pa,,,,,,1,1,1,1,17,17,
Aqueous Pressure,35834.85704,Pa,,,,,,1,1,1,1,16,16,
Aqueous Pressure,36237.83137,Pa,,,,,,1,1,1,1,15,15,
Aqueous Pressure,36540.06213,Pa,,,,,,1,1,1,1,14,14,
Aqueous Pressure,36741.54929,Pa,,,,,,1,1,1,1,13,13,
Aqueous Pressure,36943.03646,Pa,,,,,,1,1,1,1,12,12,
Aqueous Pressure,37245.26721,Pa,,,,,,1,1,1,1,11,11,
Aqueous Pressure,37648.24154,Pa,,,,,,1,1,1,1,10,10,
Aqueous Pressure,38252.70305,Pa,,,,,,1,1,1,1,9,9,
Aqueous Pressure,38957.90813,Pa,,,,,,1,1,1,1,8,8,
Aqueous Pressure,39763.8568,Pa,,,,,,1,1,1,1,7,7,
Aqueous Pressure,40267.57472,Pa,,,,,,1,1,1,1,6,6,
Aqueous Pressure,40271,Pa,,,,,,1,1,1,1,5,5,
Aqueous Pressure,56147,Pa,,,,,,1,1,1,1,4,4,
Aqueous Pressure,56147,Pa,,,,,,1,1,1,1,3,3,
Aqueous Pressure,56147,Pa,,,,,,1,1,1,1,2,2,
Aqueous Pressure,56147,Pa,,,,,,1,1,1,1,1,1,

#---
~Boundary Conditions Card
#---
2,
Top,Bare Shuttleworth-Wallace,,,
1,1,1,1,113,113,1700,
file,idaho_precip.dat,
Bottom,dirichlet Energy,Seepage Face Aqueous,Dirichlet Gas,
1,1,1,1,1,1,2,
0,day,15.0,C,101325,pa,1.0,101365,pa,1.0,
803,day,15.0,C,101325,pa,1.0,101365,pa,1.0,

#---
~Output Options Card
#---
3,
1,1,113,# 0.1 cm
1,1,50, # 1.01 m deep
1,1,1,
50,1,day,m,3,6,6,
14,
Atmospheric Solar Radiation,W/m^2,
Surface Net Long-Wave Radiation,W/m^2,
Surface Net Short-Wave Radiation,W/m^2,
Surface Sensible Heat Flux,W/m^2,
Surface Latent Heat Flux,W/m^2,
Surface Ground Heat Flux,W/m^2,
Atmospheric Temperature,C,
Surface Temperature,C,

Surface Volumetric Precipitation,cm^3/day,
Potential Evaporation,kg/day,
Actual Evaporation,kg/day,
Bare-Soil Aerodynamic Resistance,s/m,
Aqueous matric potential,cm,
Aqueous moisture content,,
10,
0.0,day,
72.0,day,
164.0,day,
254.0,day,
345.0,day,
437.0,day,
529.0,day,
619.0,day,
710.0,day,
803.0,day,
5,
Temperature,C,
Aqueous pressure,pa,
Aqueous matric potential,cm,
Aqueous moisture content,,
Aqueous relative permeability,,
#---
~Surface Flux Card
#---
7,
Potential Evaporation,kg/day,kg,Top, 1,1,1,1,113,113, #0.0 cm
Actual Evaporation,kg/day,kg,Top, 1,1,1,1,113,113, #0.0 cm
Aqueous Volumetric,cm^3/hr,cm^3,Top, 1,1,1,1,113,113, #0.0 cm
Aqueous Volumetric,cm^3/hr,cm^3,Top, 1,1,1,1,112,112, #0.2 cm
Aqueous Volumetric,cm^3/hr,cm^3,Top, 1,1,1,1,50,50, #1 m
Aqueous Volumetric,cm^3/hr,cm^3,Top, 1,1,1,1,19,19, #2 m
Aqueous Volumetric,cm^3/hr,cm^3,Top, 1,1,1,1, 1, 1, #3 m